Experimental Investigation of Interfacial Tension in Two-phase System involving Methane and Water

by

Aminu Abba Yahaya
(B.Eng., M.Sc.)

Ph.D. Thesis   2018

Experimental Investigation of Interfacial Tension in Two-phase System
involving Methane-Water

Aminu Abba YAHAYA

Petroleum and Gas Engineering Division,
School of Computing, Science and Engineering,
University of Salford, United Kingdom

Submitted in Partial Fulfilment for the Requirements of
The award of the degree of Doctor of Philosophy, June 2018

Declaration

I AMINU ABBA YAHAYA, at this moment declare that this work presented in this thesis was carried out by me. Any ideas, thoughts or quotations from other work found in the literature, published or otherwise, are fully acknowledged in accordance to the standard reference practices of the University of Salford, Manchester.

Sign   Date

Abstract

The understanding of the physical properties of reservoir fluids such as viscous and interfacial forces is critical in many oil and gas, petrochemical, and other related industries. In oil and gas industry, the production, transportation and processing of hydrocarbon fluids involve dealing with the multiphase system. Viscosity and interfacial tension (IFT) are among the fluid properties that affect fluid behaviour. These properties have significant effects on fluid flow characteristics, and thus their importance in oil and gas production and processing aspects from the reservoir to other surface facilities. Hence accurate determination of these fluid properties plays a vital role in predicting multiphase flow and managing associated problems faced by the industry such as hydrates, scale and corrosion. Surfactants are added along the line, to prevent hydrate formation, by depressing the formation temperature, and transport it as a hydrate slurry when formed to avoid pipe blockages. While significant research has been conducted in reservoir conditions, but Pipeline system, the presence of salt and polymer-surfactants which tend to alter the IFT behaviour has not been well studied.

This study investigates methane/water interfacial tension experimentally in the presence of salt (NaCl) and polymer-surfactants (PEG 8000-SDS) at operating conditions suitable for upstream and midstream industry application. Also, experimental investigation of pH, resistivity, conductivity, viscosity and density of the liquid phase (brine + polymer-surfactant) was conducted to characterises the liquid phase.

The results show that the electrical resistivity and conductivity depend significantly on the ionic concentration of NaCl presents. Resistivity decreases with increasing NaCl concentration from 0.22 Ω-m at 2.9 wt% NaCl to 0.075 Ω-m at 10.7wt% NaCl, which shows the possibility of corroding the pipe in the case of the pipeline system. The electrical conductivity measured shows an increase with increasing the concentration of NaCl from 4.55 to 13.33 S/m at 2.9 wt% and 10.7 wt% NaCl respectively. This increase in conductivity affirmed the strength of ionic concentration in the system, which could cause scaling and corrosion in the system. High electrical conductivity in the system also signifies a potentially harmful accumulation of solids in cooling towers. Conductivity was also investigated as a function of temperature. The results show that in all the concentration of NaCl studied, increasing temperature (298.15, 303.15, 308.15 and 313.15 K) led to a corresponding average increase in 0.74 S/m in the values of conductivity which shows an increase in ionisation. Results obtained also show that NaCl concentration affects the pH of the solution. The pH value was observed to increase from 6.5 to $\approx$ 7.0 at 8.2 wt% NaCl and 40 wt% PEG 8000 and decreases at 10.7 wt% NaCl at same PEG 8000 concentration to $\approx$ 6.9. Knowing the electrical resistivity, conductivity and pH of the

aqueous solutions, it is critical to accurately determine the viscosity of the solution as it determines the fluid flow and much other application.

The viscosity of PEG 8000 and SDS solution were presented at $298.15 - 313.15$ K. The shear stress obtained at $10 - 40$ wt% PEG 8000 was found to increased from 0.14 Pa at 28.1 s^{-1} to 7.6 Pa at 340.5 s^{-1} indicating Newtonian fluid behaviour. While the apparent viscosity curve obtained, show that the viscosity increased from 3.7 cP at 10 wt% PEG 8000 to 58.1 cP at 40 wt% PEG 8000. However, at each concentration, the viscosity was found to be decreasing with an increase in shear rate.

Results on interfacial tension at two-phase involving methane and water shows that the IFT is a function of pressure, temperature, salinity, and surfactant/polymer. Both increase in pressure and temperature decreases the IFT working at CH_4-H_2O. Presences of 2.9, 5.6, 8.2 and 10.7 wt% NaCl resulted in an average rise of 1.46, 2.57, 3.51 and 4.24 mN.m^{-1} respectively, in IFT. This increase in IFT due to presence of NaCl signifies the formation of corrosion in to the pipeline. Further, active presence of PEG 8000 and SDS reduces the IFT, with critical micelle-like behaviour observed at 30 and 40 wt% PEG 8000 and with more significant effect with the addition of 0.5 wt% SDS. Therefore, these percentage could be a good combination in hydrate prevention along the pipeline. Some of the results obtained were evaluated against independent experimental data gathered from open sources to validate the method and IFT data at the methane-water interface as a function of PEG 8000, and PEG 8000 + SDS were here reported for the first time.

Acknowledgements

Firstly, I would like to express my sincere thanks and gratitude to my supervisor, Doctor Godpower Chimagwo Enyi, for his untiring academic support in all possible way he could throughout my PhD programme. I also wish to thank Professor Ghasem Ghaveni Nasr for his assistance and support on the study, as my co-supervisor. To all other academic and technical staffs in the Department; Dr A. J. Abbas, Dr M. Burby, Mr Ali Kadir, Dr Nourian N, Mr Alan Mapin among others I said thank you for your kind support during this study, in one way or another.

I am very grateful to all my colleagues in the School of Computing Science and Engineering, more especially Umar, Abdullahi, Bello, Hayatu, Sunday, Emmanuel, Kabir, Mohammed (MK), Abdulhamid, Murtala, Mahmud and all others whose names were not mentioned for their commitment, solidarity and being there always for me.

I wish to particularly thank all my family members, your support have been very helpful, and to my late father Alh. Abba Yahaya have no word to use in thanking and appreciating him, all I can say now is I ask Allah to forgive all his shortcomings and grant him Jannatul Firdaus. To my mother Hajiya Aisha no words is enough for your motherly supports and everything that I have will not be without you, I ask Allah to forgive her and grant her all her wishes in this world and hereafter.

To my wife Sa'adatu for your linguistic and moral support, thanks for the courage, support and patience through this journey. You made my heart glows when returning home. To my sons Abdullah and Muhammad for being the most memorable part of this journey, your smiles, having meals with me has been a good way of forgetting the academic stresses.
Time and space will not permit me to enumerate the people in my life who made this task possible, by Allah's will. ALLAH, the almighty knows you all.

List of Content

List of Figures

Appendix List of Figure

List of Tables

List of Publications

1. Yahaya, A. A, Enyi, G. C., Abbas, A. J. and Nasr, G. G. (2017). The influence of temperature and pressure on surface tension and a bubble diameter of methane (CH4) and carbon dioxide (CO2) in water. *6th International Conference on Petroleum Engineering, 29 – 30 June, Madrid, Spain.*

2. Yahaya, A. A., Akpan, E. U., Enyi, G. C., Nasr, G. G., & Abbas, J. (2018). Experimental investigation of methane-water and methane-brine IFT measurements using pendant drop (rising bubble) method. *Journal of Engineering Technology, 6(1), pp. 394–407.*

3. Akpan, E. U, Enyi, G. C, Nasr, G. G and Yahaya, A. A (2018). Stabilizing biopolymers in water-based drilling fluids at high temperature using antioxidants, a formate salt, and polyglycol. *Journal of Engineering Technology, 7 (2) , pp. 469-486.*

Nomenclature

List of Main Symbols

K   Degree Kelvin

$^{\circ}$C   Degree Celsius

ΔT Sub-cooling Temperature

μ Chemical Potential

A   Area

ft   Foot

K_n Vapour-Solid Equilibrium Constant

lb_f Pound-Force

n   Number of moles

P   Pressure

P_c Critical Pressure

P_{pc} Pseudocritical Pressure

P_{pr} Pseudoreduced Pressure

P_r Reduced Pressure

R   Universal Gas Constant

r_c Critical Radius

T   Temperature

T_c Critical Temperature

T_{eq} Equilibrium Temperature

T_{pc} Pseudocritical Temperature

T_{pr} Pseudoreduced Temperature

T_r Reduced Temperature

x_n	Mole Fraction of Hydrocarbon Component, n, in solid on a water free basis
y_i	Molar Composition of Component i
y_n	Mole Fraction of Hydrocarbon Component, n, in gas on a water free basis
z	Compressibility Factor
a_i	Activity of the specie
IFT	Interfacial tension
PEG	Polyehthylene glycol
SDS	Sodium dodeceoul sulphate
ST	Surface tension
V	Volume
G	Gibbs free energy
K_{Li}	Langmuir adsorption constant
C_i	Concentration of components i
E	Energy per Mole of the Solute
$T_{c,h}$	Critical Temperature of Hydrocarbon Phase
CMC	Critical Micelle Concentration
EGR	Enhanced Gas Recovery
EOR	Enhanced Oil Recovery
PD	Pendant Drop
p	Perimeter of the three-phase
DP	Pressure Difference
R_1, R_2	Radius of Curvature
h	Hight of the Column

Greek Letters

β	Shape Factor
γ	Interfacial Tension
ρ	Density
Γ_i	Surface Excess Concentration
ρ_w	Density of Water
ρ_h	Density of hydrocarbon phase
Θ	Contact Angle

Chapter 1: Introduction

1.1 Preamble

This chapter aims to establish the concept of the interfacial tension (IFT) including definition, surface properties and rheology of fluids. Moreover, the chapter is divided into sections. Section 1.1 introduces the chapter while Section 1.2 presents the research background and definition. Section 1.3 and 1.4 provide the justification and contribution of the research. Furthermore, Section 1.5 gives the research questions and aim and objectives are explained in Section 1.6. Lastly, the report outline is presented in Section 1.7.

1.2 Background of the study

Flow assurance is amongst the most vital aspect of the oil and gas industry, and serves the purpose of assuring crude oil and natural gas are transported safely and economically from the reservoir to the processing facilities. It is a common practice to transport these hydrocarbon fluids from the reservoir to a platform onshore or offshore via pipelines, and frequently, most of the fluids within those pipelines come along in gaseous, liquid, and solid forms. Transport of these hydrocarbon fluids in gaseous, liquids and solid forms is referred to as multiphase flow. Transportation in multiphase flow comes with associated problems such as hydrates, scales and corrosions. These problems usually form in pipelines and caused damage or restriction of flow in the pipe, disrupting production and leading to costly repair operations(Rao et al., 2013)

One of the significant and commonly found multiphase flow in oil and gas production is the gas-liquid system. Also, numerous processes in the mineral processing, petrochemical and other related industries rely deeply on the interactions between gaseous and liquid phases. For example in the manufacture of surfactants (Gunstone & Hamilton, 2001) and Sulfuric acid (Ferguson, 1938). Also, in the processes of distillation and desiccation, the gas-liquid contacting and interaction are essential. Other areas where gas-liquid contact and interaction are essential include petroleum and natural gas production, processing and transportation (Nino-Amezquita, Enders, Jaeger, & Eggers, 2010). Furthermore, during enhanced oil recovery, absorption, separations and multiphase flow characteristics in the pipe, requires gas-liquid contact and interaction understanding. Generally, the gas-liquid contacting are most commonly attained by either automation of liquid into gas in the form of drops or by sparging of gas into the liquid pool.

Most of these processes involve interfacial phenomena containing liquid-liquid, liquid-gas and liquid-solid interfaces interactions. These interfaces are very significant in recent years' industrialisations (Mendoza et al., 2014). In the processes such as absorption, adsorption, distillation, and froth flotation, the interaction of two phases occurs through bubbling of gas into the liquid pool (Dominik & Cassel, 2015). Equipment design for such applications depends on the knowledge of the hydrodynamic parameters suitable for desired performance (Kulkarni & Joshi, 2005; Nathanson, Davidovits, Worsnop, & Kolb, 1996). Further, the physicochemical properties, specifically, viscosity, surface tension, and density of the liquid phase and few of the characteristics of the gas phase (viz. bubble size, bubble rise velocity, etc.) govern the hydrodynamics as well as flow pattern in the system. These properties can be applied to design gas and liquid phase processes on both large scale and microscale.

Additionally, the interfacial properties play a vital role in other processes such as enhanced oil recovery, corrosion and hydrate inhibitions, oil spill clean-up, gas/oil/water separation, and asphaltic emulsions. For example, viscous and capillary forces are the dominant factors that control the rate of oil recovery from hydrocarbon reservoirs. The capillary forces depend largely depends on fluid/fluid interfacial tension (Hendraningrat & Torsæter, 2014). Presence of salts significantly affects the interfacial tension and surfactant are used to reduce the interfacial tension. Further, these factors are among the critical determinant of fluid flow through a porous media (Sauerer, Stukan, Abdallah, & Buiting, 2017). Surface active constituents of the reservoir crude oil accumulate at oil-brine and oil-rock interfaces and thus change the properties of the interfaces as well as the flow characteristics (Arsalan, Buiting, & Nguyen, 2015; Atkinson, 1927). Fluctuations in the phase boundaries due to temperature, pressure and compositions variations affect the interfacial properties of the reservoir fluids (Sauerer et al., 2017). Likewise, during emulsification, the interfaces are exposed to different types of external perturbations, like expansion and compression or shear, caused by changes in size and shape of the interface. Karbaschi et al. (2014) reported that the simple, accessible dynamics interfacial quantity of interfaces is the interfacial tension. Therefore, it is of critical importance to understand the Interfacial behaviour in two-phase flow system, more especially in surface facilities such as pipeline and separators.

Moreover, the formation of solid deposits of gas hydrates, waxes and scale is a critical technical concern along the hydrocarbon stream. Because of their rapid formation, gas hydrates are considered by far the most dangerous and common problem in flow assurance in the case of deep subsea transportation compared to other solid deposits (Zerpa, Salager, Koh, Sloan, &

Sum, 2011). This phenomenon of hydrates can be utilised positively, with the aids of surfactant, in some applications such as separation of gas mixtures, CO_2 capture, methane storage and transport among others (A. Kumar, Bhattacharjee, Kulkarni, & Kumar, 2015). Hydrate formation is primarily a crystallisation process that happens at the water-gas interface and grows further in a mass transfer limited regime. Gaseous methane and liquid water is the most straightforward, two-phase system in which hydrate is formed, and interfacial tension working at each liquid-gas interface is considered one of the critical parameter dictating the dynamics in such system (Yasuda, Mori, & Ohmura, 2016). Zhang, Zhou, Wang, Wang, & Li (2013) suggested the importance of interfacial tension and other surface properties in the study of gas hydrate formation and other related application. Now there are several methods used in measuring the surface or interfacial tension of fluids. These methods employed include; capillary rise method, drop weight method, Wilhelm plate or ring methods, maximum bulk pressure methods, methods analysing the shape of the hanging liquid drop or gas bubble (pendant drop), and dynamic methods. In all these methods, pendant drop (PD) is the most suitable methods employed for gas-liquid interfacial tension measurement (Berry, Neeson, Dagastine, Chan, & Tabor, 2015).

With the technological advancement of digital imaging technology, the pendant drop technique has become a widely used method (Hansen & Rodsrud, 1991). Thus in the past decade, there has been an active drive toward understanding interfacial rheology in the context of surfactant adsorption dynamics. There exist several detailed descriptions of the adsorption activity of this and similar systems at an interface. Specifically, it is well-known that for a fluid interface coated with a surfactant, compression and expansion of the interface will result in surfactant exchange with the bulk coupled with a change in the surface tension. If one assumes that the conformational changes in molecules at the interface do not exist, and then measuring this exchange is insignificant. Nevertheless, this may not be true, as indicated by Ramírez, Stocco, Muñoz, & Miller (2012). Any molecular interactions at the interface would very likely result in an apparent rheological response. Identification of this behaviour is essential, more especially in the pipe flow. Surface tension is among the most crucial property on interface mass transfer during surface processes, such as hydrate formation. Indeed, gas hydrate is one of the significant issues in oil and gas transportations line (Sloan, 2005), and also a source of energy as there exist a several research and production of natural gas from gas hydrate deposits (Makogon & Omelchenko, 2013) with potential reserves estimate of 1.5 x 10^{16} m^3 (Makogon, Holditch, & Makogon, 2007). Another area of interest to natural gas industries is the transportation of gas in solid form (Hydrate) and have also been a subject of higher benefits (Englezos & Lee, 2005).

Interfacial properties at gas-liquid interface play a vital role in all these processes of hydrate technology. For example, at low interfacial tension at methane-water interface enhanced the gas mass transfer into the water molecules. Thus, results from this investigation will provide an insight on how the polymer-surfactant and the system isotherm influences the interface interaction between gaseous hydrocarbon (methane) and water in the presence of salt (NaCl).

However, if the understanding of mass transfer in the multiphase system can be enhanced beyond mass transfer characteristics, example in absorption and floatation process, would significantly boost management of technological advantage of the multiphase system (such as enhanced oil and gas recovery) and associated problems of transporting oil and gas in a pipeline and other processing facilities (such as hydrate, scales and corrosion) management. Mass transfer in multiphase (fluid-fluid) system is one of the significant amongst the most fundamental processes occurring in various applications related to petroleum and natural gas. In multiphase systems, the species mass transfer rate is controlled by the system pressure and temperature, as well as by the conductance of mass transfer, concentration gradient, interfacial tension, activation energy and so forth. For example, in the event that we investigate the mass transfer process, the interfacial tension variation from the interface because of mass transfer is not entirely, fluid dynamical phenomena. In any case, it has causation, which comes about into a coupling of liquid flow and mass transfer. This coupling causes non-uniform shear dispersion along the interface, which prompts interfacial instability such as surface ripples, interfacial turbulence and localised eruption (Khadamkar, Khanwale, Sawant, & Mathpati, 2017). The interfacial or surface phenomena is, therefore, a key fundamental in the study of the multiphase system.

1.3 Interfacial phenomena

The region that separates various phases caused by the imbalance of molecular forces of attractions between molecules is referred to as interfacial phenomena (Davies, 2012). At the interface of two different contacting phases, there exist more molecular attraction than in the bulk of the phases, and consequently, those atoms at the interface have different internal pressure, intermolecular spacing, and chemical potential (Israelachvili, 2011). The physical behaviour of the interfaces determines the strength of the contact phase's interfacial tension.

Before going deep into the forces that exist at the surface of the fluids due to its molecular interactions, it is essential to understand the meaning of the word "surface". The surface is used to refer to a topmost layer or boundary of two distinct phases existing together (Adamson &

Gast, 1967). However, the surface can be described geometrically, as an area where the thickness tends to zero, and chemically, as a region in which there exists some metastable properties which are different from the bulk of the two adjoining phases. Surface tension (ST) may be referred to as phenomena resulting from an imbalance of a molecule at the topmost layer, of a liquid due to the molecular attractions pulling, downward to the bulk of the liquid. The molecular attraction experienced by the molecules at the surface due to the bulk of the liquid is higher than the molecular affinity towards the medium from which the liquid is distinguishable with the surface. This molecular behaviour at the surface is due to the existence of unbalanced forces of tractions at the interface. The molecules at the bulk volume of the liquid experienced a balanced molecular attraction from the surrounding molecules of the liquid. This balance diminishes as the molecule approaches the surface. The imbalance, and consequently the surface tension, depends upon the properties of both of the phases in which the surface is the common boundary. In other words, surface tension is not a property of one phase, but a joint property of two phases exist together. Surface tension is an essential interfacial property of fluids (Cheng, Li, Boruvka, Rotenberg, & Neumann, 1990; Miller, Sedev, Schano, Ng, & Neumann, 1993; Río & Neumann, 1997). Río & Neumann (1997) described that measurement of surface tensions using automated computer software has not only improved the accuracy of the measurements considerably, but it has also permitted the study of phenomena that were not possible or difficult to investigate in the past, such as ultralow interfacial tensions, the relaxation of adsorption layers, and dynamic surface tensions.

Hence, the need to improve on the existing knowledge on the interfacial phenomena on gas-liquid (methane – liquid water and carbon dioxide – liquid water) interfaces cannot be overemphasised. Despite several methods used in the investigation of the interface phenomena, still, there is lack of literature in the area of the gas-liquid system, most especially towards processes involving gas hydrate formation along the pipeline and other related two-phase flow behaviours.

1.4 Justification of the research

Despite several efforts to understand the dynamics of the different interfaces (such as liquid-gas and liquid-liquid) interactions, investigating the interfacial phenomena involving liquid-gas interface, have always been a problem in most of the applications involving such interface process phenomena (Berry et al., 2015). The design of most of the multiphase application, especially processes involving gas-liquid system requires the knowledge of interface properties.

The responses of the interfacial tension due to the system pressure and temperature, for example, is required in gas-liquid and liquid-liquid separator design. Also, flow pattern and characteristics in pipeline require accurate measurement of interfacial tension as a function of pipe operating conditions. Most of the reservoir fluids come along with water containing a various concentration of different salts, with NaCl being the major salt present. Presence of salt in the system alters or affect the IFT measured. Further, surfactants are used in enhanced oil recovery, to reduce the interfacial tension between the fluids in the reservoir and reservoir rock, corrosion and hydrate inhibitors are also applied to prevent corrosion in the pipeline and blockages due to hydrate formation. All of these applications are surface processes, and interfacial tension and area working at these interfaces are one of the critical parameters controlling both the formation, prevention and management of corrosions and hydrates in the pipeline or any processing facilities. Therefore, knowledge of interfacial surface tension plays a crucial role in carefully selecting and designing the best options. The present study is designed to investigate the methane − liquid water interface rheology with different salt concentration and polymer-surfactant. Methane-water is the most commonly encountered two-phase system in oil and gas industry (Bilgesu, Ternyik, & Virginia, 1994) hence the selection. Also, the produced water comes along with different salts such as calcium, magnesium, potassium, sodium with sodium being the major constituents. Therefore, in this study sodium salt (NaCl) was used. Understanding the interfacial or surface rheology of the gas-liquid interface interaction will influence the design and control of most of the above mention processes. The central area of concern in this study is a pipeline and other surface facilities.

1.5 Applications and significance of interfacial tension

In many of the earlier mentioned industrial processes, understanding of interfacial tension (IFT) is critical in mass and energy transfer across the interfaces of the fluids involved and hence, it therefore dramatically influences the design of process equipment (Sattari-Najafabadi, Esfahany, Wu, & Sunden, 2018). This property also influences the quality of products such as coatings, paints, agrochemicals, drugs, and detergents as well as many other industrial processes associated with the formation of emulsions, foams, micelles, thin films and gels (Myers, 2000).

As for the petroleum industry, fluid−fluid interfacial tension affects most, if not all, processes involved in the extraction and refining of petroleum and natural gas, from the optimisation of reservoir engineering scheme to the design of the petrochemical equipment. For instance, Abubakar et al. (2015) report showed that oil−water IFT influences, significantly, the flow

characteristics in the horizontal geometry of pipes. Others (Amani, Safdari, Abolghasemi, Mallah, & Davari, 2017; Asadollahzadeh, Torab-Mostaedi, Shahhosseini, & Ghaemi, 2016) demonstrated that the pressure drop in horizontal-vertical pulsed sieve-plate column and fluid hold up, characteristic velocity and slip velocity in multi impeller column are also affected by interfacial tension. Moreover, it is well established that several rock properties such as wettability, capillary pressure and relative permeabilities strongly depend on the *IFT* between fluid phases. Thus, *IFT* is a crucial parameter that determines the displacement of hydrocarbons in the pore spaces of reservoir rock and, in turn, the amount of oil produced (Arabloo, Ghazanfari, & Rashtchian, 2016; Liang, Zhou, Lu, DiCarlo, & Nguyen, 2017).

Therefore, as observed above, accurate determination and understanding of IFT and its response to change in pressure, temperature and surfactant/polymer are necessary. More especially in the design and optimisation of oil and gas production pipelines and enhanced recovery processes. Decreases in interfacial tension increase the tendency of hydrates plug in a pipeline, and recovery of more oil in the reservoir. The decrease or increase of interfacial tension is a function of pressure, temperature, the presence of salts and polymer-surfactant.

1.6 Research contributions

The present study designed, provided the following contribution to the academia and the industry in general:

1. Provide quantitative knowledge database concerning the interfacial tension of methane bubble in liquid water at:
   a. Temperature and pressure variation (temperature 298.15 – 313.15 K, pressure up to 13.10 MPa);
   b. Different chloride salt concentration (NaCl); and
   c. Polymer (PEG 8000) and surfactant (SDS) concentration.
2. Provide surface inhibition performance and suitable among the PEG 8000, SDS and PEG 8000 + SDS investigated for preventing and promoting mass transfer across the methane-water interface.

1.7 Aim and objectives

1.7.1 Aim

The aim of this work is:

1. To investigate and establish the interfacial tension response to temperature and pressure variation, different salt and polymer-surfactant concentrations at the gas – water interface using pendant drop (risen bubble) technique.

1.7.2 Objectives

The aim of this work is going to be achieved by the goals designed as follows:

a. To characterise the typical range of industry brine, the polymer-surfactant solution regarding pH, electrical conductivity and resistivity.

b. To investigate the effect of average oil and gas pipeline salt concentrations on apparent viscosity and density of the liquid water – surfactant solution at the experimental pressure and temperature specified in Section 1.6 above.

c. To investigate the influence of temperature and pressure on interfacial tension existing in a two-phase system involving methane bubble in water/brine.

d. To investigate the effect of surfactant concentration on the interfacial tension of methane bubble in water/brine solutions.

e. To compare the existing experimental IFT data in the literature with the measured IFT data from this work.

1.8 Thesis structure

This thesis contains five chapters.

Chapter 1:   This chapter gives a prologue to the thesis regarding the research background, justification and contribution of the research, and aims and objectives of the study and then the structure of the thesis. The scientific merit and significance of the study are briefly discussed.

Chapter 2:   This chapter provides the relevant theoretical background and literature review of this work. Concepts of the interfacial phenomenon, capillary actions and multiphase flow in porous media and related fundamental theoretical equations are explained.

Chapter 3:   This chapter portrays the materials and the main experimental methodologies used, such as rheological measurement technique for the liquid samples developed in this project and gas-liquid interfacial tension measurement apparatus.

Chapter 4:   This chapter contains the main body of the thesis. It presents the experimental results and discussions of the $CH_4 - H_2O$ and $CH_4 - $ (Brine + PEG 8000 + SDS) interfacial tension and the rheology of the liquid solutions. The experimental investigations include the influence of temperature and pressure on the interfacial tension.

Chapter 5:   This chapter presents the main findings and highlights the significance of the study. The limitations, shortcomings and flaws of the study are addressed and emphasised, and future work is also proposed.

Chapter 2: Theoretical Background and Literature Review

2.1 Preamble

In this chapter, an in-depth technical review of background and studies on multiphase flow in the oil and gas industry is presented, showing the properties that affect the fluid flow characteristic, specifically interfacial tension and viscosity. The chapter is also categorised into specific sections as follows: 2.1 introduces the chapter, 2.2 describes a multiphase system and flow classification in the pipeline, and fluid properties and two-phase flow are presented in section 2.3. The interfacial phenomena are presented in sections 2.4, and lastly, surfactants fundamentals are presented in section 2.5.

2.2 Multiphase System

Most of the processes in hydrocarbon production and refining, petrochemical processing plant, minerals transport, and separators involve dealing with the multiphase system (Ahmadi, Galedarzadeh, & Shadizadeh, 2016; Bilgesu et al., 1994; Jahanandish, Salimifard, & Jalalifar, 2011; Rosenberg et al., 1992; Shannak, 2008). The processes of extraction, refining and transportation of oil and natural gas involve dealing with a mixture of hydrocarbon components with other several non-hydrocarbon components including H_2O, CO_2, H_2S and some solids materials including sand. In addition to that, transfer of species between phases during diffusion and chemical reactions involves the interaction of different molecular species.

Multiphase flow, which is the flow of the mixture of gases, liquids and solids (Brennen, 2005) is predominant in many of the processing facilities and production pipelines in the oil and gas industry (Günther & Jensen, 2006). The nature of the flow is very complicated due to the existence of different flow regimes resulting from the presence of various phases and system pressure and temperature. Usually, the phases present includes gas, liquid and solid (oil, water, gas and sand). The most commonly encountered form in multiphase flow is a two-phase system (Ali & Yeung, 2013) where a variety of flow patterns can be observed depending on the fluid properties and the geometry of the pipe (Tan, Dong, & Wu, 2007). The pipe geometry which could either be horizontal or vertical effects of the interfacial area available for mass, momentum or energy transfer between the phases.

2.2.1 Horizontal Flow

During the flow of two-phase fluid containing gas and a liquid in a horizontal pipe, the liquid, which is the heavier components settled down at the bottom due to gravity, while the gas components remained at the top (Mishima & Hibiki, 1996). In this case, when the ratio of the gas volume to total liquid volume is small, the gas gravitate to form smaller bubbles and rise to the top of the pipe. As the gas volume to total liquid increases, the bubbles become bigger and finally merge or combine with the smaller bubbles to form plugs. Moreover, further increases in the gas-liquid ratio result in plugs growing longer and thereby separating the gas and liquid phases to flow in separate layers. The flow of gas and liquid in separate layers results in forming a stratified flow in the pipe. Increasing the gas flow rate, causes the interface formed by the gas-liquid in stratified flow to becomes curvy (wavy). As the gas-liquid ratios continue to increase, the waves become higher until the peak of the waves reaches the top of the pipe to form drags of liquid which was strapped along by the gas. Continual increases in the gas-liquid ratio may cause a centrifugal motion to the liquid and result in annular flow. The liquid is dispersed into the gas stream, at extremely high gas-liquid ratios. The dispersion of the liquid into the gas stream is a function of both interfacial and viscous forces. Figure 2.1 represents diagrammatically, these flow behaviour resulting from gas-liquid flow in the horizontal pipe.
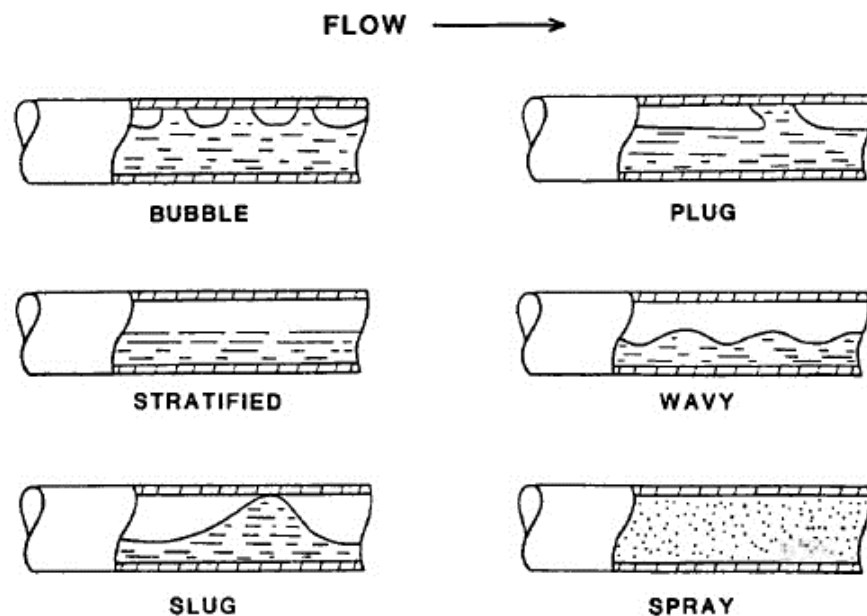
Figure 2.1: Schematic representation of horizontal two-phase pipe flow (Barnea, Luninski, & Taitel, 1983)

2.2.2 Vertical flow

In the case of vertical flow, the two-phase flow patterns involving gas and liquid varies to some extent from horizontal flow. The flow geometries can be classified as bubble, slug-annular, transition, and annular-mist in vertical flow pipe configuration. These flow patterns depend on the gas-liquid ratio as described in horizontal flow section, and they can happen in the same pipe. For instance, in a well-tubing, of a reservoir producing light oil that is near its bubble point, the flow at the bottom of the hole is a bubble regime, as the free gas present is small. As the fluid flow continuously upwards in the tubing, other regimes emanate due to the decreases in pressure resulting in the continual discharge of gas out of the solution. Most of the flow in producing wells are in the slug regime and rarely in mist. Usually, mist flow happens in condensate reservoirs or steam-stimulated wells.

During the upward flow in the vertical pipe, the bubble regime is characterised by small gas-liquid ratio at the bottom of the pipe. The gas bubbles movement is at different velocities which depend upon their respective sizes. Moreover, the upward movement of the liquid, the liquid velocity is uniform. The gas phase has no significant effect on the pressure gradient, except for its density. In the slug flow regime, the gas phase is more pronounced, although the liquid phase is still continuous. The gas bubbles coalesce and equilibrate to form bubbles of the same profile separated by slugs of liquid. The gas bubble velocity is higher than the liquid velocity and can be determined using liquid-slug velocity and the liquid film around the gas bubble (Barnea et al., 1983). The variations in liquid velocities influence the variation in wall friction losses and the liquid holdup, which influences flowing density (Dong, Liu, Deng, Xu, & Xu, 2001). In this case, both phases have significant effects on the pressure gradient. The pressure gradient increases with decreasing interfacial tension especially in gas-liquid pipe flow. In this case, interfacial tnesion has to some extent significant effect on both liquid holdup and the pressure gradient.

A change characterises the regime of transition flow from a continuous liquid phase to a continuous gas phase. The liquid drag (slug) between the bubbles almost vanishes, and a significant amount of liquid becomes entrained in the gas phase. The effects of the liquid are significant, but the gas phase is predominant in this case. For the case of annular-mist flow, the gas phase is continuous. The bulk of the liquid is entrained and carried in the gas phase. A film of liquid wets the pipe wall, but its effects are secondary. The gas phase is the controlling factor. Figure 2.2 represents schematically, these flow pattern in vertical pipe discussed, resulting from two-phase flow involving gas and liquid.

12
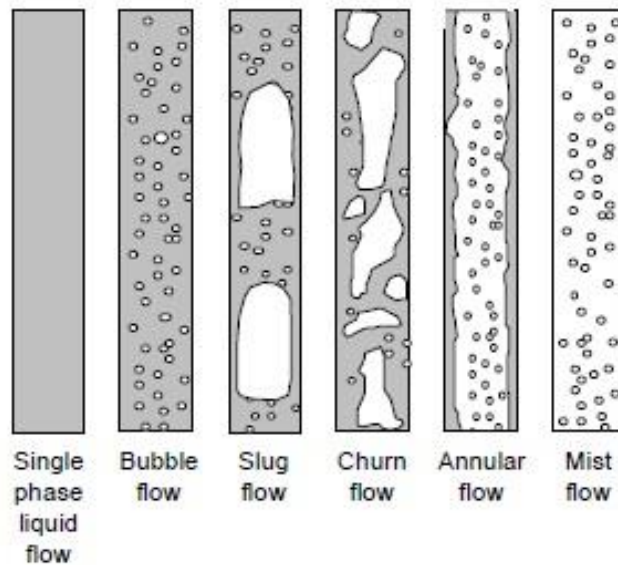
Figure 2.2: Schematic representation of vertical two-phase pipe flow (Barnea et al., 1983)

2.3 Gas-liquid properties in horizontal and vertical flow

As described in the previous sections, the flow characteristics and pattern in two-phase flow depend on properties such as density, viscosity, and interfacial tension. These properties are essential in designing processes involving multiple phases. There have been reported cases where the effects of viscosity, density, and interfacial tension of the fluids were investigated on the transitions between multiphase flow patterns in a circular pipes (Abubakar et al., 2015b; Günther & Jensen, 2006; Mishima & Hibiki, 1996; Rodriguez, 2016; Rodriguez, Mudde, & Oliemans, 2006; Utvik, Rinde, & Valle, 2001; Weisman, Duncan, Gibson, & Crawford, 1979).

Abubakar et al. (2015b) investigated the influence of low interfacial tension on flow patterns, pressure gradients and holdups of medium-viscosity oil/water flowed in the horizontal pipe and concluded that the interfacial tension influences the changes observed in the flow characteristics of oil-water flows. However, they did not indicated how change in IFT could affect the vapour-liquid behaviour (gas-liquid). Günther & Jensen (2006) summarises the importance of interfacial tension in pressure-driven, multiphase flow through microchannel involving gas-liquid and liquid-liquid systems. Rodriguez (2016) examined the effects of interfacial tension on two-phase flow comprising a liquid-liquid system. Rodriguez concluded that the stability of the flow patterns more especially at a region of extreme volumetric fractions depends on

interfacial tension and which also depend on the viscosity and the configuration of the medium through which the fluids flow. Rodriguez et al. (2006) proposed a model to locate the stratified flow pattern in horizontal and slightly inclined oil-water flow. This model recognised the importance of interfacial tension for the flow characteristics pattern stability. Hence, understanding the flow stability by varying IFT could provide a better insight into the flow pattern and stability.

In this work, a two-phase system containing methane and liquid water were investigated regarding interfacial tension and the properties of the liquid. The investigation was carried out using system conditions replica to some of the surface facilities during natural gas productions. Also, salts and polymer-surfactant were considered to analyse their significance when present in the system.

2.4 Interfacial tension definition and fundamentals

For a stable existence of an interface between two phases is that the free energy of formation of the interface is positive; where it is negative or zero, the effect of unexpected fluctuations would be to expand the surface region continuously and to lead to eventual complete dispersion of one material into the other. Example of interfaces whose free energy per unit area is such as to offer no opposition to dispersive forces would be those between two dilute gases or between two miscible liquids. Thus, in the current study, methane and water was used to study the interfacial beahviour, due to their poor miscibility.

This property of immiscible phases is one of the essential properties in dealing with various applications dealing with multiple phases. When the two immiscible fluid system, for example, liquid-liquid or gas-liquid system, exist together in equilibrium, the boundary forces between the phases are usually described using the concept of interfacial tension (IFT) or surface tension (ST). Mostly, when dealing with the liquid-liquid system, the forces existing at the interface are referred to as IFT. In the case of gas-liquid system ST are used. However, theoretical background of the IFT is indistinguishable with that of the ST. The only difference is that the interface liquids-liquids replace the interfacial liquids-gases. Also, all surfaces, whether it is gas, liquid or solid surfaces, can equally act as an interface. Hence, the term IFT includes both liquid-liquid, gas-liquid and liquid-solid interfaces, as described in Table 2.1. Therefore, the term IFT is used for describing the interfacial forces that exist at gas-liquid and liquid-liquid two-phase system for simplicity, in this work, unless otherwise stated.

In Figure 2.3 (a) and (b) a visual representation of interfaces under tensions of gas-liquid and liquid-liquid are shown schematically. The forces are acting on the molecular boundary between the two phases in contact, in all directions. In gas-liquid or liquid A – Liquid B system, the molecules in the centre of the bulk are surrounded by similar molecules and are attracted in all directions by intermolecular forces. The net force acting on the molecules at the bulk is therefore summed to zero, due to the equal pulled by neighbouring molecules in all direction. However, molecules at the interface experienced a net imbalance of forces. The molecules at the boundary are pulled inward and to the side by neighbouring molecules, creating an inward pull of molecules back to the bulk of the phases. The net effect of this imbalance force pulled is that the interfacial area tends to diminish as molecules move from a region of high energy to a state of lower energy. This contraction in the surface area continues until the molecules at the bulk phases reaches their maximum for a given volume and at that particular conditions or external forces (Davies, 2012). Therefore, in this manner, the interface remains in a state of tension, with a system being characterised by a value of interfacial tension. Based on this, the IFT (γ) is often interpreted as a mechanical quantity corresponding to the external work (ΔW) required to increase the interface area (ΔA) by an infinitesimal amount as described in equation (2.1).

$$\Delta W = \gamma \Delta A \tag{2.1}$$

Where γ is the interfacial tension measured in force per unit length (mN/m), W is the work done, and A is the change in the area. The energy of the system is minimised, the surface tends to contract so surface energy can also be expressed as a tension force per length.
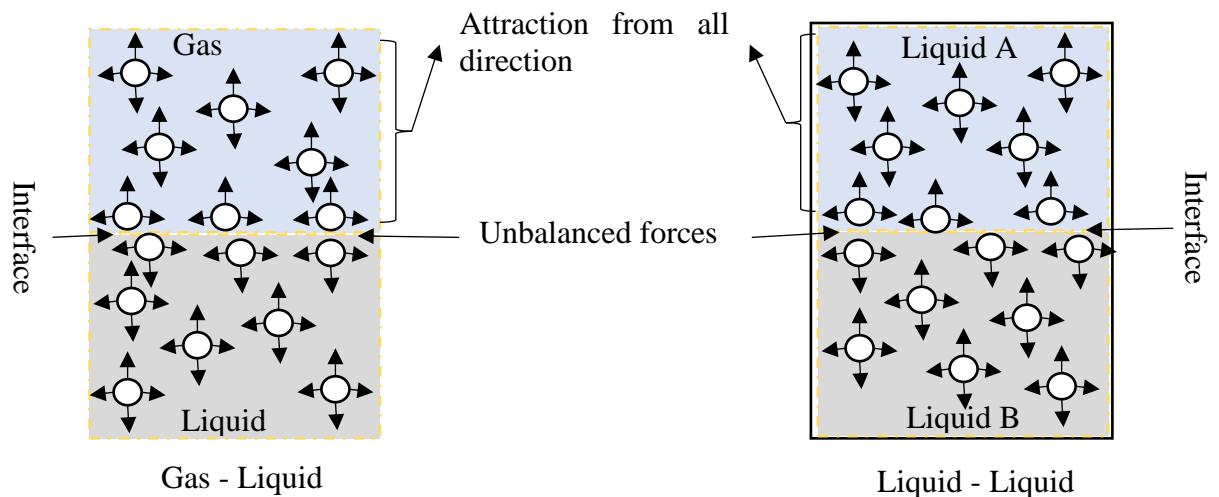
Figure 2.3: The concept of interfacial tension

The interface, however, should not be regarded simply as a plane which separates the two phases but rather as a small region of thickness Δz where properties, like density ρ, vary continuously from one bulk phase to another adjoining bulk phase, as depicted in Figure 2.4. Hence, the interface possesses an anisotropic characteristic, i.e., the magnitude of properties changes in the direction normal to the interface, and the contained fluid is said to be an inhomogeneous fluid or phase.

Table 2.1: Classification of interfaces

Phase	Interfacial Tension	Types and example of interfaces
Gas-Gas	–	–
Gas-Liquid	γ_{LG}	Liquid surface, the body of water exposed to atmosphere
Gas-Solid	γ_{SG}	Solid surface, table top
Liquid-Liquid	γ_{LL}	Liquid–liquid interface, emulsion
Liquid-Solid	γ_{LS}	Liquid–solid interface, suspension
Solid-Solid	γ_{SS}	Solid–solid interface, powder particles in contact
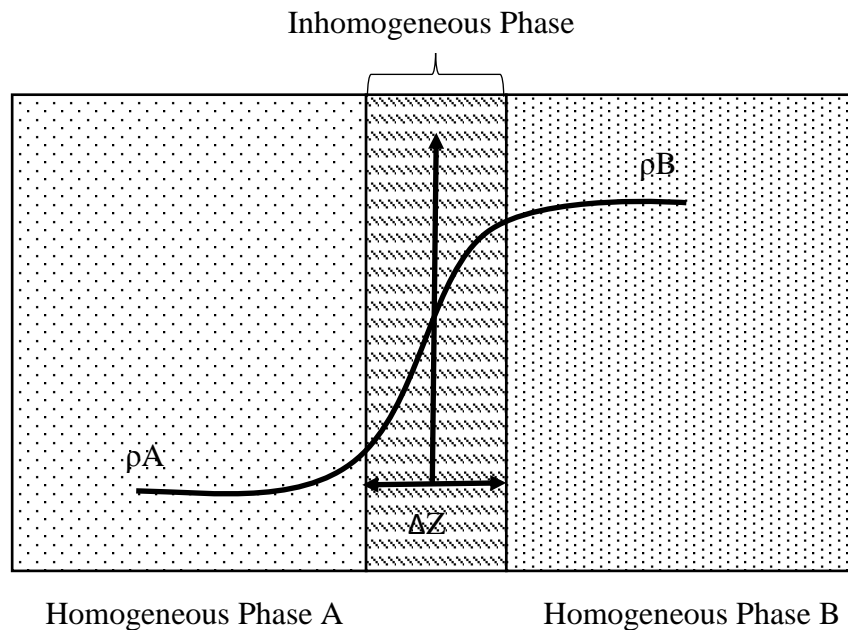
Figure 2.4: Density variation along the normal distance z in the interfacial region (Graf & Kappl, 2006)

From this viewpoint of inhomogeneouty, since the interface is very thin (typically 1 to 2 nm for fluid−fluid interfaces far from the critical point), the interface can be analysed mathematically using Gibbs formalism (Graf & Kappl, 2006). Hence, the IFT defined in thermodynamic terms

16

as the change in the Helmholtz free energy, *F*, (or Gibbs free energy, *G*) of the interface when its area is increased reversibly by an infinitesimal amount at constant temperature and composition, and at constant volume (or pressure) (Moradi, 2011). colour

$$\gamma = \left(\frac{\partial G}{\partial A}\right)_{T,\ P, n=constant} = \left(\frac{\partial F}{\partial A}\right)_{V,T,\ n=constant} \qquad (2.2)$$

Where γ is given in units of energy per unit area (J/m^2) or force per unit length (N/m). It can be concluded, from this interpretation, which is a more fundamental one, *γ* can also be regarded as interfacial free energy (or surface free energy) and is dimensionally equivalent to that obtained in Equation (2.1), *i.e.*, 1 mN/m = 0.001 J/m^2. IFT, as defined in Equations 2.1 and 2.2, are also numerically equivalent for vapour−liquid and liquid−liquid interfaces formed between bulk phases in thermodynamic equilibrium, but it may differ for non-equilibrium liquids and solids (Graf & Kappl, 2006). The interfacial tension can be related to the composition of the system through the Gibbs adsorption isotherm.

2.4.1 Gibbs adsorption isotherm

Gibbs derived a thermodynamic equation presented in Equation (2.3) to relate the change in interfacial tension γ and the change in chemical activity of the components in the solution (Tadros, 2013):

$$d\gamma = -RT \sum \Gamma_i\, d \ln a_i \qquad (2.3)$$

Where *dγ* is the change in interfacial tension of the solution, *R* is the gas constant measured in J/mol.K, *T* is the absolute temperature measured in K, and Γ_i and a_i are the surface excess concentration and the activity of the ith component in the solution, respectively. The summation is taken over all the species in the solution.

The excess surface concentration is the concentration of a species in the interfacial region which is more than the concentration of that species in bulk. It is expressed in units of moles per unit area as (Moradi, 2011).

$$\Gamma_i = \frac{n_i^{\delta}}{A} \qquad (2.4)$$

Where A, is the interfacial area.

Figure 2.5 shows the concentration profile of a solute which tends to concentrate at the interface in a liquid (say water)/gas system. The Gibbs interface, also shown, defines the boundary between the two bulk phases and is formally defined as the location where the excess concentration of the solute is zero. The excess concentration of surfactant (the solute) is

17

determined from the difference between its actual concentration and its solubility in the bulk phases.
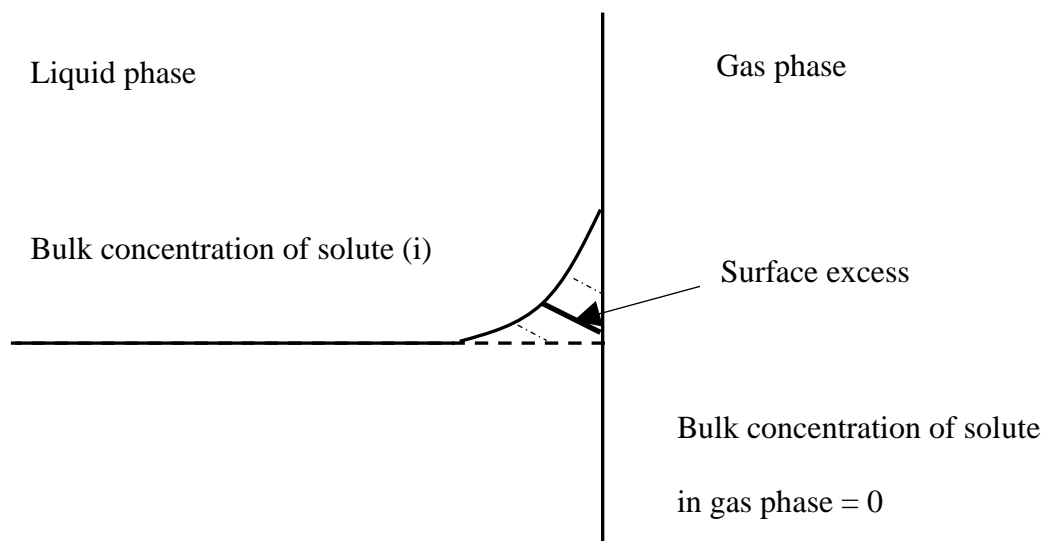
Figure 2.5: Concept of excess surface concentration (Moradi, 2011)

The solid line is the excess surface concentration near the liquid-gas interface. The dashed line is the concentration profile of surfactant (Moradi, 2011). For a binary system, the surface excess of one of the components (the solute) is zero, and the Gibbs adsorption equation can be written as:

$$d\gamma = -RT\Gamma_2 d(\ln a_2) \tag{2.5}$$

Where Γ_2 and a_2 are the surface excess concentration and activity of the solute, respectively. Since the excess surface concentration of surfactant is positive, Equation (2.5) shows that the addition of surfactant decreases the interfacial tension of a solution.

A typical plot of surface or interfacial tension versus log concentration of solute is indicated schematically in Figure 2.6. At low surfactant concentrations, the interface is only partially covered with a surfactant. As more surfactant is added, the interface becomes saturated with the surfactant, and the surface excess concentration becomes nearly constant. The interfacial tension then becomes linearly related to the log of the activity of the surfactant. For an ideal system and when the surfactant mole fraction is much lower than the solute mole fraction, the activity is proportional to the surfactant concentration (Elworthy & Mysels, 1966). Therefore, the interfacial tension becomes linearly related to the log of concentration. At low surfactant concentrations, the change in excess surface concentration with changing surfactant concentration must also be accounted for; for instance, utilising the Gibbs–Langmuir isotherm (Yarranton & Masliyah, 1996) which model's surfactant adsorption with a Langmuir isotherm.
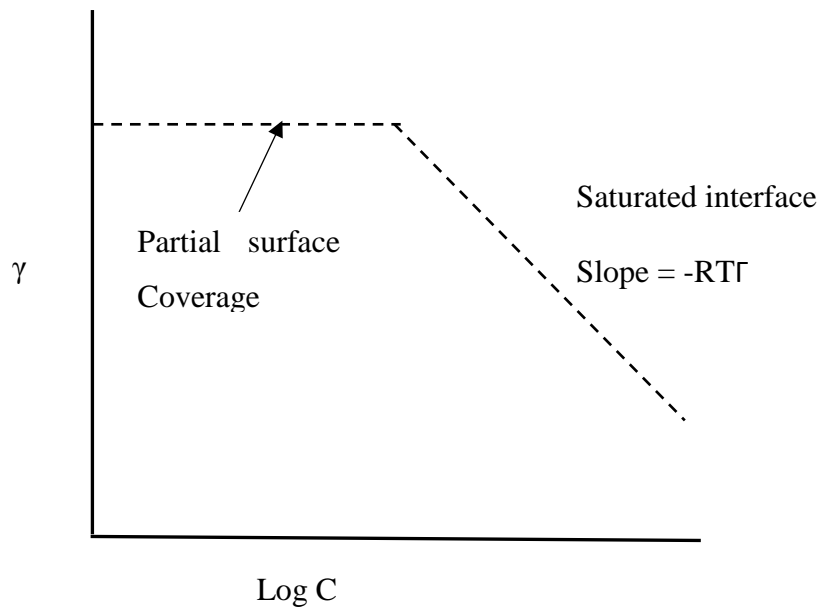
Figure 2.6: Interfacial tension versus bulk concentration of a surface-active substance

2.4.2 Gibbs-Langmuir isotherm

A system of mutually insoluble organic and aqueous phases is presented in Figure 2.7. If an insoluble monolayer interface is assumed, then it can be represented by a combination of the Gibbs and Langmuir isotherms.
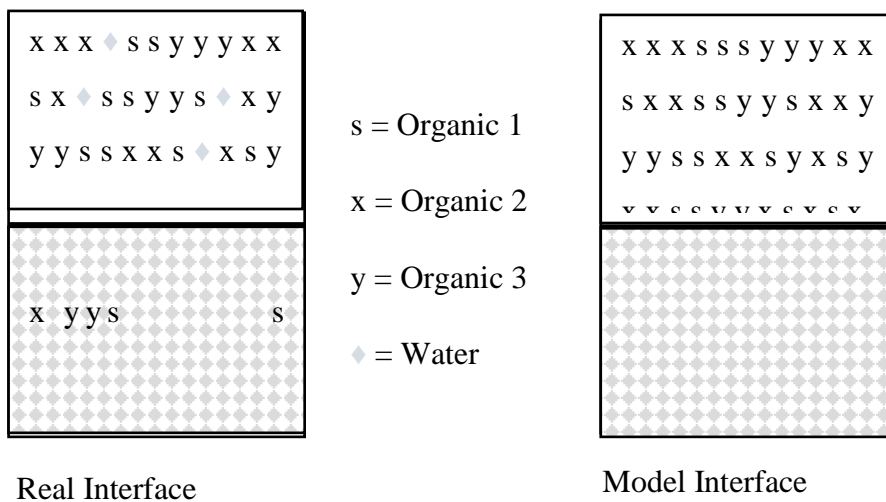
Figure 2.7: Representation of a simple model of the immiscible system interface

The excess surface concentration of a component can be expressed using Equation (2.6) as follows:

19

$$\Gamma_i = \theta_i \Gamma_{mi} \tag{2.6}$$

Where θ_i and Γ_{mi} are the fractional surface coverage and monolayer surface excess concentration of component i, respectively. The fractional surface coverage can be related to the bulk phase concentration using the Langmuir adsorption isotherm given by:

$$\theta_i = \frac{\Gamma_i}{\Gamma_{mi}} = \frac{K_{Li} C_i}{1 + K_{Li} C_i} \tag{2.7}$$

Where K_{Li} and C_i are the Langmuir adsorption constant and concentration of component i, respectively. Equation (2.7) is substituted into the Gibbs adsorption isotherm, Equation (2.2), to obtain the following:

$$d\gamma = -RT\Gamma_m \ln(1 + K_L C) \tag{2.8}$$

The adsorption constant and monolayer surface excess concentration can be found by fitting Equation (2.8) to experimental data.

For a liquid-liquid interface, the Langmuir constant K_L is directly proportional to *exp{-E/RT}*, where *E* is the energy per mole of the solute (Moradi, 2011). This relationship allows the modelling of the temperature dependence of interfacial tension at low concentrations of solute.

2.4.3 Effect of pressure and temperature on gas-water IFT

Interface behaviour due to contacting of two immiscible fluids in applications such as gas/oil/water separations (Arvoh, Skeie, & Halstensen, 2013) is critical and remain one of the problematic aspects to investigate experimentally. Other areas include emulsion (Leunissen, van Blaaderen, Hollingsworth, Sullivan, & Chaikin, 2007) and corrosion and corrosion inhibition (Pouraria, Seo, & Paik, 2016). Also, one area of significant interest in recent years is the relationship of the interfacial tension and gas hydrate management (Erfani & Varaminian, 2017; Qin, Sun, Sun, Liu, & Chen, 2016). Qin et al. (2016) suggested that mechanisms of kinetic hydrate inhibitors (KHI) adsorption behaviour can be indirectly investigated, by investigating gas/liquid interfacial properties. Determination of the interfacial tension allows deductions to be made regarding the chemical composition of fluid interfaces and the adsorption and desorption of surface-active solutes (Zhao & Middelberg, 2011). Therefore, it follows directly that accurate measurement of interfacial tension is of critical importance to gas hydrate management.

Variation of interfacial tension with temperature and pressure strongly influences the dynamic of multiphase flow a pipeline (Bachu, 2015; Khadamkar et al., 2017). In the literature,

interfacial tension data at or near the hydrate formation conditions are relatively scarce. Most of the data in the literature (Georgiadis, Maitland, Trusler, & Bismarck, 2011; Jho, Nealon, Shogbola, & King Jr., 1978; Kashefi, Pereira, Chapoy, Burgass, & Tohidi, 2016; Mahmoudi, Hasanvand, & Naderi, 2015; Massoudi & King, 1974; Ren, Chen, Yan, & Guo, 2000; Sachs & Meyn, 1995) have been measured at temperatures above 296 K. Massoudi & King (1974), for instance, presented the effect of pressure on the interfacial surface tension of water with various gases including He, CO_2, CH_4, C_2H_4 and n-C_4H_{10}, using the capillary-rise method. The variation reported using hydrostatic pressure at 298.15 K for the different gases used. It was also found that the free energy of adsorption for the n-alkanes is a linear function of the functional group. However, pendant drop method could have been a better option to investigates gas-liquid ineterfacial tension than the capillary rised methods. Sachs & Meyn (1995) presented a dependence of the interfacial surface tension in the natural gas with water on pressure and temperature at 298.15 K and pressured up to 46.8 MPa using pendant drop method. A correlation was presented based on a profile parameter which allows the estimation of the uncertainty of surface and interfacial tension data and evaluation of the achieved data be done with the few published results available. Recently, Khosharay & Varaminian (2014) presented IFT experimental data for the water-n-alkane system and water-carbon dioxide. Kashefi, Pereira, Chapoy, et al. (2016) showed IFT measurements for the methane-water system. The behaviour of the IFT of the system due to change in pressure and temperature was investigated. Yasuda et al. (2016) also investigated the influence of low pressure and temperature on IFT of the methane-water system towards hydrate formation. Finally, Ghorbani & Mohammadi (2017) presented IFT for hydrocarbon gas-oil for live crude oil system at reservoir conditions. They found that the effect of pressure was more significant than that of temperature while dealing with a system involving hydrocarbon gas and oil.

Even though the trends of the gas-water, oil-water and gas-oil IFT measurements found in the literature (as indicated in Table 2.2) are to some extent different, inconsistent and contradictory, a comparison of all data does show the effects of pressure and temperature. With some exceptions, a decrease in IFT with both increasing pressure and temperature for the gas mixtures examined were observed. Further, similar behaviour has been reported for a range of different types of gases and liquids, including both pure hydrocarbon and non-hydrocarbon (Georgiadis et al., 2011; Jho et al., 1978; Rushing, Newsham, Fraassen, Mehta, & Moore, 2008; Sachs & Meyn, 1995). The impacts of both temperature and pressure, are perhaps best be illustrated by

comparing some literature data. This comparison, shown in Figure 2.8, clearly establishes the significant of pressure on IFT. Thought both conducted their investigation within same pressure range, but obtained to a reasonable degree, different IFT values. However, both results obtained shows a decreased in IFT values with increased in pressure.

The influence of pressure and temperature on the IFT reported in the literature, showed disagreement among several trends. However, the behaviour of the IFT due to pressure and temperature as observed during the review depends on the nature of the two-phase system involved and the pressure and temperature range used. In general, the IFT between hydrocarbon gas/water decreases with increasing temperature (Sachs & Meyn, 1995), reaching a value of zero at a "critical" temperature. The zero value of IFT at critical temperature may be attributed to the disappearance of phase boundary (Teja, Garg, & Smith, 1983) at critical temperature and pressure. Another reason could be the increase in the solubility of natural gas in water (Ma & Huang, 2017), resulting from an increase in temperature. The increased solubility decreases the interfacial energy, which subsequently leads to a lower value of IFT. Further, enhance in surface mobility, may be a reason; which increases the total entropy of the surface and thereby reduces its free energy (Massoudi & King, 1974). Although the increase in pressure increases the IFT and increase in temperature led to a decrease in IFT, several authors reported different trends with regards to pressure. The effect of pressure is highly dependent on the type of system (liquid-liquid or gas-liquid) under investigation.
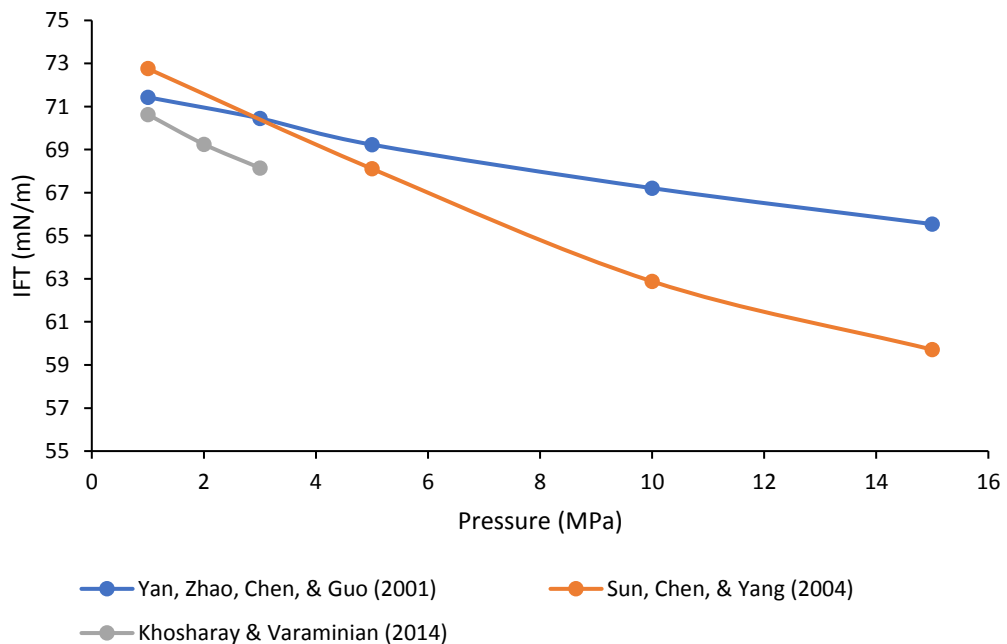
Figure 2.8: Effect of pressure on IFT of methane versus water at 298.15 K

For example, Sachs & Meyn (1995) reported the pressure and temperature effects on the interfacial tension in methane – water system, using pendant drop method (rising bubble mode) at 298.15 K, for pressures range between 0.5 and 46.8 MPa. The interfacial tension measurement was performed only at 25 ° C and pressure increases from 0.5 to 46.8 MPa. Ren, Chen, Yan, & Guo (2000) investigated the influence of pressure and temperature on IFT of a two-phase system involving (CO_2+CH_4) – water systems at the various concentration of the gases involved. They adopted same techniques as (Sachs & Meyn, 1995) at temperature ranges from 298.15 - 373.15 K and pressure ranges of 1 - 30 MPa. This investigation was subsequently followed up by Yan, Zhao, Chen, & Guo (2001), where they reported the influence of pressure, temperature and presence of impurities in the methane composition on the IFT, using pendant drop (rising bubble) method for a mono mixture of ($CH_4 + N_2$) at various concentration with water and ($CO_2 + N_2$) – water at temperature and pressure ranges of $298 - 373$ K and $1 - 30$ MPa respectively. Their investigation covers only impurities in the gas sample and without the presence of salt and polymer-surfactant in the liquid sample, which make this work unique and different from their work.

(Rushing et al., 2008)(Rushing et al., 2008)(Rushing et al., 2008)(Rushing et al., 2008)(Rushing et al., 2008)(Rushing et al., 2008)(Rushing et al., 2008)(Rushing et al., 2008)(Rushing et al., 2008)(Rushing et al., 2008)Rushing et al. (2008) measured dry gas-water interfacial tension and evaluated the effect of gas contaminant (Carbon dioxide and Nitrogen) on the gas – water interfacial tension behaviour using a pendant drop method with computer-aided image processing and analysis. They investigated a high pressure and temperature ranges of 6.89 - 137.89 MPa and temperatures of 422 - 477.6 K, while methane-water and the methane-brine mixture were not considered at this condition. Khosharay & Varaminian, (2014) reported the interfacial tension of water with lower hydrocarbon alkane including water-methane, water-ethane, water-carbon dioxide, and water-propane systems using pendant drop method at temperatures from 284.15 K to 312.15 K and pressures up to 6 MPa. Kashefi, Pereira, Chapoy, et al. (2016) obtained interfacial tension data in methane – water and methane – brine using the pendant drop and bubble rise methods for temperatures ranging from $311 - 473$ K and pressures up to 92 MPa. Yasuda et al. (2016) reported the interfacial tension of water-methane system using pendant drop method at temperatures from 278.15 - 298.15 K and pressures up to 10 MPa. The study by Yasuda et al. (2016) was followed up Hayama, Fukuzawa, Yasuda, & Ohmura, (2017), reported the interfacial tension of mixtures of methane with another hydrocarbon alkane (ethane and propane) at various proportion employing same techniques. The composition of their natural gas was 89.95% methane, 7.05% ethane and 3.00% propane

23

and 95.0% methane, 3.5% ethane and 1.5% propane. These measurements were conducted at a pressure of up to 10 MPa and temperature between 283.2 K and 298.2 K, respectively. Yahaya, Akpan, Enyi, Nasr, & Abbas (2018) reported the interfacial tension of methane-water in the presence of NaCl at moderate pipeline operating condions. However, the investigations above did not cover a broader range of temperature and pressure.

Table 2.2: Summary of some of the existing literature on gas-liquid system IFT

Author & Year	System	Temperature ($^\circ$ F)	Pressure (psi)
Massoudi & King (1974)	He, H_2, O_2, N_2, Ar, CO, CO_2, N_2O, CH_4, C_2H_4, C2H6, C_3H8, and n-C_4H10	25	146.959 - 1175.68
Jho, Nealon, Shogbola, & King Jr. (1978)			
Kashefi, Pereira, Chapoy, Burgass, & Tohidi (2016)	$CH_4 – H_2O$	100 – 392	Up to 13000
Arif, Barifcani, & Iglauer (2016)	$CO_2 – H_2O$	94 – 158	14 – 2900
Yasuda et al. (2016)	$H_2O – CH_4$	41 – 77	Up to 1450
Sachs & Meyn (1995)	CH_4 - H_2O	25 C	Up to 46.8MPa

The existing literature also suggests interfacial tension is a function of the hydrocarbon composition. For pure or single-component hydrocarbon-water systems made up of heavier molecular weight components such as butane, pentane, hexane, etc., the IFT increases steadily with increasing pressure (Sachs & Meyn, 1995). Conversely, the measured IFTs decrease with increasing pressure for the pure methane-water system and for natural gases composed mostly of lighter molecular weight hydrocarbons such as methane (Norgaard & Nygaard, 2014; Rushing et al., 2008). However, the effects of pressure and temperature have not been fully investigated for gases containing a range of both light and heavy components similar to most

gas mixtures produced from petroleum reservoirs. Therefore, the primary objective of the laboratory study was to evaluate the effects of hydrocarbon composition on gas-water IFTs.

In almost all cases, the decreasing IFT was related linearly to the increasing temperature and pressure. Some empirical relations have likewise been developed for IFT prediction between pure hydrocarbons and water. They appear to be much simpler and mostly require some standard fluid properties like density of the phases, hydrocarbon critical temperature and system temperature. These empirical correlations are easy to implement approaches for determination of IFT amongst hydrocarbons and water; yet, they are prone to predicting moderately off range values in some cases mainly because of their empirical nature. Some of the more popular empirical correlations for IFT prediction between pure hydrocarbons and water are presented.

Firoozabadi & Ramey, (1988) reported interfacial tension of some hydrocarbons and water and they found that a specific trend of single curve was formed by plotting a group that they called IFT function versus density difference amongst water and hydrocarbon. Consequently, they provided a graphical correlation that could predict interfacial tension between pure hydrocarbon and water utilizing system temperature, hydrocarbon critical temperature and the density difference between hydrocarbon and water. They characterized their IFT function as:

$$f(IFT) = \left(\frac{\gamma_{hw}^{0.25}}{\rho_w - \rho_h}\right) * \left(\frac{T}{T_{c,h}}\right)^{0.3125} \tag{2.9}$$

Danesh (1998) study the graphical correlation of Firoozabadi & Ramey, (1988) and proposed the mathematical form as:

$$\gamma_{hw} = 111\left(\rho_w - \rho_h\right)^{1.024} * \left(\frac{T_R}{T_{c,h}}\right)^{-1.25} \tag{2.10}$$

After Denesh work, Sutton (2006) tried to better fit data of Firoozabadi & Ramey, (1988) to the curve that had been represented by them. He proposed a new correlation as:

$$\gamma_{hw} = \left(\frac{1.58\left(\rho_w - \rho_h\right) + 1.76}{\frac{T_R}{T_{c,h}}}\right)^4 \tag{2.11}$$

Sutton (2009) modified his previous correlation and is represented as follows:

$$\gamma_{hw} = \left(\frac{1.53988\left(\rho_w - \rho_h\right) + 2.08339}{\left(\frac{T_R}{T_{c,h}}\right)^{0.821976 - 0.0018385T_R + 0.00000134016T_R^2}}\right)^{3.6667} \tag{2.12}$$

This correlation can predict the interfacial tension between pure hydrocarbons and water more accurately than previous relationships. Also, his model can better predict the effect of

temperature on interfacial tension between pure hydrocarbons and water in comparison to past relationships.

Most of these investigations concentrated on the reservoir conditions towards enhancing oil/gas recovery; they did not consider pipeline operating conditions and other surface processing facilities. Moreover, more investigations need to be conducted on IFT at very high pressure and temperature reservoir conditions including condensate reservoirs and natural gas reservoirs. Also, based on previous discussions on experimental investigations approaches for IFT, there is considerable interest in providing more accurate IFT data more especially at two-phase system involving hydrocarbon gases and water at a pressure and temperature typical to the pipeline system. Most of the produced oil and natural gas come along with associated water (formation water).

Hence, in this study system involving methane and water are going to be investigated at normal and critical pressures and temperatures conditions typical of the pipeline system. Also effects of the presence of salt in the produced water on the IFT exisiting at gas-water interface is going to be investigated.

2.5 Formation water and gaseous hydrocarbon

In the hydrocarbon reservoirs, rocks are permeated with fluids such as water, oil, gas or a combination of these fluids. The rock in most gas and oil-bearing sediments was wholly saturated with water before the invasion and trapping of hydrocarbon (Chilingar & Yen, 1983). The lighter hydrocarbons migrated and displaced some of the water from the formation in the trap locations. Hence, reservoir rocks usually contain both liquid and gaseous hydrocarbon and water. Sources of this water may include flow from the nearby reservoirs and injected fluids and additives resulting from production activities. Also, this water is mostly termed as connate or formation water and becomes produced water when brought to the surface along with petroleum hydrocarbons.

The produced water from conventional oil and gas production contains dispersed or dissolved, organic and inorganic compound. The organic constituents include oil, grease and an inorganic compound are mostly total dissolved salts. The total dissolved salts are the primary concerns of the present work, because. The amount of total dissolved salts (TDS) in the water is what is referred to as salinity. Electrical conductivity typically measures the salinity of the produced water. Because dissolved ions in water conduct electricity.

Presence of inorganic salts such as NaCl and CaCl in the aqueous phase results in forming a cage-like structure by the hydrogen-bonded water molecules. This cage-like hydrogen-bonded structure surrounds the salt particles as indicated schematically in Figure 2.4. At the interface, the water molecules interact with another molecules or phase, thereby creating an interfacial boundary between the two phases. The hydrogen bonding at the interface is interrupted creating a higher energy location for the inorganic ions (Na^+). Consequently, the salts near the interface depleted and have negative surface excess concentration. The effects of the presence of salts on interfacial tension were described in Gibbs adsorption isotherm. In the Gibbs adsorption isotherm, increasing the number of inorganic salts in the aqueous solution increases the interfacial tension of the system (Y. Liu, Li, & Okuno, 2016; Rashid, Harimi, & Hamidpour, 2017).
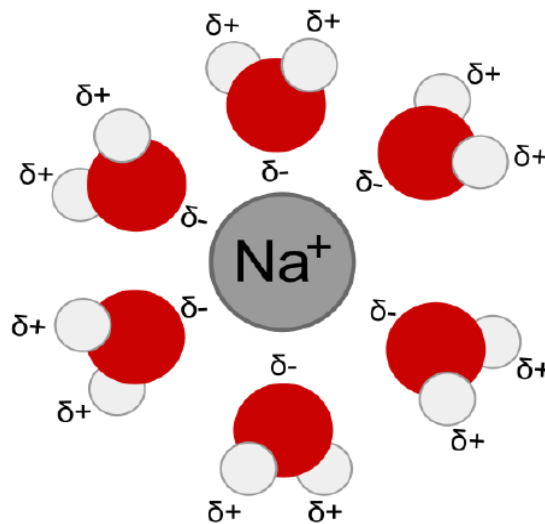
Figure 2.9: Hydrogen-bonded water molecules [Source: Kumar (2012)]

Understanding a produced water characteristics is essential for an increase in hydrocarbon productions and also in the design of other surface facilities. For example, pay zones are defined by parameters such as resistivity measurement resulting from the presence of inorganic salts (Li et al., 2008). Also, knowing the constituents of the produced water determine the application of inhibitors for scale and hydrate as well as well-treatment chemicals.

2.5.1 Influence of salinity on interfacial tension

The IFT of gas-water and gas-brine systems is one of the most critical parameters in petroleum, natural gas and petrochemical industries. For example, in the petroleum industry, the variation of IFT with pressure and temperature strongly influences the transport of the fluid in a reservoir.

Also, in natural gas industry, a product of the IFT and the cosine of the contact angle between reservoir rock and brine is one of the determining factors for the gas in place. Since the IFT is directly proportional to the capillary pressure, the variation of IFT with temperature and pressure strongly influences the transport of the fluid in a reservoir. IFT can affect water-gas contact movement and distribution of hydrocarbons in a reservoir, water alternating gas drive, gas-injected enhanced oil recovery processes, hydrate formation processes, multiphase flow behaviour and oil/gas processing (Yan et al., 2001). Injecting and storing acid gases like carbon dioxide and hydrogen sulphide separated from a stream of sour natural gas into reservoir has grown interested in the past decade (Parker, Northrop, Valencia, Foglesong, & Duncan, 2011). Accurate knowledge of this property is also of crucial importance for the efficient and economical design of potential processes. And IFT is the most critical factor in keeping approximately sixty percent of all oil discovered trapped after primary and secondary oil recovery (Alhomadhi, Amro, & Almobarky, 2014; Muggeridge et al., 2013).

There are several reported literature on the effects of salinity on interfacial tension of hydrocarbon fluids with water, in scientific and technical literature. Ozdemir, Karakashev, Nguyen, & Miller (2006) conducted an investigation on adsorption of salts at the air-water interface using Pendant Bubble (PB) method. They found that the negative adsorption of sodium carbonate and bicarbonate increases the interfacial tension at the air-water interface. The negative adsorption is usually attributed to the concentration increases and salt activities in the aqueous solutions. This behaviour of ionic salts in aqueous solutions has previously been reported by Goard (1925), using phenol, containing NaCl. Bachu & Bennion (2009) conducted the experiments to measure interfacial tensions between CO_2 and water/brine at a pressure range of 2 to 27 MPa and 20 to 125 ° C temperature by using a Pendant Drop (PD) method. Bachu & Bennion found that the water salinity or presence of salt increased the interfacial tension. The interfacial tension increases almost linearly with an increase in the salt concentration. However, they found, further that the system pressure and temperature have effects on the IFT measured. Both increased pressure and temperature decreases the CO_2-H_2O/brine IFT.

Further, Chalbaud et al. (2009) conducted the experiments to measure interfacial tension for brine (NaCl)-CO_2 at a conditions replica to geological CO_2 storage using PB method. They found that the presence of NaCl in the solution increased the IFT at brine-CO_2 interface. They further investigated the effect of the geological isotherm on the IFT and found that both increased pressure and temperature led to a corresponding decrease in the IFT at the brine (NaCl)-CO_2 system. Moreso, Akiba & Ohmura (2016) investigated the effect of salts, using

ammonium salts (TBAB) on IFT existing at a gaseous mixture of carbon dioxide and nitrogen employing PD method. Their experiments, using experimental pressure range 1 to 4 MPa, and 288.15 to 303.15 K of temperature, shows that increasing the concentration of TBAB and pressure, reduces the IFT of the system. However, Chiquet, Daridon, Broseta, & Thibeau (2007) and Massoudi & King (1974) reported that NaCl concentration has a significant effect on IFT CO_2 – brine interface, only at higher concentration.

Kashefi et al. (2016) experimented to investigate the effect of NaCl concentration on the IFT of the CH_4-H_2O interface using the PD method at pressure up to 92 MPa, and temperatures range 311 – 473 K. They found that presence of 5 and 10 wt% NaCl in the system increased the IFT at an average value of 1.4 mN/m and 4.1 mN/m respectively.

Therefore, based on the reported literature, it was observed that more work had been done on IFT involving carbon dioxide and water at condition representative to the geological storage system. Also, the reported case for methane and water interfacial tension at various salts concentration is limited, and surprisingly, all the reported cases were at reservoir conditions towards enhancing oil or gas recovery. Also, there are other reported cases for IFT of liquid-liquid systems at reservoir conditions as a function of pressure, temperature, fluid compositions and salinity (Karnanda, Benzagouta, AlQuraishi, & Amro, 2013; Lashkarbolooki, Riazi, Ayatollahi, & Hezave, 2016; Moeini, Hemmati-Sarapardeh, Ghazanfari, Masihi, & Ayatollahi, 2014; Xu, 2005).

However, this work investigated the effect of inorganic salt (NaCl) on the IFT of water at the methane-water interface. Towards understanding the effect of pressure, temperature and salinity on IFT involving two-phase system (methane-water) at a conditions replica to the surface facilities.

2.6 Surfactants-polymer in solution

Surface active agents usually abbreviated as "Surfactants" simply means any substance that, when present at low concentration in a solution, has the property of adsorbing onto the surfaces or interfaces of the solution thereby modifying to a significant extent the interfacial tensions acting on those surfaces or interfaces. Surfactants are typically used to reduce the interfacial tension, although there are instances where they are used to increase the interfacial tension (Rosen & Kunjappu, 2012). Surfactants are characterised to possess both hydrophilic and hydrophobic components as described in Figure 2.10. The hydrophilic part could be anionic, cationic, amphoteric or non-ionic. Dissolving of surfactant molecules in water above the

"*critical micelle concentration*" (CMC), form aggregates known as micelles. The surfactant hydrophobic tail group together at the inward, in the aggregates, in order to minimise their contact with water. Also, the hydrophilic heads group in a specific pattern on the outside surface to make the most of their contact with water (Chandler, 2005; Rangel-Yagui, Pessoa Jr, & Tavares, 2005) see Figure 2.11. Surfactants adsorb, even at low concentration, firmly at the interfaces of liquid/liquid and gas/liquid interface and significantly reduce the surface free energy even at low concentrations (Binks & Horozov, 2008). When surfactant molecules cover the surface or interface, the amount of work required to expand the interface is reduced, and the denser the surfactant packing, the more significant the reduction (Holmberg, Jönsson, Kronberg, & Lindman, 2003). The characterisation of surfactants is frequently constrained to surface active components that can self-assemble at higher concentrations (Adamson & Gast, 1967).

Surfactant Tail
(Hydrophilic group)

Surfactant Head
(Hydrophobic group)
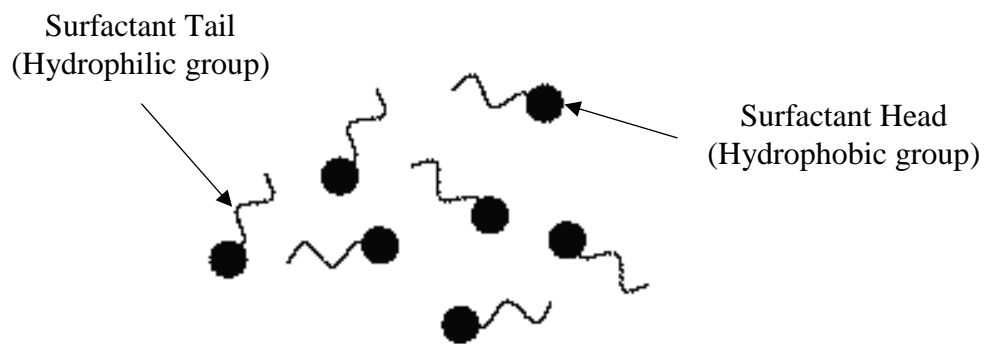
Figure 2.10: General schematic illustration of surfactants (Adamson & Gast, 1967)

There is a balance between monomers of surfactant and micelles, at the CMC. A similar behaviour, however in oleic phase with oil-soluble surfactants, is known as reverse micellization. The interfacial tension of a solution remains constant after the CMC due to the fact that the additional surfactant forms extra micelles and the convergence of free surfactant in the bulk phase and adsorbed surfactant at the interface has no significant effects on the system.
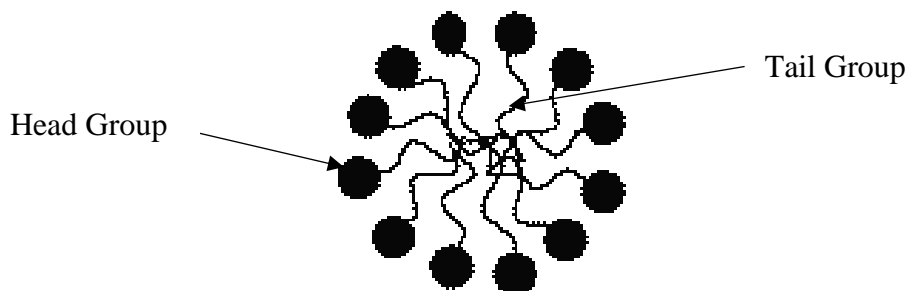
Figure 2.11: Schematic illustration of surfactant micellization (Renner, 2006)

The tail group which consists of the hydrophobic part is normally a linear or branched hydrocarbon group and fluorinated carbon chains which are broadly applied as stain repellents (Renner, 2006). Other applications of these carbon chains are preparation of superhydrophobic conductive carbon blacks (Sansotera et al., 2010). The tail group area of the hydrophobic region is mostly oil soluble. And their presence in the bulk of water is not energetically favoured as it tends to interrupt the water molecular structure.

The head group which is the hydrophilic part contains the polar group. In this region, various degrees of hydration is observed, depending on the nature of the head group. However, this part of the surfactant sections is water soluble, although some degree of solubility in oil may perhaps be observed, mostly for non-ionic surfactants (Goddard, 2017). The size of the head group varies from a few molecules to very complex structures, and its nature extensively influences the surfactant's behaviour. In fact, surfactants are generally classified into three main categories depending on the nature of their head group.

2.6.1 Ionic surfactants

Ionic surfactants are class of a surfactant that carries a net charge on the hydrophilic part, and this charge can be negative (anionic surfactant) or positive (cationic surfactants). Carboxylic acid salts ($RCOO^-M^+$), sulphonic acid salts ($RC_6H_4SO_3^-M^+$) and sulphuric acid ester salts ($ROSO_3^-M^+$) are among the general classification of anionic surfactants. All these compounds carry a permanent charge on the head group. Phosphoric and polyphosphoric acid esters are

also very common anionic surfactants, but it must be stressed that the presence of the charge in the head group depends on the pH of the solution. Generally, anionic surfactants are widely used as cleaning products because of their outstanding detergency properties.

The cationic types of surfactants generally comprise amines, and they can also carry a permanent or a pH dependent charge. Quaternary ammonium compounds ($RN^+(CH_3)_3Cl^-$), for instance, convey a perpetual charge, while other amines can either be charged or neutral depending upon the pH. The surface of most texture and hair contains locales which are negatively charged. Moreover, the positive head group of this cationic surfactant is attracted to these sites, and the long hydrophobic tail will tend to lie along the fabric or hair surface, providing a smooth covering.

2.6.2 Non-ionic surfactant

Non-ionic surfactants have either a polyether or a polyhydroxy unit as the polar groups. Their head groups carry no any charges. Their chemical structure is comparatively simple and is only composed of hydrogen, carbon and oxygen atoms. Fatty alcohols and alkyl ethoxylates are amongst the most used non-ionic surfactants, but the structure of both the head and tail group can vary significantly. These are used mainly in detergents, as emulsifying agents in paints, agrochemicals, drugs and cosmetics and as dispersing agents. Hydrophile has no charge but may contain highly polar groups. For example, polyoxyethylene (-OCH2CH2O-) or polyol (-RX (C3H5OH)nOH-) groups.

2.6.3 Amphoteric (or zwitterionic)

Amphoteric surfactants usually show comparable behavioural characteristics to non-ionic surfactants (Zana, 2002). This class of surfactants are exciting compounds, and they carry opposite charges in the head group. However, these charges could be permanent or pH dependent, so that some of these compounds can be cationic or anionic in certain conditions. The most common zwitterionic surfactants are lecithin and betaines which are particularly essential as cleansing agents and emulsifiers.

2.6.4 Surfactants solution in water

After forming the solution, the water molecules in the region of the hydrophobic tail groups arrange themselves in a cage around them, resulting in an overall increase in the free energy of the system. By concentrating the surfactant at the surface and positioning the tails out of the

water, consequently away from the solvent, the free energy of the system can be efficiently reduced.

The adsorption of surfactant molecules at the interface reduces the interfacial tension of the solution, the decrease being a function of the surfactant concentration. A typical variation of interfacial tension with increasing concentration of surfactant is illustrated in Figure 2.12. At a shallow concentration, molecular adsorption occurs, and the surface tension varies little. As the concentration increases, more adsorption occurs, and the surface tension decreases rapidly and steadily. Further increase in concentration, surfactants saturate the interface, and the surface tension becomes nearly constant, and the solution reaches critical micelle concentration (CMC).
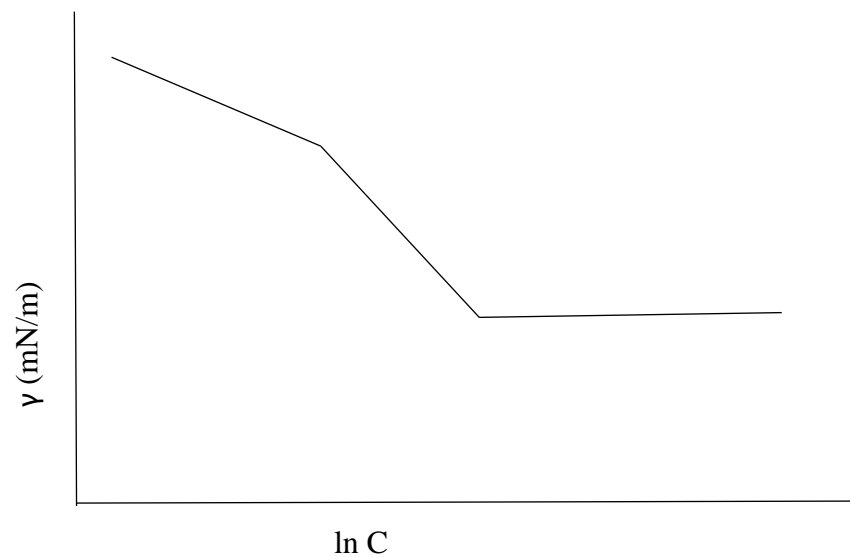
Figure 2.12: Surface tension isotherm of a generic surfactant

2.6.5 Surfactants partitioning in solution

Surfactants dissolved in either the water or oil phase tend to partition to some degree into the other phase, depending on its relative solubility between the phases. The relative solubility depends on the structure of the surfactant. For example, a highly polar hydrophilic group or a large number of polar groups will make the surfactant more water soluble and less oil soluble. And the solubility and partitioning of surfactant depend on the total amount of the salt present in the solution. This increases of surfactant concentration due to an increases of salt has been reported. For example in the oleic phase, surfactant concentration increases with a corresponding increased in the salt concentration (Opawale & Burgess, 1998). In the case of IFT in the system, unity value of a partitioning coefficient, corresponds to a minima in the IFT values. Therefore, the partitioning can be characterized by a partitioning coefficient, Ke, which is express mathematically as:

33

$$K_e = \frac{C_{sol}^a}{C_{Solv}^b} \tag{2.13}$$

where C_{sol}^a is the concentration of the solute in the oleic phase and C_{aq}^b is its concentration in the aqueous phase. The partition coefficient depends on the ionic strength, pH, oil type, co-solvents (Salager, Marquez, Graciaa, & Lachaise, 2000), temperature, and surfactant composition at the interface (Graciaa et al., 2006). For non-ionic surfactants the part,,,itioning coefficient between water and oil, *Ke*, was greater than unity for surfactants with more than 10 ethylene oxide units, which also gives high water solubility (Richards, Chaiyasit, McClements, & Decker, 2002). For naphthenic acids, the partition coefficient was correlated to the number of cyclic rings in the compound (Havre *et al.,* 2003).

2.7 Effect of surfactant on gas-water IFT

Many of the processes in petroleum and gas are in part an interfacial phenomenon. Interfacial property such as the interfacial tension of gas and water have a significant influence on enhancing gas recovery (EGR), multiphase flow pattern and hydrate formation rate. In the management of hydrate formation and other related problems such as corrosion in the pipeline, surface-active agents have been used in their management. Some surfactants will promote hydrate growth (Kalogerakis, Jamaluddin, Dholabhai, & Bishnoi, 1993). While others will delay or dispersed and transport it as slurry depending on the concentration added to the system (Ganji, Manteghian, Sadaghiani zadeh, Omidkhah, & Rahimi Mofrad, 2007). The addition of surfactant agents interferes with the interfacial tension between gas and water and thereby altering the formation rate or formation mechanism of hydrates.

Watanabe, Niwa, & Mori (2005) reported the interfacial tension of methane/water with three different sodium dodecyl sulfate (SDS) at 3.95 MPa and 275 K, conditions at which methane hydrate is thermodynamically stable. Peng et al. (2009a) conducted experiments to study the effects of VC- 713 and kinetic inhibitor (Inhibix 301 and 501) solution on interfacial tension of a methane/aqueous at hydrate forming conditions. They found that the surfactant reduces the IFT of the system thereby increasing the concentration of methane on the aqueous solution interface. Hence, increasing the hydrate formation rate. Further, Liu, Sun, Peng, Chen, & Chen (2009) experiments agree well with Peng et al. (2009a). Sun, Chen, & Yang (2004) investigated the interfacial tension existing at methane/water interface with sodium dodecyl sulfate (SDS) in the temperature range of 273.2–298.2 K and pressures of up to 10 MPa. They found that the IFT of the solution decreases with the addition of SDS. However, at the CMC, the IFT of the solution was found to be constant, even with increases in SDS concentration. Other kinetic

inhibitors and synergists were investigated, for example, Qin et al. (2016) investigated and established the performance of KHIs (PVP-E, PVP-A, PVP-BP, PVP and inhibex 501) and alcohols (Methanol, ethanol, glycol and triglycol) as synergists, based on their effects on interfacial tension. They concluded that the lower reduction of IFT the better the delay on the onset time for hydrate formation, hence the performance of the inhibitors. These kinetic data are essentials in establishing the inherent relationship between the surfactants behaviour and interfacial properties.

In this work, thermal and kinetic mechanism of a polymer with dispersive properties, and SDS were investigated by measuring, both polymer solution properties and the gas/liquid interfacial tension with respect to a system composed of methane and aqueous solution.

2.8 Chapter summary

The concept of multiphase flow and flow pattern in pipe geometry has been described. Also, interpretation of interfacial tension fundamentals has been explained along with the concepts of Gibbs free energy and surface excess concentration. The variation of interfacial tension of a system due to the presence of various solute components can be related using Gibbs adsorption isotherm. Further, the slope of the Gibbs adsorption isotherm gives the values for excess surface concentration in the system. Effect of salinity is to increase the interfacial tension of gas/water, and also the surfactant usually decreases the interfacial tension. However, there are instances where surfactant are found to increases IFT. Interfacial tension of pure gaseous hydrocarbons generally decreases with an increase in both pressure and temperature.

Critical analysis has also been performed on experimental IFT data available in the literature for binary and multicomponent systems comprising lower hydrocarbon fluids. The impact of density, diluent gases and salts on the IFT were reviewed. The systems which require further investigation were identified: gas + water/brine and gas + (water/brine Surfactant) (where gas = CH4, surfactant = PEG 8000 and SDS).

Chapter 3: Review of Experimental Techniques for Interfacial Tension Measurement

3.1 Introduction

Because of its significant role in many technical areas, many tensiometers have been developed for the experimental investigation of the IFT between fluid phases in interaction. Among all the various techniques reviewed by Dorsey (1929), only a few are still being utilised for interfacial tension measurements in fluid−liquid interfaces. The most popular techniques used today were briefly reviewed by Drelich, Fang, & White (2002) and are depicted schematically in Figure 3.1. They are also described in detail in Rusanov & Prokhorov (1996). Another valuable source of information on experimental measurement techniques of interfacial tension includes Arashiro & Demarquette (1999); Cheng et al. (1990); Harkins & Jordan (1930); Lee, Kim, & Needham (2001); Río & Neumann (1997). The Pendant Drop (PD) is arguably the most widely used methods for measuring the IFT at two-phase system involving hydrocarbon gases and liquids, due to its simplicity and ease of implementation at a gas-liquid interface under a wider range of pressure and temperature conditions.

In the context of the PD technique, a drop of a denser fluid is formed at the tip of a capillary tube and kept in equilibrium with a surrounding less dense fluid (vapour or liquid), and the shape of the drop is subsequently analysed, as depicted in Figure 3.1 (f). Once the profile of the drop or the height of the liquid column is determined, they are combined with pertinent phase density data to obtain interfacial tension values. In essence, the estimation of the IFT with the other technique relies on the balance between capillary and gravity forces, which were recently described and improved by (Berry et al., 2015). In the PD the effect of gravity on the shape of a drop of fixed volume is analysed (Drelich et al., 2002).

Most of these measurement techniques are either direct measurement using a microbalance or based on individual analysis of equilibrium between capillary and gravity forces, surface tension forces and a variable volume of liquid, distortion of a fix drop of liquid volume under influence of gravity force and techniques where the shapes of fluid drops are distorted by centrifugal forces and are used to measure ultra-low interfacial tensions.

The accurate measurement of IFT with the PD method requires a sufficiently large density difference between the phases to elongate the drop, reducing the errors that arise from the determination of the profile of the drop. For this reason, the PD drop technique is in general

preferred for systems involving gaseous and liquids phases over the other methods. Overall, these methods have been applied in the study of interfacial phenomena of a variety of fluids and interfaces over a broad range of conditions and with established high precision and repeatability (Rusanov & Prokhorov, 1996).

In this chapter, a brief historical and technical discussion of the theoretical background of these techniques are presented along with a detailed description of the apparatus used in this work to measure the interfacial tension of reservoir fluids over a broad range of experimental conditions.
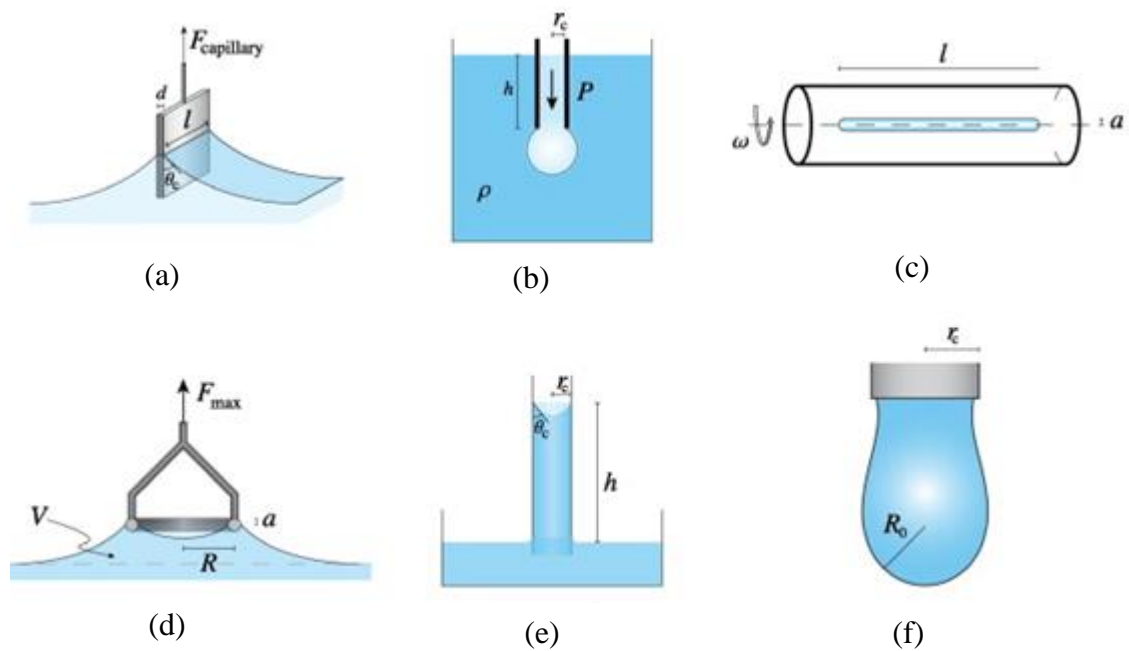
Figure 3.1: Experimental techniques used to determine interfacial tension: (a) Wilhelmy plate, (b) Maximum bubble pressure, (c) Spinning drop, (d) Du Nouy ring, (c) Capillary rise, and (f) Pendant drop (Berry et al., 2015)

3.2 Methods based on force concept

Some of the techniques used for interfacial tension measurement are based on the direct measurement using microbalance. At the fluid-liquid interfaces, the interfacial tension mirrors the excess energy related to unsaturated intermolecular interactions at the interface. This excess energy tends to drive interfaces to adopt geometries that minimise the interfacial area, and this tendency can be interpreted as a physical force per unit length (i.e., a tension) applied in the plane of the interface. The excess energy per unit area is numerically equal to force per unit length (F/L), which is numerically equal to the interfacial tension (γ). To directly measure interfacial tensions using a microbalance, a plate, ring, rod, or another probe of simple shape is

brought into contact with the interface. If one of the liquids thoroughly wet the probe, it adheres to the probe and climbs as the result of capillary force, increasing the interfacial area and leading to a force tending to pull the probe toward the plane of the interface (see Figure 3.1 (a) and (d) above).

This restoring force is directly related to the interfacial tension and can be measured by a microbalance. The force (F) acting along the three-phase contact line is precisely equal to the weight of the liquid meniscus standing above the plane of the fluid-liquid interface. This force, measured by the microbalance, is used to calculate the interfacial tension:

$$\gamma = \frac{F}{p \cos \theta}$$
(3.1)

Where p is the perimeter of the three-phase contact line and θ is the contact angle measured for the liquid meniscus in contact with the object surface. The two principal techniques used for direct measurement of interfacial tension utilising the microbalance are Wilhelmy plate and du Nou¨y ring methods.

3.2.1 Wilhelmy plate method

The Wilhelmy plate technique is one of the oldest methods used to study the interfacial phenomena between interacting fluid phases. The Wilhelmy plate technique is used in both static and detachment modes. In the static measurement, the plate remains in contact with liquid during the entire cycle of interfacial tension measurement. If the instrument operates in the detachment mode, the interfacial tension is measured by measuring the force required to separate the ring or plate from contact with the interface.

A thin vertical plate is used in this technique, which is usually made from roughened platinum-iridium alloy or platinum. The metal plate must be cleaned from organic contaminants by an organic solvent and then flamed before the experiment. Both roughening and cleaning of the plate surface are used to maintain a proper wetting of the plate by the test liquid. Other materials such as glass, mica and steel (Parsons, Bukton, & Chatham, 2012; Rusanov & Prokhorov, 1996) apart from platinum or platinum-iridium alloy have also been used. However, right wetting of the test liquid to the plate is always necessary. The use of plates made of a material other than metal is a requirement in the case of certain liquids such as during the measurements of the interfacial tension between a heavy nonpolar liquid (i.e., carbon tetrachloride) and immiscible, but lighter, polar liquid (i.e., water). For such systems, the plate should be hydrophobic. Several polymers, especially fluorinated polymers, can be used for this purpose. Adsorption and self-

assembling of organic amines on the surface of the platinum plate could also be a solution to this problem.

In the Wilhelmy plate method, the plate is put in a fixed position relative to the horizontal surface of the liquid. Then, the force (F) vertically acting on the plate by the liquid meniscus is measured by using a microbalance. The force applied to the plate is equal to the weight of the liquid meniscus uplifted over the horizontal surface. By measuring this force, the interfacial tension can be calculated using (Drelich et al., 2002):

$$\gamma = \frac{F}{p \cos \theta} \tag{3.2}$$

Where p = 2(l+t) and is the contact area between the liquid and the plate, W_p is the weight of the plate, b is the buoyancy force of an immersed part of the plate in the liquid and θ is contact angle. Modern instruments use plates of standard dimensions so that measurements of the plate size and its weight are not required. Adsorption of organic compounds from the laboratory environment or test solutions can be a significant source of experimental error when measuring surface tensions using the Wilhelmy plate method.
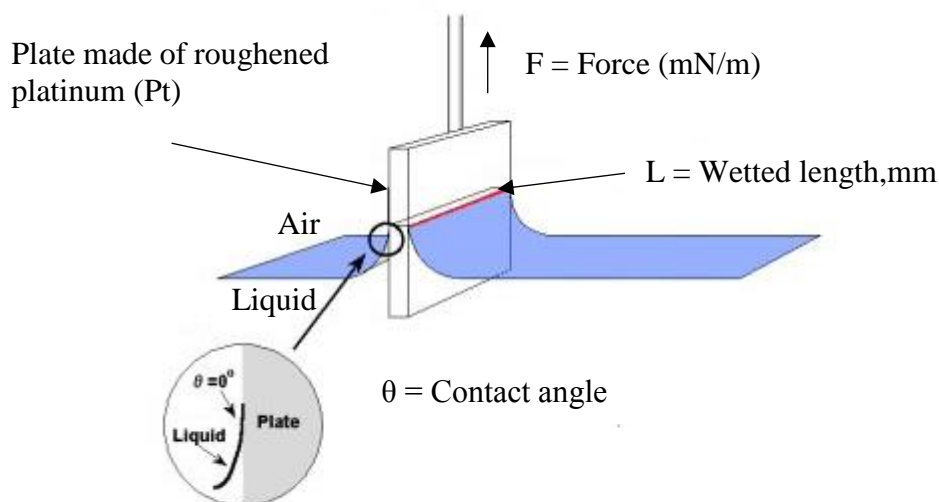
Figure 3.2: Schematic illustration of Wilhelmy plate method (Ghosh, 2009)

3.2.2 Du Nouy ring method

The du Nou¨y ring technique is one of the most widely used methods for measuring surface tension and is similar to that of the Wilhelmy plate, except that the rings is employed in detachment mode compared to the plate. The technique is named after Du Nouy who developed

the method (Lykema et al., 2000). The only difference is that du Nouy ring method uses a detachment technique strictly.

The experimental setting developed by DuNouy (1919) used in this methods is indicated in Figure 3.3. In this method, the interfacial tension relates to the force required to pull a wire ring off the interface (Drelich et al., 2002; DuNouy, 1919). As in the case of Wilhelmy plate, the ring is usually made up of platinum or a platinum-iridium alloy of a radius (R) of 2–3 cm. The radius (r) of the wire ranges from 1/30 to 1/60 of that of the ring (9).

Figure 3.3: Du Nouy ring apparatus (DuNouy, 1919)

The relation describing the calculation procedure of the method is given in Equation (3.3). Here, the perimeter (p) of the three-phase contact line is equal to twice the circumference of the ring: p =4pR. Because the additional volume of liquid is lifted during the detachment of the ring from the interface, a correction factor (f) is required:

$$\gamma = \frac{F}{p \cos\theta} f \tag{3.3}$$

The correction factor varies from about 0.75 to 1.05 and depends on the dimensions of the ring (R, r), its surface wettability (θ), and the difference in fluid density ($\Delta\rho$). The tabulated f values about R/r (for y = 0) can be found in Ref. 8, and also calculated from the following approximate equation (10):

$$f = 0.725 + \sqrt{\left(\frac{9.075 \times 10^{-4}}{\pi \Delta\rho g R^3} - \frac{1.679r}{R} + 0.04534\right)} \tag{3.4}$$

The application range of Equation 3.4 is $0.045 \leq \Delta\rho gR^3/F \leq 7.5$. The maximum force is measured by the microbalance (F) and corresponds to detachment of the ring from the interface. The F value is measured experimentally, and then Equation 3.4 is used to calculate the correction factor f. The interfacial tension is then calculated from Eq. 3.3. The interfacial tension reading made by modern computerised instrumentation does not require separate calculation of the correction factor, f since its computation is incorporated in the software.

The high-accuracy measurements with the ring method require that the plane of the ring remain parallel to the interface. The significant error in this technique is caused by deformation of the ring, which is a very delicate probe and subjects to inadvertent deformation during handling and cleaning. It is also essential that perfect wettability of the ring surface by the denser fluid be maintained ($\theta = 0$). If ideal wetting is not achieved, additional correction of the instrument reading is needed. Poor wetting of ring by the denser fluid measures interfacial tension impossible to carry out. In the case of individual measurements requiring homemade rings, huge rings should be avoided to avoid the small value of the correction factor (see Eq. 1.4). If all of the necessary experimental precautions are observed, this method can guarantee higher accuracy than any other detachment method.

3.3 Measurement based on capillary pressure concept

Interfacial tension is defined as the work required to create a unit area of the interface at a constant temperature, pressure, and chemical potential. Because it is always positive for interfaces between immiscible phases, interfacial tension still tends to decrease the area of the interface. This tendency gives rise to a pressure difference between fluids on either side of a curved interface, with the higher pressure on the concave side of the interface. This pressure difference results in phenomena such as a capillary rise, bubble and drop formation, etc. A formula describing the pressure difference (DP) across the curved interface is known as the Young-Laplace equation (Rotenberg, Boruvka, & Neumann, 1983; Scriven, 1960):

$$\Delta P = \gamma \left(\frac{1}{R_1} + \frac{1}{R_2} \right) \tag{3.5}$$

Where both R_1 and R_2 are the radii of curvature respectively.

The pressure difference across a curved interface (ΔP) can be measured in some ways (e.g., using a pressure sensor or observing a capillary rise) and then be used to calculate γ if the radii of curvature are known. The most common and probably one of the oldest methods in this group of interfacial tension measurement techniques is a maximum bubble pressure method that is

briefly described in the next paragraph. Modification of the maximum bubble pressure method based on continuous measurement of varying pressure during growing bubble or drop is now a fundamental technique in the examination of dynamic (not equilibrated) interfacial tension.

3.3.1 Maximum bubble pressure

The maximum bubble pressure method was first proposed by Simon (1851) for measuring the surface tension of liquids. This technique is structured based on measuring the maximum pressure (p*) to force a gas bubble out of a capillary into a liquid (Kovalchuk & Dukhin, 2001; Mobius & Miller, 1997). The measured pressure is the sum of capillary pressure (ΔP) caused by the interfacial tension and the hydrostatic pressure ($\rho_A g h_A$) produced by the liquid column above the orifice of the capillary and can be represented by Equation (3.6):

$$\Delta P = p^* - \rho_A g h_A \tag{3.6}$$

Therefore, the pressure can also be related to or express as the height (h) of the column of an imaginary liquid density ($\Delta\rho = \rho_A - \rho_B$):

$$h = \frac{\Delta P}{\Delta\rho g} \tag{3.7}$$

In discussing both the capillary correction and the behaviour of large bubbles, it is often advantageous to express pressures as the corresponding height, h, of the liquid and to use a natural unit of length, a. This natural unit is conveniently chosen as the ideal height of the meniscus in a wetted tube having a radius equal to that height.

Sugden (1924) derived an expression to relate h with the Laplace capillary constant $a = 2\gamma/(\Delta\rho g)$ and the bubble meniscus:

$$\frac{r}{X} = \frac{r}{b} + \left(\frac{r}{a}\right)\left(\frac{z_c}{b}\right)\left(\frac{\beta}{2}\right)^{0.5} \tag{3.8}$$

Where $X = a^2/h$, $b = 2b^2/a^2$, z_c is the height of the bubble, and b is the curvature radius at the apex (lowest point of the bubble). Then he tabulated the minimum values of X/r as dependent on a given amount of r/a within the range $0 < r/a \leq 1.5$. Then use this range to calculate the surface tension, by following an iteration procedure.

The maximum bubble and drop pressure technique or its modifications have been very useful in studying the dynamic interfacial tensions. This technique has also been attractive to an examination of surface tension for molten metals (Myers, 2000).
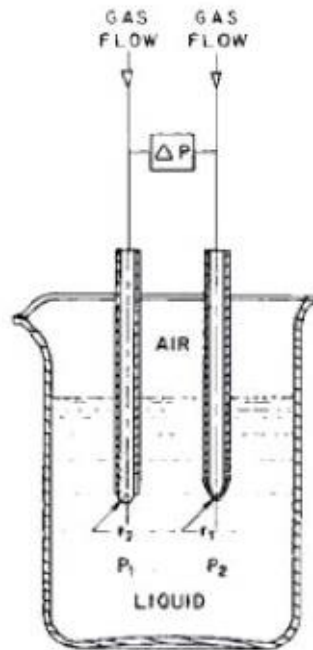
Figure 3.4: Schematic illustration of the equipment used for maximum bubble pressure technique

3.4 Concept based on a balance between capillary and gravity forces

Methods based on analysis of capillary effects, other than the shape of a drop or meniscus, such as the capillary rise and drop volume or weight, are among the oldest surface tension measurement methods in use. A short review of two techniques, capillary rise and drop weight methods are given in the following sections.

3.4.1 Capillary rise method

Surface tension measurement using capillary rise methods is among the oldest surface tension measurement methods in use today. The profile of the meniscus of the fluid rise in a circular glass tube of known inner radius, r, which is immersed in the liquid solution, as shown in Figure 3.5.
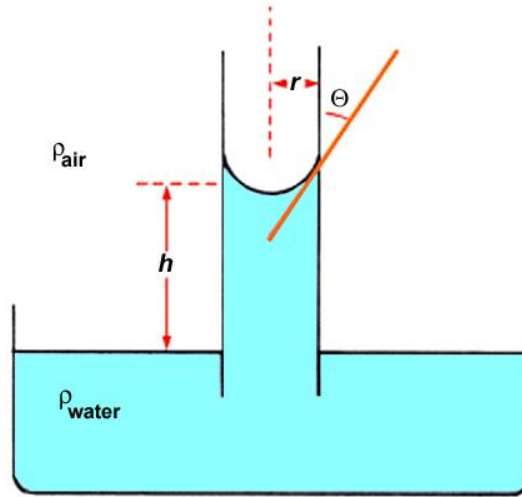
Figure 3.5: Illustration of the capillary rise method modified from (Drelich et al., 2002)

The surface tension draws the liquid into the tube due to the Laplace pressure, P, which is the difference between the pressure at the inside and outside of a curved surface (Myers, 2000). The height (h) at which the liquid reaches in the tube depends on interfacial tension. For glass tube of a smaller diameter ($r \ll h$) the shape of the meniscus is spherical, and the column of liquid in the capillary must be held up against the gravity pull by force, the so-called capillary suction. The surface tension can be determined using:

$$\gamma = \frac{\Delta\rho g h r}{2\cos\theta} \tag{3.9}$$

Though there are associated technical problems with the technique related to fabrication of uniform bare capillary tube and precise determination of its inside diameter, still can be one of the most accurate methods used to make surface tension measurements. Further, analysis of the interfacial tension between two liquids is not appropriate using this method.

3.4.2 Drop weight method

In this method, the weight or volume of a drop falling from a capillary with a radius r is measured (W. D. Harkins & Brown, 1919). The weight (W) of the drop falling off the capillary correlates with the interfacial tension through the following equation

$$W = V\Delta\rho g = 2\pi r\gamma f\left(\frac{r}{\sqrt[3]{V}}\right) \tag{3.10}$$

Where V is the drop volume, r is the radius of the capillary, and f is the correction factor required because only a portion of the drop volume is released from the capillary during detachment (2). The correction factor is a function of $r/V^{1/3}$, and this correlation was empirically determined

and tabulated by (W. D. Harkins & Brown, 1919). It can also be calculated from the practical function as reported by Drelich et al. (2002) :

$$f\left(\frac{r}{\sqrt[3]{V}}\right)=0.167+0.193\left(\frac{r}{\sqrt[3]{V}}\right)-0.0489\left(\frac{r}{\sqrt[3]{V}}\right)^2-0.0496\left(\frac{r}{\sqrt[3]{V}}\right)^3 \qquad (3.11)$$

Because of a small volume of each drop, many drops need to be collected for the accurate measurement of drop weight or volume. In modern instrumentation, the size of the liquid and the number of droplets released from the capillary can be determined very precisely and thus the weight or volume of the individual drop is not challenging to calculate.

Capillaries used in the drop weight or volume techniques are usually made of glass; however, metal capillaries are also used on occasion. Many liquids wet glass, is transparent and is relatively easy to clean. Capillary tubes fabricated explicitly for routine interfacial tension measurements are now difficult to purchase in the U.S. market; however, glass capillaries can be produced relatively quickly in glass workshops.

The measurements of interfacial tension with the drop weight or volume technique are straightforward but, unfortunately, sensitive to vibrations on the other side. Vibrations of the apparatus can cause premature separation of the drop from the end of the capillary before the drop reaches the critical size. Also, the measurements in multicomponent solutions when adsorption occurs might not reflect equilibrium saturation of the solutes at the interface.

3.5 Measurement based on gravity distorted drops

Interfacial tension causes interfaces to behave as elastic membranes that always tend to compress the liquid. In the absence of other forces (e.g., in zero gravity), the liquid surface has a natural tendency to form spherical shapes to minimise the interfacial area per unit volume of liquid and thus, to minimise the excess energy of the interface. The configuration of an interface in a gravitational field depends on the competition between the capillary and gravitational forces and can be described by the Bashforth-Adams equation (19):

$$\gamma\left(\frac{\sin\varnothing}{x}+\frac{1}{R_1}\right)=\frac{2\gamma}{b}+\Delta\rho gz \qquad (3.12)$$

And in the dimensionless form it may be written as:

$$\left(\frac{\sin\varnothing}{x/b}+\frac{1}{R_1/b}\right)=2+\frac{\Delta\rho gb^2 z}{\gamma b} \qquad (3.13)$$

Where γ is the interfacial tension; $\Delta\rho = \rho_A - \rho_B$ equals the difference in density of fluids, R_1 is the radius of curvature, x is the radius of rotation of point S around the z-axis; ϕ is the angle of

R$_2$ vector with the axis of symmetry; b is the radius of curvature at the apex of the curvature; and g is the acceleration due to gravity.

The techniques of curved interface shape analysis are particularly attractive to researchers because they do not require advanced instrumentation. The experimental setup requires a camera with a low-magnification lens to record the shape of the drop. The interfacial tension can be easily calculated from the dimensions of the pendant drop, sessile drop, or liquid meniscus taken from the photographic picture and by using numerical solutions to the above equations. Modern instruments, however, use image analysis software whose role is to match the entire drop profile to the best fit of the theoretical curve (e.g., the Bashforth-Adams equation) describing the shape of the drop. These advances significantly improved the precision of the techniques and reduced the time of the measurement, providing an opportunity for examination of the interface ageing process. Probably the most advanced software, axisymmetric drop shape analysis, was introduced by Neumann and co-workers. Since advanced instrumentation is not always available to the researcher, a brief review

3.5.1 Pendant drop method

In a simple method, two parameters of the pendant drop that should be experimentally determined are the equatorial diameter D and the diameter d at the distance D from the top of the drop. The interfacial tension is then calculated from the following equation:

$$\gamma = \frac{\Delta\rho g D^2}{H} \tag{3.14}$$

The shape dependent parameter (H) depends on a value of the ''shape factor'' $S = d/D$. Tables including the set of 1/H vs S values are available in several references. The values of 1/H can also be calculated from the following empirical formula:

$$\frac{1}{H} = \frac{B_4}{S^a} + B_3 S^3 - B_2 S^2 + B_1 S - B_0 \tag{3.15}$$

Where B_i (i = 0, 1, 2, 3, 4) and a, are empirical constants for a specific range of S, which are shown in Table 3.1.

The pendant drop technique, as other interfacial tension measurement techniques, requires extreme cleanliness to obtain good quality and reproducible results. Here, the needle used for hanging the drop should be well cleaned, and the climbing of the interface over the outer surface of the needle should be avoided. Needles made of stainless steel or glass that are relatively easy to clean with acids, bases, and organic solvents are most often used in surface chemistry laboratories. It is recommended that needles with a diameter that is less than 0.5 D be used. The

diameter of the needle should not be too small, however, because this reduces the value of d and, consequently, the precision of interfacial tension determination.

Table 3.1: Empirical Constant for Equation 1.8

S (Range)	a	B_0	B_1	B_2	B_3	B_4
0.401 - 0.460	2.567	0.181	0.841	0.976	0	0.327
0.460 - 0.590	2.597	0.133	0.501	0.469	0	0.320
0.590 - 0.680	2.624	0.053	0.158	0.117	0	0.315
0.680 - 0.900	2.643	0.059	0.147	0.092	0	0.313
0.900 - 1.000	2.846	0.210	-0.183	-1.083	-0.691	0.307

3.5.2 Sessile drop method

This method is based on the analysis of the profile of the drop sitting on a solid substrate, as shown in (Padday, 1971). It is recommended that substrates used in sessile drop measurements be poorly wetted by the drop, i.e., they should have a contact angle larger than 90 degrees. In a simple experimental approach, one first needs to locate the equator of the drop, and then measure the height from the top of the drop to its equator (z_e). For a huge sessile drop, an analytical expression for the interfacial tension is as follows (Drelich et al., 2002):

$$\gamma = \frac{\Delta \rho g Z_e^2}{2} \tag{3.16}$$

From a practical point of view, it is often difficult to precisely locate the equator of the drop and measure z_e for many drops. Although the large drop is almost flat, locating the top of the drop is sometimes experimentally tricky. It should be recognised, however, that large drops are not required if tabulated dependencies of drop shape parameters, based on the Bashford-Adams analysis Equation 3.13 are used (Bashforth & Adams, 1883; Padday, 1971).

Summary of these classic techniques used for the interfacial tension measurements are given in Table 3.2 with their accuracy and interface suitability. Also, some of them are comfortable with surfactant while others are difficult to investigate at higher pressure and temperature, whereas some are very good in any systems of interest, during the investigation.

Table 3.2: Accuracy and suitability of some techniques used for IFT measurements

Method	Accuracy [mN/m]	Suitability Surfactant Solution	Liquid-liquid System	Gas-Liquid System	HTHP
Wilhelmy Plate	0.1	Limited	Good	Good	No
Du Nouy Ring	0.1	Limited	Reduced Accuracy	Good	No
Maximum Bubble Pressure	0.1 – 0.3	Very good	Very good	Good	No
Capillary Rise	<0.1	Very good	Very good and experimentally difficult	Good	_
Drop volume	0.1-0.2	Limited	Good	Good	Yes
Pendant Drop	0.1	Very good	Very good	Good	Yes

3.6 Chapter summary

Most of the commonly used experimental set-up and their theoretical background for measuring interfacial tension has been described. The experimental set-up were described and categorised based on their theoretical concepts. Pendant (risen bubble) method has been chosen for the purpose of conducting the present investigation, because is the most suitable method for investigating interfacial tension of a system involving gas-liquid, as reviewed and described.

Chapter 4: Materials and Experimental Methods

4.1 Introduction

The measurement of methane-water interfacial tensions in this study was conducted on a laboratory scale, to investigate the influence of temperature, pressure, salinity and inhibitors on interfacial tension. The pressure and temperature conditions similar to those of gas processing facility were considered. The initial base-case test involves IFT measurement using air bubble in distilled water for calibration and establishing the accuracy and reliability of the system. The chapter describes the experimental setup, materials and methods. Further description of detailed steps required to ensure precise and accurate results are obtained was also explained. The investigation was conducted in three phases as shown in Figure 4.1, and these stages include:

Phase I: **Sample preparation and liquid characterisation:** In this phase, density resistivity and pH measurement of each of the liquid sample preparation was performed. The description of the apparatus, test materials/procedure, calibration, error and accuracy, cleaning and maintenance of the equipment used in this stage as described in Section 4.2 – 4.7. The objective of this stage was to characterise and analyse the liquid samples in terms of their density, pH, and electrical resistivity. The results obtained from the density of the samples were subsequently used in phase three for IFT measurement.

Phase II: **Rheology of solution involving PEG 8000 and SDS Analysis:** In this phase, the rheology of the surfactant and polymer used as inhibitors (hydrate inhibitors) was investigated using rheometer. The detailed descriptions of the apparatus, calibration, error and accuracy, cleaning and maintenance of the equipment were presented in Section 3.8. The objective of this stage was to study the liquid sample rheological behaviour at various concentration of each surfactant and polymer used in the present study, with or without the presence of NaCl in the solution. Also, their combination was investigated to ascertain their rheology and comparability.

Phase III: **IFT of hydrocarbon two-phase (gas-water) system:** The experimental investigation of IFT was conducted at this stage. The experimental method, procedure, calibration, error and accuracy, cleaning and maintenance of the equipment were described in section 3.9. The objective of this phase was to investigate the effects of temperature, pressure, salt concentration and inhibitors on the IFT existing at CH_4/H_2O interface.

The experimental setup, procedures, as well as precautionary measures and sources of error, are detailed in each of the preliminary stages in each of the phase designed for conducting the present study, and in their respective sections. Figure 4.1 shows the schematic presentation of the experimental and simulation stages involve in conducting this study.
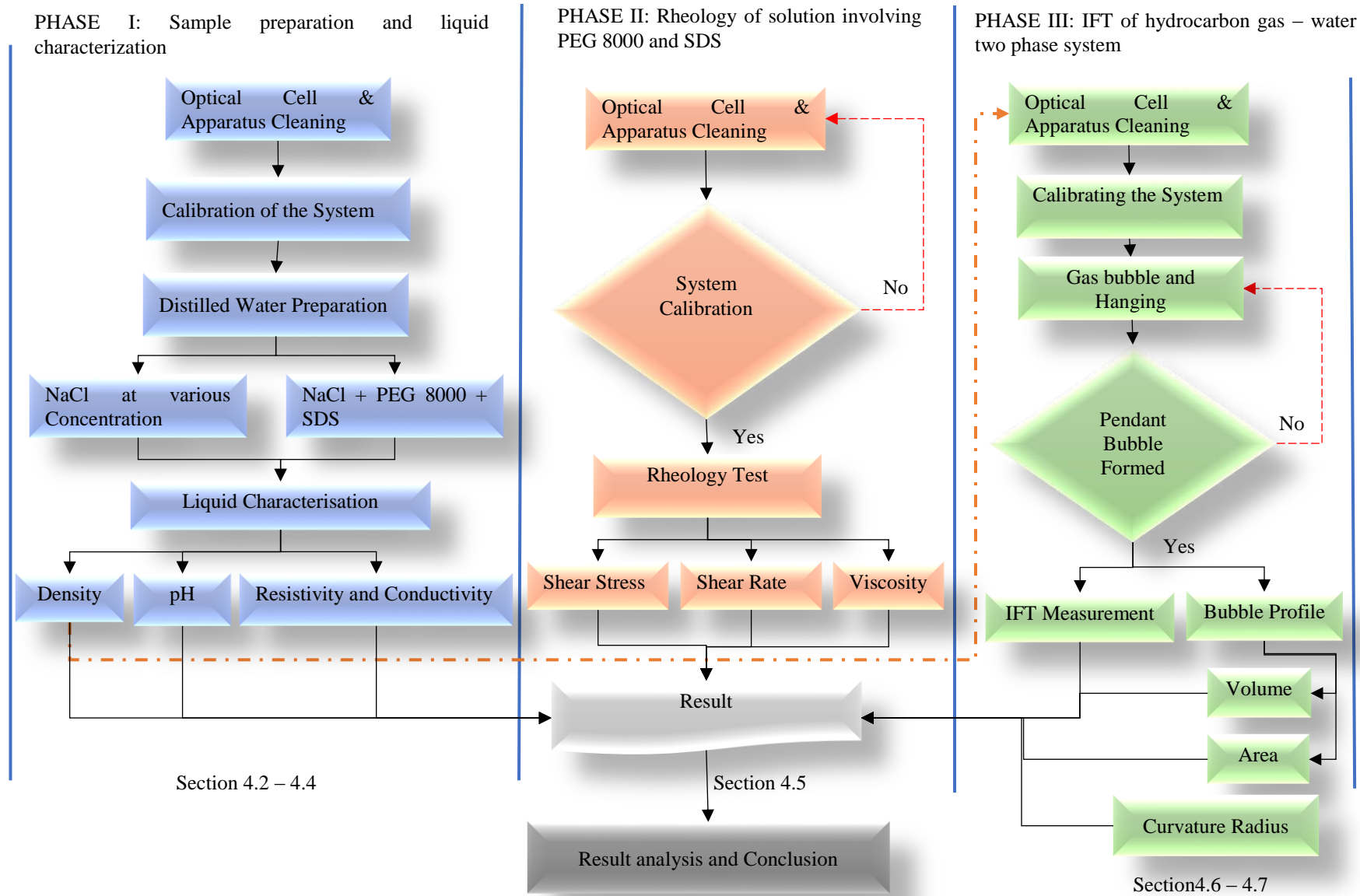
Figure 4.1: Schematic presentation of the experimental and simulations validation stages

4.2 Phase I: Sample preparation and liquid characterisation

The initial phase of conducting the present investigation was presented in this section. The phase described the materials and samples preparations for the current study. The samples prepared were then characterised. The objective of this stage was to characterise the structure of the liquid samples and analyses, to determined their respective density, pH, and electrical resistivity and conductivity. Each of the equipment used in this stage was described in the corresponding sections.

4.3 Sample preparation

4.3.1 Materials used in the present study

This sub-section described the salt and inhibitors types used in the present study. The four different chloride salts commonly found in the produced water are $NaCl$, $CaCl_2$, KCl, and $MgCl$. NaCl has the highest percentage, thus used for this work. This salt was used to prepare brine or salt-water used in the current investigations. The salt-water was prepared at a different concentration of NaCl as described in subsection 4.2.4. Table 4.1 presents the chemical formula, structure and molecular weight of the salts used with their respective suppliers and purity.

Table 4.1: Structure, types and properties of the salt used for the investigations

Component	Chemical Formula	Molecular Mass (g/mol)	Percentage Purity	Supplier
Sodium Chloride	NaCl	58.45	99.99	Fisher Scientific

Polymer and surfactant were also used in the present work. This surfactant and polymer were commonly used as an inhibitor in hydrocarbon flow through the pipeline, and include thermodynamic and low dosage inhibitors. The thermodynamic hydrate inhibitor used was Polyethylene glycol (PEG 8000) which is a polymer, while the low dosage hydrate inhibitor used was Sodium dodecyl sulphate (SDS) which are all surfactant. PEG 8000 was used at a different concentration of 10, 20 and 30 and 40 wt%, and a combination of PEG 8000 and various level at a low dosage of SDS at 0.1, 0.2, 0.3 and 0.5wt %. In Table 4.2 chemical structure, molecular weight and percentage purities of these inhibitors were presented with their corresponding suppliers.

Table 4.2: Structure, types, and properties of inhibitors used for the investigations

Component Structure/Name	Condensed Name	Molecular Weight (g/mol)	Percentage Purity	Supplier
Polyethylene glycol	PEG	8000	99.99	Fisher Scientific
Sodium dodecyl sulphate	SDS	288.38	99.99	Fisher Scientific
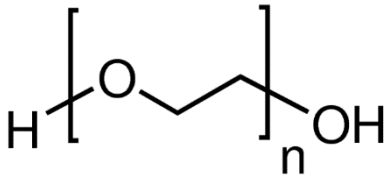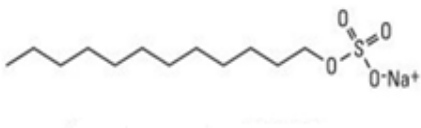
The surfactant and polymer combinations were in the presence or absence of various concentration of the salts used. As described in subsection 3.2.1 and 3.2.4 respectively.

4.3.2 Hydrocarbon gas (methane, CH$_4$)

Methane (CH$_4$) was used in the present study as it is the predominant hydrocarbon gas found in the reservoir. Table 4.3 shows the chemical and structural formula of methane with it equivalent molecular weight, percentage purity, and supplier.

Rather than using natural gas, synthetic CH$_4$ was used which allows us to control the gas purity to a predictable variation and also ensures that there are consistency and repeatability during the experimental investigation. Further, uses of synthetic CH$_4$ will eliminate any difference in the property measurements caused by the presence of contaminants such as CO$_2$, N$_2$ and other hydrocarbon presence in the system.

Table 4.3: Structure and properties of methane used during the investigations

	Component
Chemical formula	CH_4
Structural Formula	
Molecular weight (g/mol)	16.00
Critical temperature	191.15 K
Critical Pressure	4.61 MPa
Boiling point	111.67 K
Melting point	90.68 K
Gas Density	0.6
Percentage purity	99.52
Supplier	BOC Gas
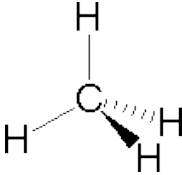
4.3.3 Preparation of distilled water (dH$_2$0)

Distilled water is water that had many of its contaminants removed by the process of boiling the water and condensing the steam into a clean reservoir/container. Thus, distilled water was prepared and used to conduct the present study. Distilled water is used to avoid having any components that may be present in the water which may affect the results of the experiment and also prevent any mineral build-up in the equipment. Other uses of distilled water during the study was in the cleaning and maintenance of the apparatus used.

4.3.3.1 Equipment description

The preparation of the distilled water was carried out using a bench mounted Distinction water still. The distillation equipment was made from the glass with a silica-sheathed by Stuart Equipment, as depicted in Figure. 4.2. The distiller was placed near a power source rated 3kW, 220-240V 50/60 Hz single phase for convenience. All units are connected to the mains supply via a double pole 30mA RCD isolating circuit breaker rated at 15A. It was also, linked to a cold-water supply source, capable of providing a minimum flow rate of 60 l/hr. Further, placed close to a wastewater drain, so that the drain pipe can fall away straight without twists or bends, to allow unrestricted flow. All water supplies and drainage systems were adequately earth bonded. A distillate collection reservoir is located beside the Still.
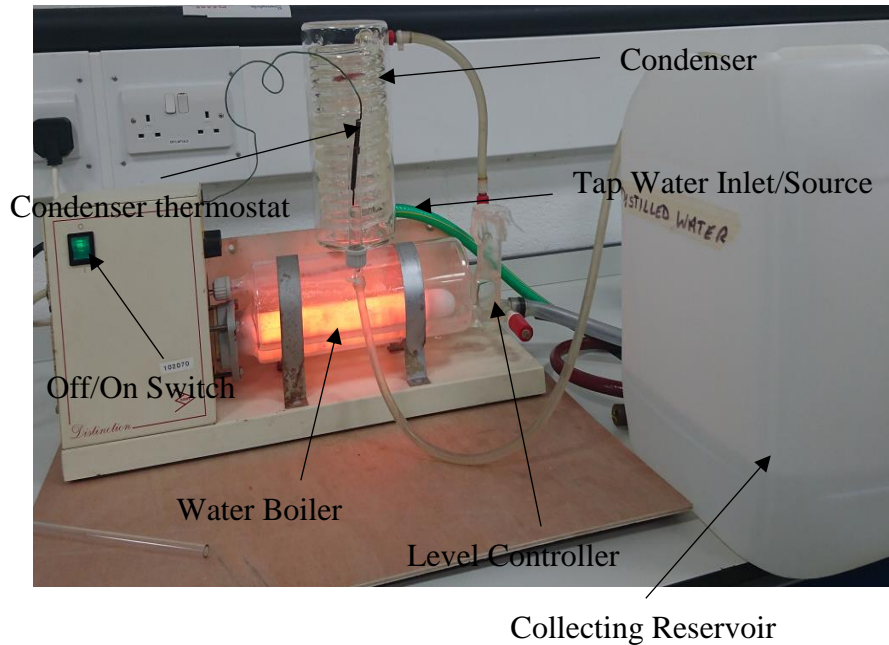
Figure. 4.2: Laboratory equipment for distilled water preparation

The system was designed with some safety controllers that will turn the heater off when the collecting reservoir is full and independent thermostats to prevent overheating in case the water source is interrupted.

4.3.3.2 Material and procedure

In the preparation of distilled water used, tap water was used as a raw material. Therefore, the method and process for the purified water preparation in the current study are described in the subsequent paragraph.

The equipment was set ready to use by suitably mounting it on the table top, and all other components placed appropriately. The cold water supply source was then turn on, and the water flow rate was adjusted to approximately 60 l/hr. The operating level of the water boiler was attained by allowing and monitoring the water flow via the condenser and into the furnace. Moreover, the excess water was allowed to flow freely to the water drain-out. The heating element was then turned on via the on/off switch located on the front panel as indicated in Figure. 4.2. The distillate emerged from the condenser after 4-7 minutes of operation and was allowed to run to drain for approximately 20 minutes, to flush out any contaminant that may be present in the line, before the collection begins.

After completing the operation, the system was shut down by turning the heating element off, and cooling water was allowed to continue for a few minutes to cool the heating element to minimum allowable temperature.

4.3.3.3 Cleaning and maintenance of water distiller

Scale build up in the neck, and the main body of the boiler chamber is non-avoidable over time of usage. Therefore, to obtain optimum performance, this scale should be removed on a regular basis. Massive scaling is known to reduce distilled water quality and can shorten the life of the heating element. However, the time span between cleaning depends significantly on the hardness of the water and the frequency of use. Hence, the need for descaling once a week whereas in a soft water area several weeks may elapse before descaling is necessary.

The descaling procedure was carried out by following instructions in conjunction with Control of Substances Hazardous to Health Regulations (COSHH) 1988 as follows:

i. The electric supply source was turned off, and the still was allowed to cool completely.

ii. The cooling water supply was also turned off.

iii. The stopcock on the constant level was removed to drained the boiler and closed back.

iv. The cooling water supply was switched, and the boiler was filled halfway to its normal operating level after which the water supply was turned off.

v. 100ml of 10% formic acid was added via the open funnel of the constant level control (Always handle strong acids with great care, and protective clothing, gloves and face-masks should be worn during the descaling operation. Remove any acid spills immediately).

vi. The system was allowed for 12-hours to dissolve the scale.

vii. Water supply point was turned on again, and the boiler filled to its normal operating level. The water flushed the acid into the boiler, and the supply point was turned off when the level was slightly below the overflow.

viii. The stopcock was opened, and the boiler was drained out. All the necessary precautions and effluent control procedures were followed.

ix. The stopcock was closed, and water supply was turned on and allowed to fill the boiler. The water supply was turned off and stopcock re-open and let the furnace to drain out. This procedure was repeated three times.

x. The Distinction water still may now be restarted by referring to the instructions given under "Operation" in this manual. Also, the stand and outer surfaces of the glassware should be cleaned using a damp cloth and a mild detergent solution.

4.3.4 Preparation of salt-water (Brine)

4.3.4.1 Equipment description

The brine solution used for conducting present investigations were prepared in the Laboratory, using the equipment described in Figure 4.3. These apparatus include electronic weighing balance, Petri dish, different salt sample containers, volumetric flask, hotplate and magnetic stirrer. For optimal brine solution, the amount in gram (g) of salt required to make an intended concentration in 1000 ml of distilled water are calculated using mass-volume. Although careful attention to proportions was adhered to, for accuracy, however, in this investigation and for certainty, the concentration was measured in percentage (%) using a refractometer.
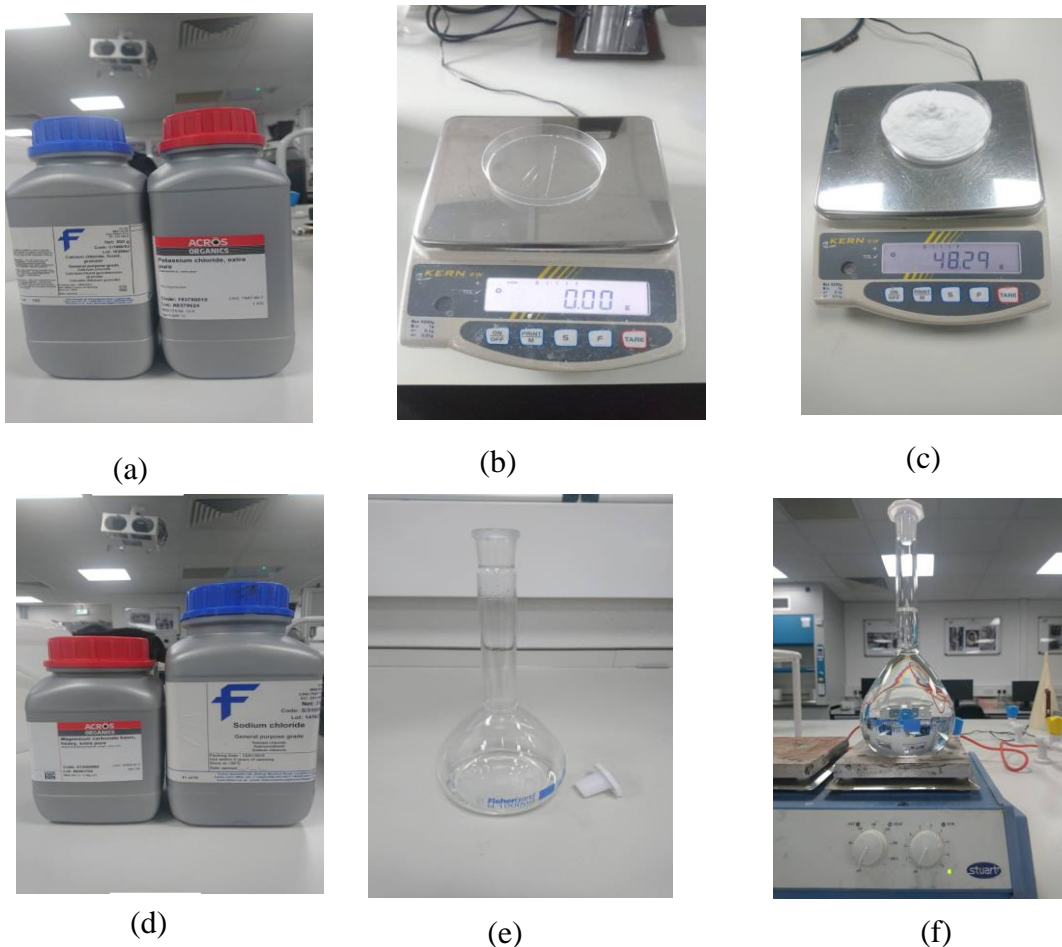
Figure 4.3: Materials and equipment used for salt-water preparation: (a) Sodium chloride and magnesium chloride salts containers, (b) Tared mass balance with Petri dish, (c) Mass balance indicating measured sample, (d) Calcium and potassium chloride salts, (e) Volumetric flask and stopcock, (f) Magnetic stirrer with brine contained in volumetric flask.

4.3.4.2 Brine preparation procedure

All the reagents and equipment (mass balance, petri dish, spatula, volumetric flask, etc.) required are collected and set ready for use. The general procedure followed for the preparation of the brine solutions in the present study are described as follows:

i. The weighing balance was plug-in to the power sources, and the start button was turned on to power the balance, making it ready to be used.

ii. The petri dish was tared, and 29.22, 58.44, 87.66 and 116.88g of NaCl are weighed.

iii. Each of the measured amounts of NaCl is carefully poured into a volumetric flask of 1000ml filled to 1/3 with distilled water.

iv. The volumetric flask was then filled to the graduation mark and then stirred with a magnetic hotplate stirrer at 350 rpm for 5-10 minutes at room temperature between 20 °C and 23 °C.

v. Steps 3 and 4, are repeated for each of the measured amounts of 29.22, 58.44, 87.66 and 116.88g of NaCl and 0.5, 1.0, 1.5 and 2.0 Molar solution of brine (NaCl) solution was prepared, respectively.

4.3.4.3 Cleaning and maintenance of the apparatus used for brine preparation

Immediately after use, the equipment was cleaned and safely placed appropriately for another use. For the preparation of brine solution, if the petri dish, volumetric flask and other useful glassware for measuring fluids and salt are tainted with oil and different materials, it keeps the glass from being consistently wetted. The fouled will affect the accuracy of the volume of liquid conveyed, and the measure of deposit is holding fast to the dividers of the compartment and mutilate the meniscus of the flask. The procedure followed for the cleaning of glasswares and other equipment used in the preparation of brine are as follows:

i. The petri dish, spatula, and the volumetric flask are cleaned and rinse with tap water immediately after use.

ii. Washed petri dish, spatula, and volumetric flask are placed in a basket with their mouth downwards for allowing them to dry completely. Sometimes oven is used.

iii. The washed and dried glassware are placed in a cabinet to protect it from dust and also a can tape a piece of paper on the mouth of the glassware to prevent dirt and dust from entering the glassware.

iv. Keep washed, cleaned, and sterilised glassware pieces in individual racks and at a distance to avoid any breakage.

4.3.5 Preparation of surfactant and polymer solution

The same equipment and procedure used in section 4.3.4 was used to measure the quantity of the surfactant required. An aqueous solution of PEG 8000 (10, 20, 30 and 40 wt%) were prepared gravimetrically using distilled water (ρ = 18.2 MΩ.cm) by measuring 100, 200, 300 and 400g of powdered PEG 8000. Also, for the polymer-surfactant solutions, 0.5, 1.0, 1.5 and 2.0 wt% SDS were prepared in each of the measured PEG 8000 concentration, to have PEG 8000 + SDS solutions. The surfactant and polymer were dispersed in distilled water by stirring at 450 rpm on a multipoint magnetic hotplate stirrer (SB 162-3 Stuart). After the preparation, the solution was kept at room temperature. An overview of the equipment set-up for hotplate stirrer is shown in Figure 4.4.

Figure 4.4: Multipoint hotplate magnetic stirrer

Table 4.4: Overview of the prepared surfactant and polymer solution with or without the presence of salts

S/N	Reagent	Corrected Concentration [wt%]			
1	PEG 8000	10	20	30	40
2	SDS	0.5	1.0	1.5	2.0

4.4 Liquid characterisation

4.4.1 pH Measurement

pH is a measure of the acidity or alkalinity of a given solution. The acidity or alkalinity of a solution is controlled by the relative number of hydrogen particles (H^+) or hydroxyl particles (OH^-) present in the solution. Any liquid solution that has a higher relative number of hydrogen ions is an acidic solution, while alkaline solutions have a higher relative amount of hydroxyl ions. Acids are substances which either separate to discharge hydrogen ions or react with water to form hydrogen ions. Bases are substances that separate to release hydroxyl particles or react with water to form hydroxyl particles. In water solutions, the result of the molar groupings of hydrogen and hydroxyl ions is equivalent to a dissociation constant (K_w). Hence, Knowing the value of K_w and the concentration of H^+ makes it possible to calculate the concentration of OH^- and vice versa. However, the product of hydrogen and hydroxyl ion is always equal to K_w and has a value of 10^{-14} as shown in the equation (4.1).

$$[H^+][OH^-] = 10^{-14} \ (Mol/L)^2 = K_w \tag{4.1}$$

It is essential to understand the acidity or alkalinity of a given liquid sample, hence the importance of pH in the solution of inhibitors in brine.

4.4.1.1 Equipment description

Figure 4.5 shows the pH meter used for the present investigations. The following subsections described the procedure, calibration and cleaning and maintenance of the pH meter.
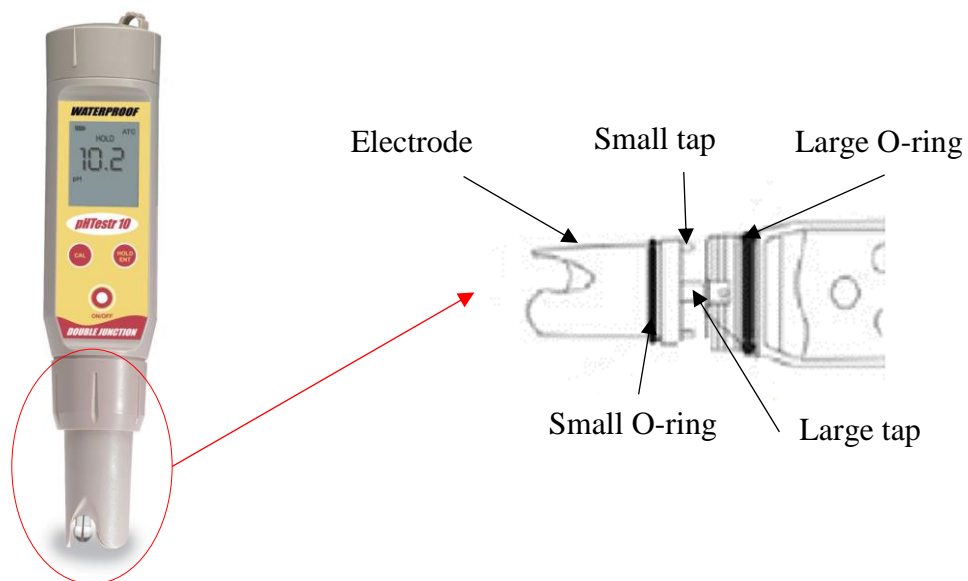
Figure 4.5: pH Measuring device

4.4.1.2 pH calibration procedure

The pH tester was usually calibrated every week, and it can be calibrated up to three points using either of the standards. For this study, USA standard was used to calibrate the meter using the following steps:

i. The pH meter was switched on by pressing ON/OFF button.

ii. The electrode was dip into the pH standard buffer solution to about 2 to 3 cm.

iii. CAL button was pressed to enter calibration mode. The 'CAL' indicator was displayed, and the upper display shows the measured reading based on the last calibration while the lower displayed value the pH standard buffer solution.

iv. The pH reading was allowed to stabilise and then confirmed the calibration point by pressing the HOLD/ENT button. The upper value displayed was calibrated to the pH standard buffer solution, and the lower value will be toggling in between readings of the next pH standard solution.

v. Steps 1-5 was repeated with other buffer solutions, and the electrode was rinsed using distilled water before dipping into the next standard solution.

4.4.1.3 pH measurement procedure of the liquid sample

Before beginning the sample pH measurement, the pH meter electrode was conditioned by immersing it in electrode storage solution or tap water for at least 30 minutes. De-ionized water is not suitable for the conditioning. After conditioning the pH meter, buffer selections were made to suit the required measurement. The tester has two standards for analysis which are USA (pH 4.01, pH 7.00 and pH 10.01) or NIST (pH 4.01, pH 6.86, and pH 9.18) standards.

4.4.1.4 pH standards selection procedure

i. HOLD/ENT button was pressed and while pressing, ON/OFF button was pressed to switch the tester.

ii. The HOLD/ENT button was released, and the display screen flashes either USA or NIST.

iii. CAL button was pressed to toggle between the two buffer set standards and USA was selected

iv. HOLD/ENT button was pressed to confirm the selection of the buffer set.

4.4.1.5 pH measurement procedure

i. The pH meter was switched on by pressing ON/OFF button.

61

ii.   The electrode was dipped into the liquid test sample to about 2 to 3 cm, stirred and the readings are allowed to stabilise.

iii.   The displayed pH value was then noted and recorded.

iv.   The pH meter was switched off after used by pressing the ON/OFF button.

v.   Steps i-iv was repeated for 2.9, 5.6, 8.2 and 10.7 wt% NaCl and the results obtained for the various concentration are shown in section 5.2.1.

vi.   Step v was repeated with the presence of 10, 20, 30 and 40 wt% PEG 8000 in each of the NaCl concentration results are also shown in section 5.2.1.

4.4.2 Resistivity measurement

Electrical resistivity is well understood in the context of current flow through materials consisting of different layers with different individual resistivities. The layers are assumed to be horizontal. Moreover, it is the measure of how well the material retards the flow of electrical current through it. The resistance per unit length and area is called the resistivity R and can be presented as shown in equation (4.2).

$$R = \frac{\Delta E}{I} * \frac{A}{L} \qquad\qquad (4.2)$$

Here R is the resistance of the sample, measured in ohm-meters (Ω-m). E is the potential difference measured in volts (V), and I is the current flowing through the sample measured in amperes (A). A is the cross-sectional area of the sample perpendicular to the current flow measured in square meter (m^2), and L is the length of the sample measured in meter (m). It is worth to note that the electrical conductivity is the reciprocal of resistivity and can be express as shown in equation (4.3).

$$C = \frac{1}{R} = \frac{1}{\Delta E} * \frac{L}{A} \qquad\qquad (4.3)$$

4.4.2.1 Equipment Description

Figure 4.6 shows the image of the resistivity meter used in the current investigations. The meter is a convenient measuring device designed to give a quick, and reliable resistivity value of a small sample of liquid measured in ohm-meters. The device accurately measured resistivity within the range of 0.01 – 10 ohm-meters. It consists of the meter itself, lucite cell with a built-in thermometer, resistivity probe, rubber suction bulb for probe, 9-volt battery and pipe cleaner. The meter has a two terminal posts which connect the cell assembly to the meter. The adjusting control knob, and the two black and red button which is used to allow the current

to pass the electrode (post) terminals. The temperature was measured using the thermometer in the cell.

Figure 4.6: Resistivity meter

4.4.2.2 The calibration procedure for the resistivity meter

   i.   The meter was calibrated by pressing and holding the black button.

  ii.   The adjusting knob was turned to set the meter pointer to the "ADJ" position.

4.4.2.3 Procedure for resistivity measurement of the samples

   i.   The sample was pulled into the suction bulb via the lucite cell by pressing and releasing it after dipping it into the sample. The compartment was emptied and refilled several times to wet the cylinder walls thoroughly.

  ii.   Filled the slot and connected the two-hole on the slot to the two terminal posts on the meter.

  iii.   The resistivity was measured and recorded by pressing and holding both black and red button at the same time.

  iv.   The temperature was also noted and recorded using the thermometer on the cell wall.

  v.   Steps i-iv were repeated using 10, 20, 30 and 40 wt% PEG 8000 in each of 2.9, 5.6, 8.2 and 10.7 wt% NaCl at temperature of 298.15, 303.15, 308.15 and 313.15 K. Results obtained are shown in section 5.2.2.

  vi.   The conductivity of each sample was determined using the relationship described in section 4.4.2.

4.4.2.4 Cleaning and maintenance of the resistivity meter

   i.   The cell was clean immediately after measuring by purging the cell with distilled water until it is clear.

  ii.   In case of deep cleaning due to dirt build up, pipe cleaner and mild soap was used and scratching the surface of the cell was avoided

 iii.   Replaced the 9-volt alkaline batteries, when it is no longer possible to calibrate the meter.

  iv.   The mercury in the sample cell thermometer is always united and if separated, reunites it by shaking it down or by placing the cell into hot water until the mercury enters the top void. Then remove the cell from the hot water and insert it into ice water to pull the loose mercury into the graduated tube.

4.4.3 Density Measurement

The density of a given volume of a liquid sample is determined in the present study by using a weighing balance and was simulated using Refprof at 298.15 – 313.15 and pressure up to 13.10 MPa.

4.4.3.1 Equipment description

Figure 4.7 shows the diagram of the mud balance used in the present study. The balance measured the density or specific gravity within the accuracy of ±0.1 and ±0.01 respectively. The mud balance consists of a constant volume cup with a lever arm and rider calibrated to read the density of the liquid directly in ppg (water = 8.33), pcf (water = 62.4), specific gravity (water = 1) and pressure gradient in psi. It also consists of measuring scales and fulcrum. The fixed volume chamber at the end of the beam was designed to be balanced by the sliding the rider at the opposite end moving along the measuring scale on the lever arm. A level bubble mounted on the shaft indicates when the system is in equilibrium.

Plastic caring case
Sliding weight
Level bubble vial
Lid
Volume chamber
Fulcrum
Messuring scale
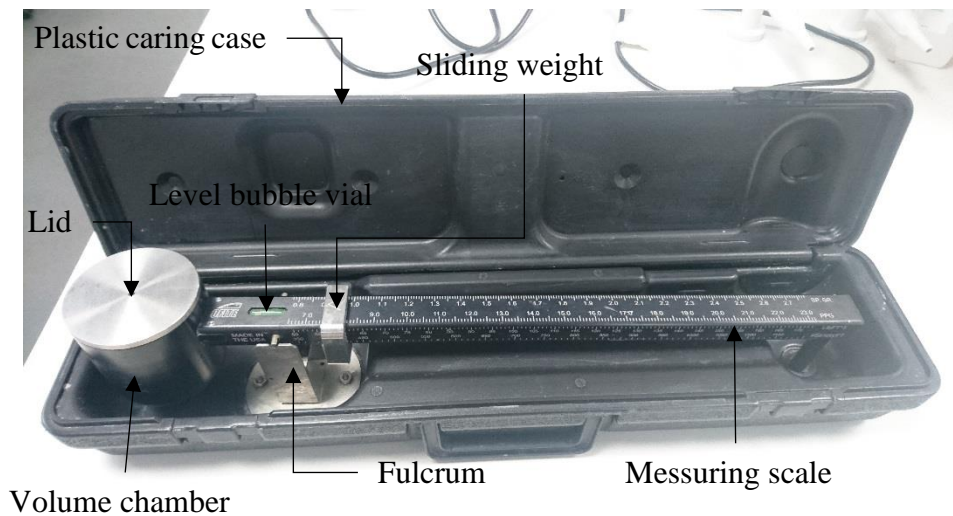
Figure 4.7: Weight balance with carrying case

4.4.3.2 Calibration

The mud balances are re-calibrated by measuring the density of fresh water using the following procedure.

  i.   The lid from the cup was removed, and the cup was filled with water.
  ii. The lid was then replaced and wiped dry.
  iii. The balance arm was then replaced on the base with knife-edge resting on the fulcrum.
  iv. The rider was then set at 8.3 pounds per gallon. Add or remove steel shot from the Shot-well until the instrument is in the balance.

4.4.3.3 Procedure for liquid density measurement using the weighing balance

  i.   The mud balance was placed on flat table top surface (in carrying case).
  ii.   The temperature of the liquid sample was measured and recorded.
  iii. The volume chamber was filled with freshly obtained liquid sample to be weighed.
  iv.   The lid was then placed to cover the cup and set it with a gentle twisting and tapping to free any trapped air.
  v.   The liquid expelled through the hole was cleaned, by covering the hole in the lid with a finger and washing the liquid from the outside of the cup and arm.
  vi.   Then thoroughly dry the entire balance with a clot.
  vii. After which the balance was then placed on the prop and move the sliding weight along from the opposite end of the arm until balanced as indicated by the bubble vial.
  viii. The density was then read and recorded.

65

ix. The balance was then emptied and then clean.

x. Steps i-xi are repeated for using 2.9, 5.6, 8.2 and 10.7 wt% NaCl at 298.15 K.

xi. For each NaCl concentration in step x, 10, 20, 10 and 40 wt% PEG 8000 was added, and step i-xi were repeated to determine their density at 298.15 K and atmospheric pressure.

4.4.3.4 Cleaning and maintenance of the weighing balance

After used, the mud balance was clean with distilled water and dried. It was placed appropriately in a drawer, after putting it in a plastic caring case.

4.5 PhaseII: Rheology of solution involving PEG 8000 and SDS containing NaCl

In this section, the method for the second phase of conducting the present investigations was described. The second phase of the investigation is the rheology of the inhibitor solution involved and the objective of the phase was to analyses and categorise the rheological behaviour of the different concentration of the inhibitors with or without the presence of salts. The phase described the equipment, procedure and accuracy of the method.

4.5.1 Viscosity

Viscosity is a degree of the resistance of a fluid to flow due to deformation by either shear stress or tensile stress. The less thick the fluid is, the higher it can flow when deformed easily. Viscosity depicts liquid's inward resistance to flow. The rheology of the inhibitor solution was measured as a part of the present study, to understand the mass transfer of the liquid. Fig. **4.8** shows the experimental setup used to perform the rheological (viscosity) measurement of the inhibitor solution in the current investigation, using rotational viscometer.
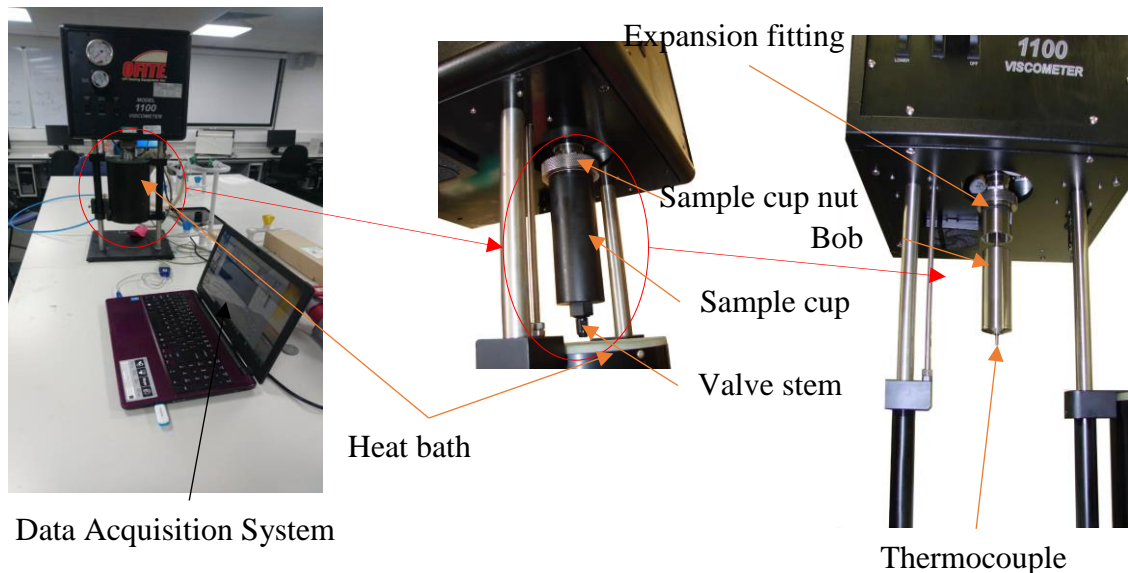
Fig. 4.8: Rotational viscometer

4.5.2 Theory and Evaluation for Coaxial Cylinder Viscometer

When a thin film of a liquid is held between two glass plates, moving the plates relative to each other requires the application of force. The liquid layers that are directly adjacent to each of the plates surfaces are held to them by forces of adhesion and forces of cohesion act between the molecules of the liquid. On movement, a linear velocity gradient is formed within the fluid between the two plates.

When a fluid is held between two surfaces and a linear velocity gradient is formed within the liquid then according to Newton's law of viscosity, the shear stress is given by equation (4.4).

$$\tau = \frac{F}{A} = \mu \frac{dv}{dy} \tag{4.4}$$

where τ is the shear stress, F is the force required to move the liquid layers, A is the area of contact between the plate and the liquid, μ is the viscosity, and dv/dy is the velocity gradient.

The rotational viscometer was employed due to its ability to work continuously at a given shear rate as compared to many different viscometers. Working continually at a given share rate enable another steady-state measurement to be carried out. Analysis at a constant share rate allows determination of time dependency viscosity of a given sample. Similarly, subsequent measurements at different share rates, temperature, etc. can be made with the same instrument. For these and other reasons, rotational viscometers are used for rheological analysis of the liquid sample under the current investigations.

4.5.3 Equipment description
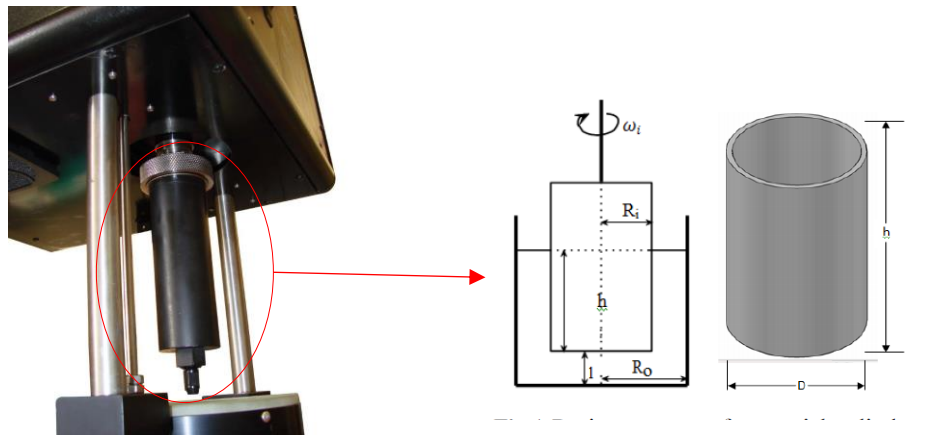
Figure 4.9: Basic components of the viscometer

4.5.4 Procedure for viscosity measurement

4.5.5 Test preparation

The following steps were followed for the viscosity measurement of the liquid sample for characterising before the IFT measurement.

i. The water source and drain hose were connected to the appropriate fittings on the viscometer as indicated in Figure 1.7.

ii. The heater cable was screwed from the heat bath into the bottom of the cabinet.

iii. The thermocouple was plugged from the heat bath into the bottom of the cabinet.

iv. The viscometer was connected to the computer via USB serial adopter.

v. The viscometer was turned on by plugging the power cord into an AC power source and switching on by pressing ON/OFF into ON position.

vi. The computer was then turn on, and ORCADA software was started.

vii. 42ml of the sample was then measured using a cylindrical beaker and transferred into the sample cup.

viii. The RB1 bob was then positioned at the centre of the sample cup, and the sample cup was then pushed up past the O-ring and screwed in to place.

ix.   The heat bath was positioned under the sample cup and then raised automatically with the lift and lower switch.

4.6 Phase III: IFT of hydrocarbon two-phase gas and water system

This is the final phase of the investigation, in which the IFT existing at the methane-water interface were investigated. Therefore, this section described the equipment, procedure and accuracy of the method. The objective of this final phase was to analyses the influence of operating conditions, salt and inhibitors on IFT of a two-phase system involving methane and water.

4.6.1 IFT of methane bubble at the methane-water interface

The IFT measurement of the methane-water, methane-brine and methane-inhibitor solution was performed according to the set up shown in Figure 4.10, and Figure 4.11 shows the process flow diagram of the system. In this investigation, the interfacial tension of gas-liquid was determined using pendant drop technique, which is a standout amongst the most convenient and reliable methods for measuring gas-liquid interfacial tension. The Rig was initially designed to accommodate liquid-liquid system, but for conducting present work, the Rig was re-configured to accommodate gas-liquid system at the pressure and temperature conditions intended for the current investigations.

Figure 4.10: Experimental set-up for IFT measurement (1-Data acquisition system; 2-Temperature and pressure recorder; 3-Illuminator; 4-IFT Measurement Chamber; 5-Back-

pressure regulator; 6-Rame-hart Camera; 7-Methane cylinder; 8-Vibration control table; 9-water sample cylinder; 10-Manual pump; 11-Automatic pump)
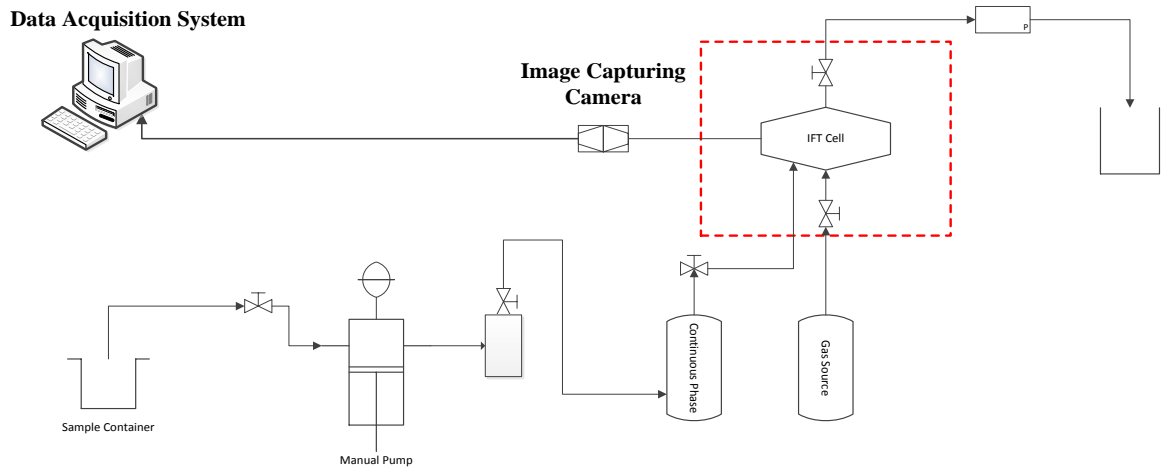
Figure 4.11: Simplified process flows diagram for interfacial tension measurement using re-configured IFT-10.

4.6.2 Theory behind pendant drop (hanging bubble) technique and profile evaluation

The pendant drop (hanging bubble) techniques use axisymmetric drop or bubble shape analysis (ADSA) to determine interfacial properties through ascertaining the profile of the liquid droplet or hanging bubble formed as the case may be. This experimental profile is then fitted with the general Laplace equation reported by Cheng, Li, Boruvka, Rotenberg, & Neumann, (1990). Hydrodynamic equilibrium is a requirement for this technique, and this means that only gravity forces and interfacial forces are acting on the drop or bubble (Berry et al., 2015; Río & Neumann, 1997). Figure 4.12 shows the schematic of a pendant bubble.
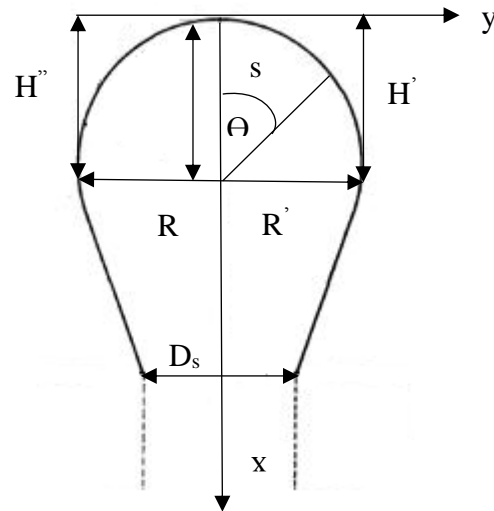
Figure 4.12: Pendant bubble profile with variables adopted and modified from (Hansen & Rodsrud, 1991)

The symbol, s, represents the distance along the bubble profile from the bubble apex, whereas $H^{'}$ is the distance from the centre of the curvature to the drop apex.

IFT of the pendant bubble is determined by measuring the size parameters R_i (radius of the curvature), and β (shape factor) from the hanging bubble profile. Using R_i and β obtained, the IFT calculated using equation (4.5):

$$\gamma = \Delta\rho g \left(\frac{R_i^2}{\beta}\right) \tag{4.5}$$

Where $\Delta\rho$ is the density difference between the hanging bubble and the surrounding liquid, g is the acceleration due to gravity, R_i is the radius of curvature at the drop apex, and β is the shape factor. The $\Delta\rho$ is given by equation (4.6):

$$\Delta\rho = \rho_{gas\ phase} - \rho_{liquid\ phase} \tag{4.6}$$

Equation (4.7) – (4.9) were driven from Young-Laplace in dimensionless form, and these equations described the bubble profile (Hansen & Rodsrud, 1991).

$$\frac{d\theta}{dS} = 2 - \beta Y - \frac{\sin\theta}{X} \tag{4.7}$$

$$\frac{dX}{dS} = \cos\theta \tag{4.8}$$

$$\frac{dY}{dS} = \sin\theta \tag{4.9}$$

Where X, Y and S are dimensionless quantity drive by dividing x, y and s with R_i as presented in equation (4.10) – (4.12) as:

71

$$X = \frac{x}{R_i} \tag{4.10}$$

$$Y = \frac{y}{R_i} \tag{4.11}$$

$$S = \frac{s}{R_i} \tag{4.12}$$

A large number of theoretical dimensionless profiles were computed for the entire possible β-range, from $\beta = -0.55$ to 10^{20} utilising Kutta-Merson's numerical integration calculation with programmed step length change. The most extreme relative error was set to 10^{-4}. Each profile was measured numerically by using cubic interpolation. Along these lines curves connecting the parameters β and R_i with quantifiable metrics as demonstrated in Figure 4.12 were produced, and these curves were fitted with linear polynomials by the technique of least squares method.

For pendant drops or bubbles that are sufficiently long in order to measure D_S, then the ration of D_s and D_E was given by (3.13) is used:

$$\sigma = \frac{D_s}{D_E} \tag{4.13}$$

Here D_E is the maximum diameter, and D_S is the diameter at a distance D_E from the drop apex. Therefore, the equation found is presented in equation (4.14) and (4.15) and also the β is negative:

$$\beta = -0.12836 + 0.7577\sigma - 1.7713\sigma^2 + 0.5426\sigma^3 \tag{4.14}$$

Also

$$\frac{D_E}{2R_i} = 0.9987 - 0.1971\beta - 0.0734\beta^2 - 0.34708\beta^3 \tag{4.15}$$

For pendant drops too short for the determination of D_S, the drop height (H), and the radius (R) is used. R is given as:

$$R = \frac{D_E}{2} \tag{4.16}$$

Moreover, equation (4.4) may be re-written in term of H as:

$$\gamma = \Delta\rho g \left(\frac{H^2}{B}\right) \tag{4.17}$$

It is effortlessly watched that H will have an ultimate point in light of the maximum hydrostatic pressure the IFT may stand up to or resist. At the end when the drop turns out to be infinitely wide, just a single radius of curvature will be essential, and the limiting value of β is 2.0. Equation (4.16) is significantly more advantageous for small pendant bubbles. Another

parameter B may develop from Equation (4.4) and (4.16) as a component of the proportion ξ = H/R, as presented in equation (4.17) and (4.18)

$$B = \beta* \left(\frac{H}{R_0}\right)^2 = f(\xi) \tag{4.18}$$

$$\frac{H}{R_0} = g(\xi) \tag{4.19}$$

Combining equation (4.18) and (4.19) yields (4.20):

$$b = f(\xi)/g(\xi)^2 \tag{4.20}$$

The function B = f (ξ) has a highest B = 2.290 at ξ = 0.285 that compares to ca. β = 5000, and it implies the drop "height", H likewise should have a greatest at this value of ξ. These values must represent an optimum for the sum of the two radii of curvature, implying that at higher drop volumes, the curvature in the horizontal plane must decrease stronger more than the opposing increase in the vertical plane.

The function B = f (ξ) might be numerically approximated by various functions, depending on the ξ-domain and the desired accuracy. Though exact analytical solutions have not been found, instead experiments show that ordinary linear polynomials give agreeable fit in most cases, utilising ξ-1 as the independent variable and driving the consistent term to 0. Around ξ=1 it might approximate by a straight line with an incline of 4.38, while for all values ξ>0.34 (i.e. β<1000) we may utilise a fourth order polynomial with a standard error of 0.0018. Due to the opposite curvature of the positive and negative parts of the curve, the enhanced approximation is obtained by utilising separate conditions as given by equation (4.21) and (4.22).

$$\xi<1:\ f(\xi)=-4.1788(\xi-1)+1.9086(\xi-1)^2+4.5738(\xi-1)^3 \tag{4.21}$$

$$\xi>1:\ f(\xi)=-4.3626(\xi-1)+1.1961(\xi-1)^2 \tag{4.22}$$

Equations (1.20) and (1.21) provide perfect estimates of B over all regions of practical interest and the slope at ξ = 1 is 1.723. In order to obtain reasonable estimates for the whole area of ξ > 0.34, two separate polynomials as given in equation (4.23) and (4.24) that provide a standard error of 0.0007 are chose.

$$\xi<1:\ g(\xi)=1+1.6795(\xi-1)-0.58334(\xi-1)^2-1.4257(\xi-1)^3 \tag{4.23}$$

$$\xi<1:\ g(\xi)=1+1.7356(\xi-1)-0.40869(\xi-1)^2 \tag{4.24}$$

With these two functions, R_0 and β are easily determined for all values of β<1000 from the measurement of H and R and equations (4.17) and (4.18).

The objective function used in the optimisation is the standard mean square deviation (MSD) between theoretical and experimental points, given by equation (4.25):

$$\Delta f = \frac{\Delta y}{\sqrt{1+\left(\frac{dy}{dx}\right)^2}} \qquad (4.25)$$

Where the mean square in the y-direction, Δy, is given by (4.26):

$$\Delta y^2 = \frac{\sum (y-\dot{y})^2}{N} \qquad (4.26)$$

The mean square is computed between $x = 0.2\ R_0$ and the most extreme value in the dataset. N is the number of data points. The theoretical value is calculated at each experimental x-value using cubic interpolation.

4.6.3 Equipment description

4.6.3.1 Bubble chamber and vibration control

The bubble chamber is the primary component of the system as this is where both the liquid and gaseous sample are coming into contact with each other, to create the interface. Figure 4.13 shows the measurement chamber and vibration control table. The chamber was made of stainless steel metal and rated up to 68.95 MPa at 477.6 K. The total inside volume of the chamber is 39 cm^3, with a sealed port at the bottom for the needle insertion while at the top is the overflow valve and linked to the back-pressure controller.

Figure 4.13: Experimental section of the IFT-10 showing the bubble chamber with other components attached to it.

The chamber was mounted and centred on the vibrational control bench mate. The vibrational control bench minimises the error of IFT measurement due to vibration. The platform air-

mounts of the bench mate is inflated using manual pump according to the schematic as shown in Figure 4.14.

(a)   (b)
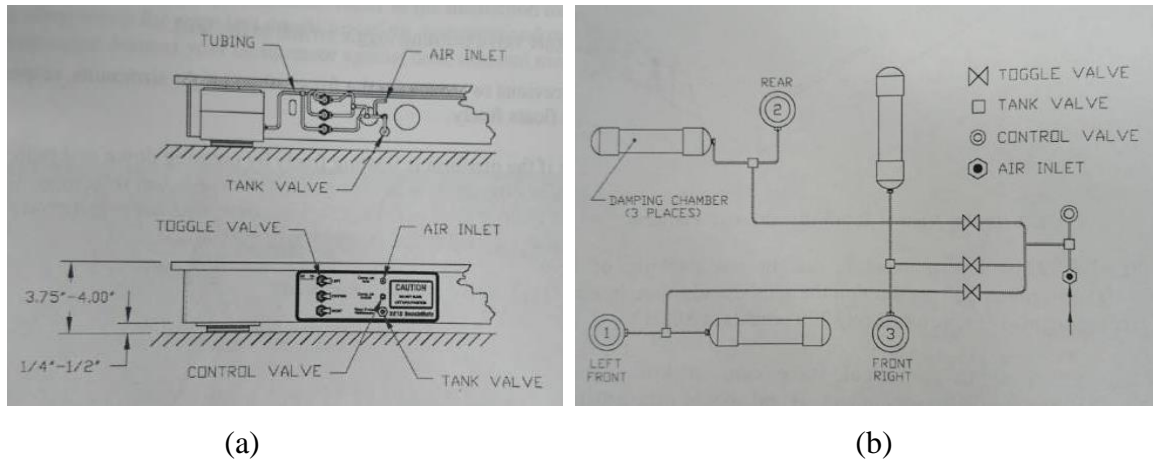
Figure 4.14: Vibrational control schematic: (a) control panel and air fill illustration, (b) airline schematic

The front end of the chamber is the viewing window, which enabled the capturing camera to capture and record a live image of the bubble or droplet. While at the back end of the cell is the illuminating light mate, which illuminates the fluid in sight the cell to allow viewing of the inside of the cell.

The bottom of the needle fastens to the lower valve assembly which connected the gas source to the capillary tube. Rotating the knurled stem positions the needle tip into the appropriate place in the cell for bubble or drop generation.

4.6.3.2 Automatic and manual pump

Figure 4.15 shows the automatic and manual pump used during the IFT measurement. The automatic pump is QX series pump (QX-6000), is entirely integrated, connected to the data acquisition system and controlled, via a Quizix Pump Works software. It contains a pump controller, which coordinates the activity of two independent, positive displacement piston pumps A and B. These two piston pumps can each be used separately for single stroke volumes, or as a pair to give pulseless continuous fluid flow for a single fluid. It can exert a maximum pressure of 41.2MPa, with a maximum flow rate of 50 cm^3 per minute, having stroke volume of approximately 12 cm^3 and piston diameter of 0.375in. The manual pump is used for pressure build-up in the cell.
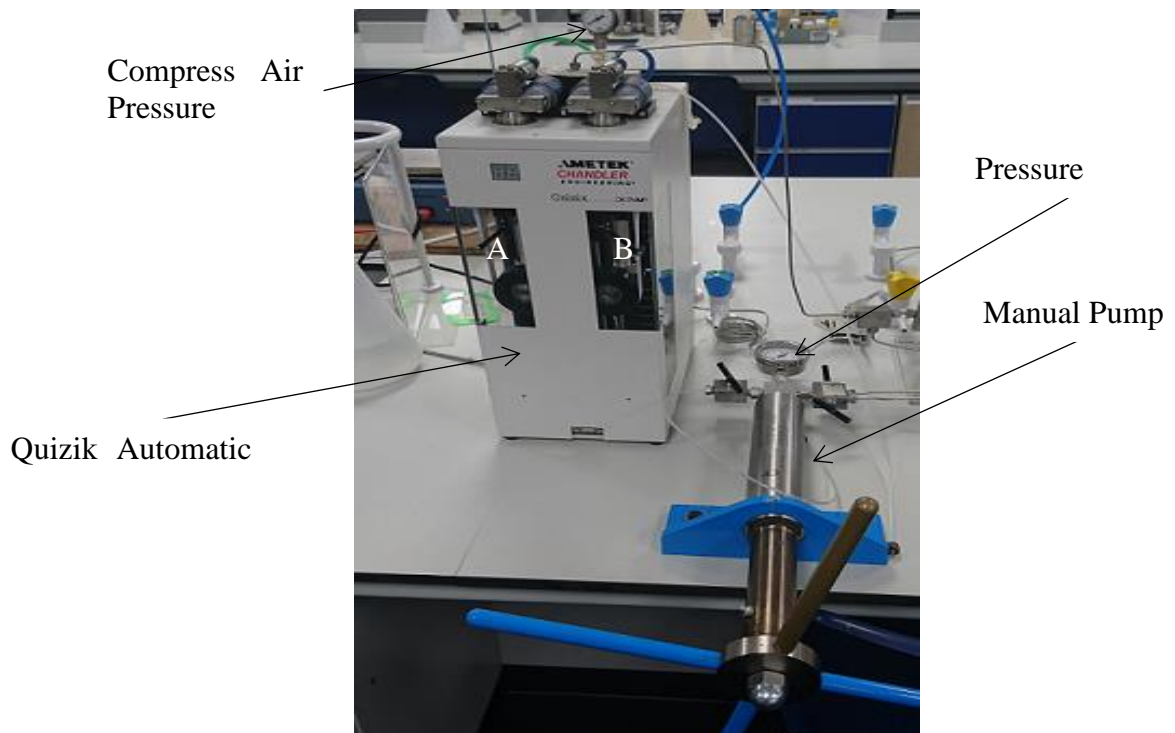
Figure 4.15: Section showing automatic and manual pump

4.6.3.3 The live image capturing camera (*Rame-hart*)

A visual record of the drop or bubble created inside the cell was captured using a *Rame-hart* digital video camera mounted outside the viewing chamber of the cell.

4.6.3.4 Data acquisition system

Rame-hart camera connected to the PC allowed the supplied the drop image software with the live image for analysis. The suit is attached to the *Rame-hart* camera, which provided the live image of the drop generated in the cell for further analysis using Advanced Image software.
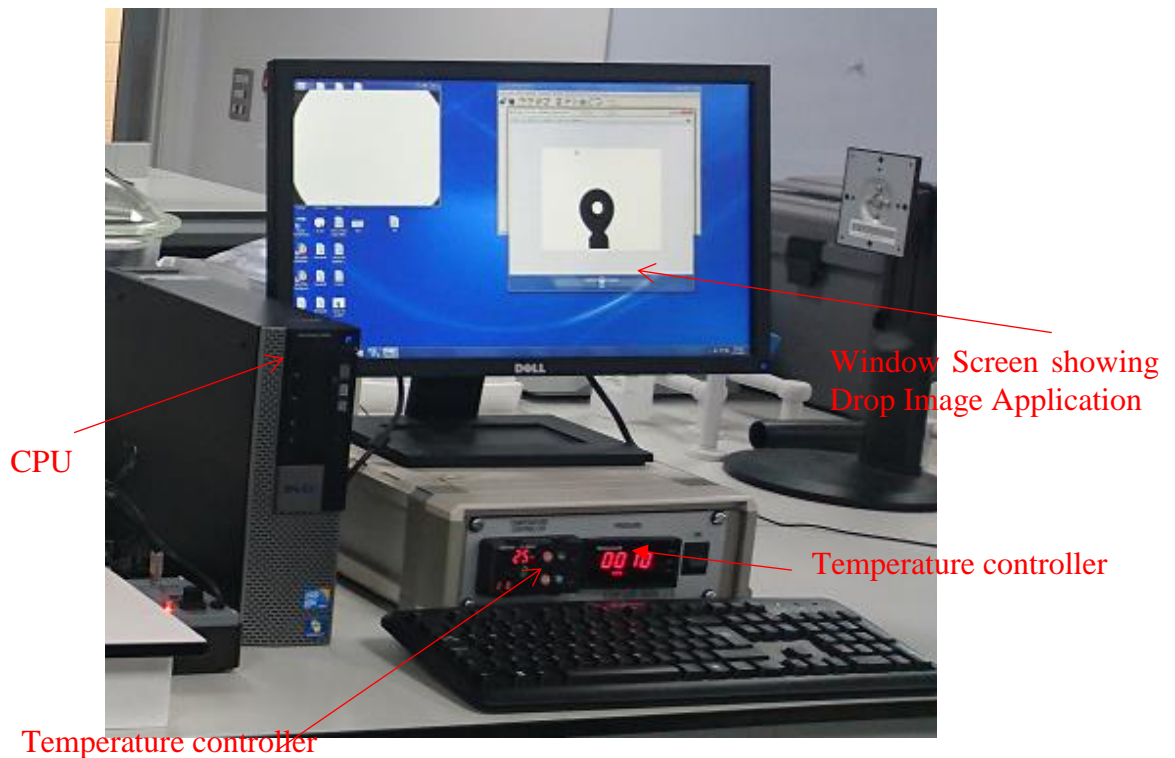
Figure 4.16: Section showing the Data Acquisition System

4.6.4 IFT measurement procedure

4.6.4.1 Charging the IFT chamber with test liquid

The idea of the pendant drop techniques or method for IFT investigation at two-phase system consisitng of two immiscible fluid, is based on suspending a droplet of heavier phase (e.g liquid) surrounded by a lighter phase (e.g vapour) in the equlibrium conditions as shown in Fig. 4.16. However, pendant bubble is employed by hanging bubble of a lighetr phase surrounded by heavier phase as shown in Fig. 4.17.

In the present study, the liquid phase was first feed into the IFT chamber using the automatic pump described in section 4.9.4. The valve supplying air to the pump was turned on by turning it to open position, and the pressure gauge was controlled between 4 – 8 bar range. The pump was then turned on by switching the electrical source by pressing the ON/OFF button into the ON position. The Quizix PumpWorks software was initiated by double-clicking on the Quizix on the desktop, after launching the pump safety operating pressure was set to 1000 psi (700 kPa) and flow rate set to 40 ml/min.

After which, the suction of the pump was placed into the liquid sample container (500ml beaker) and watched for air bubbles as the piston extends, and the air is pushed out of the

cylinder barrel. The valve connecting the automatic pump to the more substantial phase (100cm^3 accumulator) was fully opened (counter-clockwise). Also, valve above the accumulator linking the accumulator and the IFT chamber was open, and the valve connecting the manually operated pump line to accumulator was closed. Valve above the IFT chamber was opened, and the bottom valve connected with the injection needle for the lighter phase was closed. The Back Pressure (BP) regulator was turned entirely counter-clockwise.

The quizix software was then used to control the pump and filled the chamber with the liquid sample. The fill valve button was clicked to open the valve, and deliver valve was click to closed the delivery valve to retract the sample into the pump 2A cylinder and allowed up to the maximum retracted position. Then the fill valve was shut and deliver valve was open to extend the liquid sample into sample cylinder by allowing the piston to reach the maximum extend position. These steps was repeated until the IFT chamber was completely filled with the liquid sample. Finally, the automatic pump was then isolated by closing the valve that connects the pump and the heavier phase accumulator and then switched off from the power source.

4.6.4.2 Pressurizing the IFT Chamber

The chamber was pressurised using both manual pump and back pressure regulator to the desired pressure for IFT measurement at the two-phase system. First, the liquid sample charged into the chamber was used to fill the manual pump cylinder by placing the suction line of the pump into the 500 ml beaker containing the liquid sample. The suction or inlet valve was open. The pump discharge valve was closed and the vacuum barrel of the hand pump was filled with the liquid sample by turning the pump handle fully counter-clockwise. The inlet valve was then closed and discharge valve open that connect the manual pump to the heavier phase accumulator to the manual pump.

To develop the pressure into the chamber the hand pump was slowly turned clockwise and the back-pressure regultor turned counter-clockwise simultaneously. When the required pressure was reached, the valve at the bottom of the outer phase accumulator was closed to allow the pressure to stabilise. The valve below the IFT cell was slowly opened with fine adjustment to control the sample bubble. To de-pressurize the cell, the heater was first turned off, and the cell was allowed to cool off gradually. At room temperature, the remaining pressure was released slowly.

4.6.4.3 Pendant bubble generation

The shape of the bubble can define the interfacial tension value. This technique is known as a mere mathematical approach which is derived from a force balance between buoyancy and gravitational forces. The dimensions of the droplet, d_e and d_s, and the density difference of the adjacent phases are used for interfacial tension measurement using equation (4.5). The IFT measurement procedures were repeated using 2.9, 5.6, 8.2 and 10.7 wt% NaCl solutions at 298.15 – 313.15 K and pressure up to 13.10 MPa. It was also repeated for the NaCl concentrations with PEG 8000 and PEG 8000 + SDS at same temperature and pressure conditions. The results obtained are presented in section 5.4.

4.6.5 Cleaning and maintenance

A very important procedure in achieving reliable results for interfacial tension and the contact angle is a thorough cleaning of the apparatus since contamination of trace amounts can alter the measurement results.

i. The procedure outline in section 4.6.4.1 was flowed using Hexane as the outer phase and sample phase in order to flush out any contaminants from the system.

ii. The valve under the IFT cell was unscrewed using spanner (size 19) which allowed the draining of Hexane. The screwing of the valve followed immediately.

iii. Steps i-ii were repeated with Acetone as the outer phase and sample phase to flush out Hexane.

iv. Steps i-ii were repeated with distilled water as the outer phase and sample phase to flush out the Acetone.

v. After which the cell was charged with distilled water and heating the cell to at least a temperature of 100 ^{o} C for 15 mins, where necessary. Temperature adjustment was achieved using the up and down arrow buttons in the Watlow temperature controller to set the needed temperature.

vi. The system was allowed to cool down to room temperature, before repeating step ii to expel the distilled water from the cell.

4.6.6 Precautions

Precautions must be taken since the IFT cell is a high-pressure/temperature system of which some will aid in having accurate results:

i. Avoid close viewing of a high-pressure cell without protective eyewear in case of a sudden glass window failure.

ii.   It is also advisable to place shields at each end of the window axis, especially if the cell is left unattended.

iii. Do not view the cell directly in line with the window: use the video system to see the cell indirectly, or use a mirror to see the cell at an angle.

iv.   Avoid contact with exterior surfaces of the IFT Cell as it can become very hot.

v.   It is necessary to always change the associated fluid densities in the software. This associated fluid density will ensure an accurate calculation.

vi.   The cell should be cleaned periodically to remove any heavy fluid build-up.

4.7 Error propagation

In the experimental measurements, where there are many measurements of the same quantity, the mean value is defined by equation 4.27.

$$\bar{x} = \frac{1}{N}\sum_{i=1}^{N} x_i \tag{4.27}$$

Where x_i is the ith measured value, and N is the total number of measurements. The uncertainties of each of the experimental value obtained were reported in this work. These calculations were performed using the standard deviation (s.d) given by equation 4.28.

$$s.d = \sqrt{\frac{\sum_{i=1}^{N}(x_i - \bar{x})^2}{N}} \tag{4.28}$$

Hence the absolute and relative errors are defined as presented in equation 4.29 and 4.30, assuming a function f = f(x,y,z).

$$\partial f = \sqrt{\left\{ \left[\left(\frac{\partial f}{\partial x} \right) \delta x \right]^2 + \left[\left(\frac{\partial f}{\partial y} \right) \delta y \right]^2 + \left[\left(\frac{\partial f}{\partial z} \right) \delta z \right]^2 \right\}} \tag{4.29}$$

$$\frac{\partial f}{f} = \frac{1}{f} \sqrt{\left\{ \left[\left(\frac{\partial f}{\partial x} \right) \delta x \right]^2 + \left[\left(\frac{\partial f}{\partial y} \right) \delta y \right]^2 + \left[\left(\frac{\partial f}{\partial z} \right) \delta z \right]^2 \right\}} \tag{4.30}$$

4.8 Chapter summary

The methodology adopted for conducting the present investigation was described in the current chapter. Due to the importance of fluid characteristics in a various industrial application, the liquid sample was characterised based on resistivity, pH and density. Viscosity and interfacial tension are among the most critical parameters on fluid behaviour. These properties have significant effects on fluid flow characteristics and therefore in many hydrocarbon production and processing aspects from porous media to surface facilities. Hence, accurate measurement of the mentioned properties plays a vital role in process development and equipment design. The analysis of salt-water resistivity was conducted using resistivity meter to measure the electrical resistivity and conductivity of the sample. While the pH meter and the weighing balance were used for the pH and density analysis of the salt-water respectively. The pH analysis was conducted to determine the alkalinity of the water while the density is crucial for interfacial tension measurement. Viscometer and pendant drop cell (IFT-10) was used for viscosity and interfacial tension analysis of the system. The viscosity was conducted qualitatively to confirm the fluid behaviour of the water-surfactant in a two-phase system involving gas-liquid. The interfacial tension measurement trials were conducted at the methane-water interface using characterised fluid sample. The invetsigation was to establish the effects of different salts and surfacatant on the interfacial behaviour of the system.

The next chapter provides the discussions and analysis of the results obtained from various experiments in this chapter. The presented results followed the same pattern in which the experimental description followed as shown in Figure 4.1.

Chapter 5: Results and Discussion

5.1 Introduction

This chapter presented the results obtained from the experimental investigation carried out according to the scheme set out in Figure 4.1. According to the aims and objectives of this study, in utilising the novel technique to synthesises the influence of operating conditions representatives of surface facilities on CH_4-H_2O Interfacial Tension (IFT) at the two-phase system in the presence of NaCl, PEG 8000 and SDS. The characterisation of the fluid sample was conducted in terms of resistivity, pH, density and rheology of the brine and brine + surfactants (PEG 8000 and SDS), before the IFT measurement trials. Therefore, the present chapter is divided into three phases, Phase I, Phase II and Phase III, according to the experimental techniques proposed, as described in Chapter 4.

Phase I: The first phase presents the investigation results, the analysis and a discussion of the fluid characterisation, in term of resistivity, pH and density of the salt-water (brine) and a combination of salt-water (brine) + inhibitors (PEG 8000 and SDS) solutions. The density of each prepared brine and brine + inhibitors (PEG 8000 and SDS) were measured and analyses. The density is one of the critical properties in the study of interfacial tension in liquid-liquid and gas-liquid (Chalbaud et al., 2009)(Chalbaud et al., 2009)(Chalbaud et al., 2009)(Chalbaud et al., 2009)(Chalbaud et al., 2009)(Chalbaud et al., 2009)(Chalbaud et al., 2009)(Chalbaud et al., 2009)(Chalbaud et al., 2009)(Chalbaud et al., 2009)(Chalbaud et al., 2009)(Chalbaud et al., 2009)interface.

Phase II: The second phase deals with the results, analysis and discussion on the rheological analysis of the brine + surfactants (PEG 8000 and SDS) solution. Also, the rheological (viscosity) study of the brine + surfactant was conducted to enable establishing the rheological characteristics of the brine + inhibitors. The aim of performing the rheology was to established the structural behaviour of the aqueous solution of brine-surfactant viscosity when subjected to various deformation and classified the fluids.

Phase III: The third phase, which is the final stage of the investigation presents the results, analysis and discussions on methane-water, methane-brine and methane-(brine-surfactants) IFT at various pressure and temperature that may be categorised as normal and extreme pipeline operating conditions.

Therefore, this chapter focuses on addressing and filling in some experimental gaps found in the literature for the IFT of systems composed of methane and water in the presence of NaCl, PEG 8000, and SDS. Prior, to IFT analysis, resitivity, conductivity, pH, density and viscosity

of the aqueous solution containing NaCl, PEG 8000 and SDS were characterised and presented. Further, where the results obtained under various conditions have no significant effects, only at one condition was reported in this section while the remaining were shown in the appendices.

5.2 Phase I: Characterization of the aquous solution

The sample prepared as described in Section 4.2 of this thesis have been characterised in term of resistivity, pH and density. Therefore, this section presented the results and discussion for the investigated results obtained in Phase I. The results consist of resistivity (Ω-m), pH and density, ρ (kg/m^3) for the brine and brine-surfactants at various pressure and temperature conditions.

5.2.1 pH of brine and brine-surfactant-polymer

Figure 5.1 shows the variation of pH value with a concentration of NaCl and 10, 20, 30 and 40% PEG 8000. As indicated in the plot, the initial pH measured for the water without the addition of the NaCl and PEG 8000 shows a value of 6.5, however, the addition of NaCl and PEG 8000 to the system was observed to influence the pH value. The pH value increases from 6.5 to 0% of both NaCl and PEG 8000 to a maximum value of 6.98 at 8.2% NaCl and 40% PEG. However, a decrease in pH value was observed at 10.7% NaCl and 40% PEG 8000 to a value of 6.92 from 6.98 at 8.2% NaCl and the same concentration of PEG 8000. The same behaviour was observed for the other concentrations of NaCl and PEG 8000.

83
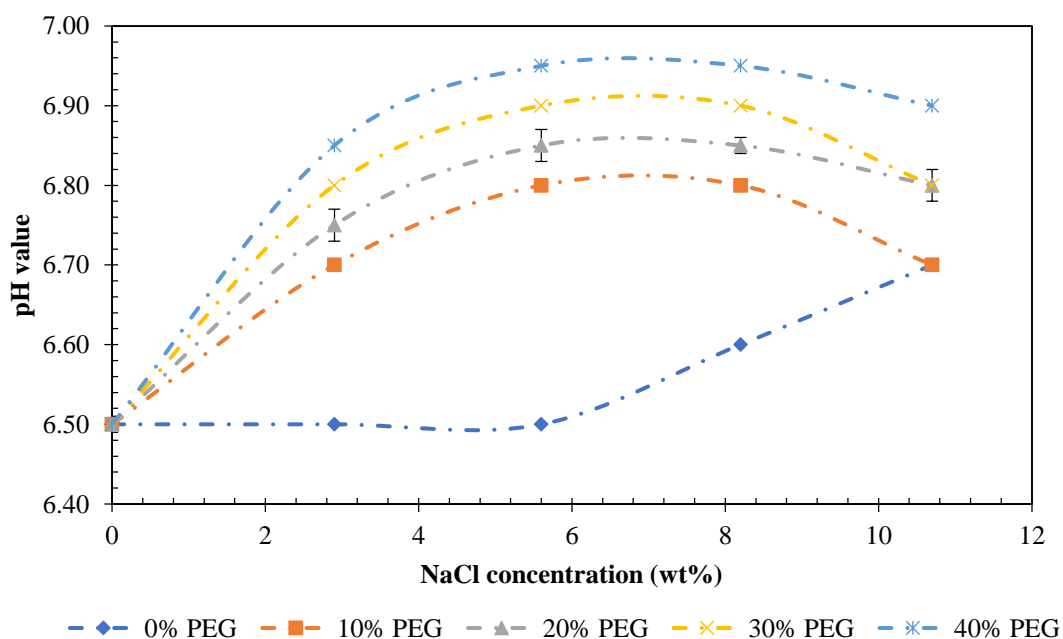
Figure 5.1: pH value of the liquid sample at various concentrations of NaCl and PEG

The increase in pH value due to NaCl was attributed to its the basicity nature and also the chemical nature of the water. The reason is that the basicity characteristic of the NaCl tend to push the H^+ concentration towards the centre value if the concentration is low. Whereas the concentration of H^+ is high, the NaCl then pushed it down towards the neutral value. Thus, the presence of PEG 8000 polymer in the solution does not have a significant effect on the pH value. Instead the concentration of NaCl influences the behaviour. Therefore, in the case of PEG 8000, yet, affect the pH and ionic strength due to ageing, however, in this case, it enhances the NaCl activity to influence the increase or the decrease in the pH value as the case may be. Both pH and ionic strength are essential variables for crystallisation, hence there significance in the determination of scale and corrosion in the tubing or pipeline.

5.2.2 The resistivity/conductivity of an aqueous solution of NaCl and PEG 8000

In trying to highlight the importance of surfactants and brine solution in two-phase pipe flow involving methane and water, it became relevant to establish the characteristics nature of the produced water (liquid) phase and the gaseous hydrocarbon. The assessment of the temperature influence on the electrical resistivity and conductivity of the water phase at various NaCl concentration is required for thermodynamic analysis of a two-phase system involving methane-water and also in separators and other related systems. The methane-water system consisting of a nonconductive gas matrix (methane) and conductive water (brine) system move in a tortuous path when subjected to pressure and temperature conditions. If it is assumed that no transport takes place through the gas matrix and that there is no interaction between the ionic constituents of the liquid water and the gas matrix, the bulk resistivity of the system is then a function of liquid water and tortuosity. The characterisation of the water in terms of electrical conductivity is obtained in the present study as a function of temperature and salinity (NaCl concentration) covering a range of temperatures from 293.15 – 313.15 K and a variety of salinity (NaCl) from 2.9 – 10.7 wt% relevant to pipeline conditions.

Figure 5.2 presented the experimental results obtained for resistivity and conductivity of the water as a function of NaCl concentration at 293.15 K. The resistivities were measured experimentally while the conductivity was calculated as the inverse of the resistivity using equation (4.3). The salt-water resistivity shows a decreasing trend with an increase in the concentration of NaCl, because of the increase in the ion mobility and strength of NaCl.

However, this increase in ionic movement of the electrolytes led to the rise in the conductivity as indicated in the same figure. The electrical resistivity and conductivity of the produced water, depend significantly on the fluid chemistry and the electrolyte concentration. In the quantitative determination of gas saturation, knowledge of salt-water or produce water are essential.

The resisitivity were found to be decreasing with increasing salt concentration from 0.22 Ω-m at 2.9 wt% NaCl to 0.075 Ω-m at 10.7wt% NaCl. This decreased in resistivity signifies the high content of salt concentration in the system. Therefore, it indicates the posibility of corrosion in the case of pipline conditions, due to high presence of salts in the water. Further, corroding pipes represents a good nucleation site for hydrate formation at appropriate temperature and pressure conditions. The electrical conductivity measured shows an increase with increasing the concentration of NaCl from 4.55 to 13.33 S/m at 2.9 wt% and 10.7 wt% NaCl respectively. This increase in conductivity affirmed the strength of ionic concentration in the system, which could cause scaling and corrosion in the system. High electrical conductivity in the system also signifies a potentially harmful accumulation of solids in cooling towers. Conductivity was also investigated as a function of temperature. The results show that in all the concentration of NaCl studied, increasing temperature (298.15, 303.15, 308.15 and 313.15 K) led to a corresponding average increase in 0.74 S/m in the values of conductivity which shows an increase in ionisation.

Figure 5.2: Resistivity and conductivity of water as a function of NaCl concentration

The dissolution of NaCl into Na^+ and Cl^- ion in water led to energetic ion mobility and fluidity of water which influences the conductivity of the water molecules. Many measurements of relatively dilute NaCl solutions have been made, with salinities comparable to those of formation water, at temperatures between 0 °C and 50 °C. There are fewer measurements at higher concentrations and higher temperatures, but even so, NaCl is relatively well-studied compared to many other salts. However, it is essential that the effect of NaCl concentration on the parameters (resistivity and Conductivity) are investigated in the current work, due to their corresponding influence on the surfactant adsorption at the methane-water interface.

From the highlight above, it can be concluded that one of the essential methods for analysing the presence and behaviour of ions in an aqueous solution is the measurement of their electrical conductance. Presence of ions has a significant influence in the surfactant activity at the interface of two immiscible fluid. Figure 5.3 shows the temperature dependence of water conductivity at a different concentration of NaCl. It has been observed as reported in the literature, that the electrical conductance is not a function of NaCl only but also temperature.
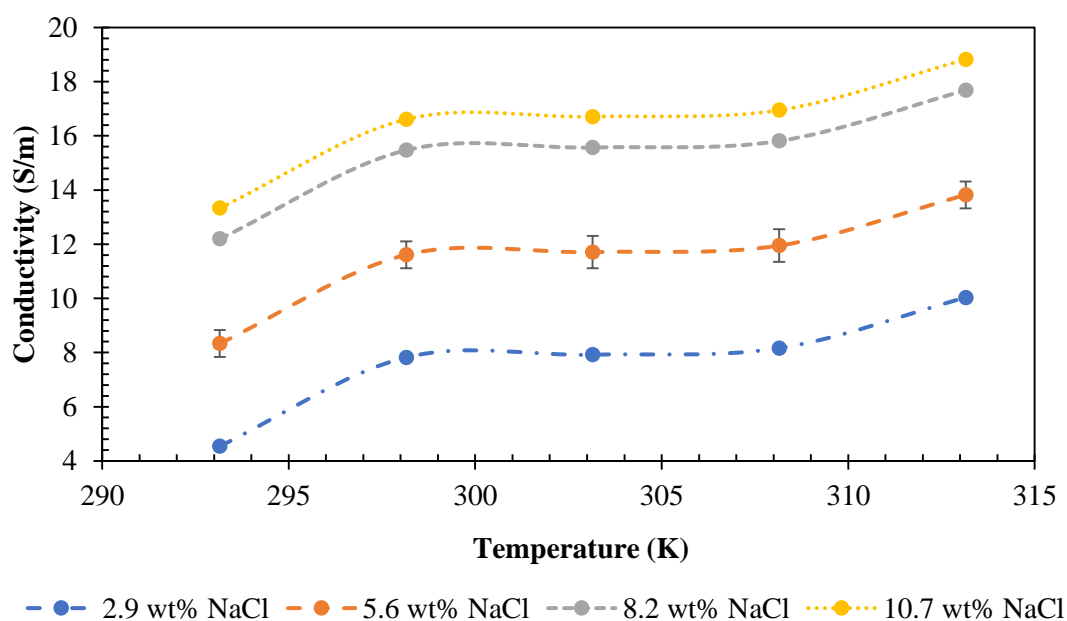
Figure 5.3: Various water salinity (NaCl) conductivity as a function of temperature

Since electrical conductivity has a strong dependence on ionic strength, it is conventional to discuss a related parameter, the equivalent conductivity Λ. The correlation between the water equivalent conductivity and molality of the solute is shown in Figure 5.4. This parameter described the relationship between the Na^+ and Cl^- from the dissociation of NaCl in water and H^+ and OH^- from the water molecules.
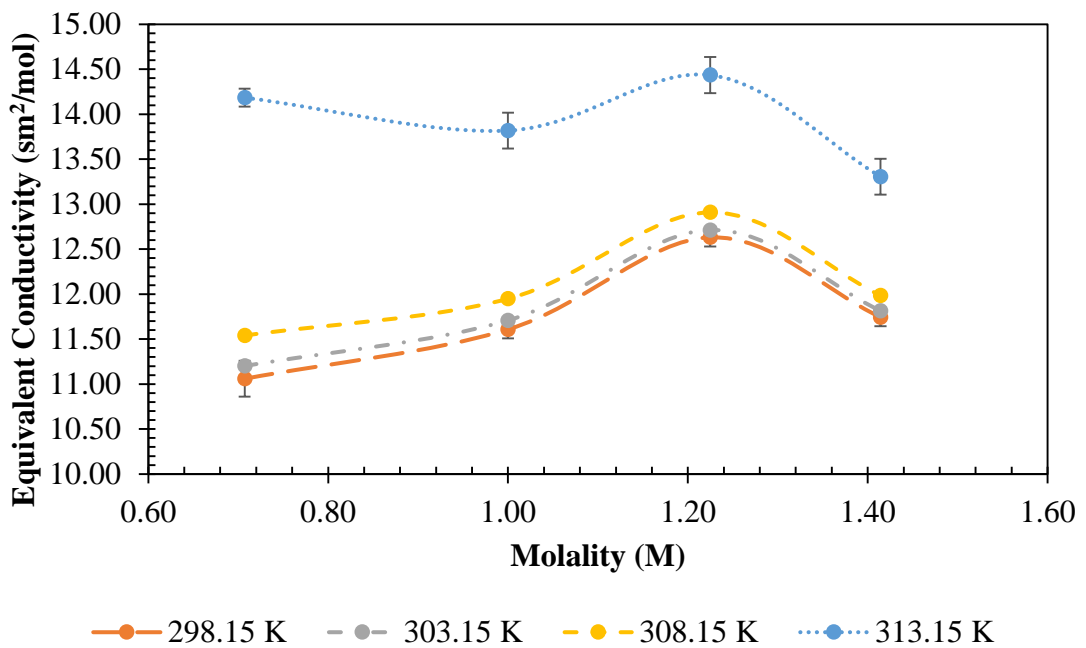
Figure 5.4: Equivalent conductivity as a function of square root of molality

Figure 5.5 shows the influence of adding 10% PEG to the brine solution on the conductivity and the resistivity of the system. As indicated in the plot, there is an average increase of 0.062 Ω-m in the values of resistivity while compared to that obtained in the absence of PEG 8000. Also, the conductivity responds with an average decrease of 2.808 S/m as compared with the values obtained without PEG 8000. This behaviour suggested the polydispersity of the sample due to the presence of PEG 8000 in the NaCl solution. Saeki, Kuwahara, Nakata, & Kaneko (1977) described the effects of PEG on critical solution and phase separation temperature in water-NaCl. However, is possible that PEG 8000 interferes with the activity of Na^+ and Cl^- ions present in the solution, thereby leading to the corresponding decrease in the conducvity of the system. The amount of the ions present and their mobility were responsible for the electrical conductance of the water. However, adding PEG 8000 to the system does not have the significant effects on the parameters as compared to NaCl concentration and temperature variation.
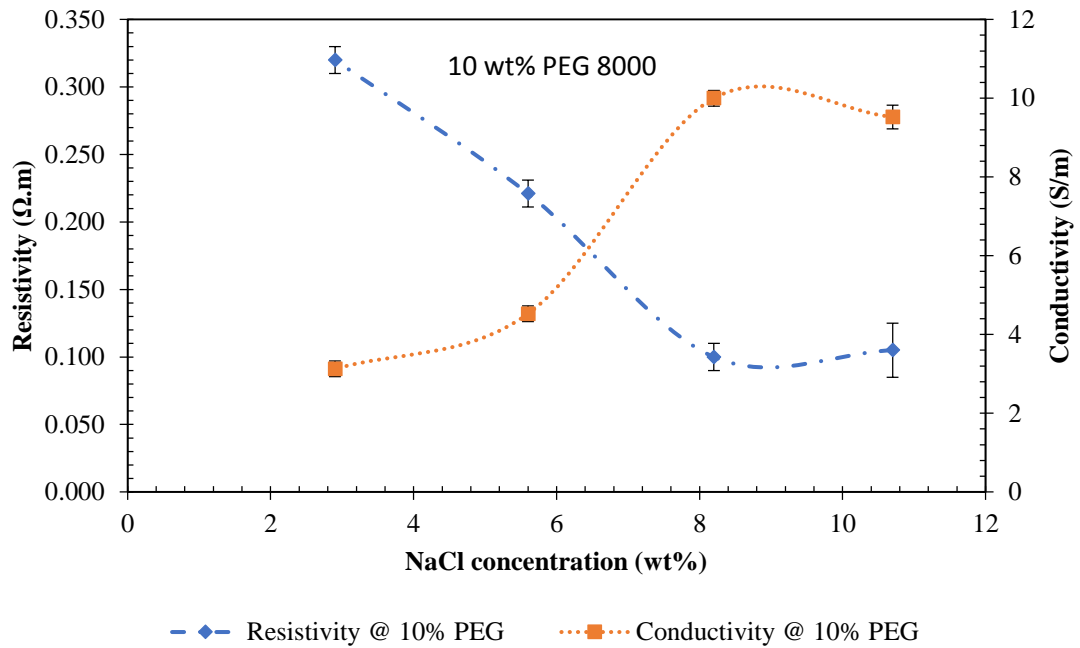
Figure 5.5: Resistivity and conductivity at different concentrations of NaCl at 10% PEG

The produce water properties vary from one reservoir to another as well as within formations, and this affected the hydrocarbon gas and liquid transportation along the down-hole tubing and surface and sub-sea pipeline, due to corrosion and other associated problems with the presence of salts in the system. Hence their significance in determining the multiphase flow pattern in a pipeline. The composition of the produced water depends on some parameters, including depositional environment, mineralogy of the formation, its pressure and temperature history and the influx or migration hydrocarbon. Therefore, water properties can change over time as the water and rock interact, and as reservoir fluids are produced and replaced with water from other formations, injected water or other injected fluids.

5.2.3 The density of an aqueous solution of NaCl and PEG 8000

The density of the aqueous solution containing 2.9, 5.6, 8.2 and 10.7 wt% NaCl was measured at the different experimental temperature and plotted in Figure 5.6. It was found that the density of the aqueous solution increases as the NaCl concentration increases and decreases as the temperature increases. It is pertinent that increasing the mass of the solution by dissolving NaCl increases the density of the system. However, increasing the temperature of the system, led to a corresponding expansion of water molecules. Hence the decreased in the density.
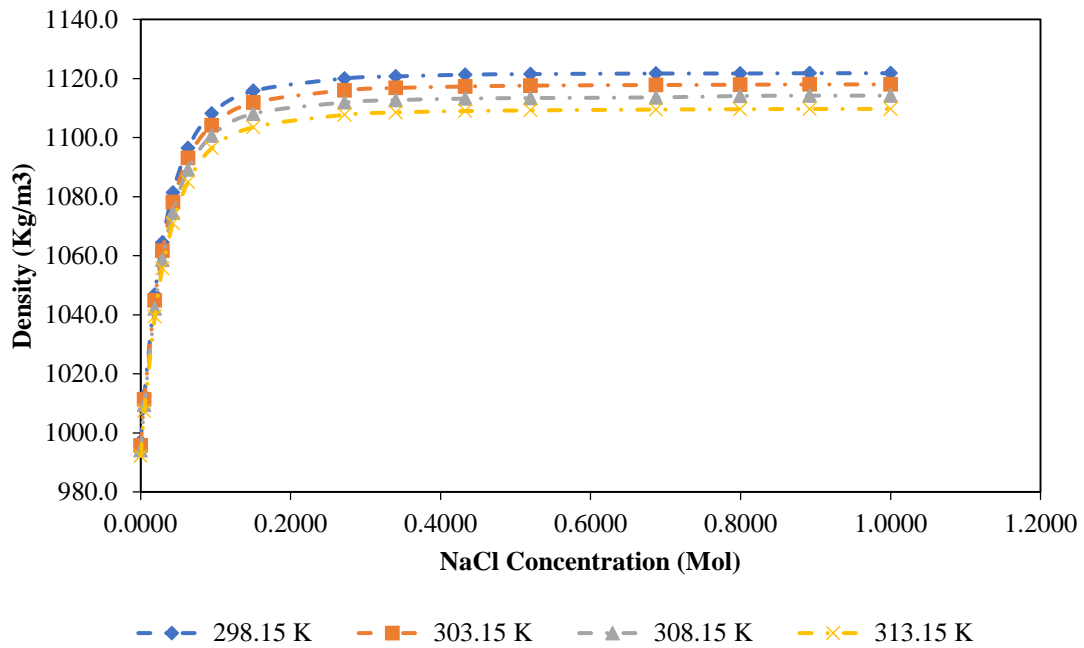
Figure 5.6: Effect of NaCl concentration on the density at a various temperature

Figure 5.7 and Figure 5.8 shows the results obtained for the density of PEG 8000 and PEG 8000 + NaCl solutions respectively. Figure 5.7 shows the density results obtained for various concentration of PEG 8000 at 298.15, 303.15, 308.15 and 313.15 K. There is an increase in the density as the concentration of PEG 8000 increases at both temperatures under investigation. This pattern shows a linear variation in the density values with the PEG 8000 concentration at each temperature. While in Figure 5.8 the densities of the binary solutions of PEG 8000 at various concentration and NaCl at a concentration of 2.9, 5.6, 8.2 and 10.7 wt% is shown. The almost linear variation was also observed. Therefore, both PEG 8000 and NaCl increases the density of water with the significant effect seen due to the presence of NaCl. The significant impact due to NaCl is as a result of the increase of the mass of the water resulting from the dissolution of NaCl in the water without affecting the volume of the water. However, in the case of PEG 8000, its dissolution in water affected both mass and volume of the water, with more impact on the mass increased. Hence the density change due to PEG 8000 concentration is less significant, compared to the presence of NaCl in the solution.
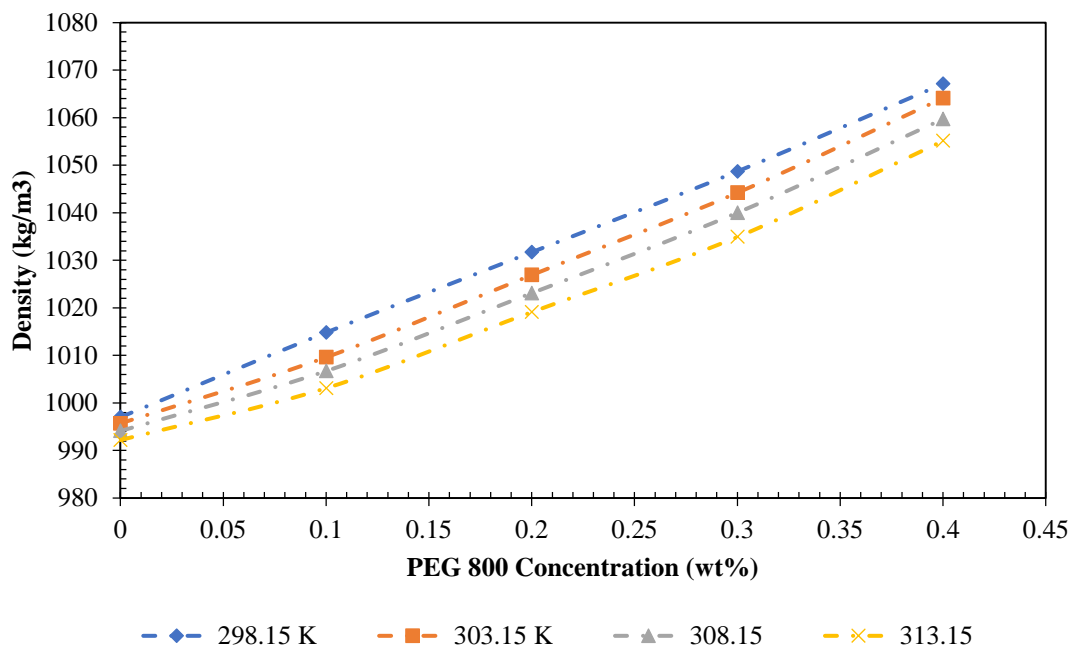
Figure 5.7: Density variation with PEG 8000 concentration at a different temperature
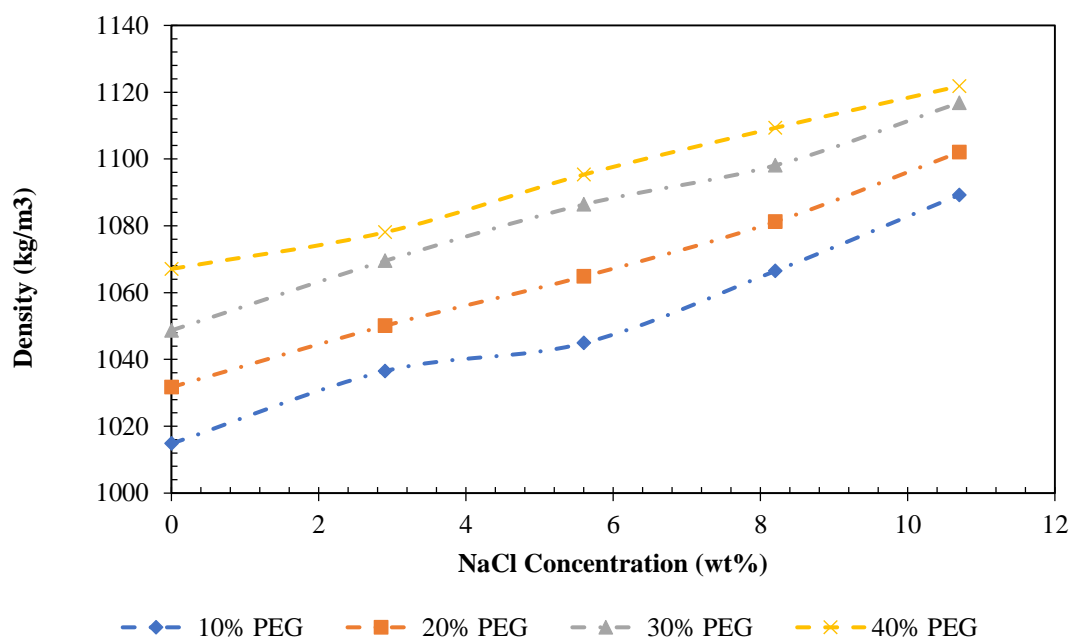
Figure 5.8: Experimental density with a concentration of NaCl and PEG 8000

Numerous experimental methods have been applied to aqueous PEG solutions to ascertain the properties of the water; the number of water said to be associated per monomer unit varies from 1 to more than 10. However, one of the most remarkable properties is the lack of effect on water activity. Even when significant fractions of the volume are filled with PEG, relatively small changes in water activity are seen (Lüsse & Arnold, 1996).
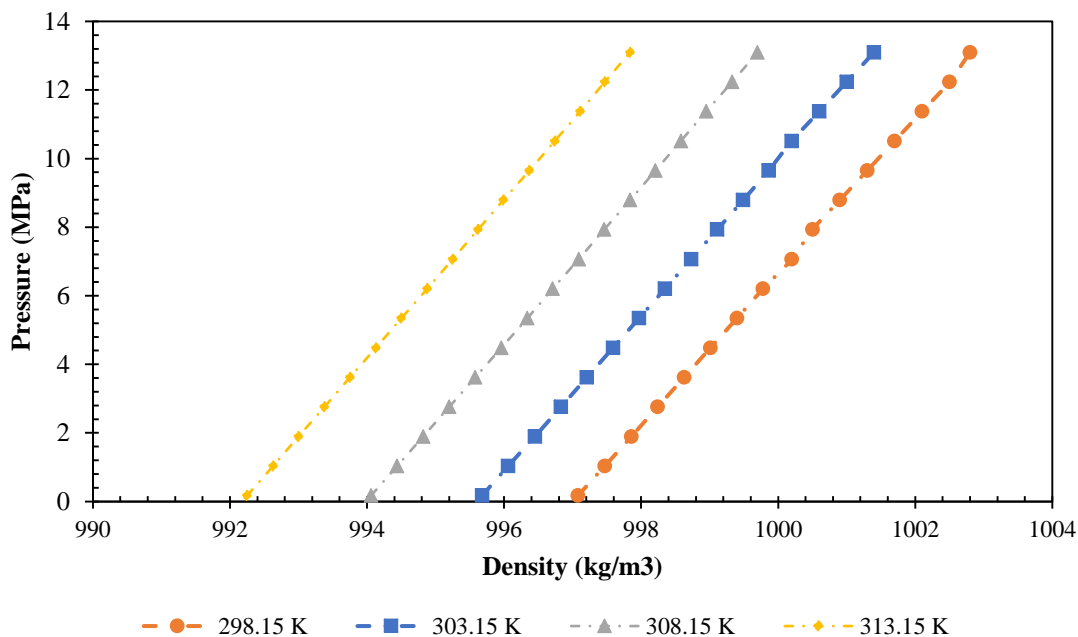
Figure 5.9: Pure water density variation with pressure at a given temperature

5.3 Phase II: Rheological characteristics of the polymer-surfactant in water

The rheology test was performed to understand the physiognomies behaviour of the polymer-surfactant. In this work, PEG 8000 and SDS are the polymer and surfactant used. The apparent viscosity of the PEG 8000 and SDS binary mixture (Polymer-surfactant) with various concentration of NaCl at 298.15, 303.15, 308.15 and 313.15 K at atmospheric pressure were investigated. The apparent viscosity tests were conducted to ascertain and classified the behaviour of PEG 8000-SDS mixtures in water as a function of shear stress and shear rate. The detailed descriptions of the facility, procedure and method used in the laboratory as well as the details on the materials, compositions and preparation of the mentioned fluids were presented in Chapter 4.

PEG 8000 was selected due to its limited information in the literature, for this investigation. In order to study the influence of PEG 8000 and SDS concentration on the apparent viscosity, solutions and the evolution of the degree of a solution of the PEG 8000 in the water, different samples with 10, 20, 30 and 240 wt.% PEG 8000 concentration were processed. The PEG 8000 solution is categorised as a homogenous or simple liquid, after dissolving in water with or without the addition of NaCl, to form a stable phase. Various concentration of PEG 8000 solution was subjected to different deformation and the results obtained for shear stress, and

dynamic viscosity as a function of shear rate are presented and discussed in the following sub-sections.

5.3.1 The apparent viscosity of PEG 8000

The apparent viscosity tests were performed on the above PEG 8000/SDS solutions and different concentration of NaCl. The temperature for these series of apparent viscosity tests were 298.15, 303.15, 308.15 and 313.15 K at atmospheric pressure.

The experimental viscosity values for the PEG 8000 at a various concentration and as a function of shear rate are plotted in Figure 5.10. The apparent viscosity at each shear rate increases noticeably with PEG 8000 concentration. However, in all cases, the viscosity decreases with increase in shear rate, the solutions exhibit shear thinning behaviour at rates > 10 while at a lower rate the curves approach the Newtonian plateau. In all the concentration, as shown in Figure 5.11 over the range of σ investigated the various PEG 8000 solutions behaves as Newtonian fluid - shear stress is linearly increasing with increasing (σ). Figure 5.10 Below $\sigma \approx 111$ s^{-1}, a sharp decrease in viscosity was observed as seen in Figure 5.10, while above that, the viscosity is constant being $1.1.7 \pm 0.1$, 3.7 ± 0.2, 10.8 ± 0.3 and 10.9 cP, for 5, 10, 20 and 30% PEG 8000 respectively.
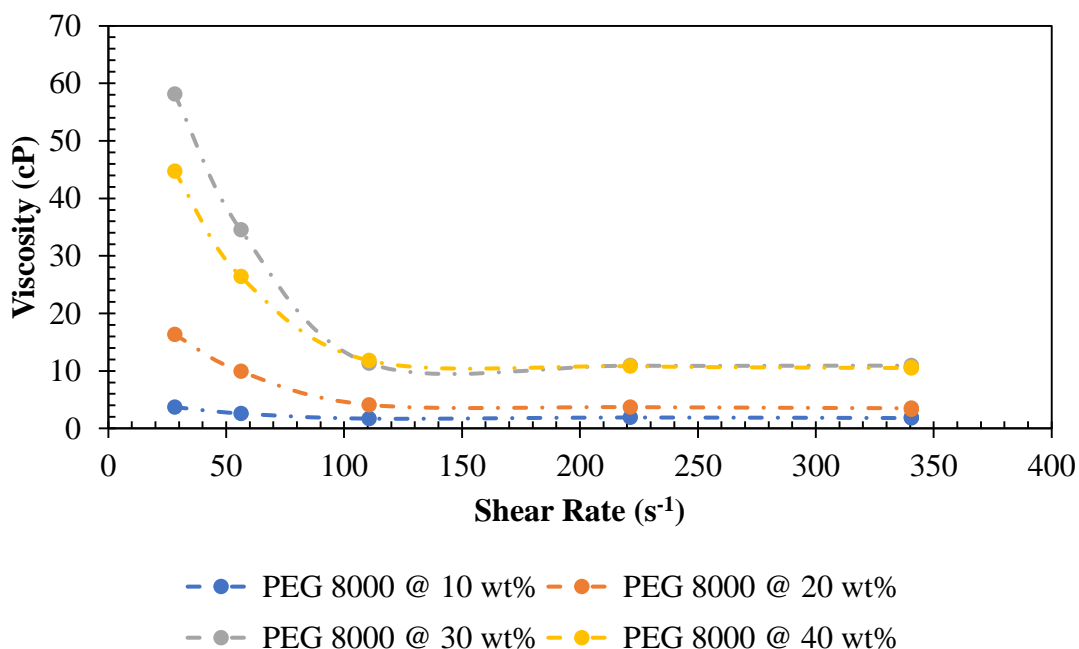
Figure 5.10: Dependence of dynamic viscosity on the shear rate of various concentration of PEG 8000 at 298.15K

It is pertinent that the shear rate causes the structure of the PEG 8000 solution to partially breaks causing a reduction of viscosity. Therefore, it has been established that the aqueous

solution of PEG 8000 below specific values of shear rate (σ) behave as a Newtonian fluid. However, when the shear rate exceeds a particular value, which depends on PEG 8000 viscosity, PEG 8000 show abnormal property - immediate flow cessation that is inherent to dilatant liquids during the sharp increase of viscosity as reported by Brikov, Markin, & Sukhoverkhov (2015).

Figure 5.11 shows the values of shear stress (τ) of various concentration of PEG 8000 as a function of shear rate at 298.15 K and atmospheric pressure. In all cases, two regions was observed: the first one comprised between the onset of the transient test and the maximum shear stress, and the second one ranging between this maximum and the equilibrium or steady-state shear stress. The shear stress increases for example at 30 wt% PEG 8000 from 1.1 Pa.s at 28.1 s^{-1} to 7.6 Pa.s at 340.5 s^{-1}.
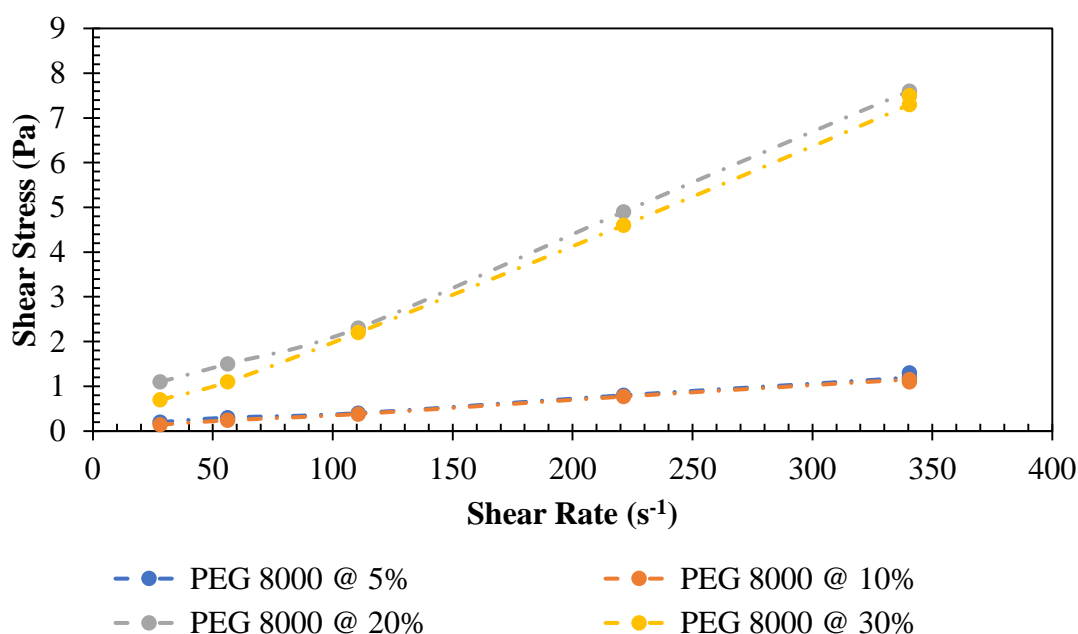
Figure 5.11: Dependence of shear stress on the shear rate of various concentration of PEG 8000 at 298.15K

Similar behaviour was seen for the remaining concentration investigated, but lower values were obtained at 10 and 20 % PEG 8000. However, both levels show a Newtonian fluid behaviour with an increase in shearing rate.

5.3.2 Effects of NaCl concentration on 10% PEG 8000 viscosity

The apparent viscosity of the 10wt% of PEG 8000 along with the presence of NaCl at various concentration is plotted in Fig. 5.8 and also in Figure 5.12, the dependence of shear stress on shear rate is shown at 298.15K.

93

In Figure 5.12, the apparent viscosity as a function of shear rate was presented in the presence of 2.7 and 8.2 wt% NaCl. A slight decrease of the viscosity was observed due to the presence of NaCl. However, an abrupt drop of the viscosity was observed at a shear rate below $\gamma \approx 111$ s^{-1}, and 5.6 and 10.7 wt% NaCl led to an increase in the viscosity with a similar reduction at below $\gamma \approx 111$ s^{-1} for both trends. However, at a shear rate above $\gamma \approx 111$ s^{-1}, the dynamic viscosity maintained a constant pattern with increasing shear rate. Rheology of PEG 8000 at 10% with a different concentration of NaCl has been established at a temperature of 298.15

K.
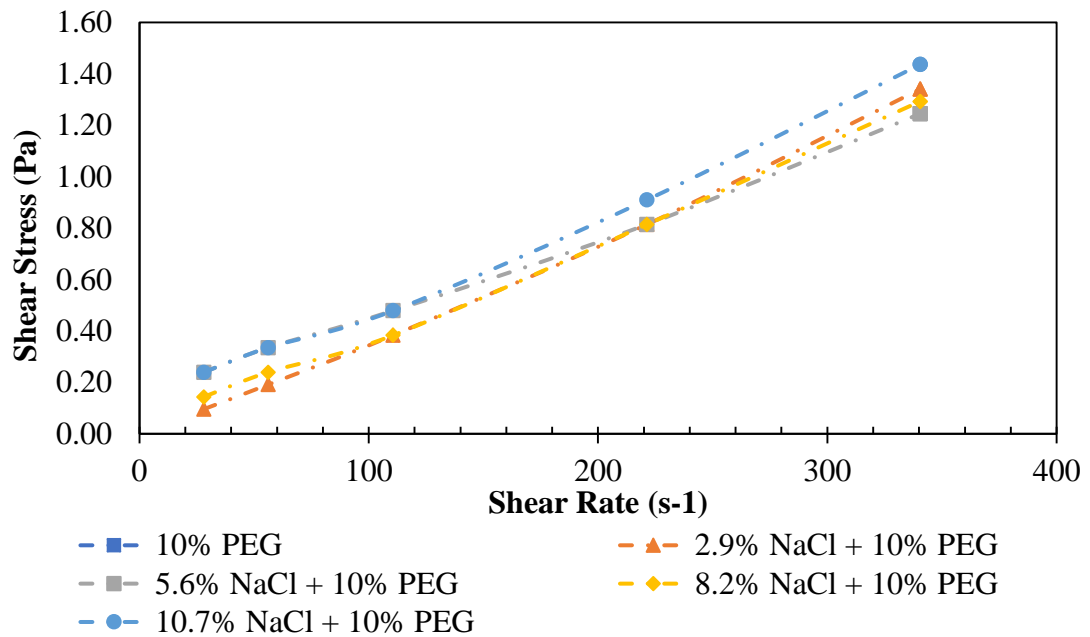
Figure **5.13**, γ increase linearly with an increase in shear rate.
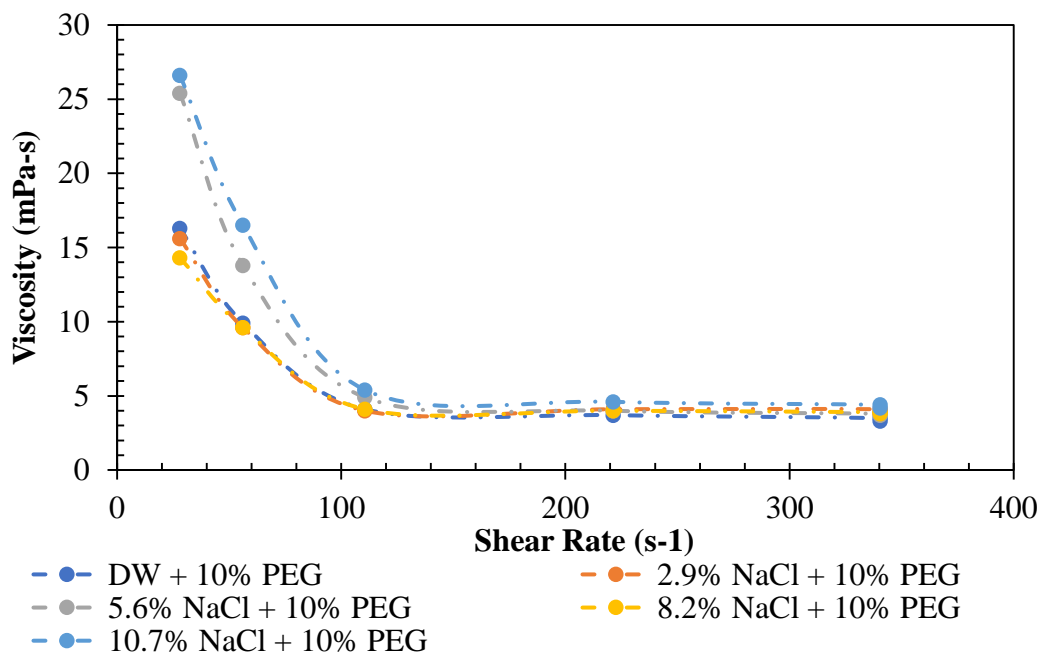
Figure 5.12: Viscosity as a function of shear rate of 10% PEG 8000 and different concentration of NaCl at 298.15 K
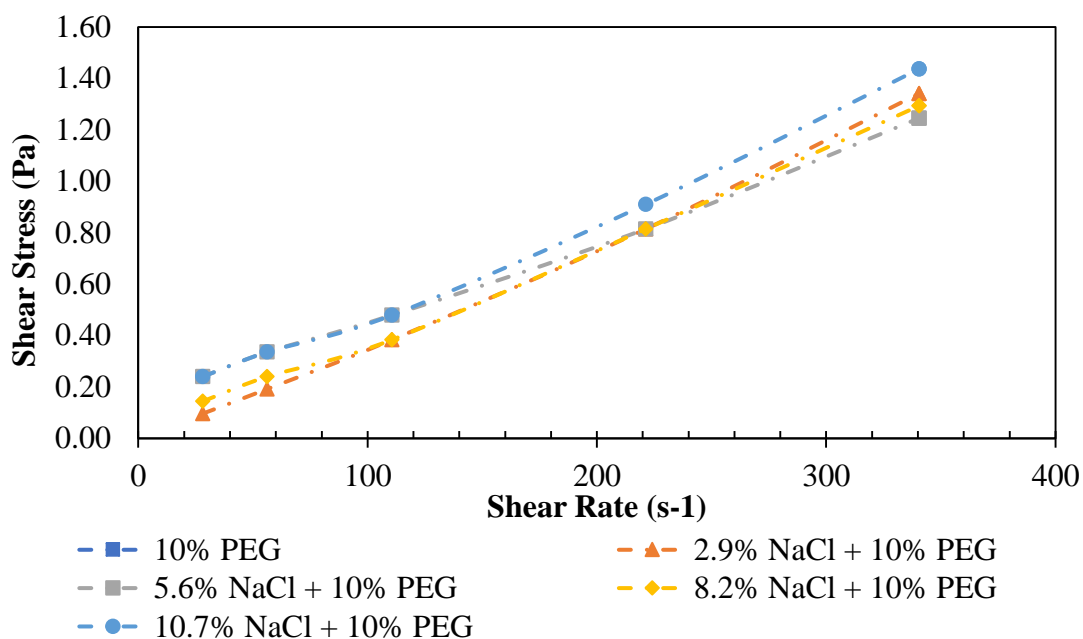
Figure 5.13: Shear stress as a function of shear rate of 10% PEG 8000 and various concentration of NaCl at 298.15 K

The shear stress of the PEG 8000 solution in both scenarios increases with an increase in shear rate, whereas the viscosity decreases with increasing shear rate. The decrease in the solution viscosity due to variation in shear rate represents a shear thinning behaviour as such the PEG 8000 + H_2O is characterised as non-Newtonian flow and a pseudo-plastic fluid. The increase in shear stress, due to increase in shear rate also confirmed the solution to be a pseudo-plastic fluid. It was observed clearly that presence of NaCl does not affect the fluid behaviour as it shows Newtonian fluids as can be seen in

5.3.3 Effects 0.5wt% SDS on 10% PEG 8000 apparent viscosity

Figure 5.14 shows the change in viscosity of the PEG 8000 (10%) solution in the presence of NaCl due to the variation of shear rate at a temperature of 298.15, 303.15, 308.15 and 313.15 K respectively. The viscosity of the sample decreases with increase in the shear rate, as indicated for example in Figure 5.12. This decrease in viscosity due to increase in shear rate shows a shear thinning behaviour as indicated for example in Figure 5.12. This behaviour of the viscosity due to the variation of shear rate represents a non-Newtonian flow, and the PEG 8000 in brine was classified as pseudo-plastic fluid. The viscosity decreases drastically as the shear rate increases from $28.2 - 110.6$ s^{-1} in both cases. At the higher shear rate, the viscosity fluctuated and tried to be settled at a constant value in all the cases observed. More so, the temperature increases decrease the viscosity of the sample as seen from the Figures.
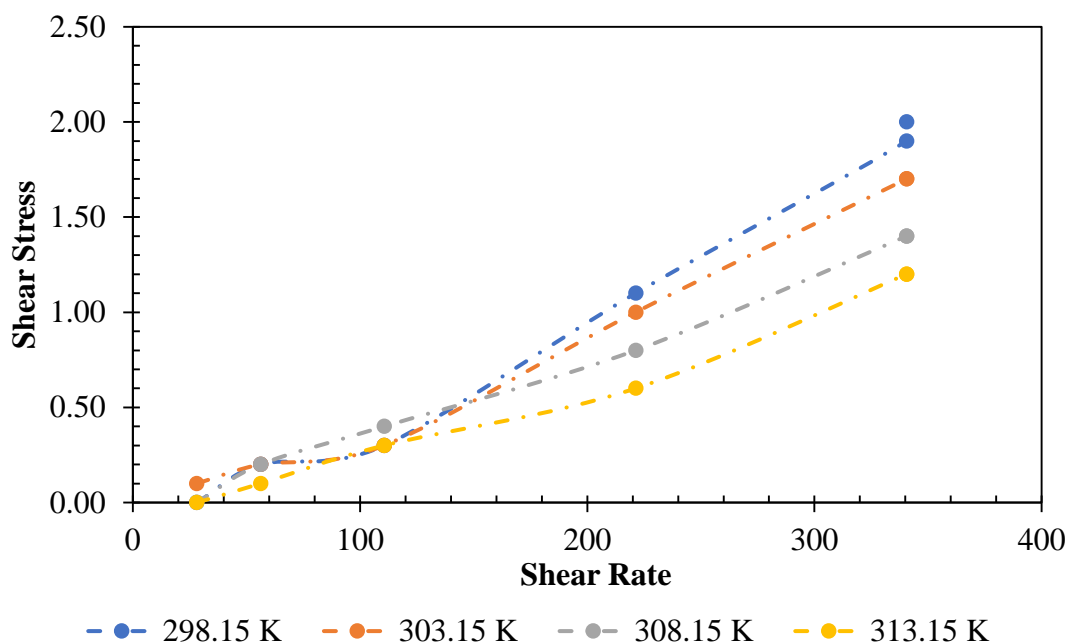
Figure 5.14: Dependence of shear stress of 10% PEG + 0.5% SDS on the shear rate at a various temperature

Figure 5.14 shows the shear stress dependence on the shear rate for 10% PEG 8000 + 0.5%SDS at various temperature. The sample followed Newtonian behaviour with some fluctuation or unstable at a lower shear rate between 28 – 120 1/s was observed. Therefore, the addition of SDS into the solution has no effect on the rheology at the higher shear rate.

5.4 Phase III: Interfacial tension (IFT) of methane-water two-phase system

The IFT of methane was measured against distilled water, brine and polymer-surfactant. Three different sets of brines were prepared at 2.9, 5.6, 8.2 and 10.7 wt% NaCl content. Also, four different sets of polymer solution (PEG 8000) were prepared at 10, 20, 30 and 40 wt%, SDS was also combined with PEG 8000 at each prescribed concentration in the presence or absence of NaCl. The density of methane, brines and polymer-surfactant mixtures were required to calculate the IFT from the drop profile using ADSA. The density of the aqueous solution was measured and are presented in Table 5.1. The density of methane and other related properties were taken from the supplier fact sheet (BOC) and are reported in Table 5.2.

Table 5.1: Density of aqueous NaCl solution as measured using a density meter

Concentration (wt%)	Density (kg/m^3)
2.9	1017.2
5.6	1037.01
8.2	1054.48
10.7	1073.1

Table 5.2: Some physical properties of methane used in this work

Melting Point (°C)	Boiling Point (°C)	Critical Temperature (°C)	Vapour Pressure (MPa)	Vapour Density	Relative Density	Dynamic Viscosity (mPa.s) @ 20 °C
-182.47	-161.48	-82.0	62.12	0.6	0.42	0.109

5.4.1 Methane-water (CH$_4$-H$_2$O) IFT

The interfacial tension (IFT) of the methane-water system was measured to validate the method adopted in conducting the investigation with the literature data as well as for comparison with the results obtained using aqueous solution and surfactants. The comparative results observed the effect of both salts and surfactants. Further, the effect of system pressure and temperature were also investigated by measuring the IFT at different pressure and temperature.

The experiments were performed over a temperature range of 298.15 to 313.15K and pressure of 0.72 – 13.1 MPa. The generated results for brine and brine+surfactant were then compared with the results of the methane-water systems to investigate the effect of salinity and surfactant on IFT. Also, the effect of pressure and temperature were observed and reported.

5.4.2 Pressure and temperature influence on IFT

Figure 5.15 and Figure 5.16 displays graphically, the IFT measured at various pressure and temperature for a CH$_4$ bubble in H$_2$O. The pressure ranges from 0.172-13.10MPa while temperatures were at 298.15, 303.15, 308.15 and 313.15 K, respectively. In general, the IFT was observed to be decreasing as both pressure and temperature increases. This behaviour indicated that at two-phase system involving CH$_4$ and H$_2$O at typical pipeline operating conditions the IFT decreases as pressure increases at a given temperature, and temperature

increases, although the pressure was found to have more significant effects than the temperature. This behaviour indicated that as the pressure increases more of the CH_4 molecules tends to concentrate at the surface of the water, thereby having more active transfer across the interface association tendency in the water. Moreover, the CH_4 transfer across the interface enhances as the IFT decreases.
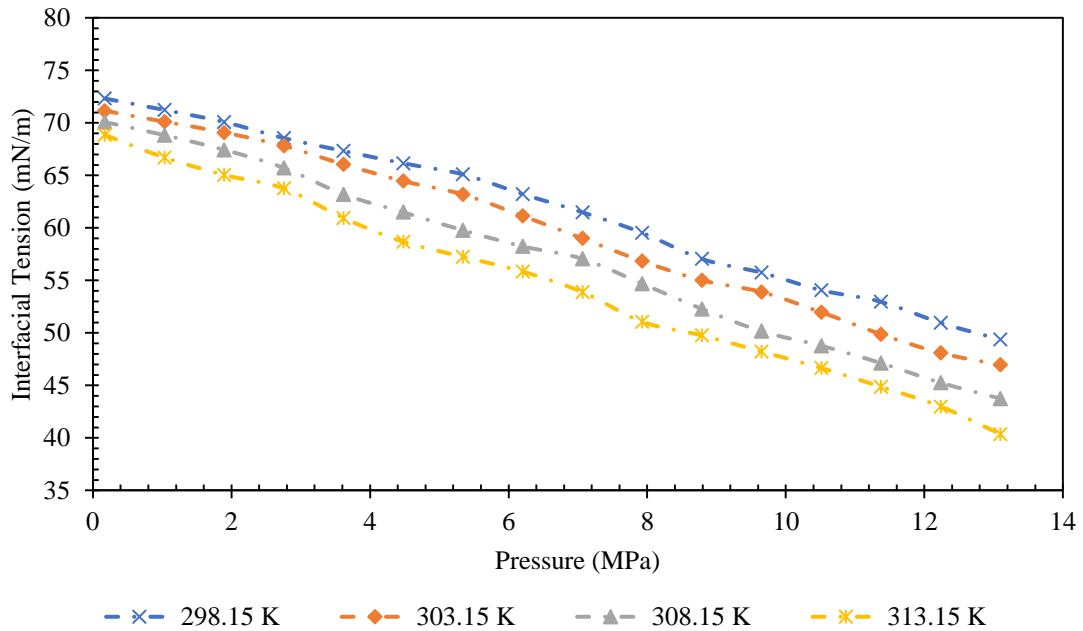
Figure 5.15: Effect of pressure and temperature variation on IFT of methane-water (CH_4-H_2O) two-phase system
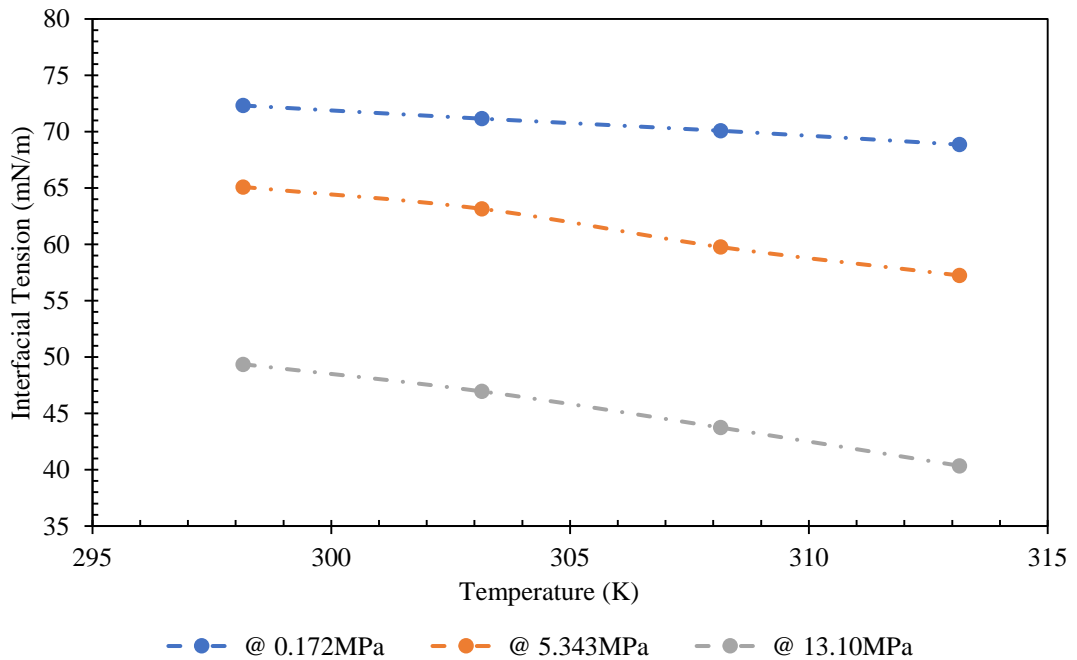
Figure 5.16: IFT response to temperature variation at a given pressure for CH_4-H_2O two-phase system

The results obtained for gas-liquid IFT responses to pressure is entirely different from some of the liquid-liquid systems where pressure increases led to a rise in the IFT (ref). In both system, however, the IFT response to pressure and temperature depend on the system compositions. Several data on CH_4-H_2O IFT at wide range of pressures and temperatures have been reported (Ghorbani & Mohammadi, 2017; Hayama et al., 2017; Jho et al., 1978; Kashefi, Pereira, Chapoy, et al., 2016; Khosharay, 2015; Khosharay & Varaminian, 2014; Peng et al., 2009b; Ren et al., 2000; Rushing et al., 2008; Sachs & Meyn, 1995; Schmidt, Folas, & Kvamme, 2007; Yasuda et al., 2016). However, only Khosharay & Varaminian (2014); Yan, Zhao, Chen, & Guo (2001); and Yasuda, Mori, & Ohmura (2016) measured isotherms are adequately close for correlation with the IFT data from the present study. Hence, Figure 5.17 compared the IFT values obtained between the present study and the literature.
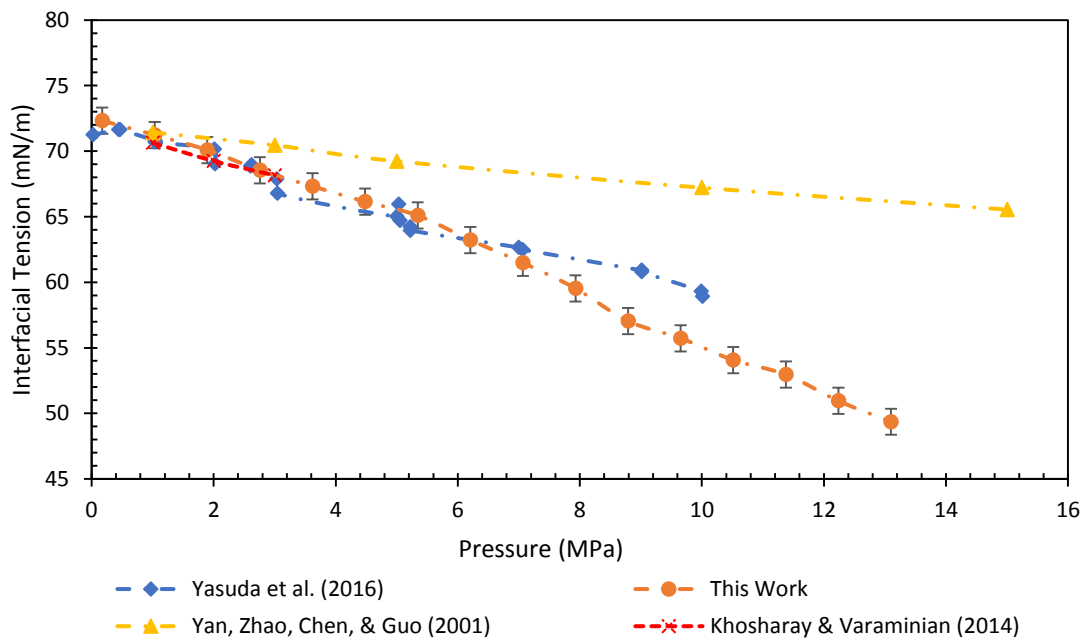
Figure 5.17: A comparison of IFT response to pressure variation at 298.15 K for the CH_4-H_2O

This work is in good agreement with the data of Khosharay & Varaminian (2014) and Yasuda et al. (2016), except for Yan et al. (2001) at lower pressure. Though, the results obtained from Yasuda et al. agree well with this work with an average deviation of 1.03 mN/m above 7.02 MPa at 298.15 K. However, there is significant disparity while compared to the data obtained by Yan et al. (2001) within the same investigated conditions and uncertainties of the present study. Therefore, this comparative analysis of the IFT results obtained validated both the methodology and the equipment employed for the current investigation.

5.4.3 Effect of salinity

The influence of salinity on CH_4-H_2O IFT was investigated by first evaluating the presence of NaCl at various concentration. The NaCl content used is 2.9, 5.6, 8.2 and 10.7 wt% NaCl for simplicity and the results obtained are plotted in Figure 5.18. Presence of NaCl led to a corresponding increased in the IFT values at the experimental condition investigated. This behaviour has been depicted in Figure 5.18. Generally, the addition of 2.9, 5.6, 8.2 and 10.7 wt% NaCl in the water, causes a corresponding average increase of 1.4, 2.57, 3.51 and 4.24 mN/m, respectively, in the IFT values obtained. The increased in the IFT values was observed by comparing the results with that of CH_4-H_2O in the absence of NaCl. Moreover, the variation in the IFT values for the CH_4-H_2O in the presence of NaCl with the experimental pressure and temperature was found to be in a similar pattern to that of the CH_4-H_2O without NaCl as stated earlier.
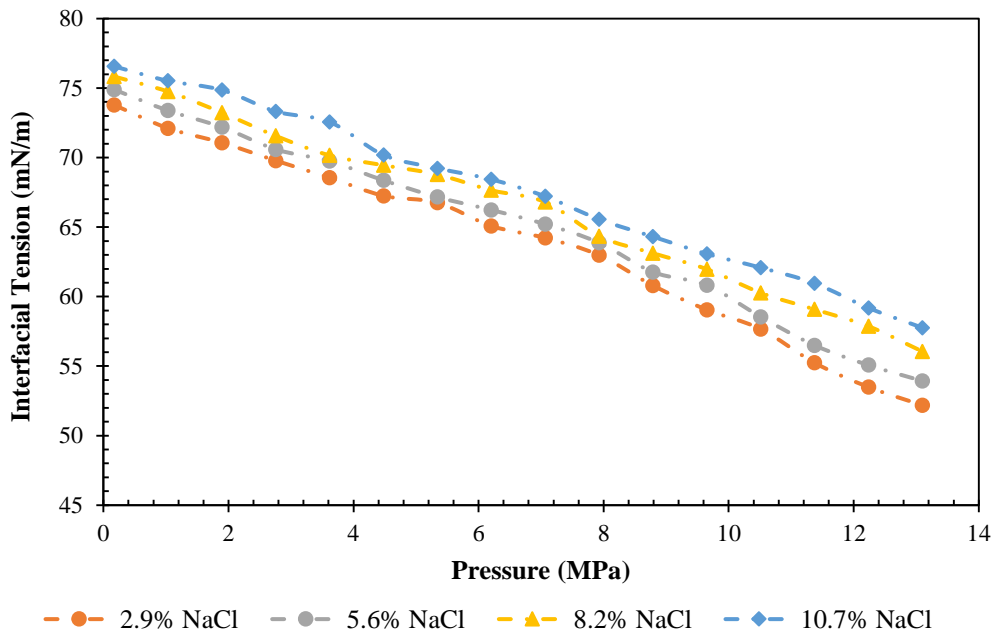
Figure 5.18: Influence of NaCl concentration on CH_4-H_2O IFT at a variable pressure at 298.15K

The modification of the orientation of a first and second layer of the water molecules at the surface by the localisations of cations and anions that may be present close to the interface causes the increase of the interfacial tension and the resident time of the of interfacial water molecules(C. Zhang & Carloni, 2012). Hence, the presence of the Na^+ and Cl^- at the various ionic strength (concentration of NaCl) are responsible for the increase in the interfacial tension of the CH_4-H_2O system presented in the current investigation (see Figure 5.19). However, both pressure and temperature affected the way both ions change or modify the first two layers of the water molecules from the interface region.

Figure 5.19 shows the variation of the IFT due to an increase in NaCl concentrations at pressure of 0.172, 5.343, and 13.1 MPa and at system temperature of 298.15 K. Lima, De Melo, Baptista, & Paredes (2013) described the increase of IFT due to the presence of different salts at various concentrations of a system containing an aqueous phase. Lima et al. (2013) conducted their investigations based on the concentration profile of different ions in the locale of the interface and at a given temperature and pressure.
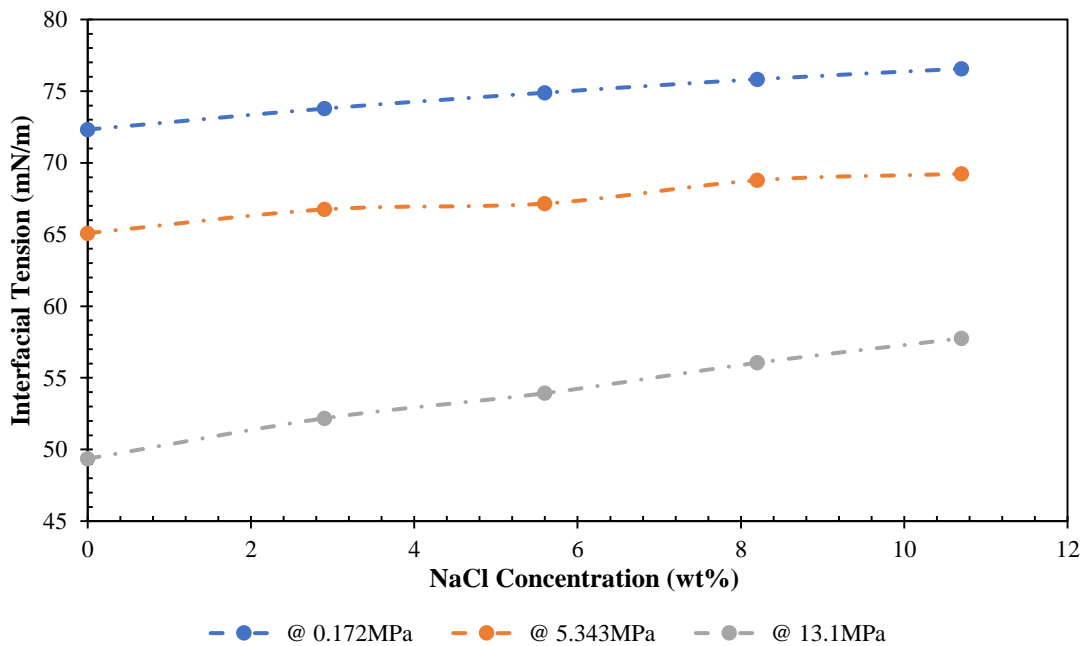
Figure 5.19: Effect of NaCl concentration on methane – brine IFT measurement at 298.15 K at a various pressure

To examine the accuracy of the method employed for the determination of CH_4-H_2O IFT obtained in which the liquid system contains a certain amount of NaCl, the results of the present work was compared against the literature. Figure 5.20 shows the comparison of the IFT results obtained for the methane-water system between current investigation at 5.6 and 10.7 wt% NaCl and Kashefi, Pereira, Chapoy, et al. (2016) at 5.01 and 10.02 wt% NaCl. It was assumed that the difference in the concentration of the NaCl between the two studies is insignificant. There is a significant deviation between the current investigation and that of Kashefi, Pereira, Manuel, et al. (2016), which could be attributed to the method employed and also the accuracy of the pendant bubble created. However, the IFT results agreed to the fact that both pressures, temperature and presence of NaCl has a significant effect on the behaviour of the methane-water phase boundary. The increase in pressure and temperature has a decreasing impact on the IFT at methane-water interface while the increase in the

concentration of NaCl has a corresponding increasing effect on IFT at the methane-water interface.
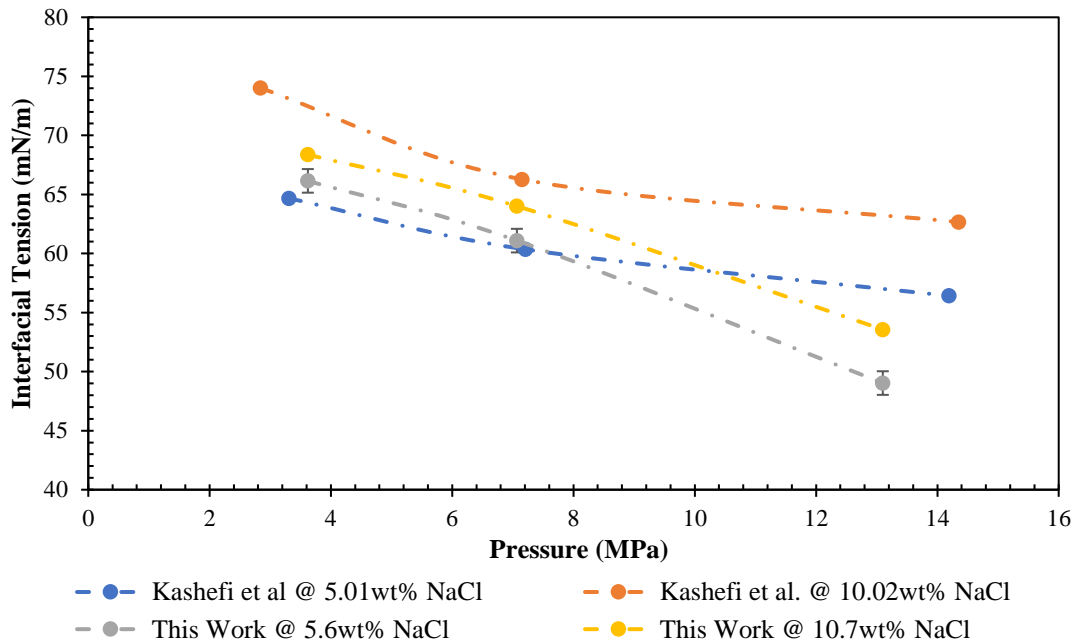
Figure 5.20: A comparison of IFT-pressure diagrams for methane-brine between this work and data obtained in some of the literature

5.4.4 Effect of surfactant on IFT

An aqueous solution of PEGs has long been an object of investigations of water-soluble polymers by various researchers. The results of such studies appear in many cases to be contradictory with others, and it is not surprising since the properties of the solution obtained differ depending on the average mass of the oligomer or polymer as well as the concentration of each and other properties such as the concentration and identities of added salts.

The interfacial tension of the $CH_4 + H_2O$ systems was measured with the addition of various concentrations of PEG 8000 ranging from $10 - 40$wt% to provide a reference for the determination of the effectiveness of the surfactant. The further measurement was carried out for PEG 8000 + SDS at various low dosage concentration to investigate their suitability and effectiveness. Presence of various concentration of NaCl was also investigated with the surfactants.

5.4.4.1 10 wt% PEG 8000 and different NaCl concentration

The IFT of CH_4-H_2O at a various concentration of PEG 8000 with or without the presence of NaCl has been investigated. Figure 5.21 shows the plot of IFT as a function of pressure and

102

temperature for the CH$_4$-H$_2$O system at 10% PEG 8000. In general, increasing the pressure and temperature decreases the interfacial tension. Also, the presence of PEG 8000 into the system lowers the IFT. The effect of PEG 8000 was observed considering the values obtained as described in the previous section (Figure 5.15) which presented the IFT values obtained in the methane-water under the same conditions. Further, the effect of temperature changes from 298.15 to 308.15 K, as seen in Figure 5.21 shows a significant difference while increasing the temperature from 308.15 to 313.15 K the effects was high at low pressure with less change as the pressure tends to a high value.
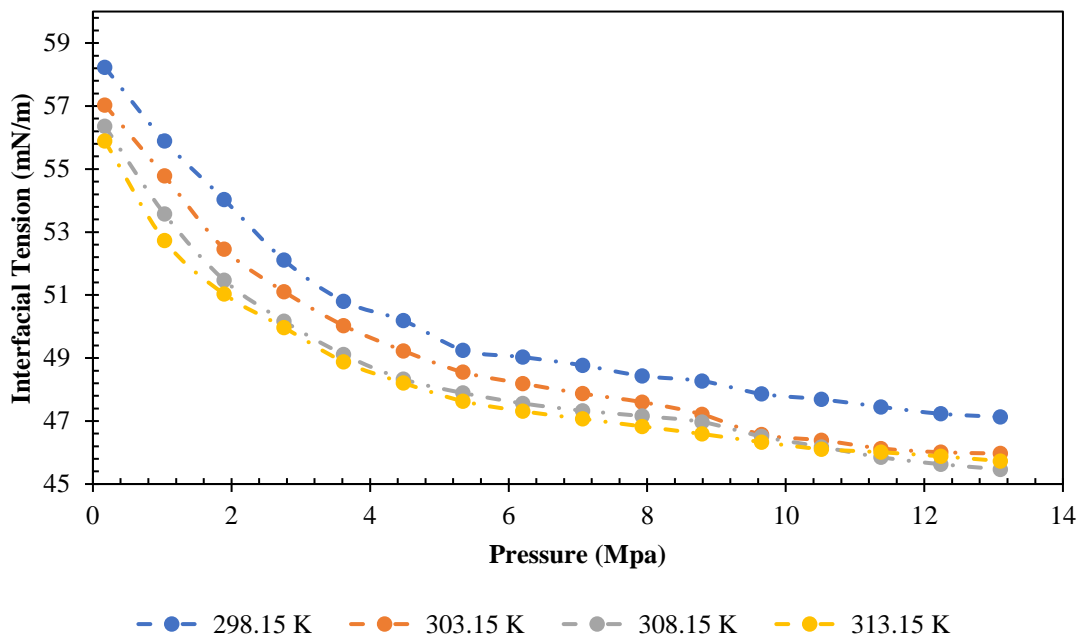
Figure 5.21: Influence of temperature and pressure on methane-water IFT at 10% PEG 8000

Figure 5.22 shows the behaviour of IFT of the CH$_4$-H$_2$O system responses to pressure and temperature at 10% PEG 8000 in the presence of 2.9 wt% NaCl. Increasing the concentration of NaCl (**see Appendix C, C1.2.1** for 5.6, 8.2 and 10.7 wt% NaCl) led to a corresponding increase in IFT values in the presence of the PEG 8000, though there was a reduction in the initial IFT measured without the polymer. The effect of PEG 8000 was observed to be more pronounced at a lower temperature in the system. Hence, temperature affects the presence of polymer in water (PEG 8000)
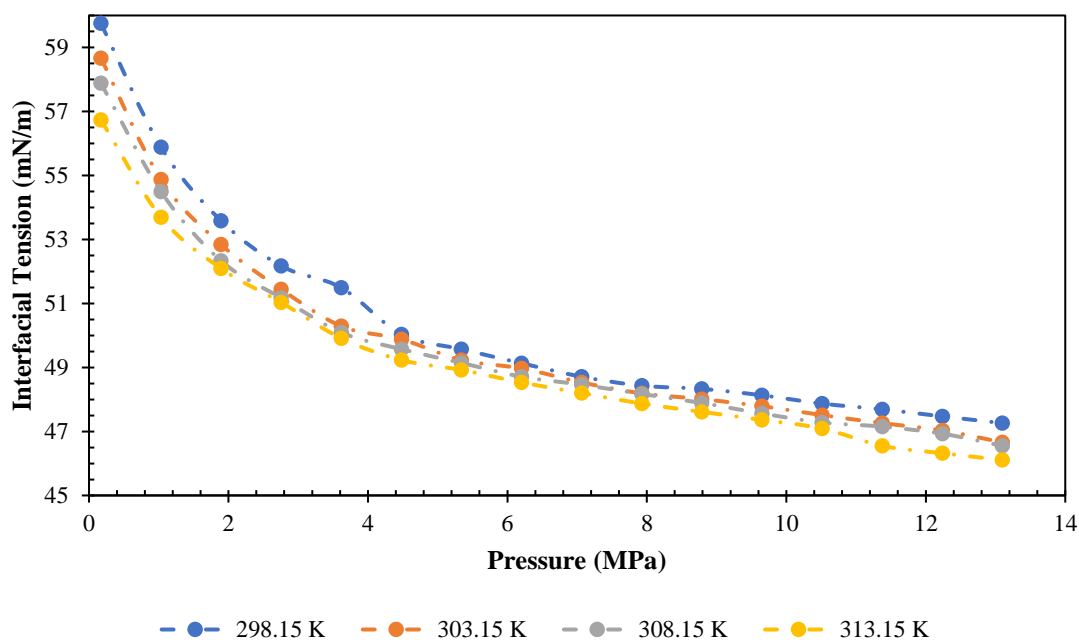
Figure 5.22: Methane-water IFT response to change in pressure at 2.9 wt% NaCl and 10% PEG 8000

5.4.4.2 20 wt% PEG 8000 and various NaCl Concentration

Figure 5.23 presented graphically, the results of IFT as a function of pressure and temperature for the CH_4-H_2O system at 20% PEG 8000. Presence of 20 wt% PEG 8000 into the system decreases the IFT further compared to 10 wt% PEG 8000. The variation of the IFT values, as observed at a lower pressure up to 2.76 MPa, indicated that there are significant decreases in IFT. The decreased in IFT values was seen at higher temperature change from 298.15 to 313.15 K, and slight changes were observed at 298.15 – 308.15 K. However, at 298.15 K increased in pressure has a lesser effect on IFT reduction, but at 303.15 – 313.15 there was a significant reduction in IFT. Similar behaviour was observed in the presence of 2.9 wt% NaCl as shown in Figure 5.24, though there was increased in the IFT due to the NaCl. Therefore, generally, increasing the concentration of NaCl (**see Appendix C, C1.2.2** for 5.6, 8.2 and 10.7 wt% NaCl) led to a corresponding increase in IFT values even with the presence of the PEG 8000. The influence of temperature was observed to be affected by the presence of PEG 8000 in the system. The effect of PEG 8000 was observed to be more pronounced at a lower temperature in the system.
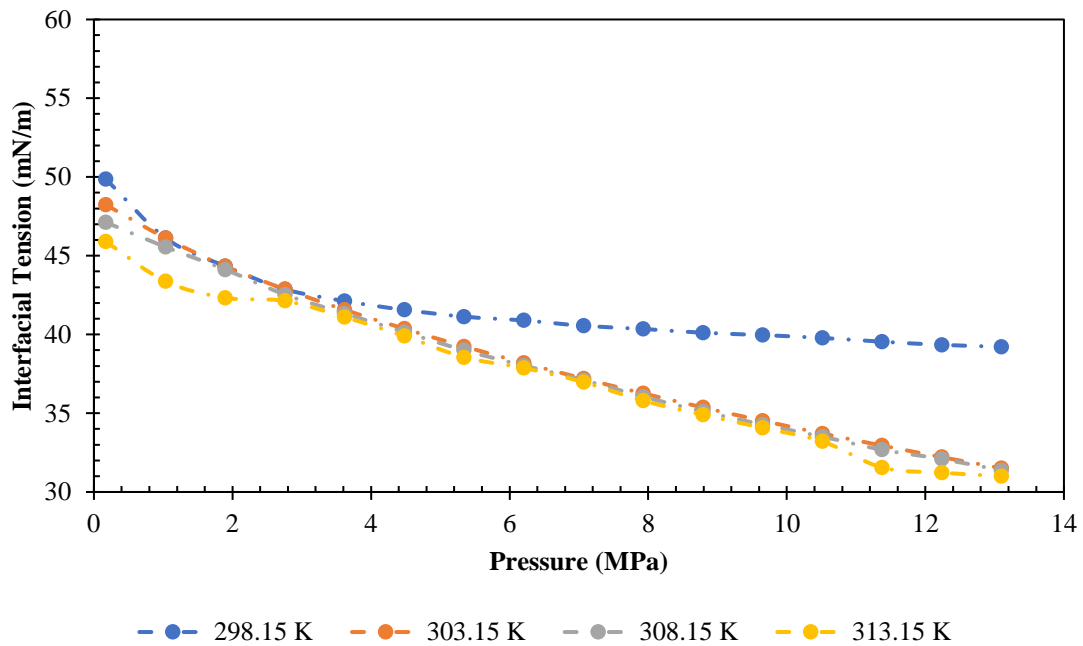
Figure 5.23: Methane-water IFT response to change in pressure at 20% PEG 8000 and a given temperature
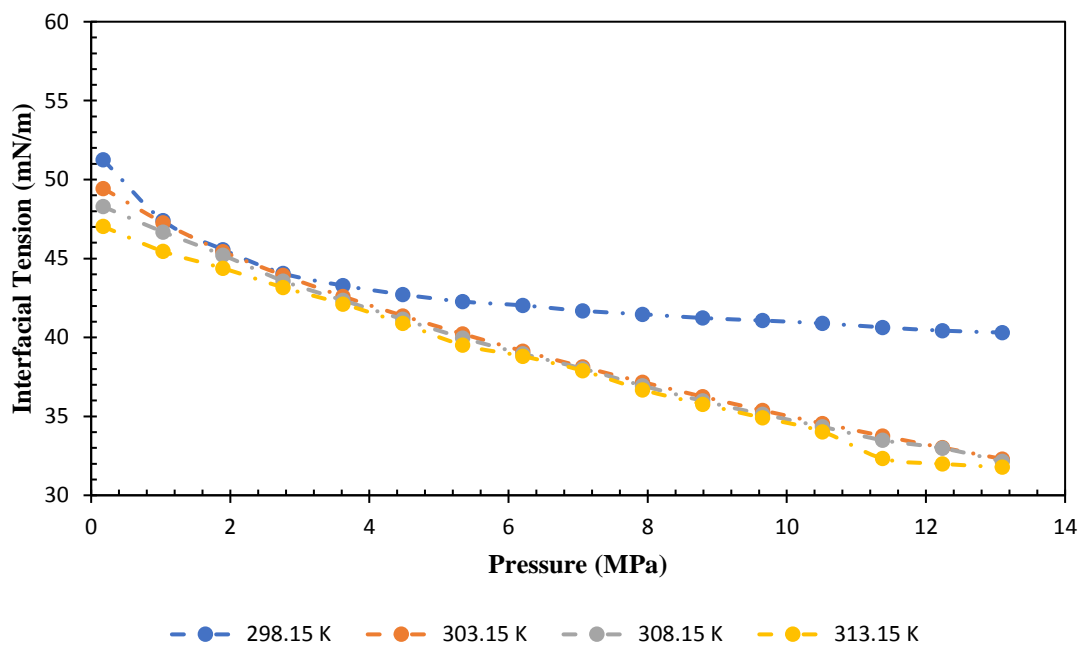
Figure 5.24: Methane-water IFT response to change in pressure at 2.9 wt% NaCl and 20% PEG 8000 at a given temperature

5.4.4.3 30 wt% PEG 8000 and various NaCl Concentration

Figure 5.25 and Figure 5.26 represents the IFT response to pressure and temperature at 30 wt% PEG 8000 and 30 wt% PEG 8000 + 2.9 wt% NaCl respectively. In Figure 5.25 further reduction in IFT was observed as compared to decreased in IFT seen at 20 wt% PEG 8000. A significant decreased in IFT values was observed up to a pressure of 8.79 MPa, from which

the values remained almost constant at both temperatures. Therefore, at this point, the PEG 8000 formed a bridge at the interface. Further, the effect of temperature changes from 298.15 to 308.15 K shows a significant decreased in the IFT values. However, at lower temperature change there was no much difference in IFT values as observed. Similar behaviour was observed in the presence of 2.9 wt% NaCl as depicted in Figure 5.26. In general, increasing the concentration of NaCl (see **Appendix C, C1.2.3** for 5.6, 8.2 and 10.7 wt% NaCl) led to a corresponding increase in IFT values even with the presence of the PEG 8000. The influence of temperature was observed to be affected by the presence of PEG 8000 in the system. The effect of PEG 8000 was observed to be more pronounced at a lower temperature in the system.
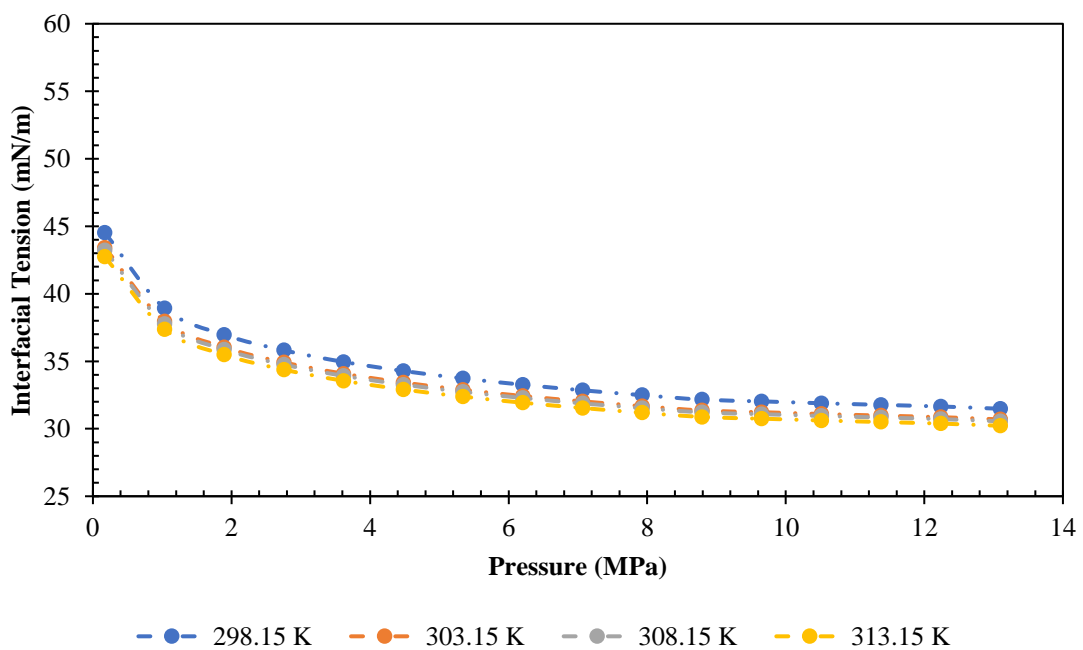
Figure 5.25: Methane-water IFT response to change in pressure at 30% PEG 8000
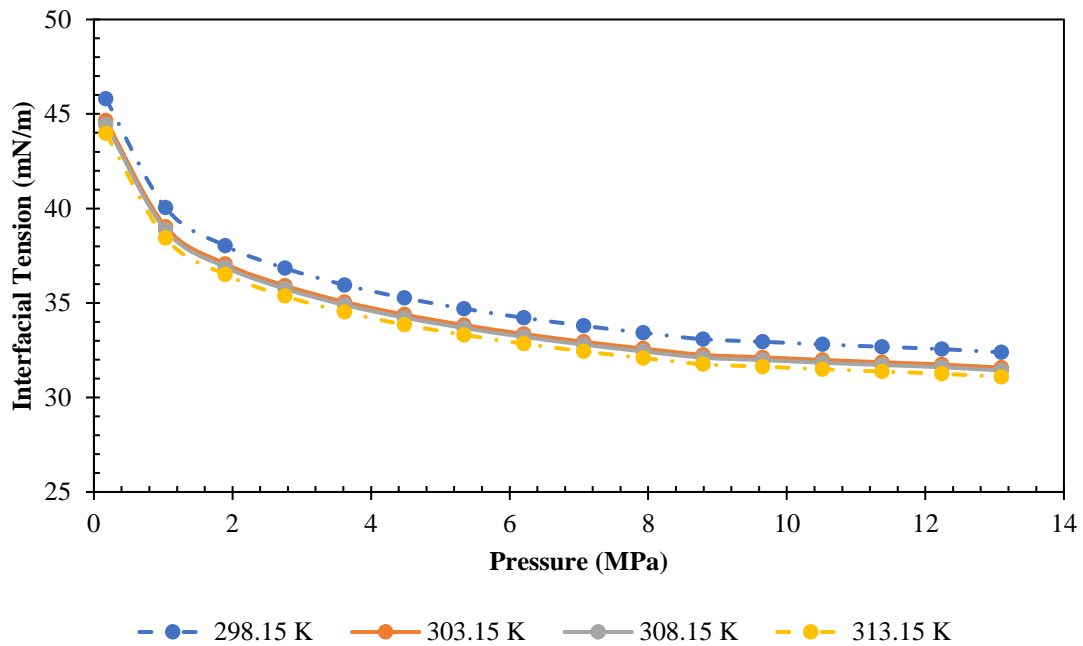
Figure 5.26: Methane-water IFT response to change in pressure at 2.9 wt% NaCl and 30% PEG 8000

5.4.4.4 40 wt% PEG 8000 and various NaCl Concentration

Figure 5.27 and Figure 5.28 depicted graphically, the results obtained for IFT as a function of pressure and temperature for the CH_4-H_2O system at 40 wt% PEG 8000 and 2.9 wt% NaCl respectively. In Figure 5.27, it was observed that increasing pressure led to a corresponding decrease in IFT. However, the temperature changes from 298.15 to 303.15 K shows a decreasing trend, but with less change observed with an average increase of 5 K after that. Figure 5.28 shows the behaviour of IFT of the CH_4-H_2O system responses to pressure and temperature at 40% PEG 8000 in the presence of 2.9 wt% NaCl. Increasing the concentration of NaCl (see Appendix C, C1.2.4 for 5.6, 8.2 and 10.7 wt% NaCl) led to a corresponding increase in IFT. Values even with the presence of the PEG 8000. The influence of temperature was observed to be affected by the presence of PEG 8000 in the system. The effect of PEG 8000 was observed to be more pronounced at a lower temperature in the system.
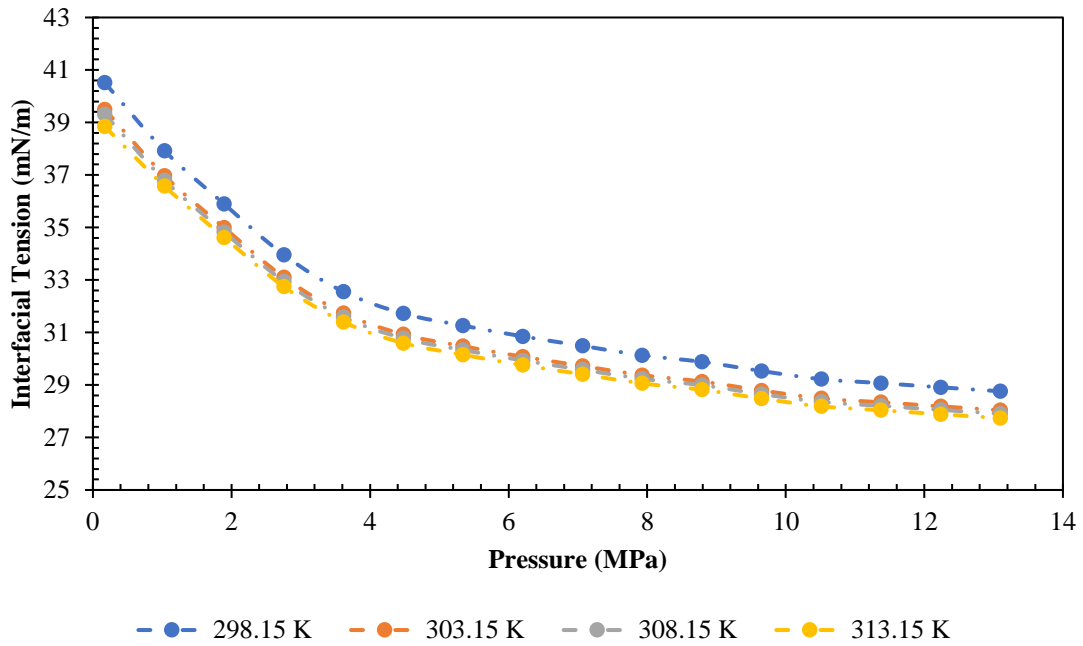
Figure 5.27: Methane-water IFT response to change in pressure at 40% PEG 8000
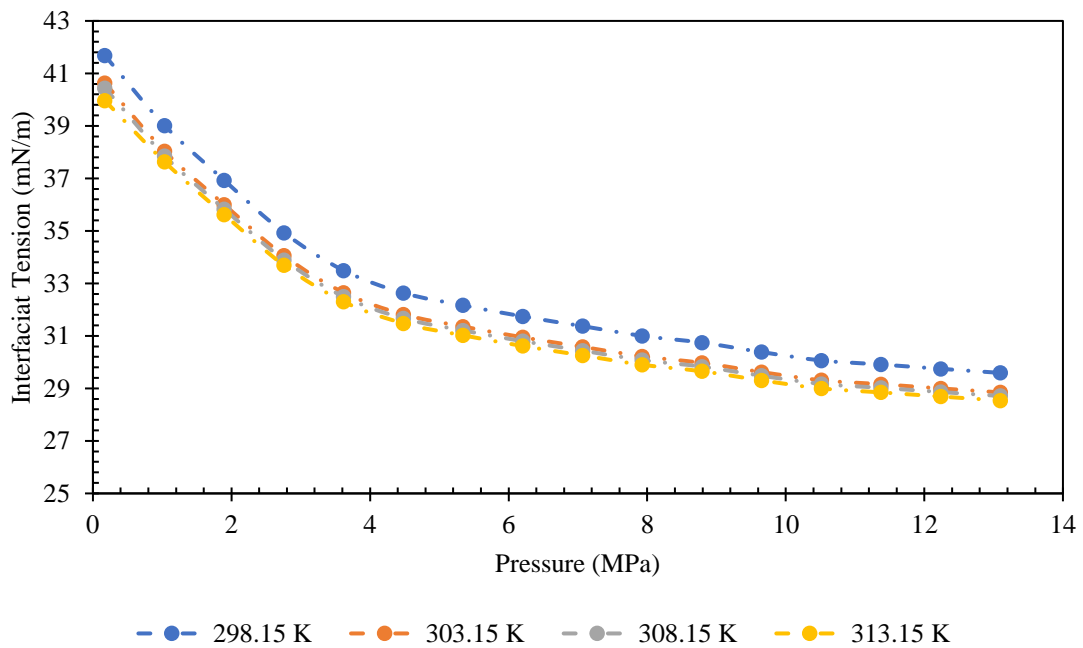
Figure 5.28: Methane-water IFT response to change in pressure at 2.9 wt% NaCl and 40% PEG 8000

Figure 5.29 shows the IFT results obtained as a function of both pressure and PEG 8000 concentrations. The effect of PEG 8000 concentration on IFT existing at CH_4-H_2O interface, indicated that increasing PEG 8000 concentrations decrease IFT. For example, IFT at 10 wt% PEG 8000 decrease from 55.03 mN/m at 2.76 MPa to 44.96 mN/m at 20 wt% PEG. However, at the higher concentration, as shown in Figure 5.29, the decrease in the IFT values begin to shrink, as the concentration increases. Example, at 30 wt% PEG 8000 IFT decreases from

37.52 mN/m to 35.58 mN/m at 40 wt%. The reduction of the IFT due to PEG 8000 is an indication of its dispersive properties. However, the IFT is observed to be the function of pressure and PEG 8000 concentration. The dependence of IFT at CH_4/PEG 8000 agrees well with the previous reported literature using CO_2/PEG at lower molecular weight of 400 and 600 PEGs (Hrnčič, Kravanja, Škerget, Sadiku, & Knez, 2015).
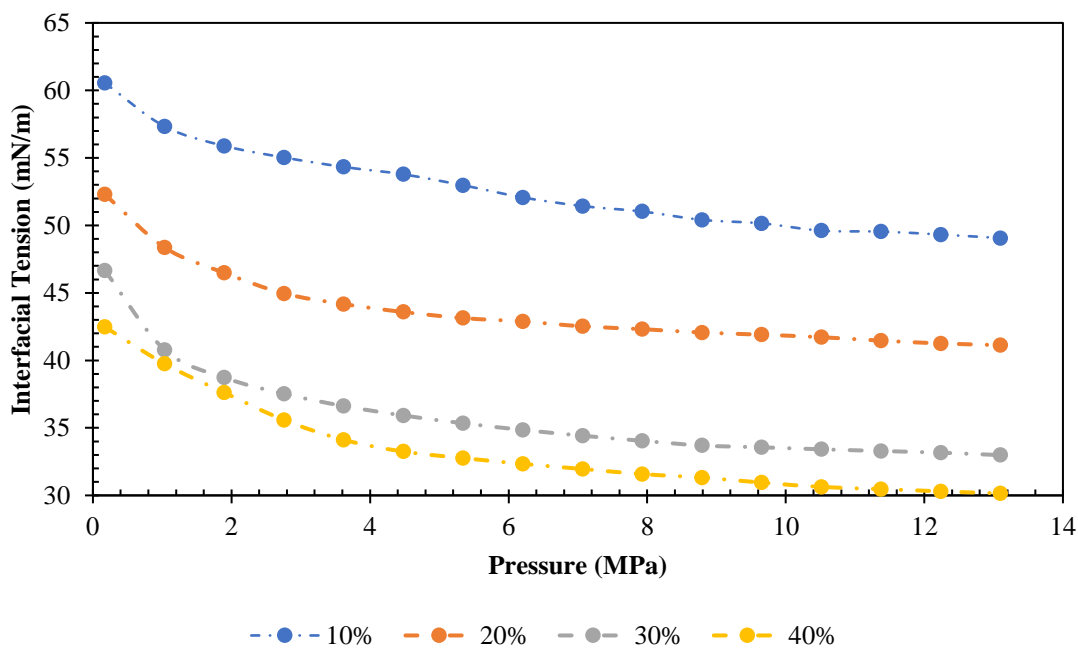
Figure 5.29: Influence of pressure and PEG 8000 on IFT at CH_4-H_2O interface at 298.15K

According to Figure 5.30, it is observed, that IFT at the CH_4/H_2O interface decreases with increasing PEG 8000 concentrations. Further, it increases with increasing NaCl concentrations. In all the conditions investigated, the decreasing or increasing trends is almost linearly as the case may be. For example, the IFT decreases from 63.22 mN/m at 0 wt% PEG 8000 to 30.85 mN/m at 40 wt% in the absence of NaCl. Also, at 2.9 wt% NaCl, the IFT decreases from 66.33 mN/m at 0 wt% PEG 8000 to 31.74 mN/m at 40 wt% PEG 8000. However, in the case of NaCl concentrations, for instance, at 20 wt% PEG 8000 the IFT increases from 40.89 mN/m at 2.9 wt% NaCl to 44.93 mN/m at 10.7 wt% NaCl.
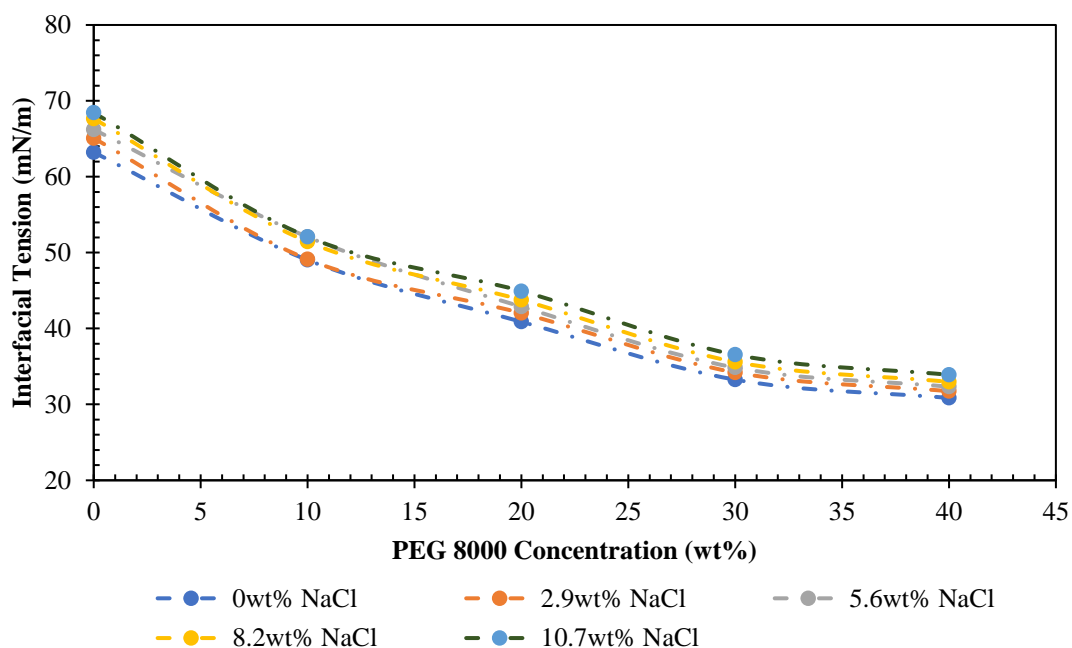
Figure 5.30: Influence of PEG 8000 and NaCl concentration on IFT at CH4-H2O interface at 298.15K and 6.21MPa

5.4.5 Effects of PEG 8000 + SDS

The interfacial tension of the (PEG 8000 + SDS) + H_2O was measured at T = 298.15, 303.15, 308.15 and 313.15 K and pressures up to 13.10 MPa. Figure 5.31 - Figure 5.33 shows the IFT isotherms at CH_4-H_2O interface containing 10 wt% PEG 8000 and 0.5 wt% SDS, at 0, 2.9 and 10.7 wt% NaCl respectively. In all the scenarios observed, it indicates that, at low pressures below 5.34 MPa, IFT decreases approximately linearly with increasing pressures at the same temperatures. This behaviour of IFT due to the isotherms observed correspond to the so-called Henry regime (Y. Liu et al., 2016). At the endpoint of the Henry regime, increasing pressure has less or no effect on the IFT reduction. When pressure increases to a certain higher value, the IFT remain constant. Generally, IFTs for CH4/H2O system is found to be decreasing with increasing both pressure and temperature.

In the case of PEG 8000 + SDS concentrations, it was observed at all the isotherms investigated that the IFT decreases drastically due to the presence of 0.5 wt% SDS. IFT reduces from 60.55 mN/m at 10 wt% PEG 8000 to 23.66 mN/m at 10 wt% PEG 8000 + 0.5 wt% SDS at 0.172 MPa and 298.15 K, see Appendix C, C2.1 for 20, 30 and 40 wt% PEG 8000 + 0.5 wt% SDS. The PEG 8000 and SDS combinations show excellent characteristics in the reduction of IFT at CH4/H2O interface.
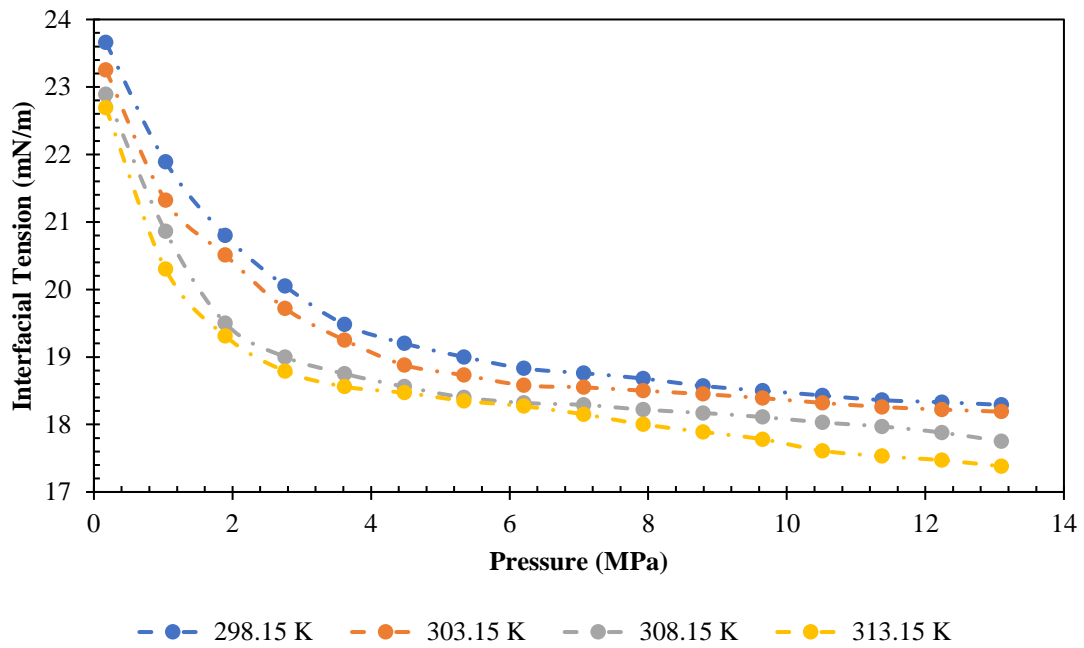
Figure 5.31: IFT as a function of pressure and temperature at 10% PEG 8000 + 0.5% SDS
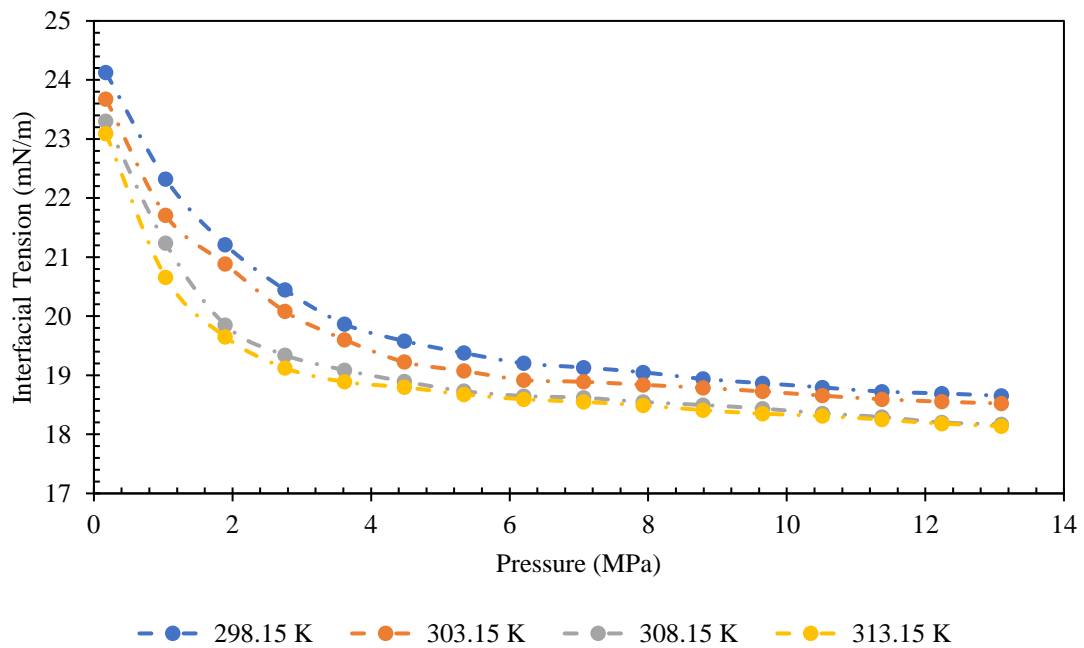
Figure 5.32: IFT as function of pressure and temperature at 10% PEG 8000 + 0.5% SDS and brine (2.9wt% NaCl)
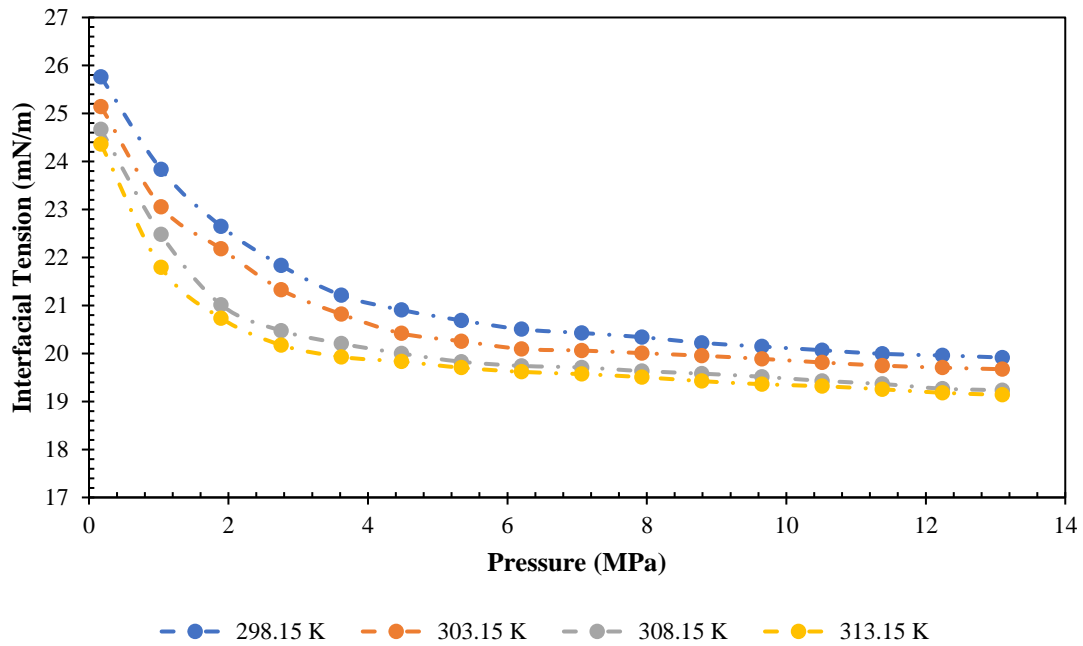
Figure 5.33: IFT as function of pressure and temperature at 10% PEG 8000 + 0.5% SDS and brine (10.7wt% NaCl)

5.5 Chapter summary

The interfacial tension of the CH_4-H_2O system has been investigated over the temperature range 298.15 to 313.15 K and for pressures up to 13.10 MPa. Also, effects of the presence of NaCl, PEG 8000 and SDS on IFT were studied. The results obtained shows that PEG 8000 and SDS could be a good synergies inhibitors for methane hydrate management. Also presence of NaCl has no significant effect on methane mass transfer across the interface in the system containing both PEG 8000 and SDS. Both the equipment and methodology were validated through comparison of measurements with selected literature data. The data reported helped to fill in the experimental gap found in literature and allowed the study of the behaviour of CH_4−H_2O *IFT* over a range of pressure and temperature conditions in the presence of PEG 8000 and SDS. The combine effect of PEG 8000 and SDS on IFT was reported for the first time. Resistivity, pH, density and the dynamic viscosity of the aqueous system at a various concentration of PEG 8000 and PEG 8000 + SDS have been measured over the temperature range 298.15 to 313.15 K at atmospheric pressure. The results obtained for resistivity could be used to ascertained methane gas saturatio. While the pH results indicated that the system has operates within the stable range for corrosion and emulsion formation in the system. Viscosity of PEG 8000 and PEG 8000 + SDS has been investigated as a function of shear rate at 298.15, 303.15, 308.15 and 313.15 K at atmospheric pressure. Results obtained from the

experiment shows that the flow pattern could be predicted using the viscosity analysis in the system.

Chapter 6: Conclusions and Recommendations

6.1 Introduction

In this thesis, the interfacial tension of two-phase fluid system involving CH_4-H_2O has been investigated. The investigations covered experimental characterisation of the liquid samples and the interfacial tension of gas−liquid interfaces in hydrocarbon and aqueous systems over a broad range of conditions (from ambient up to 313.15 K and 13.10 MPa). The examined systems comprised binary synthetic mixtures including methane, water, salts and polymer-surfactant. Though most of the systems studied here were single components of gaseous methane and mixture of liquid water with salt and polymer-surfactant, which are not devoid of complexities as obtainable in the real tubing, pipeline and other processing facilities. Interfacial tensions were observed to span from near complete miscibility (low *IFT* values) to immiscible (high *IFT* values) at two-phase equilibria conditions. More specific details on the experimental achievements and results of this thesis are briefly outlined below, and recommendations for future investigations are also described in this chapter.

6.2 Conclusions

The experiments were conducted to investigate IFT for CH_4-H_2O system along four isotherms between 298.15 and 313.15 K, at pressures up to 13.10 MPa. Effect of salinities and polymer-surfactant were also investigated. The apparatus used to measure the interfacial tension between liquid-liquid phases were modified to measure IFT for gas-liquid phases in the present investigation. The equipment was based on the Pendant Drop method and the axisymmetric drop shape analysis technique. Therefore, the following conclusions can be drawn from this work which has successfully used polymer-surfactant into the interfacial phenomena existing at two-phase system involving methane and liquid water, in the presence of salts and at three temperature of 298.15, 303.15, 308.15 and 313.15 K and pressure up to 13.10 MPa, as follows:

- The IFT of methane-water has been investigated and was found to be the function of system temperature, pressure and composition.
- Presence of salt (NaCl) was found to increase the interfacial tension. This could influence the the methane transfer to the liquid water system. It could led to corrosion in the system.

- PEG 8000 was found to significantly reduces the interfacial tension of methane-water, and hence could be used as a dispersant, for example, to transport hydrate as slurry when formed in a pipeline.

- PEG 8000 and SDS were found to be a right combination for altering interfacial tension existing at the methane-water interface and could be a good synergies for hydrate management.

- Interfacial tension could be used to map the flow pattern in the multiphase system during pipeline flow and in some separators design.

- The pH, electrical resistivity and conductivity, and density can be used to determined the corrosion and emulsion, methane saturation, and flow pattern of the system respectively.

- The viscosity of PEG 8000 – SDS has been identified to influence the behaviour of a two-phase system involving gas and water, and this has a significant effect on the flow pattern of the system.

- Further, these investigations provide a new data to quantify the effects of NaCl, PEG 8000 and SDS at the methane-water IFT at pipeline operating conditions.

6.3 Recommendations

Although this work considered details procedure and modification of the experimental facilities used, and high level of breakthrough was achieved regarding liquid characterisation and IFT involving polymer-surfactant and gaseous methane. Still, there are needs to carry out another task which were considered out of the scope of this investigation but may also contribute to a knowledge gap. These tasks may include the following:

- Time-dependent interfacial tension could be considered which enable the influence of both time and the system isotherm on the IFT.

- In this work, pure methane was considered, however, the natural gas mixture could be considered which will represent the effects of some gaseous contaminants on IFT during two-phase flow in a pipeline.

- The polymer-surfactant considered in this work were PEG 8000 and SDS. However, an alternative combination of polymer-surfactant such as PVCap and Inhibex 500 might be a right combination which could affect the interfacial properties of the gas-liquid system more especially towards hydrate management.

- Other salts such as $CaCl_2$, KCl, MgCl and other carbonates salts usually found in the formation water may be considered and also their combination. These salts were not considered within the scope of the present investigations.
- Surface dilation of the methane bubble in the liquid sample was not considered in the present study which could give a better understanding of the surface relaxation and energy during mass transfer across the gas-liquid interface.

References

Abubakar, A., Al-Wahaibi, Y., Al-Wahaibi, T., Al-Hashmi, A., Al-Ajmi, A., & Eshrati, M. (2015a). Effect of low interfacial tension on flow patterns, pressure gradients and holdups of medium-viscosity oil/water flow in horizontal pipe. *Experimental Thermal and Fluid Science*, *68*, 58–67. https://doi.org/10.1016/j.expthermflusci.2015.02.017

Abubakar, A., Al-Wahaibi, Y., Al-Wahaibi, T., Al-Hashmi, A., Al-Ajmi, A., & Eshrati, M. (2015b). Effect of low interfacial tension on flow patterns, pressure gradients and holdups of medium-viscosity oil/water flow in horizontal pipe. *Experimental Thermal and Fluid Science*, *68*, 58–67. https://doi.org/https://doi.org/10.1016/j.expthermflusci.2015.02.017

Adamson, A. W., & Gast, A. P. (1967). Physical chemistry of surfaces.

Ahmadi, M. A., Galedarzadeh, M., & Shadizadeh, S. R. (2016). Low parameter model to monitor bottom hole pressure in vertical multiphase flow in oil production wells. *Petroleum*. https://doi.org/10.1016/j.petlm.2015.08.001

Akiba, H., & Ohmura, R. (2016). Interfacial tension between (CO2 + N2) gas and tetrabutylammonium bromide aqueous solution. *Journal of Chemical Thermodynamics*, *97*, 83–87. https://doi.org/10.1016/j.jct.2016.01.014

Alhomadhi, E., Amro, M., & Almobarky, M. (2014). Experimental application of ultrasound waves to improved oil recovery during waterflooding. *Journal of King Saud University - Engineering Sciences*, *26*(1), 103–110. https://doi.org/10.1016/j.jksues.2013.04.002

Ali, S. F., & Yeung, H. (2013). Two-phase flow patterns in large diameter vertical pipes. *Asia-pacific journal of chemical engineering*, *9*(June), 105–116. https://doi.org/10.1002/apj

Amani, P., Safdari, J., Abolghasemi, H., Mallah, M. H., & Davari, A. (2017). Two-phase pressure drop and flooding characteristics in a horizontal-vertical pulsed sieve-plate column. *International Journal of Heat and Fluid Flow*, *65*, 266–276. https://doi.org/10.1016/j.ijheatfluidflow.2017.01.003

Arabloo, M., Ghazanfari, M. H., & Rashtchian, D. (2016). Wettability modification, interfacial tension and adsorption characteristics of a new surfactant: Implications for enhanced oil recovery. *Fuel*, *185*, 199–210. https://doi.org/10.1016/j.fuel.2016.06.088

Arashiro, E. Y., & Demarquette, N. R. (1999). Use of the pendant drop method to measure interfacial tension between molten polymers. *Materials Research*, *2*(1), 23–32.

https://doi.org/10.1590/S1516-14391999000100005

Arif, M., Barifcani, A., & Iglauer, S. (2016). Solid/CO2 and solid/water interfacial tensions as a function of pressure, temperature, salinity and mineral type: Implications for CO2-wettability and CO2 geo-storage. *International Journal of Greenhouse Gas Control*, *53*, 263–273. https://doi.org/10.1016/j.ijggc.2016.08.020

Arsalan, N., Buiting, J. J., & Nguyen, Q. P. (2015). Surface energy and wetting behavior of reservoir rocks. *Colloids and Surfaces A: Physicochemical and Engineering Aspects*, *467*, 107–112. https://doi.org/10.1016/j.colsurfa.2014.11.024

Arvoh, B. K., Skeie, N. O., & Halstensen, M. (2013). Estimation of gas/liquid and oil/water interface levels in an oil/water/gas separator based on pressure measurements and regression modelling. *Separation and Purification Technology*, *107*, 204–210. https://doi.org/10.1016/j.seppur.2013.01.045

Asadollahzadeh, M., Torab-Mostaedi, M., Shahhosseini, S., & Ghaemi, A. (2016). Holdup, characteristic velocity and slip velocity between two phases in a multi-impeller column for high/medium/low interfacial tension systems. *Chemical Engineering and Processing: Process Intensification*, *100*, 65–78. https://doi.org/10.1016/j.cep.2015.11.013

Atkinson, H. (1927). Recovery of Petroleum from Oil Bearing Sands. *US Patent Office*.

Bachu, S. (2015). Review of CO2 storage efficiency in deep saline aquifers. *International Journal of Greenhouse Gas Control*, *40*, 188–202. https://doi.org/10.1016/j.ijggc.2015.01.007

Bachu, S., & Bennion, D. B. (2009). Interfacial tension between CO2, freshwater, and brine in the range of pressure from (2 to 27) MPa, temperature from (20 to 125) 0C, and water salinity from (0to334 000)mgL-1. *Journal of Chemical and Engineering Data*, *54*(3), 765–775. https://doi.org/10.1021/je800529x

Barnea, D., Luninski, Y., & Taitel, Y. (1983). Flow pattern in horizontal and vertical two phase flow in small diameter pipes. *The Canadian Journal of Chemical Engineering*, *61*(5), 617–620.

Bashforth, F., & Adams, J. C. (1883). *An attempt to test the theories of capillary action*. University Press.

Berry, J. D., Neeson, M. J., Dagastine, R. R., Chan, D. Y. C., & Tabor, R. F. (2015).

Measurement of surface and interfacial tension using pendant drop tensiometry. *Journal of Colloid and Interface Science*, *454*, 226–237. https://doi.org/10.1016/j.jcis.2015.05.012

Bilgesu, H. L., Ternyik, J., & Virginia, W. (1994). A New Multi-Phase Flow Model for Horizontal, Inclined, and Vertical Pipes.

Binks, B. P., & Horozov, T. S. (2008). Colloidal particles at Liquid Interfaces : An Introduction. *Colloidal Particles at Liquid Interfaces*, *34*(c), 1–74. https://doi.org/10.1039/b705094a

Brennen, C. E. (2005). *Fundamentals of multiphase flows*. California: Cambridge University Press 2005.

Brikov, A., Markin, A., & Sukhoverkhov, S. (2015). Rheological Properties of Polyethylene Glycol Solutions and Gels. *Industrial Chemistry*, *1*(1), 1–5. https://doi.org/10.4172/2469-9764.1000102

Chalbaud, C., Robin, M., Lombard, J. M., Martin, F., Egermann, P., & Bertin, H. (2009). Interfacial tension measurements and wettability evaluation for geological CO2 storage. *Advances in Water Resources*, *32*(1), 98–109. https://doi.org/10.1016/j.advwatres.2008.10.012

Chandler, D. (2005). Interfaces and the driving force of hydrophobic assembly. *Nature*, *437*(7059), 640.

Cheng, P., Li, D., Boruvka, L., Rotenberg, Y., & Neumann, A. W. (1990). Automation of Axisymmetric Drop Shape Analysis for Measurement of Interfacial Tensions and Contact Angles. *Colloids Surf.*, *93*, 151.

Chilingar, G. V, & Yen, T. F. (1983). Some notes on wettability and relative permeabilities of carbonate reservoir rocks, II. *Energy Sources*, *7*(1), 67–75.

Chiquet, P., Daridon, J. L., Broseta, D., & Thibeau, S. (2007). CO2/water interfacial tensions under pressure and temperature conditions of CO2 geological storage. *Energy Conversion and Management*, *48*(3), 736–744. https://doi.org/10.1016/j.enconman.2006.09.011

Davies, J. T. (2012). *Interfacial phenomena*. Elsevier.

Dominik, M., & Cassel, K. W. (2015). Analysis of Initial Bubble Acceleration Using the

Level-Set Method. *Journal of Computational Multiphase Flow*, (1), 129–142. https://doi.org/10.1260/1757-482X.7.3.129

Dong, F., Liu, X., Deng, X., Xu, L., & Xu, L. (2001). Identification of two-phase flow regimes in horizontal, inclined and vertical pipes. *Measurement Science and Technology*, *12*(8), 1069.

Dorsey, W. E. (1929). The investigation of surface tension and associated phenomena. *Bull. Nat. Res. Conn*, (69), 56–118.

Drelich, J., Fang, C., & White, C. L. (2002). Measurement of Interfacial Tension in Fluid-Fluid Systems. *Encyclopedia of Surface and Colloid Science*, 3152–3166. https://doi.org/10.1081/E-ESCS-120000636

DuNouy, L. P. (1919). A new apparatus for measuring surface tension. *Journal of General Physiology*, *1*(5), 521–524. Retrieved from https://www.ncbi.nlm.nih.gov/pmc/articles/PMC2140330/

Elworthy, P. H., & Mysels, K. J. (1966). The Surface tension of sodiun dodecylsulfate solutions and the phase separation model of micelle formation. *Journal of Colloid and Interface Science*, *7*, 331–347.

Englezos, P., & Lee, J. D. (2005). Gas Hydrates : A Cleaner Source of Energy and Opportunity for Innovative Technologies. *Korean Journal of Chemical Engineering*, *22*(5), 671–681.

Erfani, A., & Varaminian, F. (2017). Experimental investigation on structure H hydrates formation kinetics: Effects of surfactants on interfacial tension. *Journal of Molecular Liquids*, *225*, 636–644. https://doi.org/10.1016/j.molliq.2016.11.043

Ferguson, R. B. (1938, January 11). Manufacture of sulphuric acid. Google Patents.

Firoozabadi, A., & Ramey, H. J. (1988). Surface tension of water-hydrocarbon systems at reservoir conditions. *J. CAN. PET. TECHNOL.*, *27*(3, May–Jun. 1988), 41–48. Retrieved from https://www.scopus.com/inward/record.uri?eid=2-s2.0-0023703242&partnerID=40&md5=1dbcabaf4b398cc6c2ff3f4b4dd60b12

Ganji, H., Manteghian, M., Sadaghiani zadeh, K., Omidkhah, M. R., & Rahimi Mofrad, H. (2007). Effect of different surfactants on methane hydrate formation rate, stability and storage capacity. *Fuel*. https://doi.org/10.1016/j.fuel.2006.07.032

Georgiadis, A., Maitland, G., Trusler, J. P. M., & Bismarck, A. (2011). Interfacial Tension

Measurements of the (H2O + n-Decane + CO2) Ternary System at Elevated Pressures and Temperatures. *Journal of Chemical & Engineering Data*, *56*(12), 4900–4908. https://doi.org/10.1021/je200825j

Ghorbani, M., & Mohammadi, A. H. (2017). Effects of temperature, pressure and fluid composition on hydrocarbon gas - oil interfacial tension (IFT): An experimental study using ADSA image analysis of pendant drop test method. *Journal of Molecular Liquids*, *227*, 318–323. https://doi.org/10.1016/j.molliq.2016.11.110

Ghosh, P. (2009). *Colloid and interface science*. PHI Learning Pvt. Ltd.

Goard, A. K. (1925). CCCXXXIII.—Negative adsorption. The surface tensions and activities of some aqueous salt solutions. *Journal of the Chemical Society, Transactions*, *127*, 2451–2458.

Goddard, E. D. (2017). *Interactions of Surfactants with Polymers and Proteins: 0*. CRC press.

Graciaa, A., Andérez, J., Bracho, C., Lachaise, J., Salager, J.-L., Tolosa, L., & Ysambertt, F. (2006). The selective partitioning of the oligomers of polyethoxylated surfactant mixtures between interface and oil and water bulk phases. *Advances in Colloid and Interface Science*, *123*, 63–73.

Graf, K., & Kappl, M. (2006). *Physics and chemistry of interfaces*. John Wiley & Sons.

Gunstone, F. D., & Hamilton, R. J. (2001). *Oleochemical manufacture and applications* (Vol. 4). CRC Press.

Günther, A., & Jensen, K. F. (2006). Multiphase microfluidics: from flow characteristics to chemical and materials synthesis. *Lab on a Chip*, *6*(12), 1487–1503.

Hansen, F. K., & Rodsrud, G. (1991). Surface Tension by Pendant Drop I. A Fast Standard Instrument Using Computer Image Analysis. *Journal of Colloid and Interface Science*, *141*(I).

Harkins, W. D., & Brown, F. E. (1919). The determination of surface tension (free surface energy), and the weight of falling drops: The surface tension of water and benzene by the capillary height method. *Journal of the American Chemical Society*, *41*(4), 499–524. https://doi.org/10.1021/ja01461a003

Harkins, W., & Jordan, H. (1930). A Method for the Determination of Surface and Interfacial Tension from the Maximum Pull on a Ring. *Jacs*, *52*(1892), 1751–1772.

https://doi.org/10.1021/ja01368a004

Hayama, H., Fukuzawa, K., Yasuda, K., & Ohmura, R. (2017). Interfacial tension between (methane+ethane+propane) gas mixture and water from 283.2K to 298.2K under up to 10MPa. *The Journal of Chemical Thermodynamics*, *108*, 71–75. https://doi.org/10.1016/j.jct.2017.01.007

Hendraningrat, L., & Torsæter, O. (2014). Effects of the initial rock wettability on silica-based nanofluid-enhanced oil recovery processes at reservoir temperatures. *Energy and Fuels*. https://doi.org/10.1021/ef5014049

Holmberg, K., Jönsson, B., Kronberg, B., & Lindman, B. (2003). *Surfactants and polymers in aqueous solution* (Vol. 2). Wiley Online Library.

Hrnčič, M. K., Kravanja, G., Škerget, M., Sadiku, M., & Knez, Ž. (2015). Investigation of interfacial tension of the binary system polyethylene glycol/CO_2 by a capillary rise method. *Journal of Supercritical Fluids*, *102*, 9–16. https://doi.org/10.1016/j.supflu.2015.03.015

Israelachvili, J. N. (2011). *Intermolecular and surface forces*. Academic press.

Jahanandish, I., Salimifard, B., & Jalalifar, H. (2011). Predicting bottomhole pressure in vertical multiphase flowing wells using artificial neural networks. *Journal of Petroleum Science and Engineering*. https://doi.org/10.1016/j.petrol.2010.11.019

Jho, C., Nealon, D., Shogbola, S., & King Jr., A. D. (1978). Effect of Pressure on the Surface Tension of Water: Adsorption of Hydrocarbon Gases and Carbon Dioxide on Water at Temperatures between 0 and 50 C. *J. Colloid Interface Sci.*, *65*(1), 141–154.

Kalogerakis, N., Jamaluddin, A. K. M., Dholabhai, P. D., & Bishnoi, P. R. (1993). Effect of Surfactants on Hydrate Formation Kinetics. In *SPE International Symposium on Oilfield Chemistry*. https://doi.org/10.2118/25188-MS

Karbaschi, M., Lotfi, M., Krägel, J., Javadi, A., Bastani, D., & Miller, R. (2014). Rheology of interfacial layers. *Current Opinion in Colloid and Interface Science*, *19*(6), 514–519. https://doi.org/10.1016/j.cocis.2014.08.003

Karnanda, W., Benzagouta, M. S., AlQuraishi, A., & Amro, M. M. (2013). Effect of temperature, pressure, salinity, and surfactant concentration on IFT for surfactant flooding optimization. *Arabian Journal of Geosciences*, *6*(9), 3535–3544.

Kashefi, K., Pereira, C., Manuel, L., Chapoy, A., Burgass, R. W., & Bahman, T. K. (2016). Measurement and modelling of interfacial tension in methane/water and methane/brine systems at reservoir conditions. *Fluid Phase Equilibria*, *409*, 301–311. https://doi.org/10.1016/j.fluid.2015.09.050

Kashefi, K., Pereira, L. M. C., Chapoy, A., Burgass, R., & Tohidi, B. (2016). Measurement and modelling of interfacial tension in methane/water and methane/brine systems at reservoir conditions. *Fluid Phase Equilibria*, *409*, 301–311. https://doi.org/10.1016/j.fluid.2015.09.050

Khadamkar, H. P., Khanwale, M. A., Sawant, S. S., & Mathpati, C. S. (2017). On nature of mass transfer near liquid-liquid interface in the presence of Marangoni instabilities. *Chemical Engineering Science*, *170*, 176–183. https://doi.org/10.1016/j.ces.2017.02.016

Khosharay, S. (2015). Linear gradient theory for modeling investigation on the surface tension of (CH_4+H_2O), (N_2+H_2O) and (CH_4+N_2)+H_2O systems. *Journal of Natural Gas Science and Engineering*, *23*, 474–480. https://doi.org/10.1016/j.jngse.2015.02.029

Khosharay, S., & Varaminian, F. (2014). Experimental and modeling investigation on surface tension and surface properties of ($CH_4 + H_2O$), ($C_2H_6 + H_2O$), ($CO_2 + H_2O$) and ($C_3H_8 + H_2O$) from 284.15 K to 312.15 K and pressures up to 60 bar. *International Journal of Refrigeration*, *47*, 26–35. https://doi.org/10.1016/j.ijrefrig.2014.08.003

Kovalchuk, V. I., & Dukhin, S. S. (2001). Dynamic effects in maximum bubble pressure experiments. *Colloids and Surfaces A: Physicochemical and Engineering Aspects*. https://doi.org/10.1016/S0927-7757(01)00721-X

Kulkarni, A. a, & Joshi, J. B. (2005). Bubble Formation and Bubble Rise Velocity in Gas - Liquid Systems : A Review. *Industrial & Engineering Chemistry Research*, *44*, 5873–5931. https://doi.org/10.1021/ie049131p

Kumar, A., Bhattacharjee, G., Kulkarni, B. D., & Kumar, R. (2015). Role of Surfactants in Promoting Gas Hydrate Formation. *Industrial and Engineering Chemistry Research*, *54*(49), 12217–12232. https://doi.org/10.1021/acs.iecr.5b03476

Kumar, B. (2012). *Effect of Salinity on the Interfacial Tension of Model and Crude Oil Systems*. University of Calgary.

Lashkarbolooki, M., Riazi, M., Ayatollahi, S., & Hezave, A. Z. (2016). Synergy effects of ions, resin, and asphaltene on interfacial tension of acidic crude oil and low–high salinity

brines. *Fuel*, *165*, 75–85.

Lee, S., Kim, D. H., & Needham, D. (2001). Equilibrium and Dynamic Interfacial Tension Measurements at Microscopic Interfaces Using a Micropipet Technique. 1. A New Method for Determination of Interfacial Tension. *Langmuir*, *17*(18), 5537–5543. https://doi.org/10.1021/la0103259

Leunissen, M. E., van Blaaderen, A., Hollingsworth, A. D., Sullivan, M. T., & Chaikin, P. M. (2007). Electrostatics at the oil-water interface, stability, and order in emulsions and colloids. *Proceedings of the National Academy of Sciences of the United States of America*, *104*(8), 2585–2590. https://doi.org/10.1073/pnas.0610589104

Li, Q., Chou, L., Omeragic, D., Yang, L., Dumont, A., & Hu, L. (2008). Directional electromagnetic wave resistivity apparatus and method. Google Patents.

Liang, T., Zhou, F., Lu, J., DiCarlo, D., & Nguyen, Q. (2017). Evaluation of wettability alteration and IFT reduction on mitigating water blocking for low-permeability oil-wet rocks after hydraulic fracturing. *Fuel*, *209*(July), 650–660. https://doi.org/10.1016/j.fuel.2017.08.029

Lima, E. R. A., De Melo, B. M., Baptista, L. T., & Paredes, M. L. L. (2013). Specific ion effects on the interfacial tension of water/hydrocarbon systems. *Brazilian Journal of Chemical Engineering*, *30*(1), 55–62. https://doi.org/10.1590/S0104-66322013000100007

Liu, P., Sun, C. Y., Peng, B. Z., Chen, J., & Chen, G. J. (2009). Measurement of interfacial tension between methane and aqueous solution containing hydrate kinetic inhibitors. *Journal of Chemical and Engineering Data*, *54*(6), 1836–1839. https://doi.org/10.1021/je800937u

Liu, Y., Li, H. A., & Okuno, R. (2016). Measurements and Modeling of Interfacial Tension for CO2/CH4/Brine Systems under Reservoir Conditions. *Industrial and Engineering Chemistry Research*. https://doi.org/10.1021/acs.iecr.6b02446

Lüsse, S., & Arnold, K. (1996). The Interaction of Poly(ethylene glycol) with Water Studied by [1] H and [2] H NMR Relaxation Time Measurements. *Macromolecules*. https://doi.org/10.1021/ma9508616

Lykema, J., Fleer, G. J., Kleijn, J. M., Leermakers, F. A. M., Norde, W., & Van Vliet, T. (2000). Fundamentals of interface and colloid science, volume III: Liquid-fluid

interfaces. Academic Press London, UK.

Ma, J., & Huang, Z. (2017). Experiments of methane gas solubility in formation water under high temperature and high pressure and their geological significance. *Australian Journal of Earth Sciences*, *64*(3), 335–342. https://doi.org/10.1080/08120099.2017.1294108

Mahmoudi, B., Hasanvand, M. Z., & Naderi, A. (2015). Experimental Measurements and Modeling of Interfacial Tension for Injected Gas + Live Oil Systems at Elevated Pressures. *Journal of Petroleum & Coal*, *57*(1), 1–5.

Makogon, Y. F., Holditch, S. A., & Makogon, T. Y. (2007). Natural gas-hydrates - A potential energy source for the 21st Century. *Journal of Petroleum Science and Engineering*, *56*(1–3), 14–31. https://doi.org/10.1016/j.petrol.2005.10.009

Makogon, Y. F., & Omelchenko, R. Y. (2013). Commercial gas production from Messoyakha deposit in hydrate conditions. *Journal of Natural Gas Science and Engineering*, *11*, 1–6. https://doi.org/10.1016/j.jngse.2012.08.002

Massoudi, R., & King, A. D. (1974). Effect of pressure on the surface tension of water. Adsorption of low molecular weight gases on water at 25°. *The Journal of Physical Chemistry*, *78*(22), 2262–2266. https://doi.org/10.1021/j100615a017

Mendoza, A. J., Guzmán, E., Martínez-Pedrero, F., Ritacco, H., Rubio, R. G., Ortega, F., … Miller, R. (2014). Particle laden fluid interfaces: Dynamics and interfacial rheology. *Advances in Colloid and Interface Science*, *206*, 303–319. https://doi.org/10.1016/j.cis.2013.10.010

Miller, R., Sedev, R., Schano, K.-H., Ng, C., & Neumann, A. W. (1993). Relaxation of adsorption layers at soiution / air interfaces using axisymmetric drop-s) hape analysis. *Colloids and Surfaces*, *69*, 209.

Mishima, K., & Hibiki, T. (1996). Some characteristics of air-water two-phase flow in small diameter vertical tubes. *International Journal of Multiphase Flow*, *22*(4), 703–712.

Mobius, D., & Miller, R. (1997). *Drops and bubbles in interfacial research* (Vol. 6). Elsevier.

Moeini, F., Hemmati-Sarapardeh, A., Ghazanfari, M.-H., Masihi, M., & Ayatollahi, S. (2014). Toward mechanistic understanding of heavy crude oil/brine interfacial tension: The roles of salinity, temperature and pressure. *Fluid Phase Equilibria*, *375*, 191–200.

Moradi, O. (2011). Thermodynamics of Interfaces. In *Thermodynamics - Interaction Studies*

- Solid, Liquids and Gases (pp. 201–250). https://doi.org/10.1002/9781444305401.ch3

Muggeridge, A., Cockin, A., Webb, K., Frampton, H., Collins, I., Moulds, T., & Salino, P. (2013). Recovery rates, enhanced oil recovery and technological limits. *Philosophical Transactions of the Royal Society A: Mathematical, Physical and Engineering Sciences*, *372*(2006), 20120320–20120320. https://doi.org/10.1098/rsta.2012.0320

Myers, D. (2000). *Surfaces, Interfaces and Colloids: Principles and Applications. Talanta* (Second Edi, Vol. 51). New York. https://doi.org/10.1016/S0039-9140(99)00305-7

Nathanson, G. M., Davidovits, P., Worsnop, D. R., & Kolb, C. E. (1996). Dynamics and kinetics at the gas-liquid interface. *Journal of Physical Chemistry*, *100*(31), 13007–13020. https://doi.org/10.1021/jp953548e

Nino-Amezquita, O. G., Enders, S., Jaeger, P. T., & Eggers, R. (2010). Measurement and Prediction of Interfacial Tension of Binary Mixtures. *Industrial & Engineering Chemistry Research*, *49*(2), 592–601. https://doi.org/10.1021/ie901209z

Norgaard, H., & Nygaard, L. (2014). *Measurement and Calculation of Surface Tension of Oil , Gas and Glycol*. Norwegian University of Science and Technology.

Opawale, F. O., & Burgess, D. J. (1998). Influence of interfacial properties of lipophilic surfactants on water-in-oil emulsion stability. *Journal of Colloid and Interface Science*, *197*(1), 142–150.

Ozdemir, O., Karakashev, S. I., Nguyen, A. V., & Miller, J. D. (2006). Adsorption of carbonate and bicarbonate salts at the air-brine interface. *International Journal of Mineral Processing*, *81*(3), 149–158. https://doi.org/10.1016/j.minpro.2006.07.016

Padday, J. F. (1971). The profiles of axially symmetric menisci. *Phil. Trans. R. Soc. Lond. A*, *269*(1197), 265–293.

Parker, M. E., Northrop, S., Valencia, J. A., Foglesong, R. E., & Duncan, W. T. (2011). CO_2 management at ExxonMobil's LaBarge field, Wyoming, USA. *Energy Procedia*, *4*, 5455–5470. https://doi.org/10.1016/j.egypro.2011.02.531

Parsons, G. E., Bukton, G., & Chatham, S. M. (2012). Comparison of measured wetting behaviour of materials with identical surface energies, presented as particles and plates. *Journal of Adhesion Science and Technology*. https://doi.org/10.1163/156856193X00231doi.org/10.1163/156856193X00231

Peng, B. Z., Sun, C. Y., Liu, P., Liu, Y. T., Chen, J., & Chen, G. J. (2009a). Interfacial properties of methane/aqueous VC-713 solution under hydrate formation conditions. *Journal of Colloid and Interface Science*, *336*(2), 738–742. https://doi.org/10.1016/j.jcis.2009.04.028

Peng, B. Z., Sun, C. Y., Liu, P., Liu, Y. T., Chen, J., & Chen, G. J. (2009b). Interfacial properties of methane/aqueous VC-713 solution under hydrate formation conditions. *Journal of Colloid and Interface Science*, *336*(2), 738–742. https://doi.org/10.1016/j.jcis.2009.04.028

Pouraria, H., Seo, J. K., & Paik, J. K. (2016). A numerical study on water wetting associated with the internal corrosion of oil pipelines. *Ocean Engineering*, *122*, 105–117. https://doi.org/10.1016/j.oceaneng.2016.06.022

Qin, H. B., Sun, C. Y., Sun, Z. F., Liu, B., & Chen, G. J. (2016). Relationship between the interfacial tension and inhibition performance of hydrate inhibitors. *Chemical Engineering Science*, *148*, 182–189. https://doi.org/10.1016/j.ces.2016.04.002

Ramírez, P., Stocco, A., Muñoz, J., & Miller, R. (2012). Interfacial rheology and conformations of triblock copolymers adsorbed onto the water-oil interface. *Journal of Colloid and Interface Science*, *378*(1), 135–143. https://doi.org/10.1016/j.jcis.2012.04.033

Rangel-Yagui, C. O., Pessoa Jr, A., & Tavares, L. C. (2005). Micellar solubilization of drugs. *J. Pharm. Pharm. Sci*, *8*(2), 147–163.

Rao, I., Zerpa, L. E., Sloan, E. D., Koh, C. A., Sum, A. K., & Danielson, T. J. (2013). Multiphase Flow Modeling of Gas-Water-Hydrate Systems. *Otc*.

Rashid, S., Harimi, B., & Hamidpour, E. (2017). Prediction of CO2-Brine interfacial tension using a rigorous approach. *Journal of Natural Gas Science and Engineering*, *45*, 108–117. https://doi.org/10.1016/j.jngse.2017.05.002

Ren, Q. Y., Chen, G. J., Yan, W., & Guo, T. M. (2000). Interfacial tension of (CO2 + CH4) + water from 298 K to 373 K and pressures up to 30 MPa. *Journal of Chemical and Engineering Data*, *45*(4), 610–612. https://doi.org/10.1021/je990301s

Renner, R. (2006). The long and the short of perfluorinated replacements. ACS Publications.

Richards, M. P., Chaiyasit, W., McClements, D. J., & Decker, E. A. (2002). Ability of

surfactant micelles to alter the partitioning of phenolic antioxidants in oil-in-water emulsions. *Journal of Agricultural and Food Chemistry*, *50*(5), 1254–1259.

Río, O., & Neumann, A. (1997). Axisymmetric Drop Shape Analysis: Computational Methods for the Measurement of Interfacial Properties from the Shape and Dimensions of Pendant and Sessile Drops. *Journal of Colloid and Interface Science*, *196*(2), 136–147. https://doi.org/10.1006/jcis.1997.5214

Rodriguez, O. M. H. (2016). Instability due to interfacial tension in parallel liquid-liquid flow. In *AIP Conference Proceedings* (Vol. 1738). https://doi.org/10.1063/1.4952120

Rodriguez, O. M. H., Mudde, R. F., & Oliemans, R. V. A. (2006). Stability analysis of slightly-inclined stratified oil-water flow, including the distribution coefficients and the cross-section curvature. In *5th North American Confernce on Multiphase Technology* (Vol. 2006, pp. 229–245).

Rosen, M. J., & Kunjappu, J. T. (2012). *Surfactants and interfacial phenomena*. John Wiley & Sons.

Rosenberg, E., Legmann, R., Kushmaro, A., Taube, R., Adler, E., & Ron, E. Z. (1992). Petroleum bioremediation - a multiphase problem. *Biodegradation*. https://doi.org/10.1007/BF00129092

Rotenberg, Y., Boruvka, L., & Neumann, A. W. (1983). Determination of surface tension and contact angle from the shapes of axisymmetric fluid interfaces. *Journal of Colloid and Interface Science*, *93*(1), 169–183.

Rusanov, A. I., & Prokhorov, V. A. (1996). *Interfacial tensiometry* (Vol. 3). Elsevier.

Rushing, J. A., Newsham, K. E., Fraassen, K. C. Van, Mehta, S. a, & Moore, G. R. (2008). Laboratory Measurements of Gas-Water Interfacial Tension at HP/HT Reservoir Conditions. *CIPC/SPE Gas Technology Symposium 2008 Joint Conference*. https://doi.org/10.2118/114516-ms

Sachs, W., & Meyn, V. (1995). Pressure and temperature dependence of the surface tension in the system natural gas/water. *Colloids and Surfaces A: Physicochemical and Engineering Aspects*, *94*, 291–301.

Saeki, S., Kuwahara, N., Nakata, M., & Kaneko, M. (1977). Phase separation of poly (ethylene glycol)-water-salt systems. *Polymer*, *18*(10), 1027–1031.

Salager, J.-L., Marquez, N., Graciaa, A., & Lachaise, J. (2000). Partitioning of ethoxylated octylphenol surfactants in microemulsion− oil− water systems: Influence of temperature and relation between partitioning coefficient and physicochemical formulation. *Langmuir*, *16*(13), 5534–5539.

Sansotera, M., Navarrini, W., Resnati, G., Metrangolo, P., Famulari, A., Bianchi, C. L., & Guarda, P. A. (2010). Preparation and characterization of superhydrophobic conductive fluorinated carbon blacks. *Carbon*, *48*(15), 4382–4390. https://doi.org/10.1016/j.carbon.2010.07.052

Sattari-Najafabadi, M., Esfahany, M. N., Wu, Z., & Sunden, B. (2018). Mass transfer between phases in microchannels: A review. *Chemical Engineering and Processing - Process Intensification*, *127*(March), 213–237. https://doi.org/10.1016/j.cep.2018.03.012

Sauerer, B., Stukan, M., Abdallah, W., & Buiting, J. (2017). Toward Determining Interfacial Tension at Reservoir Conditions Based on Dead Oil Measurements. *SPE Journal*, (Lenormand 1990).

Schmidt, K. A. G., Folas, G. K., & Kvamme, B. (2007). Calculation of the interfacial tension of the methane-water system with the linear gradient theory. *Fluid Phase Equilibria*, *261*(1–2), 230–237. https://doi.org/10.1016/j.fluid.2007.07.045

Scriven, L. E. (1960). Dynamics of a fluid interface equation of motion for Newtonian surface fluids. *Chemical Engineering Science*, *12*(2), 98–108.

Shannak, B. A. (2008). Frictional pressure drop of gas liquid two-phase flow in pipes. *Nuclear Engineering and Design*. https://doi.org/10.1016/j.nucengdes.2008.08.015

Simon, M. (1851). Recherches sur la capillarité. In *Annales de Chimie et de Physique* (Vol. 32).

Sloan, E. D. (2005). A changing hydrate paradigm - From apprehension to avoidance to risk management. *Fluid Phase Equilibria*, *228–229*, 67–74. https://doi.org/10.1016/j.fluid.2004.08.009

Sugden, S. (1924). The determination of surface tension from the maximum pressure in bubbles. Part II. *Journal of the Chemical Society, Transactions*, *125*, 27–31.

Sun, C. Y., Chen, G. J., & Yang, L. Y. (2004). Interfacial tension of methane + water with surfactant near the hydrate formation conditions. *Journal of Chemical and Engineering*

Data, *49*(4), 1023–1025. https://doi.org/10.1021/je049948p

Sutton, R. P. (2009). An improved model for water-hydrocarbon surface tension at reservoir conditions. In *Proceedings - SPE Annual Technical Conference and Exhibition* (Vol. 6, pp. 3968–3985). Marathon Oil Company, United States. Retrieved from https://www.scopus.com/inward/record.uri?eid=2-s2.0-78349303418&partnerID=40&md5=2837d3680803c91fd506dc26793411a7

Tadros, T. (2013). Gibbs Adsorption Isotherm. In T. Tadros (Ed.), *Encyclopedia of Colloid and Interface Science* (p. 626). Berlin, Heidelberg: Springer Berlin Heidelberg. https://doi.org/10.1007/978-3-642-20665-8_97

Tan, C., Dong, F., & Wu, M. (2007). Identification of gas/liquid two-phase flow regime through ERT-based measurement and feature extraction. *Flow Measurement and Instrumentation*, *18*(5–6), 255–261. https://doi.org/10.1016/j.flowmeasinst.2007.08.003

Teja, A. S., Garg, K. B., & Smith, R. L. (1983). A method for the calculation of gas-liquid critical temperatures and pressures of multicomponent mixtures. *Industrial & Engineering Chemistry Process Design and Development*, *22*(4), 672–676. https://doi.org/10.1021/i200023a022

Utvik, O. H., Rinde, T., & Valle, A. (2001). An experimental comparison between a recombined hydrocarbon-water fluid and a model fluid system in three-phase pipe flow. *Journal of Energy Resources Technology, Transactions of the ASME*, *123*(4), 253–259. https://doi.org/10.1115/1.1410365

Watanabe, K., Niwa, S., & Mori, Y. H. (2005). Surface tensions of aqueous solutions of sodium alkyl sulfates in contact with methane under hydrate-forming conditions. *Journal of Chemical and Engineering Data*, *50*(5), 1672–1676. https://doi.org/10.1021/je050139v

Weisman, J., Duncan, D., Gibson, J., & Crawford, T. (1979). Effects of fluid properties and pipe diameter on two-phase flow patterns in horizontal lines. *International Journal of Multiphase Flow*, *5*(6), 437–462.

Xu, W. (2005). Experimental investigation of dynamic interfacial interactions at reservoir conditions.

Yahaya, A. A., Akpan, E. U., Enyi, G. C., Nasr, G. G., & Abbas, J. (2018). Experimental investigation of methane-water and methane-brine IFT measurements using pendant drop

(rising bubble). *Journal of Engineering Technology*, *6*(1), 394–407.

Yan, W., Zhao, G.-Y., Chen, G.-J., & Guo, T.-M. (2001). Interfacial Tension of (Methane + Nitrogen) + Water and (Carbon Dioxide + Nitrogen) + Water Systems. *J. Chem. Eng. Data*, *46*, 1544–1548. https://doi.org/10.1021/je0101505

Yarranton, H. W., & Masliyah, J. H. (1996). Gibbs-Langmuir model for interfacial tension of nonideal organic mixtures over water. *Journal of Physical Chemistry*, *100*(5), 1786–1792. https://doi.org/10.1021/jp952017n

Yasuda, K., Mori, Y. H., & Ohmura, R. (2016). Interfacial tension measurements in water−methane system at temperatures from 278.15 K to 298.15 K and pressures up to 10 MPa. *Fluid Phase Equilibria*, *413*, 170–175. https://doi.org/10.1016/j.fluid.2015.10.006

Zana, R. (2002). Dimeric and oligomeric surfactants. Behavior at interfaces and in aqueous solution: a review. *Advances in Colloid and Interface Science*, *97*, 205–253. https://doi.org/10.1016/S0001-8686(01)00069-0

Zerpa, L. E., Salager, J., Koh, C. A., Sloan, E. D., & Sum, A. K. (2011). Surface Chemistry and Gas Hydrates in Flow Assurance. *Industrial & Engineering Chemistry Research*, *50*, 188–197.

Zhang, C., & Carloni, P. (2012). Salt effects on water/hydrophobic liquid interfaces: A molecular dynamics study. *Journal of Physics Condensed Matter*, *24*(12). https://doi.org/10.1088/0953-8984/24/12/124109

Zhang, L., Zhou, S., Wang, S., Wang, L., & Li, J. (2013). Surfactant Surface Tension Effects on Promoting Hydrate Formation: An Experimental Study Using Fluorocarbon Surfactant (Intechem-01) + SDS Composite Surfactant. *Journal of Environmental Protection*, *04*(05), 42–48. https://doi.org/10.4236/jep.2013.45A005

Zhao, C. X., & Middelberg, A. P. J. (2011). Two-phase microfluidic flows. *Chemical Engineering Science*, *66*(7), 1394–1411. https://doi.org/10.1016/j.ces.2010.08.038

Appendices

List of Appendices

Appendix A

DropImage Advanced Software

A1.1: The DROPimage Advanced Software

It is possible to record the evolution of liquid drop into another liquid, or gas bubble into liquid as a function of time, Using a pendant drop system. Live images of the drop or bubble are taken at a specific recurrence which relies upon the experimental duration. The images captured are digitised by a frame grabber which interface the rame-hart camera to the data acquisition system. The contours of the bubbles are evaluated to infer interfacial tension from the captured profile of the bubble using different programs. The whole process of digitisation and analysis of the bubble lasts less than 40 seconds. It consists of four steps:

i.   Capture and digitisation of the image of the pendant bubble.

ii. Extraction of the drop contour, and determination of the radius of curvature at the apex necessary for the calculation of interfacial tension

iii. Smoothing of the extracted curve of the bubble using polynomial regression as described in section 1.10.1.

iv. Profile comparison between the theoretical and experimental bubble, inferring the IFT value.

A1.2: Program futures

The DROPimage Advanced program has various futures that influence the procedure of IFT measurement flexible and straightforward. The kind of measurement, number and timing, calibration, data presentation and analysis are for the most part controllable inside the program, and the transfer of data with another application by standard Windows procedures make further presentation and analysis convenient.

The primary measurement capabilities include the type of drops (pendant, inverted pendant, sessile and captive bubble), type of results (Surface/interfacial tension, contact angle, the surface energy of solids, drop or bubble dimensions, surface elasticity and viscosity). Also, type of measurements (constant volume drops, volume steps and relaxation, Oscillation) are among the critical futures of the programme.

 shows the screen of the data acquisition system window, which contained live video and captured image windows. The captured image window is the primary window. This image is scalable and is utilised to set the limits and start position of the edge recognition algorithm.

The recognised edge is likewise plotted in this image as a visual sign of the accurate operation of the edge identification. In addition to this image, a live display of the camera output is also available, either in a 1:1 or a 1:2 scale. The real-time display might be turned on and off by using the Start pass thru/Stop pass thru flip on the View menu.
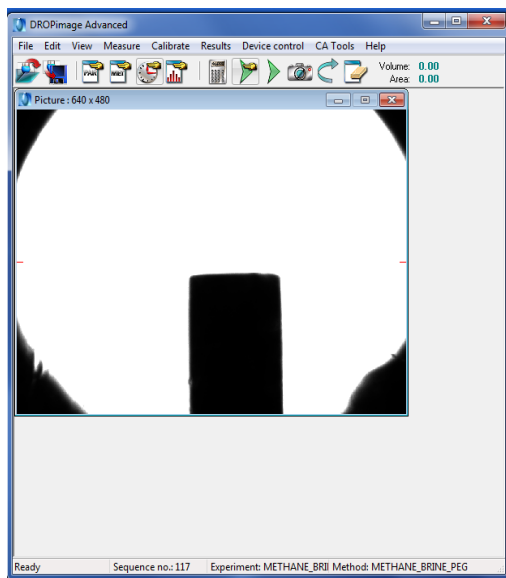
Figure A-1: Display screen showing inserted capillary tube in the chamber

After calibrating and setting up the instrument according to the instruction provided, the micro-syringe assembly is then filled with the test liquid, while the straight needle to the syringe is attached firmly. The dispensing valve on the micro-syringe is then turned on to remove air from the needle. The DROPimage Advanced software is then started. The micro-syringe is adjusted into the fixture so that the tip of the needle is visible in the centre top of the DROPimage live image as indicated in.

A1.3: DROPimage experimental setting

A new experiment is begun using the experiment Wizard, by clicking on File > New Experiment Wizard or using the shortcut on the keyboard by hitting Ctrl-T. The dialogue box will appear as shown in

Figure A-2: Screen displayed for setting up a new experiment dialogue box

For the purpose of the present investigation, "Surface tension – pendant" is selected. By clicking on the next button, the dialogue box will change as indicated in Figure A-3 , where the specific experimental name is entered, in this case, "Methane_Brine2.9%_10%PEG". In the current study, the experimental name is written to represent the types and percentage components of the fluids under investigation.
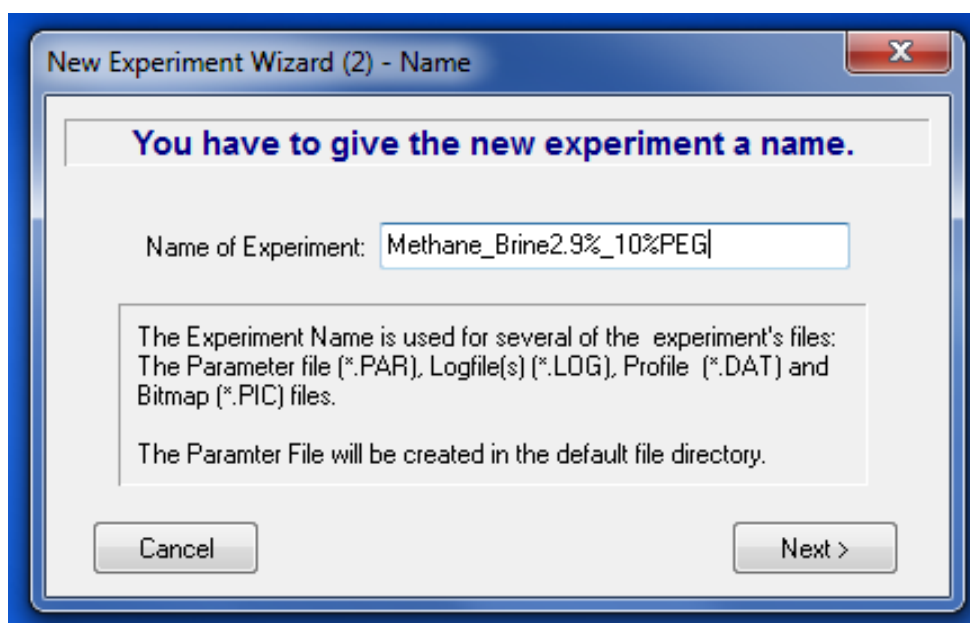
Figure A-3: Screen displayed dialogue box for naming the new experiment

135

Figure A-4 shows the dialogue box that will appear after naming the test. In this dialogue box, the bubble or droplet and surrounding phase are specified. In the current display the droplet phase, 'Methane' was selected from the list while 'Water' was selected for the external phase. The solid phase is the needle which was made from steel. Hence steel was chosen for the solid phase.
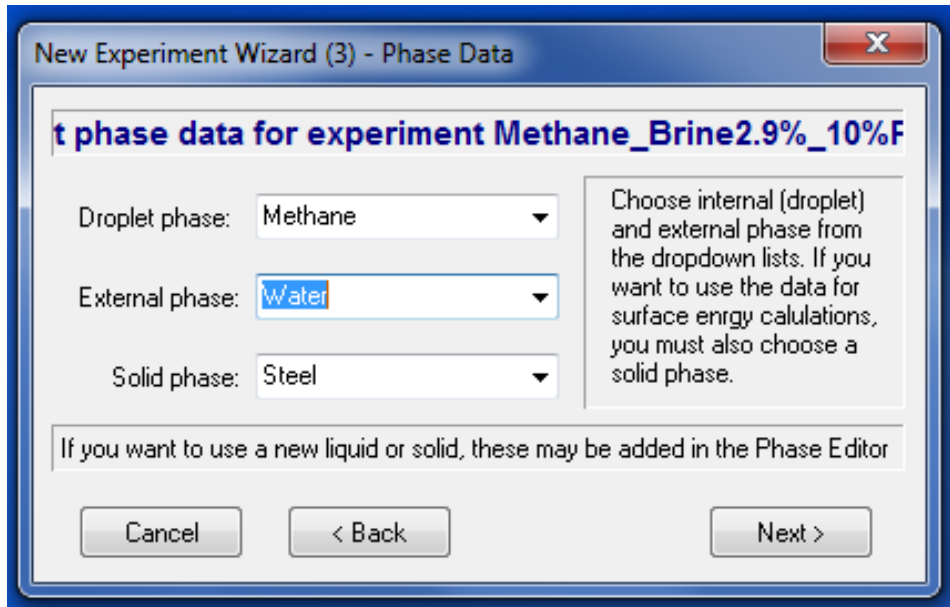
Figure A-4: Dialogue box indicating phase input data for the IFT measurement

By clicking on the next button, the experimental timing dialogue box will appear as presented in **Figure A-5**.
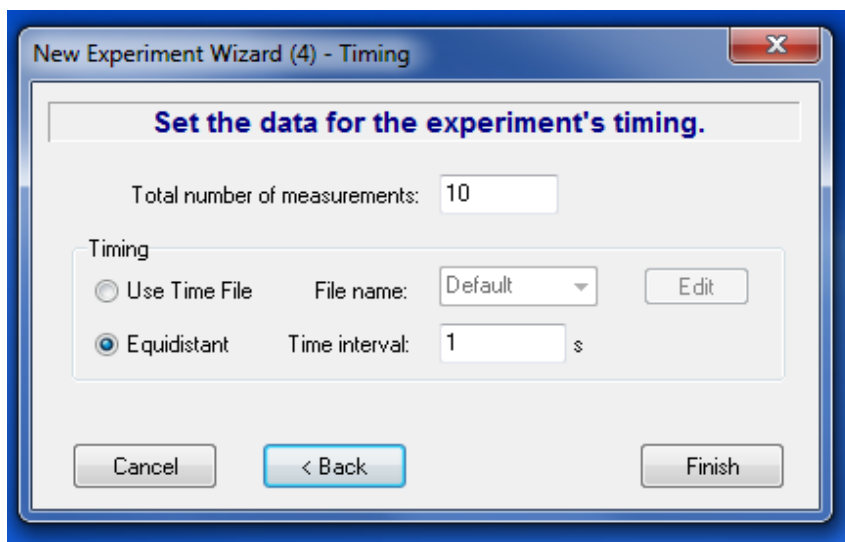
Figure A-5: Dialogue box indicating timing input data for the IFT measurement

In the current investigation, the average of 10 IFT measurements was taken over 10 seconds at 1 second time interval and equidistant timing. Hence, all the required data was entered as indicated in the dialogue box.

After the timing data is entered, then the finish button was clicked to finish the setting for the subsequent IFT measurement after generating the bubble and making sure the experimental conditions are set.

On clicking the finish button, the DROPimage will create a Parameter and Method file for the experiment with the displayed final dialogue box as shown. Clicking on yes button will continue to run the test if the bubble or drop and the experimental conditions are set. However, if not the NO button is clicked to allowed setting the drop or bubble under the experimental condition.

Figure A-6: Information display showing final step in setting the new experiment

Figure A-7 shows the real-time measurement window indicating the methane bubble, the cross hair lines and measure command dialogue box. The valve connected to the needle is used to dispense the test gas thereby producing a pendant bubble (of methane gas) as shown in Figure A-7
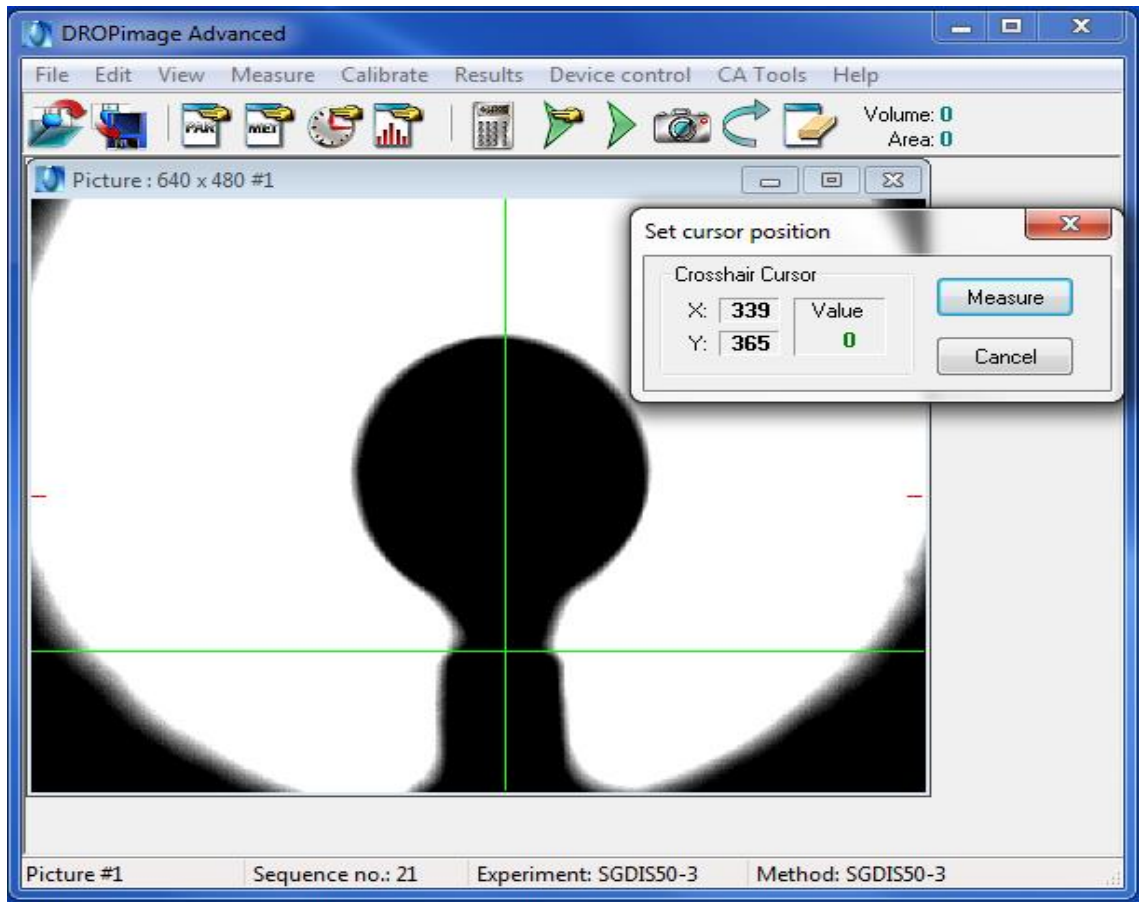
Figure A-7: Drop film showing the crosshair lines

Subsequent to making the bubble, it was vital to ensure that the illumination is set appropriately via video setup in the edit menu of the programme. For the purpose of the current study, in the net video control the brightness is set to 432, gain to 129. The shutter is set to 727 while the auto exposure is left automatic. This setting will set the interface between the bubble phase methane and the surrounding phase water to be crisp. The crosshair line was placed just at the interface between the bubble and the needle and the vertical line pass through the centre of the bubble and the needle appeared in Figure A-7.

A1.4: IFT Results Tabulation Window

All IFT experimental measurement results were displayed in a tabular form in the program's results window as presented in Figure A-8. This window contains two menu button for IFT (surface tension) and contact angle depending on the experiment being carried out. Hence for the present investigation IFT results window were considered.

Figure A-8: IFT/Surface tension results window

The result window provided the following information:

1. No.: run number.

2. Time: precise time in seconds of measurement relative to the start of the current run.

3. Gamma: surface tension in mN/m.

4. Beta: shape factor; as a rule, a number between 0.2 and 0.4 is good.

5. RO: the radius of curvature at the drop's apex in nm.

6. Area: the drop surface area in mm^2.

7. Volume: the drop volume in mm^3.

8. Theta: the contact angle at the drop limit (horizontal) baseline.

9. Height: the total measured the distance from baseline to the drop apex in mm.

10. Width: the dimension in mm at the maximum width.

11. Opt: the number of optimisations performed.

12. Messages: errors or other messages.

A1.5: Method Driven Measurement

A method comprises of a collection of parameters that portrays how and when measurements are made and how results are saved and presented. All IFT measurements depend on Measurement Methods**.** A method's parameters are saved in a text file. Methods are created and edited in the Method Editor. All measurement of interfacial tensions must refer to a

method, and quite a lot of measurements can utilize the same method. The method file window is shown in Figure A-9.
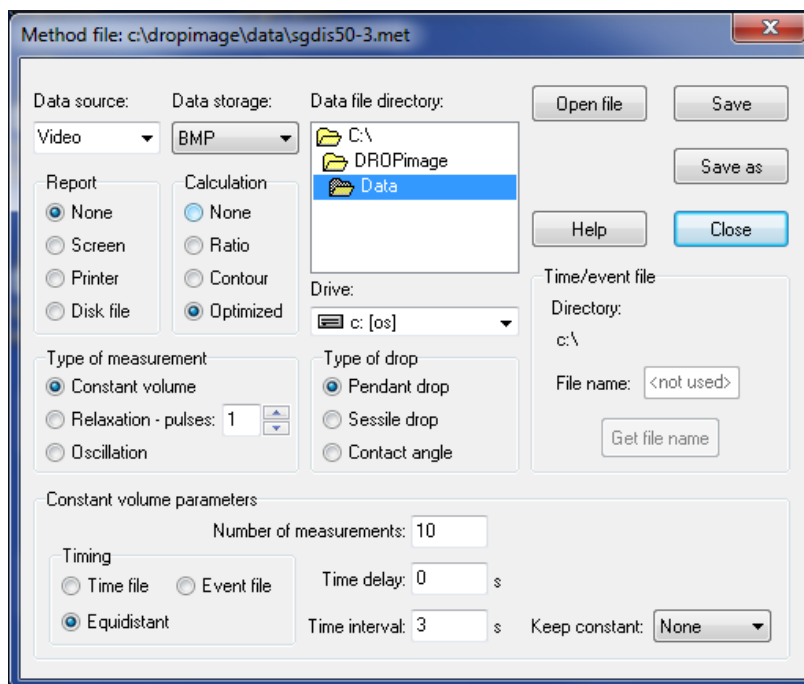
Figure A-9: Method editor without the oscillation option.

There are two categories of methods, depending on the first field, *Data source*. If this is set to *Video*, data are taken from the edge grabber board for further treatment as per alternate parameters. On the off chance that *Data source is Disk file* then this is a Recalculation method that tells the program to read data from a disk file, which must have been produced by a method where the data source is *Video*.

A1.6: Measurement parameters

Keeping in mind, the end goal is to calculate surface tensions; the program must know the densities of the two phases (drop and continuous phase), and the image amplification. These data are saved in a Parameter File seen in Figure 3.24. The parameters are created and edited in the Parameter Editor. This editor is connected to the Phases data file that contains the density data of numerous mainstream liquids and gases. This data file is retained in a different Phase Editor. Notwithstanding the input parameters in the Parameter editor, two parameters are consequently included from the calibration values. Using the measurement parameters, surface tension can be measured by a simple basic methodology leading to single or multiple readings as indicated by the method in the parameter file.
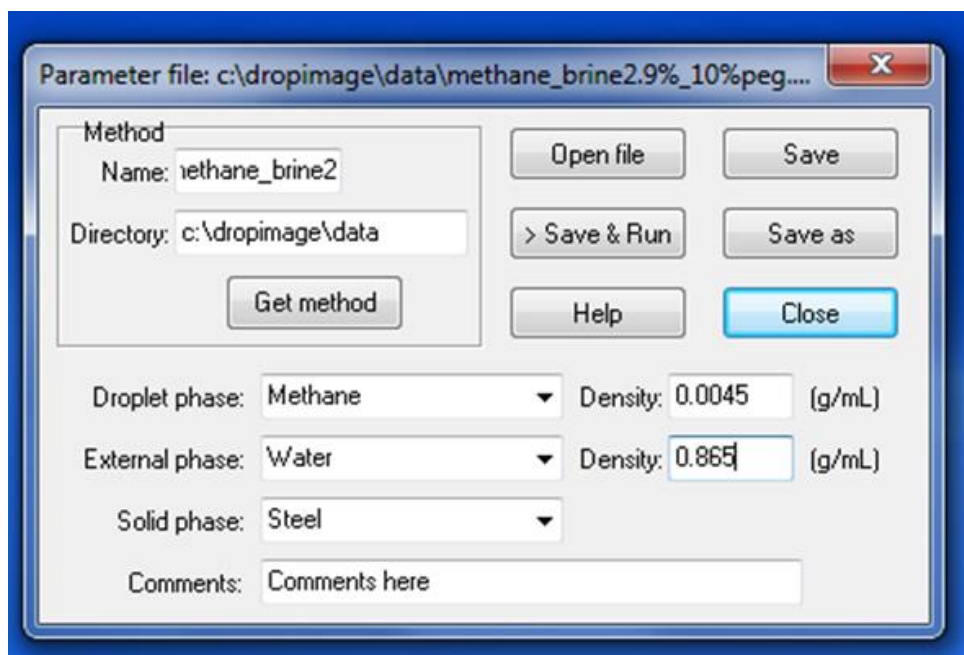
Figure A-10: Parameter file

A1.7: Experimental run/IFT measurement

i.   Droping.exe file on the desktop was initiated, which opened a new experiment wizard option box. Surface Tension-Pendant was selected.

ii.   On clicking next, an option box to name the new experiment was displayed, and SVU_IFT was entered.

iii.   The drop phase was oil and formation water mixed with bio-surfactant was selected as the outer phase. The solid phase was steel, which refers to the tip of the needle.

iv.   This followed by setting the data for the experiment's timing. A number of experiment was selected to ten (10), and time interval of two (3) seconds. The wizard then saved the choices in new parameter and method files.

v.   The yes button was then clicked to start the experiment. The measure parameter box appeared with the crosshair lines (vertical and horizontal).

vi.   The drop was released to the near buoyant point. A picture of the drop was taken using the camera button on the tool bar. Then the crosshairs were positioned correctly on the drop for accurate readings, and the measure button was clicked to take measurements. The IFT values were recorded.

vii.   Before the readings were taken, the video setup was selected from the view option box on the main window to adjust the video properties. This was necessary for clearer viewing of the drop profile. The camera zoom was adjusted to 100%

Appendix B

The apparent viscosity of the polymer-surfactant mixture in water

B1.1: Viscosity, shear stress as a function of shear rate

Figure B-1 and Figure B-2 shows the corresponding results obtained for shear stress and viscosity as a function of shear rate of PEG 8000 and various concentration of NaCl at 303.15 K. The viscosity has been reported at 298.15, 308.15 and 313.15 K in this work. The shear stress was seen to be increasing as the shear rate increases. This behaviour represents the Newtonian fluid characteristics, hence the classification of the PEG 8000 in the presence of NaCl. The viscosity was also observed to be decreasing with the corresponding increase in the shear rate, confirming the fluid characterisitcs. This fluid characteristics can be seen in Figure B-2. can be seen It has been observed that increasing the temperature of the system has significant effect on the viscosity of the polymer-surfatactant mixture, due to the increase in the molecular activity of the solution.
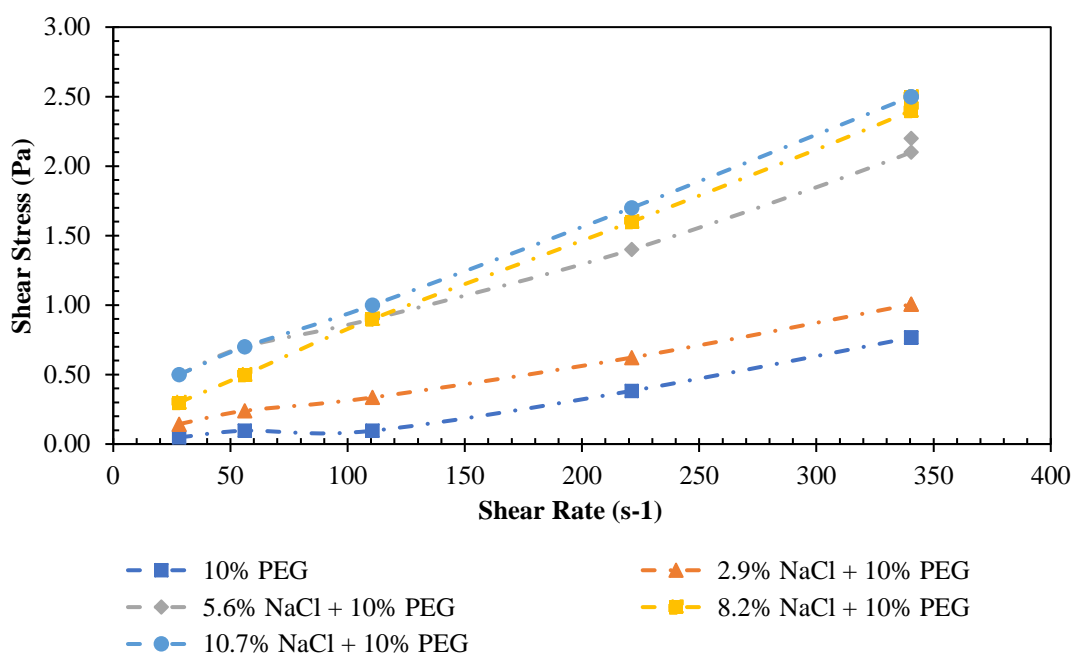
Figure B-1: Shear stress vs shear rate of 10% PEG 8000 and various concentration of NaCl at 303.15 K
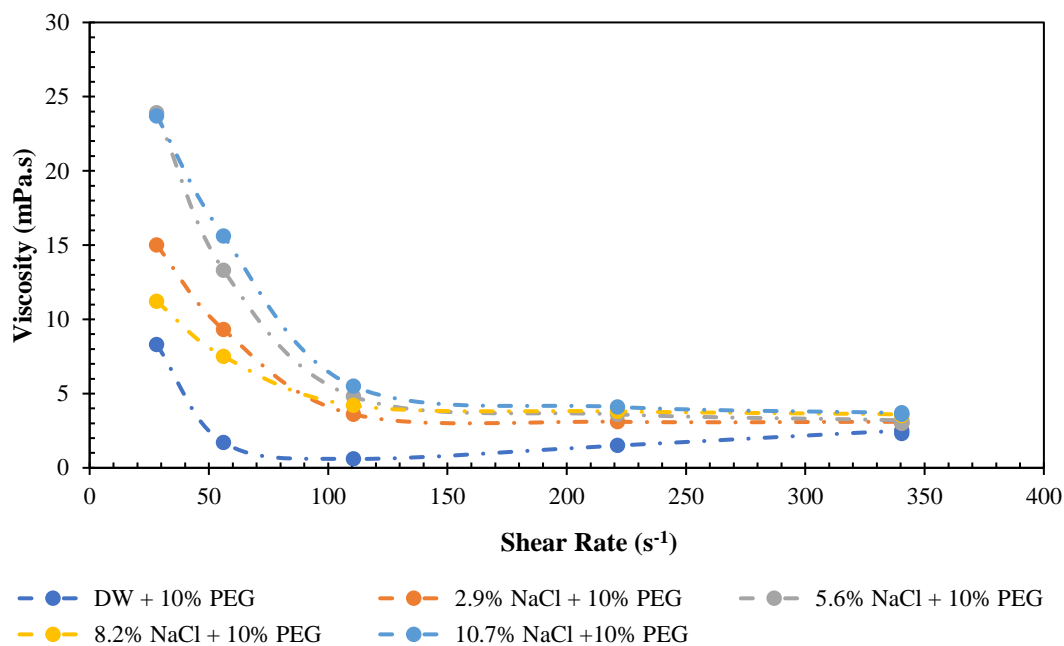
Figure B-2: Viscosity as a function of shear rate of 10% PEG 8000 and various concentration of NaCl at 303.15 K

As shown in Figure B-3 and Figure B-4, decrease in the viscosity were generally observed as compared to the results obtained at 298.15 K. There was no observed change in fluid behaviour due to temperature increase. The sample maintains non-Newtonian flow and pseudo-plastic nature.

The observed trend of shear stress and viscosity due to variation in the shear rate at 308.15 K are shown in Figure B-3 and Figure B-4 respectively. At this temperature of 308.15 K, an instability was observed for the shear stress at a lower shear rate of $28 - 60$ s^{-1}, however at a shear rate above 60 s^{-1} a stable increase in shear stress with an increase in shear rate was achieved.
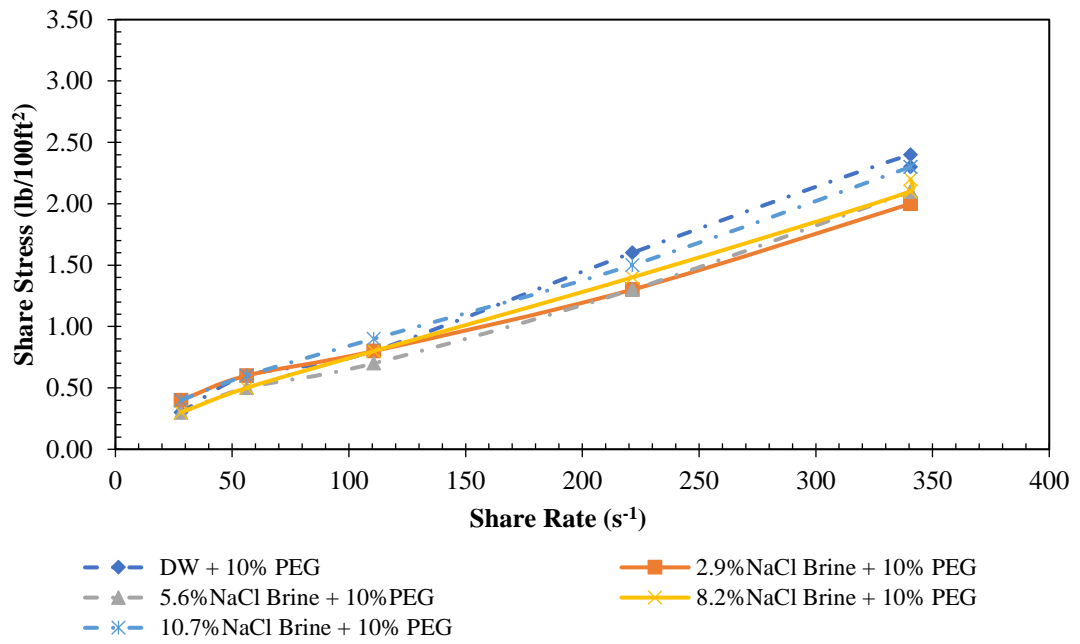
Figure B-3: Shear stress as a function of shear rate of 10% PEG 8000 and various concentration of NaCl at 308.15 K
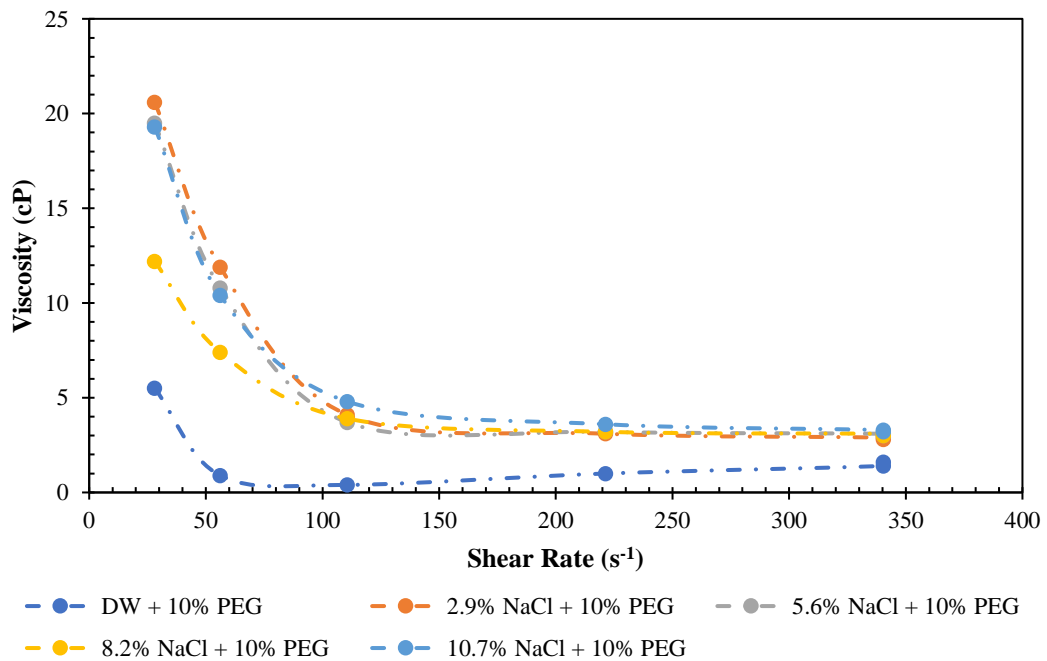
Figure B-4: Viscosity as a function of shear rate of 10% PEG 8000 and various concentration of NaCl at 308.15 K

Also, a significant effect was observed at this temperature in the viscosity of PEG 8000 and H_2O in the absence of NaCl, as seen in Fig. the higher behaviour of the solution one can

The rheology of PEG 8000 and various concentration of NaCl at 313.15 K are presented in (Fig ?) and (Fig ?) respectively.
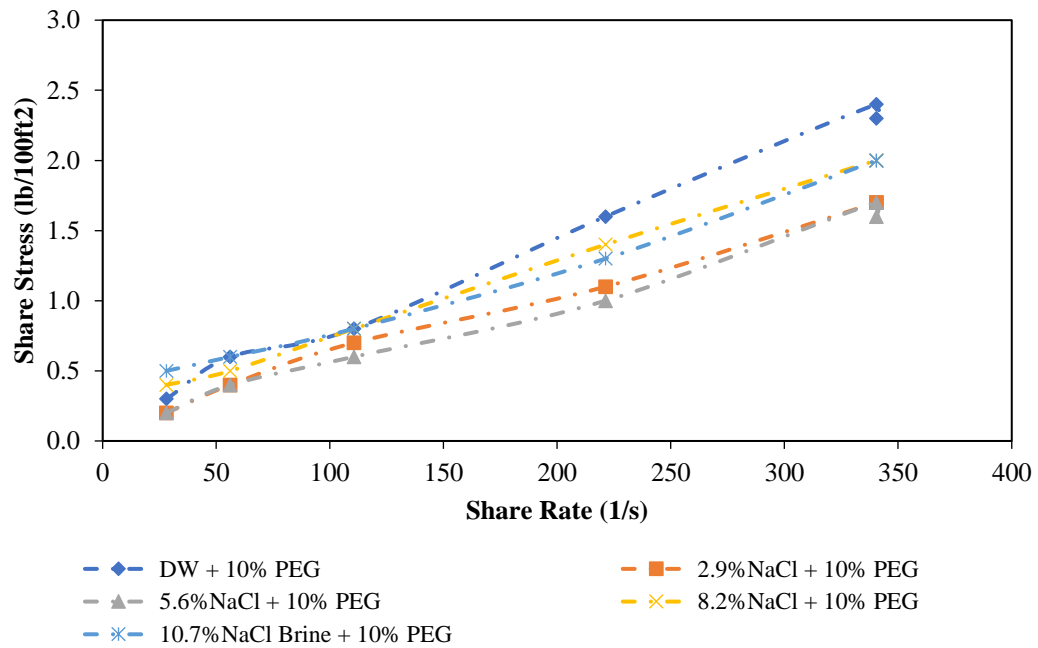
Figure B-5: Shear stress as a function of shear rate of 10% PEG 8000 and various concentration of NaCl at 313.15 K
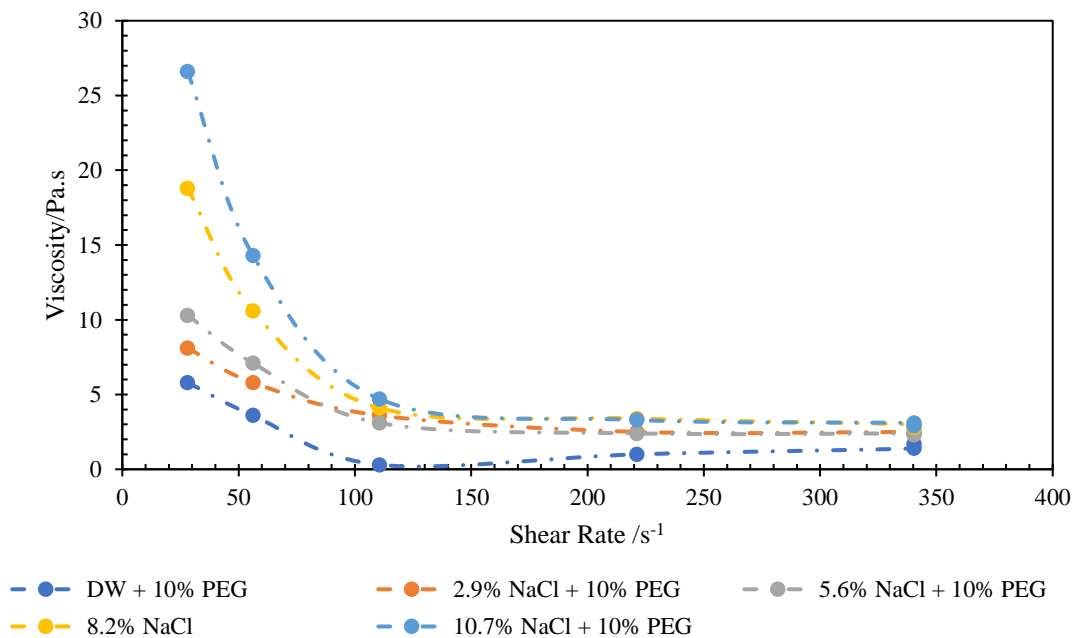
Figure B-6: Viscosity dependence on the shear rate at different concentration of NaCl and 10% PEG at 313.15 K

Overall as seen in Fig. 4.9 – 4.16 shows the change in viscosity and shear stress due to variation in the shear rate of 10% PEG 8000 solution in water and the presence of 2.9, 5.6, 8.2 and 10.7 wt% NaCl. Also, the investigation was carried out each at 298.15, 202.15, 308.15 and 313.15 K of temperature. The results indicated that 10% PEG 8000 solution and in the presence of various concentration of NaCl is characterised to be a pseudo-plastic fluid with a non-Newtonian behaviour. Further, the temperature effects were more pronounced in the absence of NaCl in the temperature range investigated in the present study. Additionally, as observed the presence of NaCl increases the viscosity of the system.

DW+5%PEG @ 298.15 K			DW+5%PEG @ 303.15 K			DW+5%PEG @ 308.15 K			DW+5%PEG @ 313.15K		
S. Rate	S. Stress	Viscosity	S. Rate	S. Stress	Viscosity	S. Rate	S. Stress	Viscosity	S. Rate	S. Stress	Viscosity
28.1	0.2	3.7	28.1	0.2	6.8	28.1	0.2	10	28.1	0.2	8.8
56.2	0.3	2.6	56.2	0.3	3.9	56.2	0.3	5.3	56.2	0.3	5.2
110.6	0.4	1.7	110.6	0.4	2.1	110.6	0.4	2	110.6	0.4	1.9
221.3	0.8	1.9	221.3	0.8	2	221.3	0.7	1.6	221.3	0.7	1.5
340.5	1.2	1.8	340.5	1.3	1.9	340.5	1.1	1.6	340.5	1.1	1.5
340.5	1.3	1.9	340.5	1.3	1.9	340.5	1.1	1.5	340.5	0.9	1.3

DW + 10%PEG @ 25			DW + 10%PEG @ 30			DW + 10%PEG @ 35			DW + 10%PEG @ 40		
S. Rate	S. Stress	Viscosity	S. Rate	S. Stress	Viscosity	S. Rate	S. Stress	Viscosity	S. Rate	S. Stress	Viscosity
28.1	0.14	16.3	28.1	0.05	0.5	28.1	0.05	1.5	28.1	0.05	5.8
56.2	0.24	9.9	56.2	0.10	1.7	56.2	0.05	1.5	56.2	0.05	3.6
110.6	0.38	4.1	110.6	0.10	0.6	110.6	0.10	0.4	110.6	0.05	0.3
221.3	0.77	3.7	221.3	0.38	1.5	221.3	0.34	1.1	221.3	0.29	1

S. Rate	S. Stress	Viscosity	S. Rate	S. Stress	Viscosity	S. Rate	S. Stress	Viscosity	S. Rate	S. Stress	Viscosity
340.5	1.15	3.5	340.5	0.77	2	340.5	0.62	1.6	340.5	0.53	1.4
340.5	1.10	3.3	340.5	0.77	2.3	340.5	0.62	1.9	340.5	0.57	1.7

DW + 20% PEG @ 25			DW+20% PEG @ 30			DW+20% PEG @ 35			DW+20%PEG @ 40		
S. Rate	S. Stress	Viscosity	S. Rate	S. Stress	Viscosity	S. Rate	S. Stress	Viscosity	S. Rate	S. Stress	Viscosity
28.1	1.1	58.1	28.1	1.7	71	28.1	1.6	68.5	28.1	1.5	72
56.2	1.5	34.5	56.2	1.5	34.2	56.2	1.9	41.9	56.2	1.6	40.5
110.6	2.3	11.3	110.6	2.2	11.2	110.6	2.4	13.7	110.6	2.4	13.7
221.3	4.9	10.9	221.3	4.5	10	221.3	3.8	8.6	221.3	3.5	8.2
340.5	7.6	10.9	340.5	6.8	9.6	340.5	5.8	8.5	340.5	5.2	7.4
340.5	7.5	10.6	340.5	6.4	9	340.5	5.9	8.3	340.5	4.8	6.7

DW + 30%PEG @ 25	DW + 30%PEG @ 30	DW + 30%PEG @ 35	DW+ 30%PEG @ 40

S. Rate	S. Stress	Viscosity	S. Rate	S. Stress	Viscosity	S. Rate	S. Stress	Viscosity	S. Rate	S. Stress	Viscosity
28.1	0.7	44.7	28.1	1.2	50.4	28.1	1.1	46.6	28.1	1	46.4
56.2	1.1	26.4	56.2	1.6	28.2	56.2	1.4	26.3	56.2	1.3	26
110.6	2.2	11.8	110.6	2.5	12.4	110.6	2.1	10.7	110.6	2	10
221.3	4.6	10.8	221.3	4.4	10.3	221.3	3.7	8.8	221.3	3.4	8.1
340.5	7.3	10.5	340.5	6.8	9.9	340.5	5.8	8.4	340.5	5.2	7.7
340.5	7.5	10.6	340.5	6.8	9.6	340.5	5.7	8	340.5	5.1	7.2

Appendix C

Interfacial tension measurement

C1.1: Effect of salinity at 303.15, 308.15 and 313.15 K
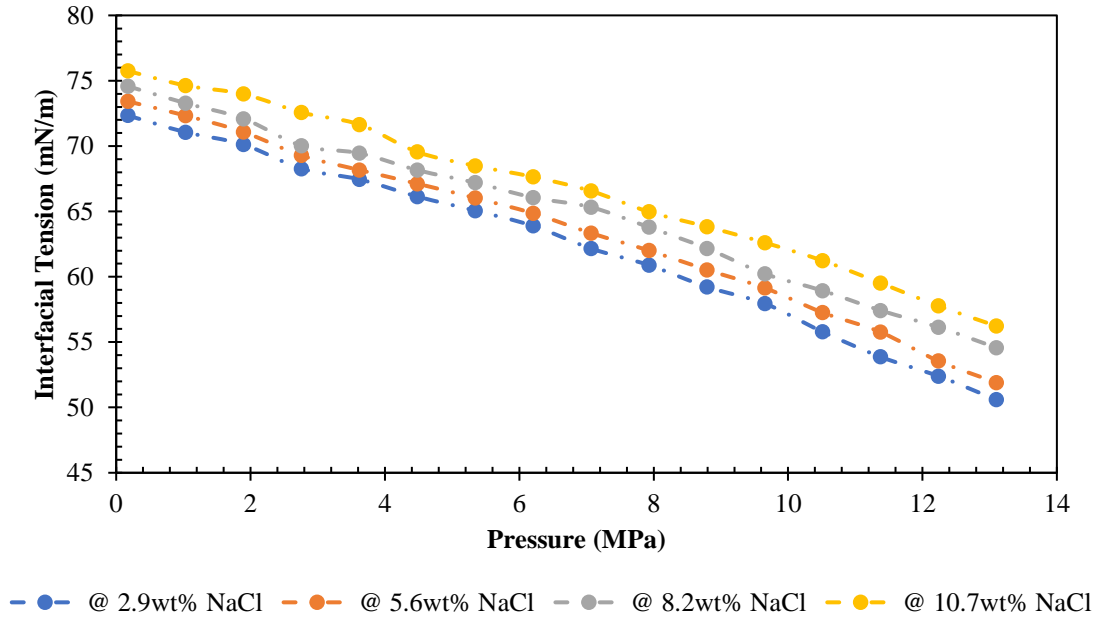
Figure C-1: IFT-pressure diagram for methane – brine measured at 303.15K and various concentration of NaCl
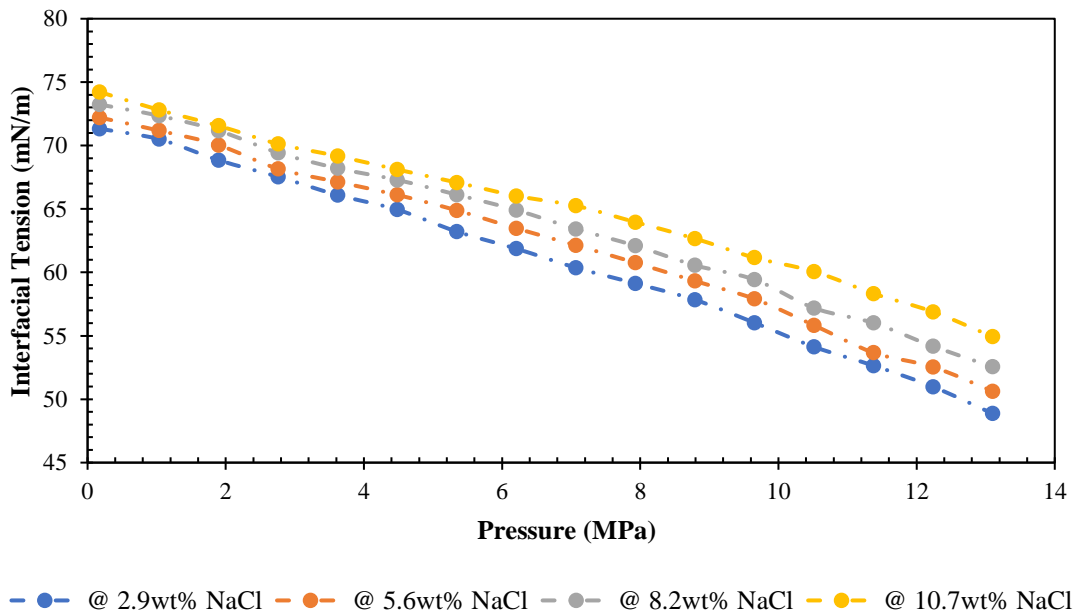
Figure C-2: IFT-pressure diagram for methane – brine measured at 308.15K and various concentration of NaCl
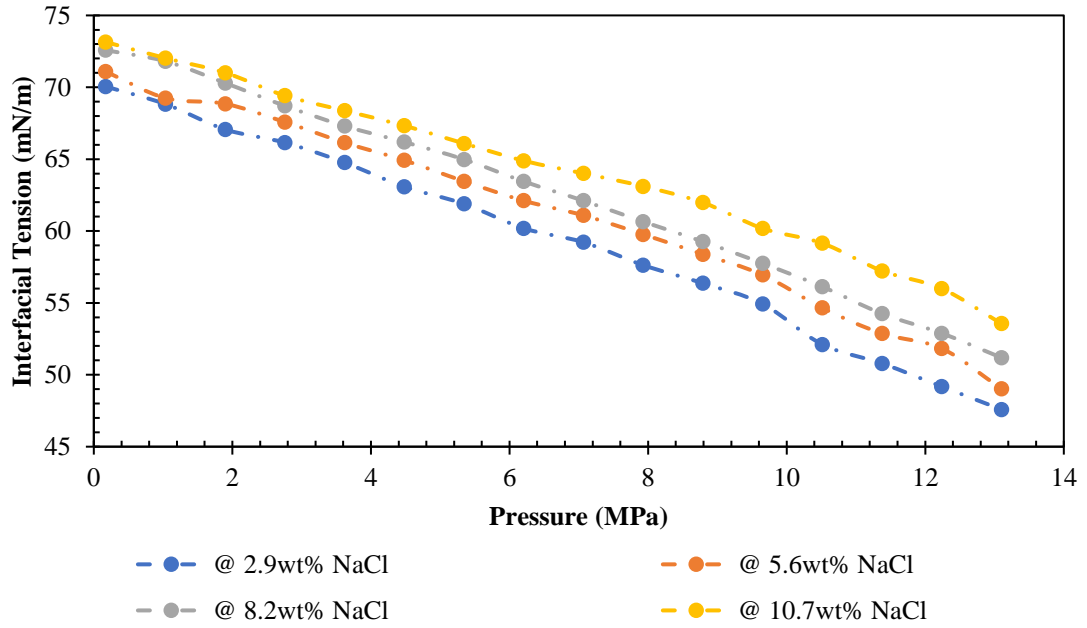
Figure C-3: IFT-pressure diagram for methane – brine measured at 313.15K and various concentration of NaCl

C1.2: Effect of surfactant and salinity

C.1.2.1: 10% PEG 8000 and 5.6, 8.2 and 10.7 wt% NaCl
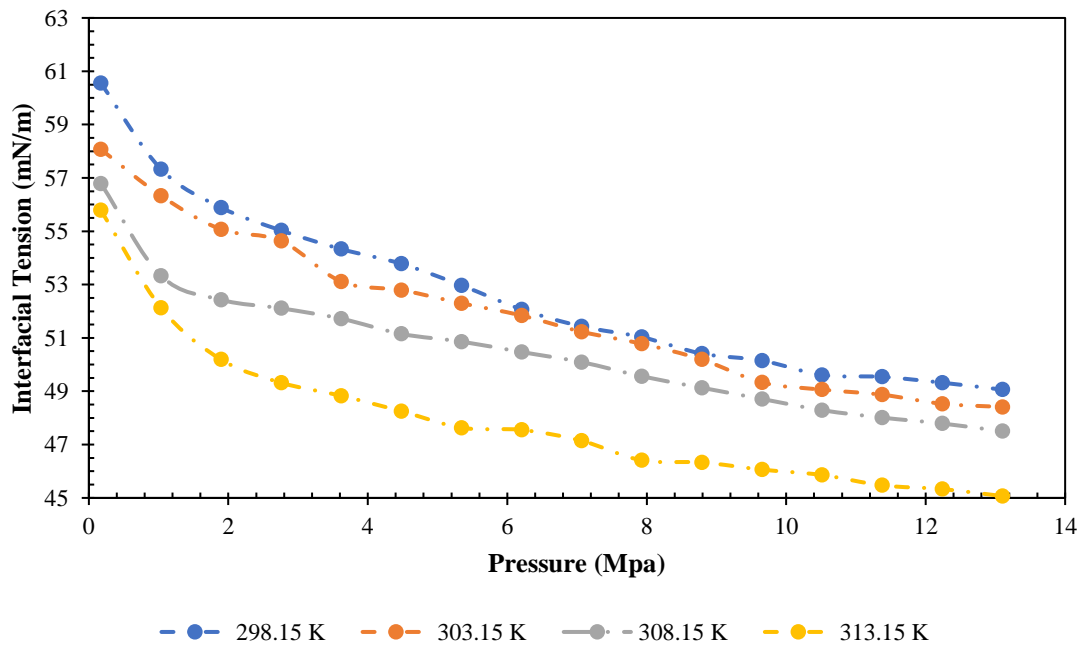
Figure C-4: Methane-water IFT response to change in pressure of 5.6 wt% NaCl and 10% PEG 8000
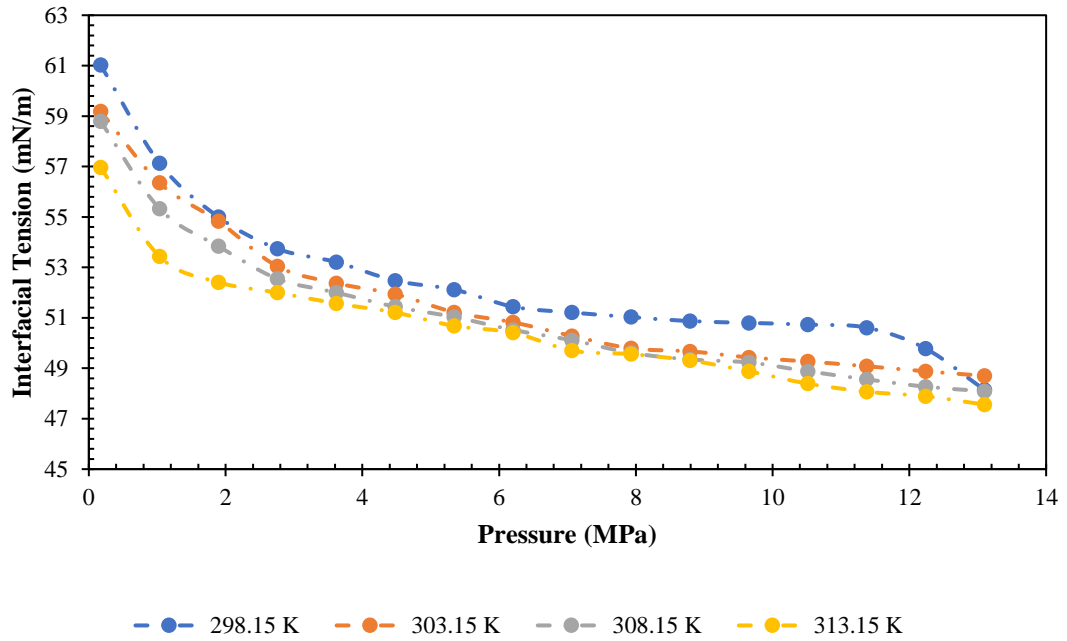
Figure C-5: Methane-water IFT response to change in pressure of 8.2 wt% NaCl and 10% PEG 8000
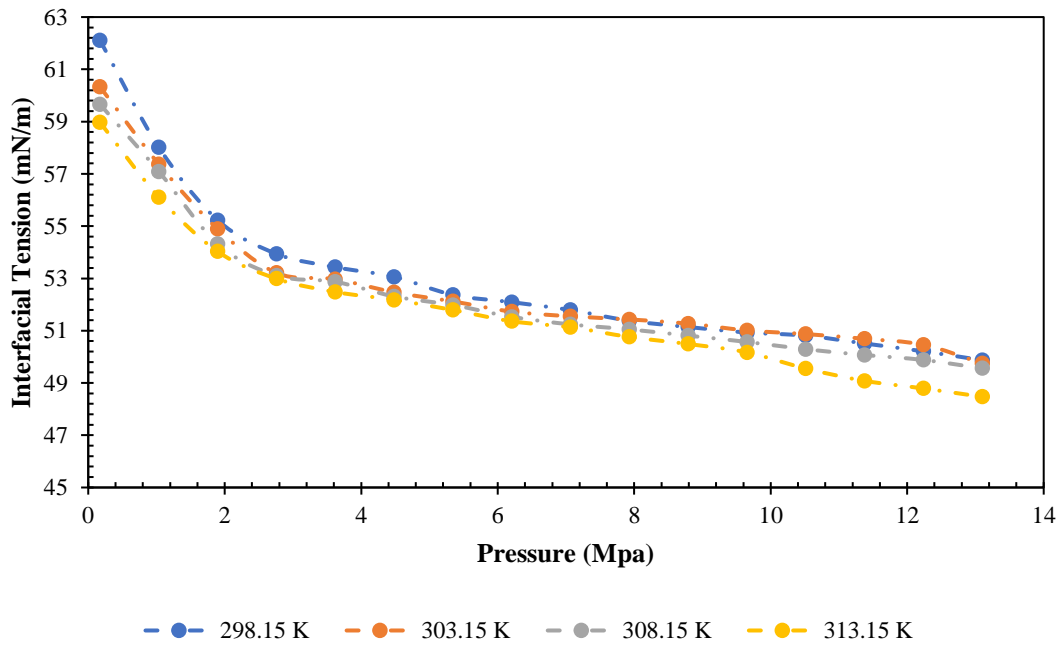
Figure C-6: Methane-water IFT response to changes in pressure of 10.7 wt% NaCl and 10% PEG 8000

C1.2.2: 20% PEG 8000 and 5.6, 8.2 and 10.7 wt% NaCl
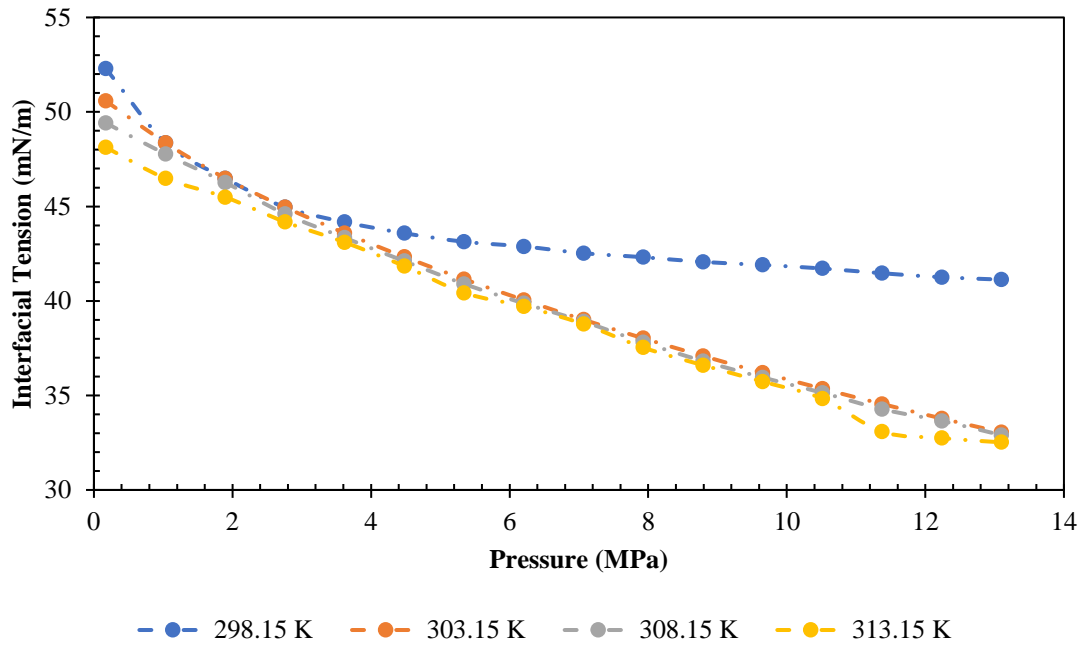
Figure C-7: Methane-water IFT response to change in pressure at 5.6 wt% NaCl and 20% PEG 8000
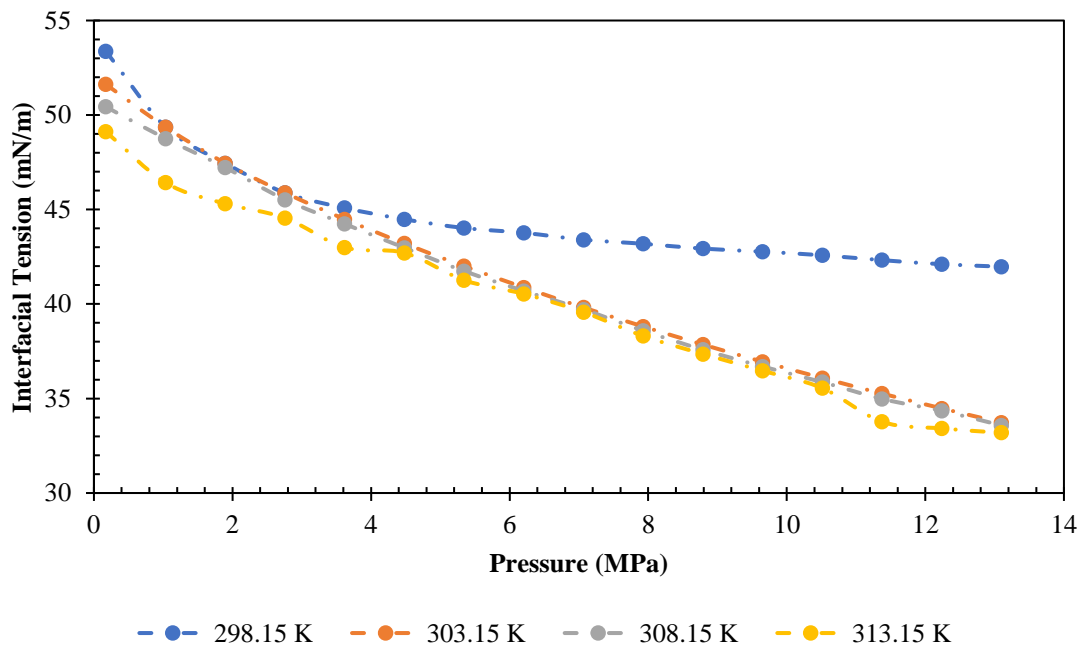
Figure C-8: Methane-water IFT response to change in pressure at 8.2 wt% NaCl and 20% PEG 8000
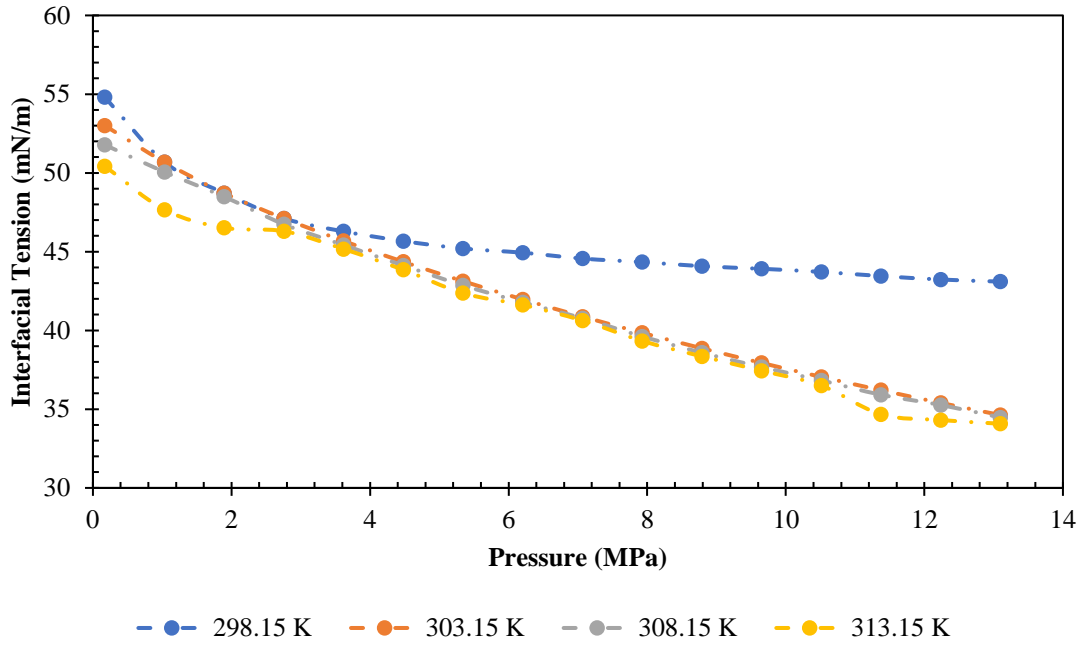
Figure C-9: Methane-water IFT response to change in pressure of 10.7 wt% NaCl and 20% PEG 8000

C1.2.3: 30% PEG 8000 and 5.6, 8.2 and 10.7 wt% NaCl
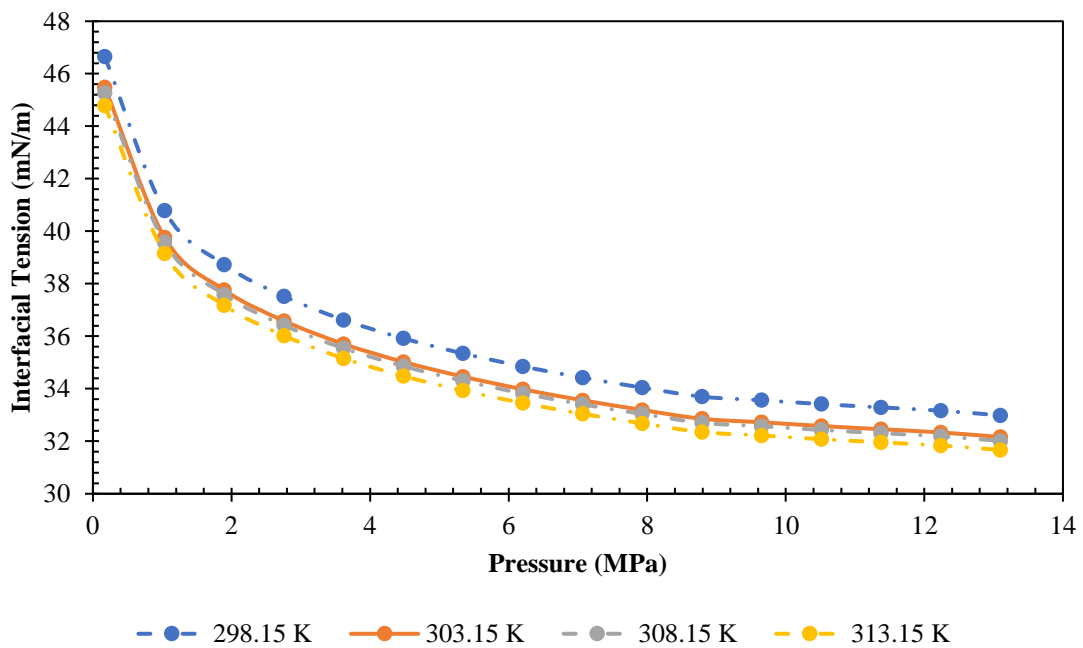
Figure C-10: Methane-water IFT response to change in pressure of 5.6 wt% NaCl and 30% PEG 8000
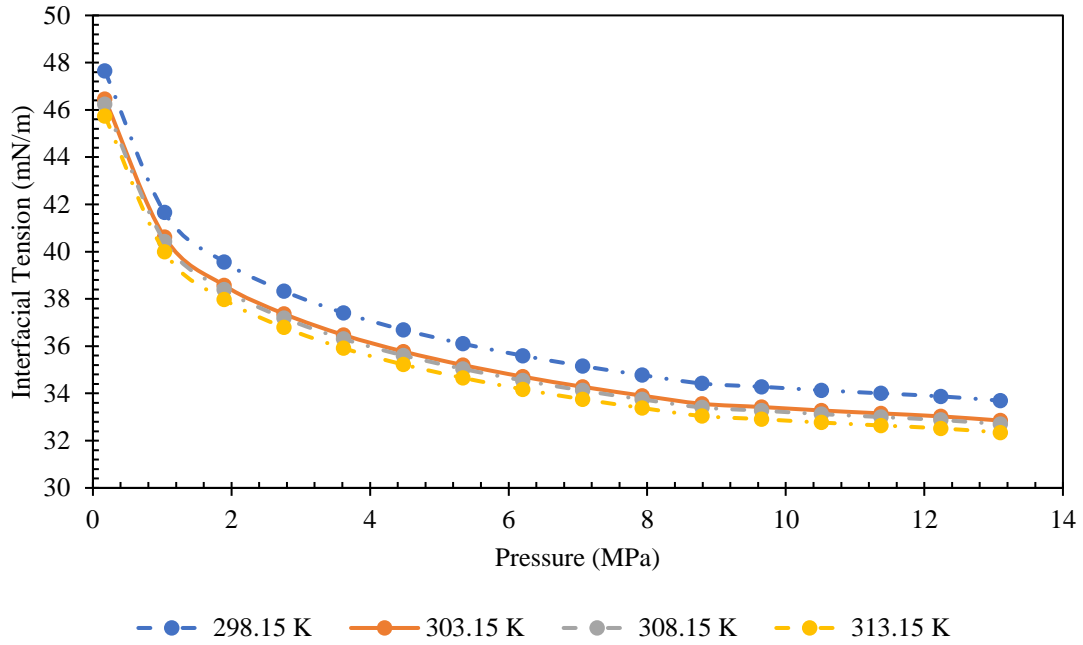
Figure C-11: Methane-water IFT response to change in pressure at 8.2 wt% NaCl and 30% PEG 8000
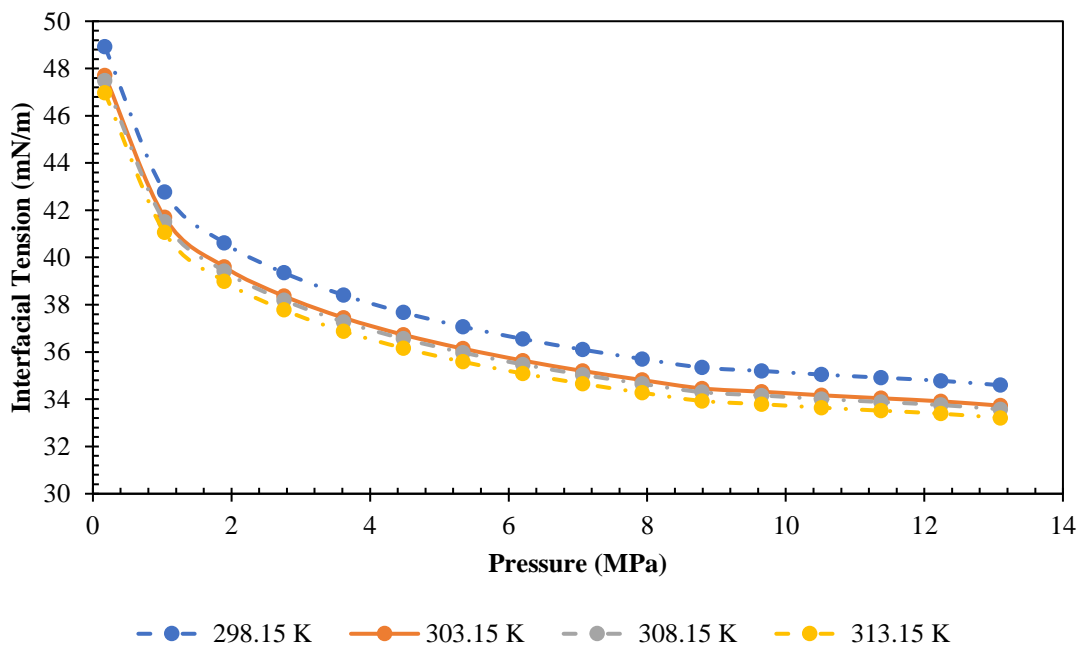
Figure C-12: Methane-water IFT response to change in pressure of 10.7 wt% NaCl and 30% PEG 8000

C1.2.4: 40% PEG 8000 and 5.6, 8.2 and 10.7 wt% NaCl
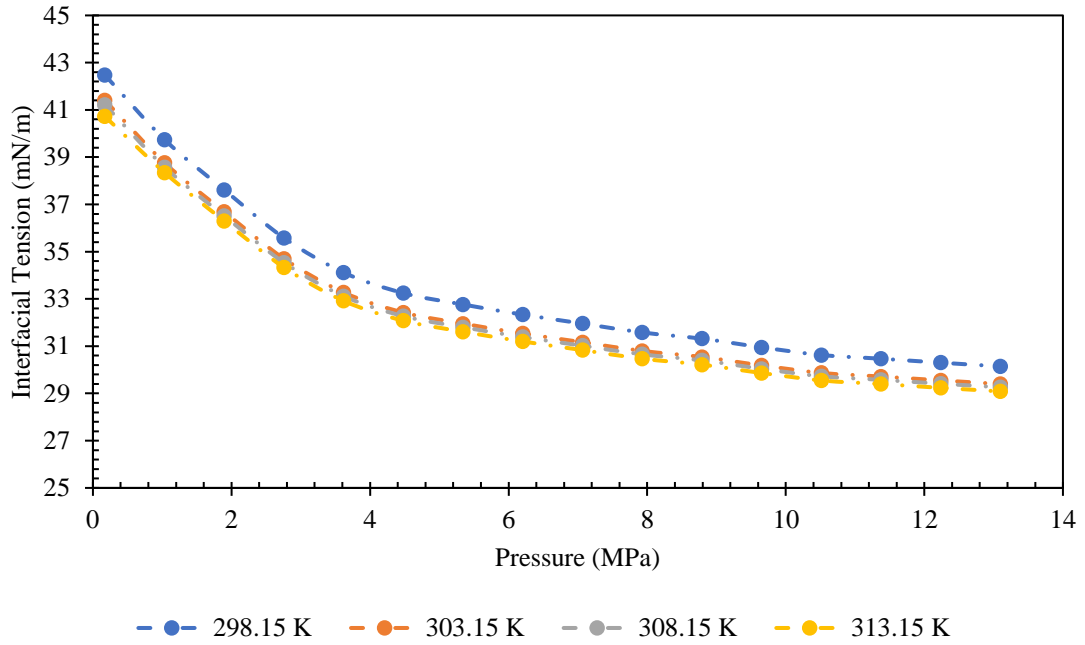
Figure C-13: Methane-water IFT response to change in pressure at 5.6 wt% NaCl and 40% PEG 8000
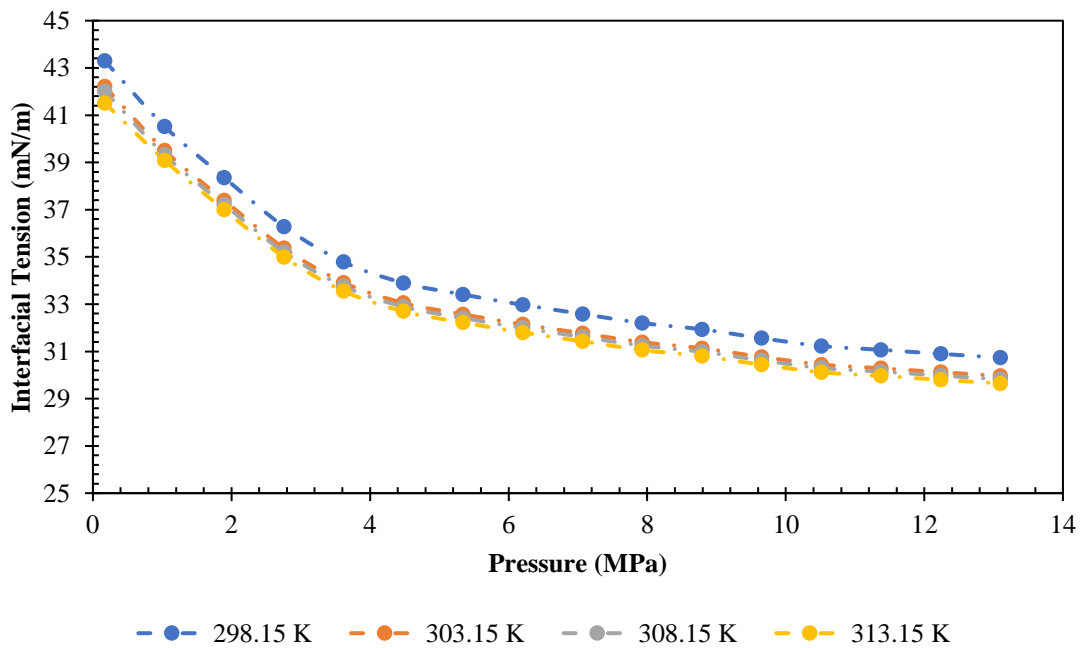
Figure C-14: Methane-water IFT response to change in pressure at 8.2 wt% NaCl and 40% PEG 8000
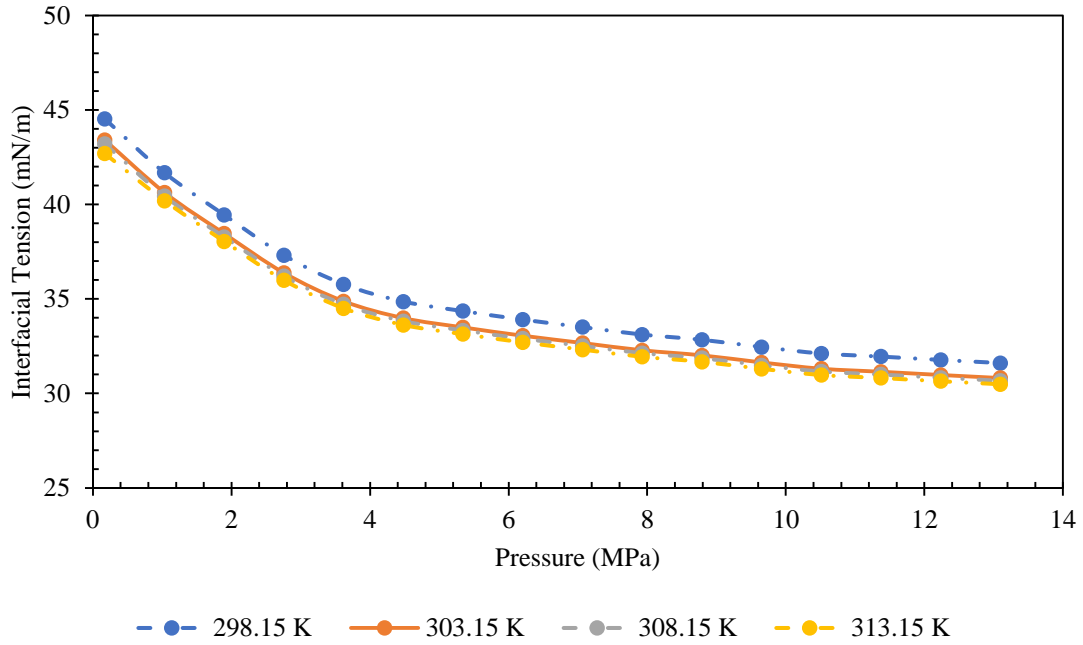
Figure C-15: Methane-water IFT response to change in pressure at 10.7 wt% NaCl and 40% PEG 8000

C2.1: Effect of PEG 8000 + SDS
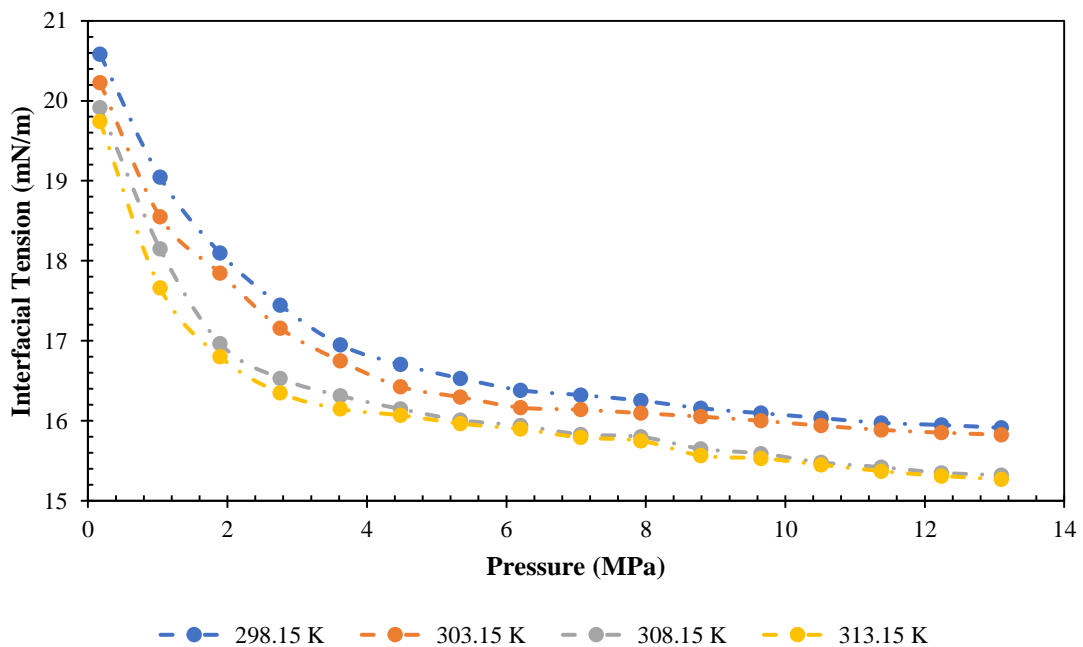
Figure C-16: IFT as function of pressure and tempresture at 20% PEG 8000 + 0.5% SDS
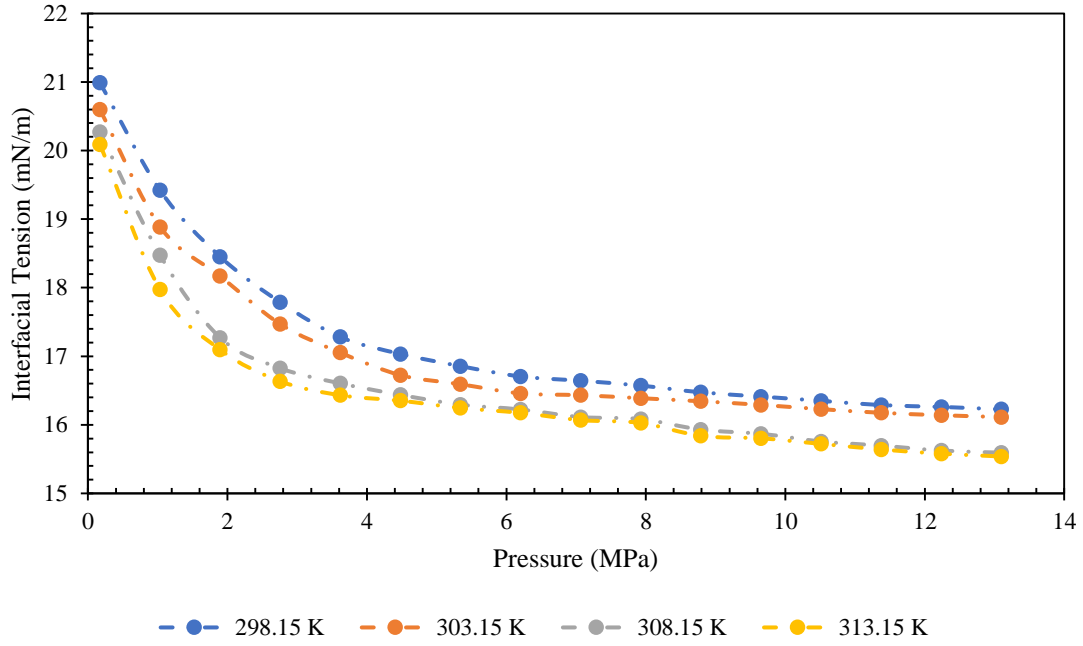
Figure C-17: IFT as function of pressure and tempresture at 20% PEG 8000 + 0.5% SDS and brine (2.9wt% NaCl)
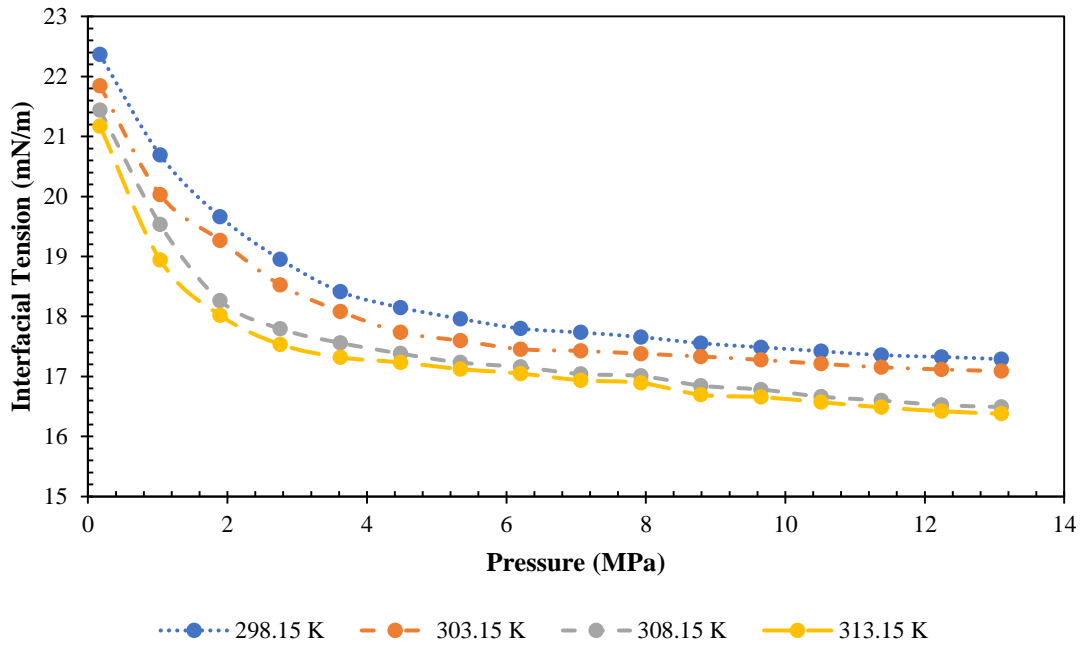
Figure C-18: IFT as function of pressure and tempresture at 20% PEG 8000 + 0.5% SDS and brine (10.7wt% NaCl)
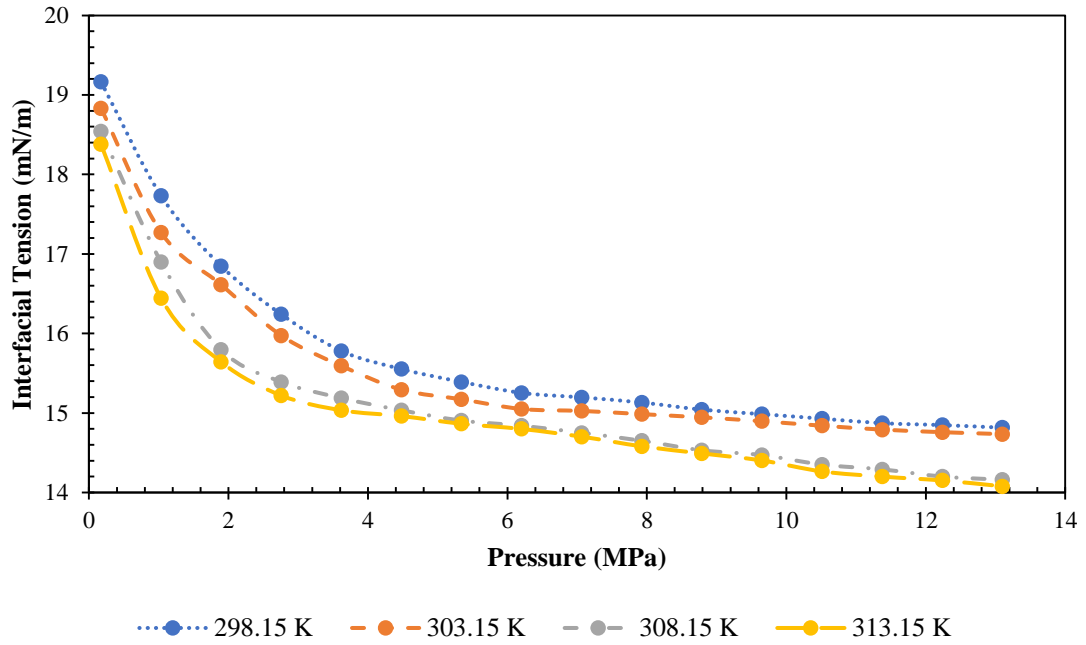
Figure C-19: IFT as function of pressure and tempresture at 30% PEG 8000 + 0.5% SDS
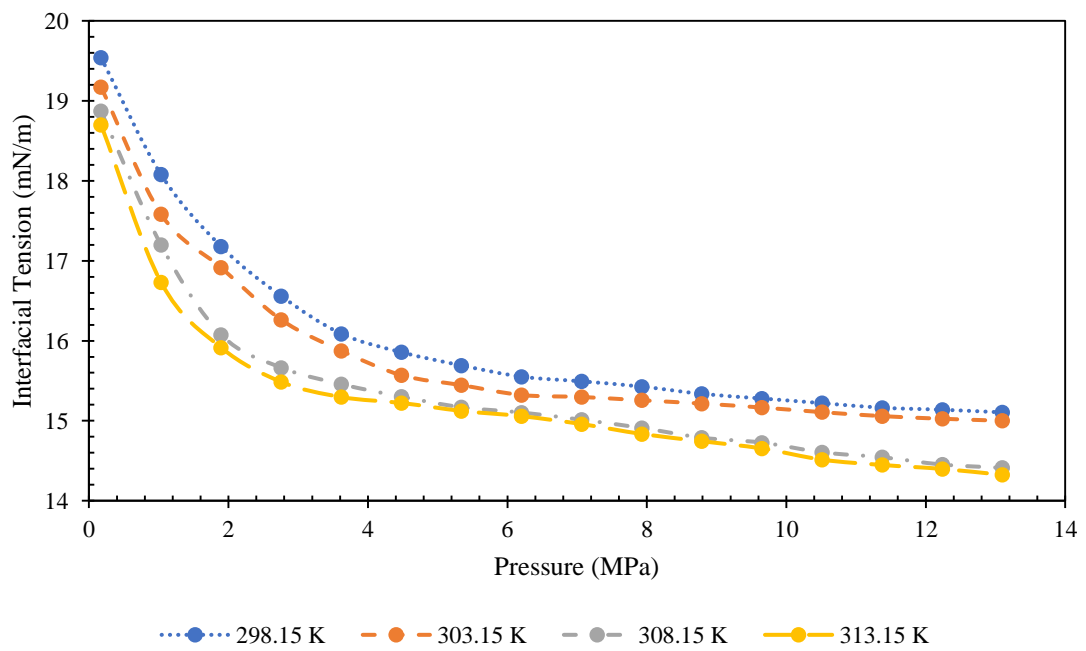
Figure C-20: IFT as function of pressure and tempresture at 30% PEG 8000 + 0.5% SDS and brine (2.9wt% NaCl)
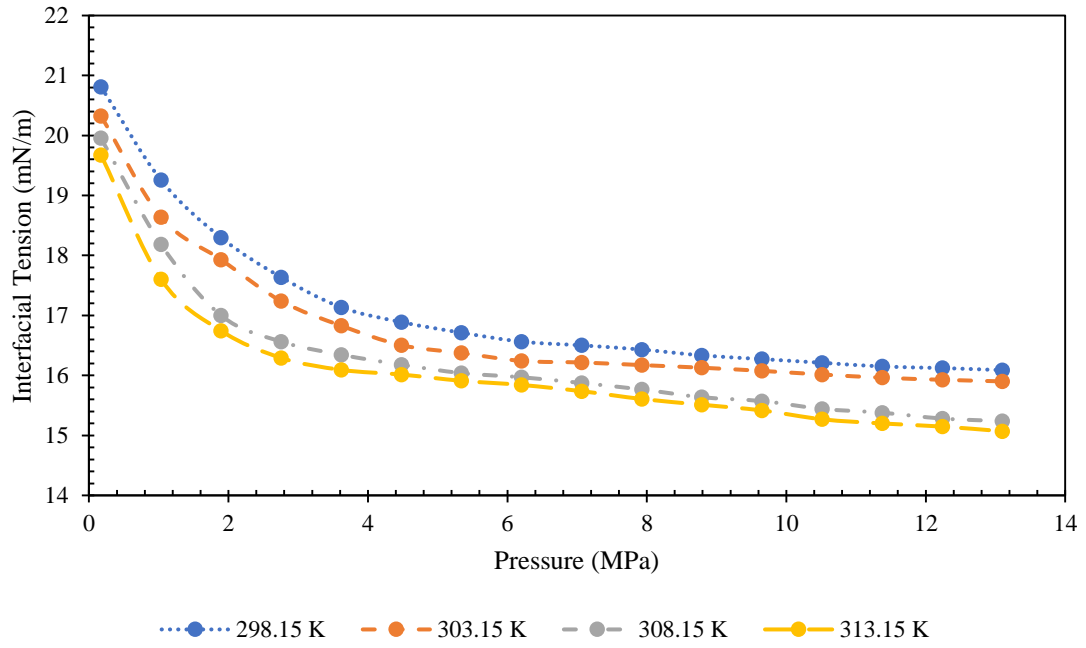
Figure C-21: IFT as function of pressure and temperature at 10% PEG 8000 + 0.5% SDS and brine (10.7wt% NaCl)

Appendix B

Temperature = 298.15 K

Pressure = 0.172 MPa

No.	Time	Gamma	Beta	R0	Area	Volume	Theta	Height	Width	Opt Messages
1	0.0	72.41	0.303	1.496	37.87	20.73	72.05	4.816	3.084	4
2	1.0	72.23	0.303	1.496	37.85	20.77	72.51	4.810	3.084	4
3	1.9	72.26	0.303	1.496	37.86	20.76	72.33	4.814	3.084	3
4	3.0	72.33	0.303	1.496	37.85	20.75	72.36	4.813	3.085	4
5	3.9	72.32	0.303	1.496	37.84	20.75	72.29	4.814	3.084	4
6	5.0	72.29	0.303	1.496	37.87	20.77	72.28	4.816	3.083	4
7	6.0	72.31	0.303	1.496	37.84	20.76	72.65	4.808	3.085	4
8	6.9	72.35	0.303	1.496	37.87	20.76	72.13	4.818	3.084	4
9	8.0	72.35	0.303	1.496	37.86	20.75	72.13	4.817	3.083	4
10	8.9	72.35	0.303	1.496	37.87	20.75	71.96	4.821	3.083	4

Mean: 72.32 0.303 1.496 37.86 20.76 72.27 4.815 3.084

Stand.dev.: 0.02 0.000 0.000 0.00 0.00 0.07 0.001 0.000

Methane_DH2O

161
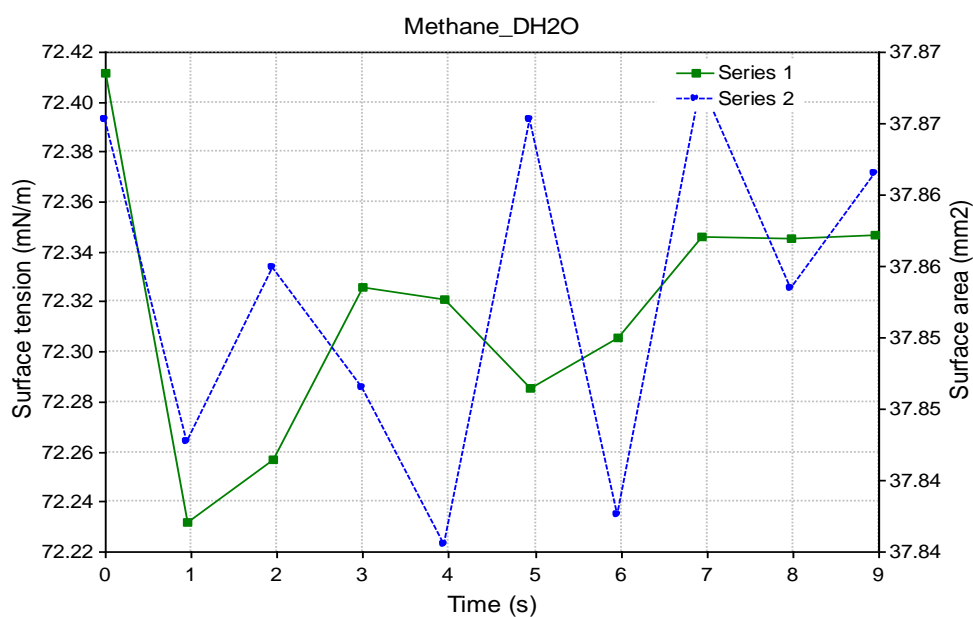
Pressure   = 1.034 MPa

No.	Time	Gamma	Beta	R0	Area	Volume Messages	Theta	Height	Width	Opt
1	0.0	71.19	0.290	1.442	34.41	17.91	69.12	4.614	2.960	4
2	0.9	71.17	0.290	1.441	34.41	17.91	69.29	4.611	2.966	4
3	2.0	71.18	0.290	1.442	34.42	17.91	69.24	4.611	2.963	3
4	2.9	71.16	0.290	1.442	34.41	17.91	69.25	4.612	2.964	3
5	3.9	71.03	0.290	1.441	34.40	17.89	69.25	4.610	2.963	3
6	5.0	71.28	0.290	1.441	34.39	17.90	69.22	4.611	2.963	3
7	5.9	71.29	0.290	1.441	34.40	17.90	69.25	4.610	2.961	4
8	7.0	71.27	0.290	1.441	34.41	17.92	69.40	4.609	2.964	3
9	7.9	71.19	0.290	1.441	34.40	17.90	69.28	4.609	2.962	3
10	9.0	71.13	0.290	1.441	34.38	17.89	69.37	4.609	2.966	4

Mean: 71.23   0.290   1.441   34.40   17.90   69.27   4.611   2.963

Stand.dev.:   0.01   0.000   0.000   0.00   0.00   0.02   0.001   0.001

Methane_DW

Pressure   = 1.896MPa

No.	Time	Gamma	Beta	R0	Area	Volume	Theta	Height	Width	Opt
					Messages					

==
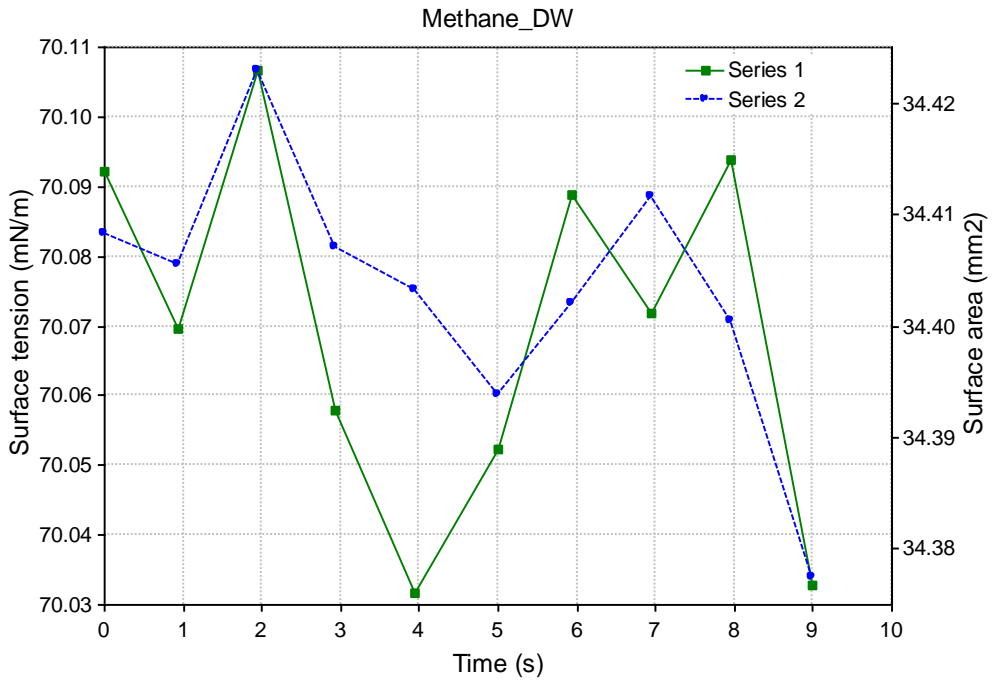
No.	Time	Gamma	Beta	R0	Area	Volume	Theta	Height	Width	Opt
1	0.0	69.78	0.303	1.478	36.75	19.89	72.71	4.744	3.048	4
2	0.9	70.09	0.303	1.478	36.73	19.87	72.68	4.744	3.046	4
3	2.0	69.80	0.303	1.478	36.77	19.90	72.76	4.744	3.048	4
4	2.9	70.08	0.303	1.478	36.75	19.88	72.66	4.745	3.047	4
5	3.9	69.84	0.303	1.479	36.76	19.89	72.62	4.746	3.046	4
6	4.9	70.11	0.302	1.479	36.76	19.90	72.72	4.744	3.048	4
7	6.0	70.21	0.302	1.479	36.78	19.91	72.69	4.746	3.049	4
8	7.0	69.91	0.303	1.478	36.73	19.87	72.48	4.748	3.046	4
9	7.9	69.96	0.302	1.479	36.78	19.91	72.62	4.747	3.048	4
10	9.0	69.99	0.302	1.479	36.77	19.90	72.38	4.752	3.047	4

==

Mean: 70.08   0.302   1.479   36.76   19.89   72.63   4.746   3.047

Stand.dev.:   0.01   0.000   0.000   0.01   0.00   0.04   0.001   0.000
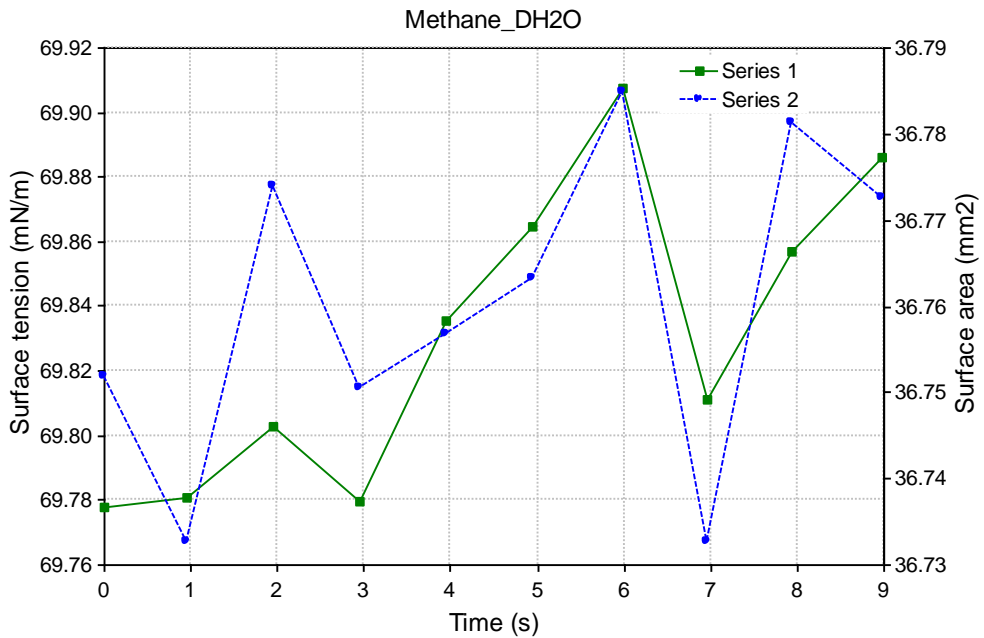
==

Methane_DH2O

Pressure   = 2.758MPa

No.	Time	Gamma	Beta	R0	Area	Volume	Theta	Height	Width	Opt Messages
1	0.0	68.28	0.304	1.471	36.53	19.72	73.36	4.717	3.032	4
2	0.9	68.29	0.304	1.471	36.51	19.71	73.39	4.715	3.032	4
3	1.9	68.26	0.304	1.470	36.53	19.72	73.29	4.719	3.031	4
4	3.0	68.23	0.304	1.470	36.51	19.70	73.21	4.719	3.031	4
5	3.9	68.20	0.304	1.470	36.52	19.71	73.37	4.716	3.032	4
6	5.0	68.30	0.304	1.471	36.53	19.71	73.26	4.719	3.033	4
7	6.0	68.27	0.304	1.470	36.53	19.71	73.23	4.719	3.032	4
8	6.9	68.30	0.304	1.471	36.54	19.73	73.27	4.719	3.032	4
9	7.9	68.30	0.304	1.471	36.54	19.72	73.18	4.721	3.034	4
10	9.0	68.32	0.304	1.471	36.54	19.73	73.26	4.719	3.035	4

Mean: 68.55 0.304 1.471 36.53 19.72 73.28 4.718 3.032

Stand.dev.: 0.01   0.000 0.000 0.00 0.00 0.02 0.001 0.000

Methane_DH2O
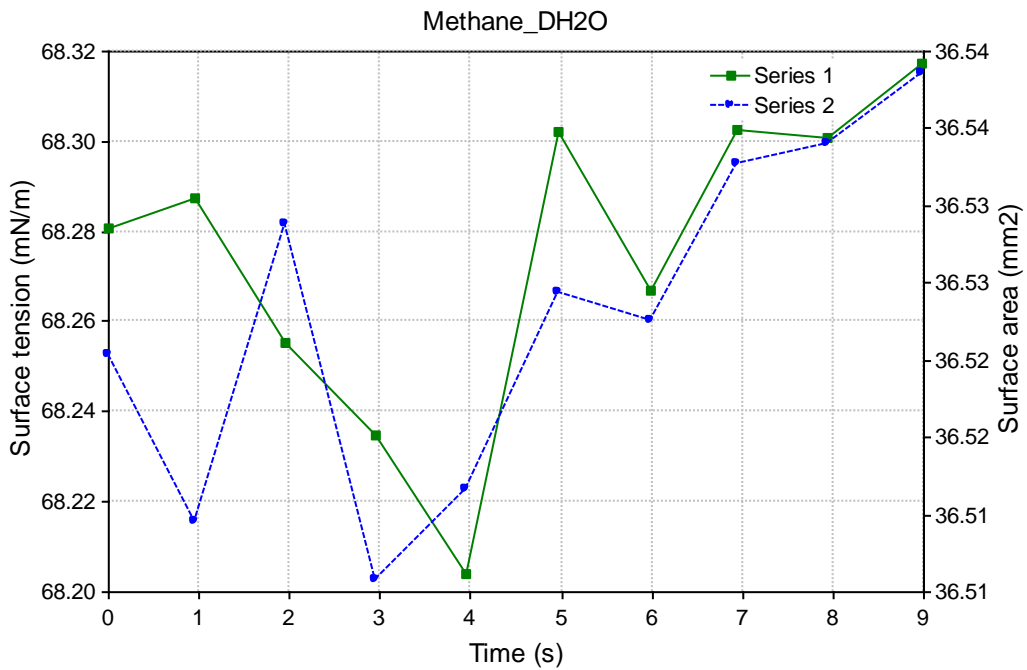
Pressure = 3.620MPa

No.	Time	Gamma	Beta	R0	Area	Volume Messages	Theta	Height	Width	Opt
1	0.0	67.65	0.283	1.416	32.76	16.61	66.12	4.545	2.891	4
2	0.9	67.69	0.283	1.416	32.80	16.63	66.20	4.545	2.888	4
3	1.9	67.70	0.283	1.416	32.79	16.64	66.25	4.543	2.890	4
4	3.0	67.70	0.283	1.416	32.81	16.64	66.19	4.545	2.891	4
5	3.9	67.71	0.283	1.416	32.82	16.64	66.11	4.546	2.891	4
6	4.9	67.81	0.283	1.417	32.80	16.64	66.08	4.547	2.891	4
7	5.9	67.80	0.283	1.417	32.81	16.65	66.01	4.549	2.892	4
8	7.0	67.83	0.283	1.417	32.81	16.65	66.09	4.548	2.891	4
9	8.0	67.84	0.283	1.417	32.84	16.66	66.04	4.549	2.892	4
10	9.0	67.84	0.283	1.417	32.82	16.66	66.04	4.549	2.893	4

Mean: 67.32 0.283 1.417 32.81 16.64 66.11 4.547 2.891

Stand.dev.: 0.02   0.000 0.000 0.01 0.00 0.02 0.001 0.000

Methane_DH2O
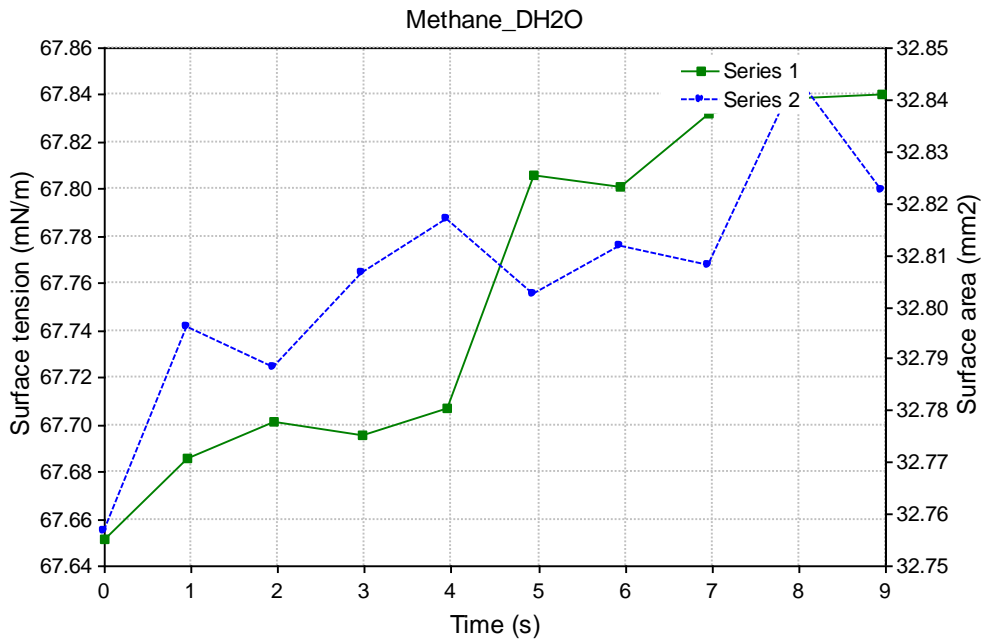
Pressure   = 4.482MPa

No.	Time	Gamma	Beta	R0	Area	Volume	Theta	Height	Width	Opt	Messages
1	0.0	66.27	0.304	1.463	36.15	19.34	71.36	4.732	3.012	4	
2	1.0	66.26	0.304	1.463	36.15	19.34	71.26	4.734	3.011	4	
3	2.0	66.28	0.304	1.463	36.18	19.36	71.26	4.736	3.011	4	
4	3.0	66.29	0.305	1.463	36.17	19.35	71.03	4.741	3.009	4	
5	4.0	66.31	0.305	1.464	36.21	19.38	71.04	4.743	3.010	4	
6	4.9	66.35	0.304	1.464	36.22	19.39	71.04	4.743	3.011	4	
7	6.0	66.37	0.304	1.464	36.23	19.39	71.02	4.744	3.011	4	
8	6.9	66.41	0.304	1.464	36.21	19.38	70.96	4.745	3.011	4	
9	8.0	66.46	0.304	1.465	36.25	19.41	70.90	4.748	3.012	4	
10	9.0	66.47	0.304	1.465	36.26	19.42	70.88	4.749	3.014	4	

Mean: 66.15   0.304   1.464   36.20   19.38   71.08   4.742   3.011

Stand.dev.:0.03   0.000   0.000   0.01   0.01   0.05   0.002   0.000

Methane_DH2O
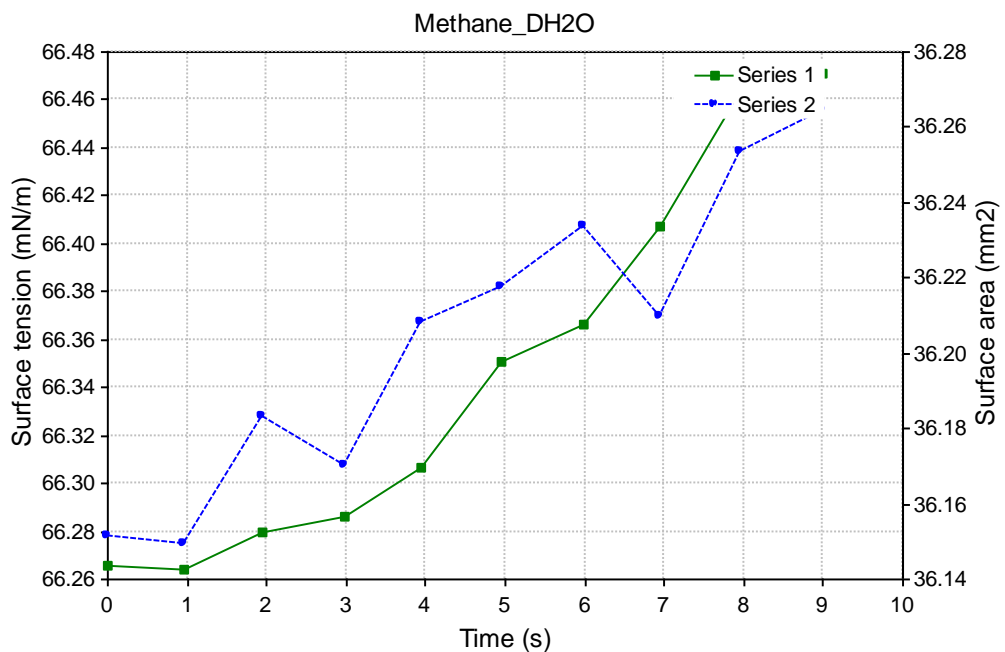
Pressure   =   5.343MPa

No.	Time	Gamma	Beta	R0	Area	Volume	Theta	Height	Width	Opt	Messages
1	0.0	64.43	0.304	1.436	34.74	18.27	72.98	4.609	2.964	4	
2	0.9	64.49	0.304	1.436	34.74	18.27	73.09	4.607	2.963	4	
3	1.9	64.54	0.304	1.436	34.73	18.28	73.17	4.606	2.965	4	
4	3.0	64.64	0.303	1.437	34.77	18.32	73.29	4.606	2.968	4	
5	4.0	64.59	0.303	1.437	34.80	18.32	73.06	4.609	2.965	4	
6	4.9	64.67	0.303	1.437	34.80	18.33	73.08	4.611	2.967	4	
7	6.0	64.61	0.303	1.437	34.80	18.31	72.89	4.613	2.965	4	
8	6.9	64.64	0.303	1.437	34.79	18.32	72.96	4.612	2.967	4	
9	7.9	64.68	0.303	1.437	34.81	18.33	72.93	4.613	2.967	3	
10	9.0	64.70	0.303	1.438	34.83	18.34	72.80	4.616	2.967	4	

Mean: 65.09 0.303 1.437 34.78 18.31 73.03 4.610 2.966

Stand.dev.: 0.03   0.000 0.000 0.01 0.01 0.05 0.001 0.001

Methane_DH2O
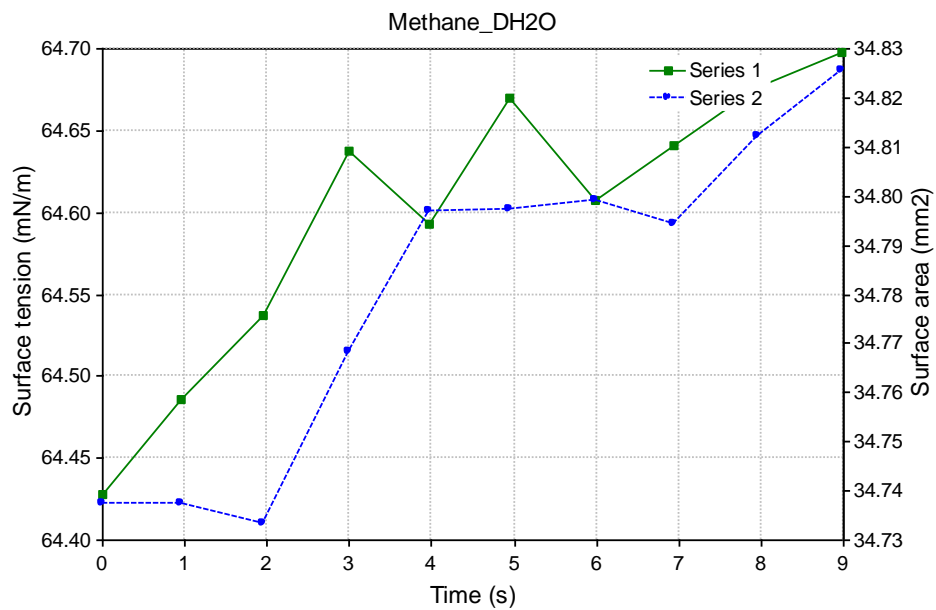
Pressure   = 6.205MPa

No.	Time	Gamma	Beta	R0	Area	Volume Messages	Theta	Height	Width	Opt
1	0.0	63.56	0.350	1.516	40.42	23.85	90.02	4.682	3.206	3
2	0.9	62.60	0.350	1.516	40.43	23.85	90.03	4.681	3.207	3
3	1.9	63.61	0.350	1.516	40.44	23.86	90.08	4.681	3.206	3
4	3.0	62.58	0.350	1.516	40.43	23.86	90.04	4.681	3.205	3
5	4.0	63.62	0.350	1.517	40.44	23.87	90.08	4.681	3.208	3
6	4.9	62.61	0.350	1.516	40.45	23.86	90.05	4.681	3.208	3
7	6.0	63.59	0.350	1.516	40.43	23.86	90.05	4.682	3.206	3
8	7.0	63.61	0.350	1.517	40.46	23.87	90.05	4.682	3.207	3
9	8.0	63.59	0.350	1.516	40.43	23.85	89.96	4.682	3.207	3
10	8.9	63.65	0.350	1.517	40.45	23.87	90.08	4.681	3.207	3

Mean: 63.22 0.350 1.516 40.44 23.86 90.04 4.681 3.207

Stand.dev.:   0.01 0.000 0.000 0.00 0.00 0.01 0.000 0.000

Methane_DH2O
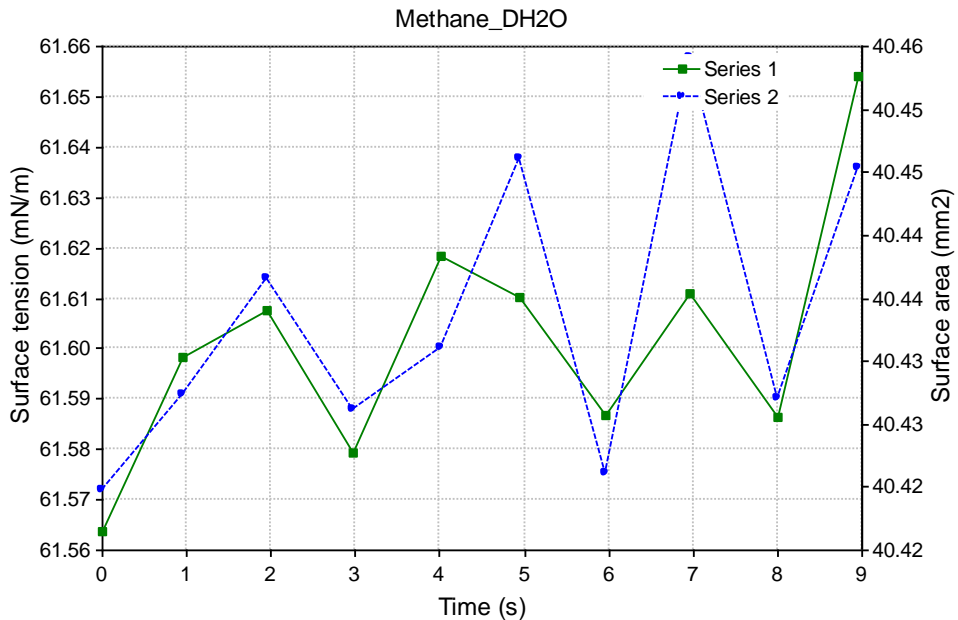
Pressure   = 7.067MPa

No.	Time	Gamma	Beta	R0	Area	Volume Messages	Theta	Height	Width	Opt
1	0.0	61.88	0.349	1.504	39.84	23.29	89.29	4.659	3.181	3
2	1.0	61.81	0.349	1.504	39.78	23.26	89.40	4.657	3.180	3
3	1.9	61.40	0.349	1.504	39.88	23.32	89.30	4.658	3.181	3
4	3.0	61.24	0.349	1.504	39.79	23.27	89.37	4.658	3.182	3
5	3.9	61.47	0.349	1.504	39.83	23.30	89.34	4.659	3.179	3
6	5.0	61.43	0.349	1.504	39.81	23.28	89.36	4.659	3.179	3
7	6.0	61.45	0.349	1.504	39.84	23.30	89.33	4.659	3.183	3
8	6.9	61.26	0.349	1.504	39.84	23.30	89.33	4.659	3.184	3
9	8.0	61.26	0.349	1.504	39.84	23.29	89.28	4.660	3.183	3
10	9.0	61.25	0.349	1.504	39.84	23.30	89.29	4.660	3.183	3

Mean: 61.48 0.349 1.504 39.83 23.29 89.33 4.659 3.182

Stand.dev.:0.01   0.000 0.000 0.01   0.01   0.01 0.000 0.001
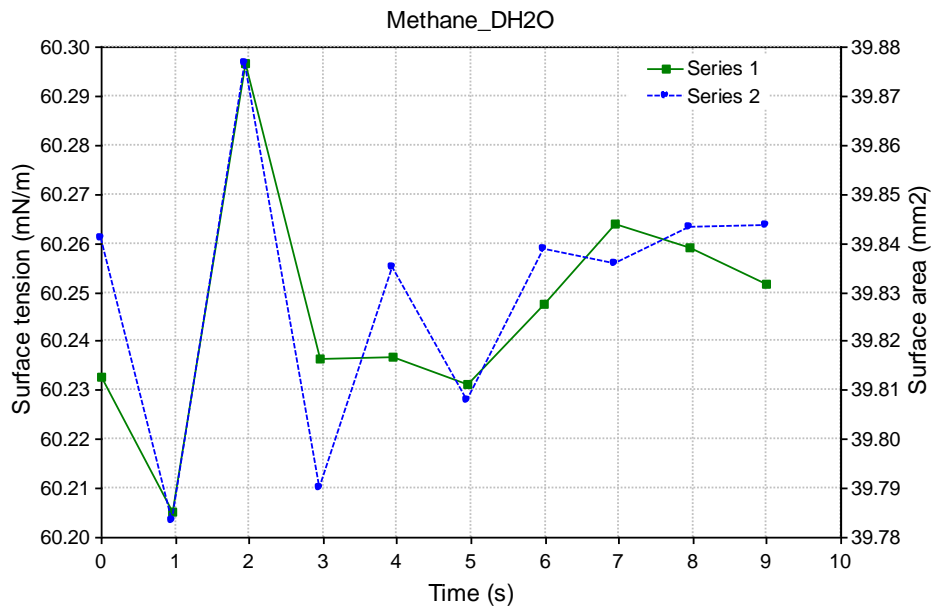
Methane_DH2O

Pressure   = 7.929MPa

No.	Time	Gamma	Beta	R0	Area	Volume	Theta	Height	Width	Opt
						Messages				
1	0.0	59.76	0.344	1.479	38.38	21.95	88.26	4.597	3.117	4
2	0.9	58.79	0.344	1.479	38.38	21.95	88.30	4.597	3.119	3
3	2.0	59.11	0.344	1.479	38.38	21.95	88.26	4.597	3.116	3
4	3.0	59.11	0.344	1.480	38.39	21.96	88.30	4.597	3.119	3
5	4.0	59.75	0.344	1.479	38.39	21.95	88.25	4.598	3.118	4
6	5.0	59.81	0.344	1.480	38.39	21.96	88.27	4.598	3.119	3
7	6.0	59.81	0.344	1.480	38.40	21.96	88.29	4.597	3.120	3
8	6.9	58.12	0.344	1.480	38.38	21.95	88.26	4.598	3.121	3
9	7.9	58.34	0.344	1.480	38.40	21.97	88.27	4.598	3.120	3
10	9.0	58.77	0.344	1.479	38.39	21.96	88.28	4.597	3.119	3

Mean: 59.53   0.344 1.480 38.39 21.96 88.27 4.597 3.119

Stand.dev.: 0.01   0.000 0.000   0.00   0.00   0.01 0.000 0.000
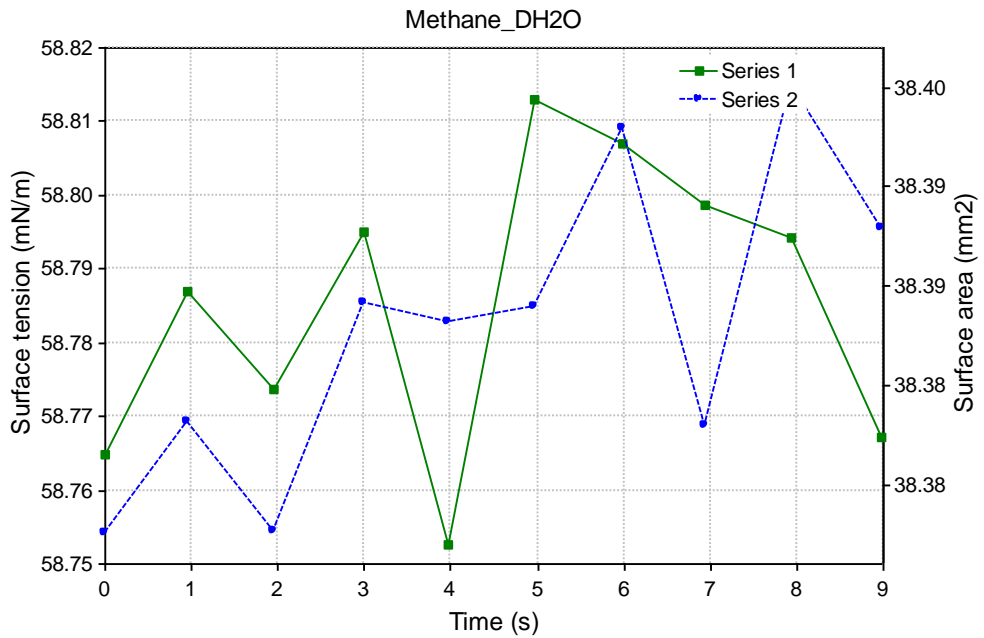
Methane_DH2O

Pressure   = 8.791MPa

No.	Time	Gamma	Beta	R0	Area	Volume	Theta	Height	Width	Opt
						Messages				

===

1	0.0	56.86	0.355	1.483	38.58	22.46	93.05	4.508	3.141	3
2	0.9	56.85	0.355	1.483	38.58	22.45	93.02	4.508	3.140	3
3	1.9	56.81	0.355	1.483	38.57	22.45	93.03	4.507	3.141	3
4	3.0	56.81	0.355	1.483	38.57	22.44	92.98	4.508	3.140	3
5	3.9	56.84	0.355	1.483	38.60	22.47	92.92	4.509	3.140	3
6	5.0	56.83	0.355	1.483	38.54	22.43	93.05	4.508	3.141	3
7	5.9	56.83	0.355	1.483	38.57	22.45	93.00	4.509	3.140	3
8	7.0	56.81	0.355	1.483	38.56	22.44	93.00	4.508	3.140	3
9	7.9	56.80	0.355	1.483	38.56	22.44	93.01	4.507	3.140	3
10	9.0	56.83	0.355	1.483	38.55	22.44	93.06	4.506	3.140	3

===

Mean: 57.04 0.355 1.483 38.57 22.45 93.01 4.508 3.140

Stand.dev.: 0.01   0.000 0.000   0.01   0.00   0.01 0.000 0.000

===

Methane_DH2O

171
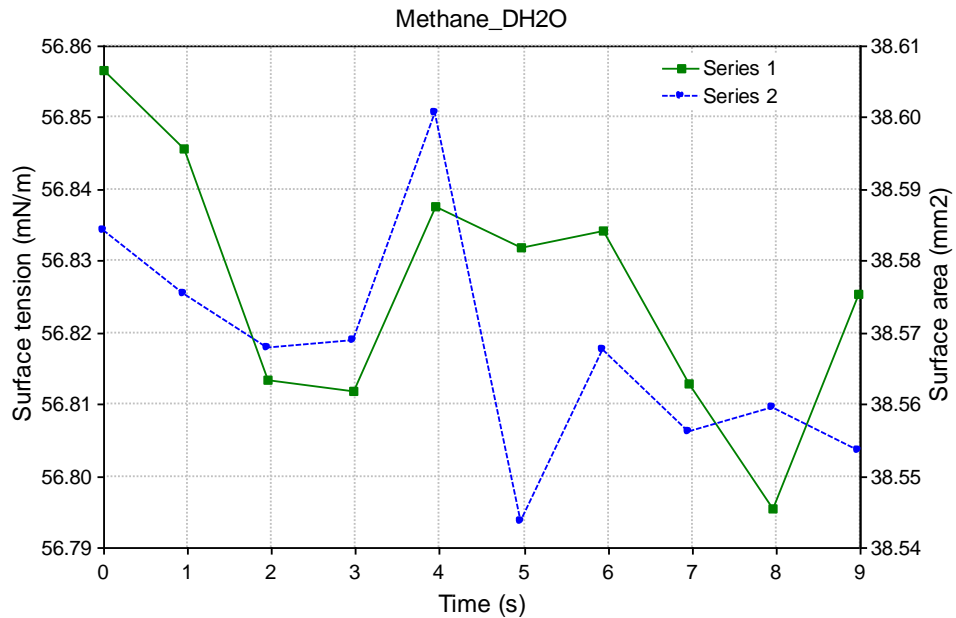
Pressure   = 9.653MPa

No.	Time	Gamma	Beta	R0	Area	Volume Messages	Theta	Height	Width	Opt
1	0.0	55.71	0.313	1.384	32.55	16.78	80.74	4.347	2.876	3
2	0.9	55.72	0.313	1.384	32.56	16.78	80.78	4.347	2.876	4
3	1.9	55.74	0.313	1.385	32.56	16.79	80.82	4.347	2.877	4
4	3.0	55.70	0.313	1.384	32.55	16.78	80.81	4.347	2.876	4
5	3.9	55.72	0.313	1.384	32.56	16.77	80.77	4.348	2.876	4
6	5.0	55.73	0.313	1.385	32.57	16.78	80.80	4.348	2.875	4
7	6.0	55.76	0.313	1.385	32.57	16.78	80.77	4.349	2.878	4
8	7.0	55.72	0.313	1.385	32.58	16.78	80.80	4.348	2.876	4
9	7.9	55.78	0.313	1.385	32.57	16.80	80.82	4.348	2.877	4
10	9.0	55.76	0.313	1.385	32.57	16.80	80.76	4.349	2.878	4

Mean: 55.73 0.313 1.385 32.56 16.78 80.79 4.348 2.877

Stand.dev.: 0.01   0.000 0.000 0.00 0.00 0.01 0.000 0.000

Methane_DH2O
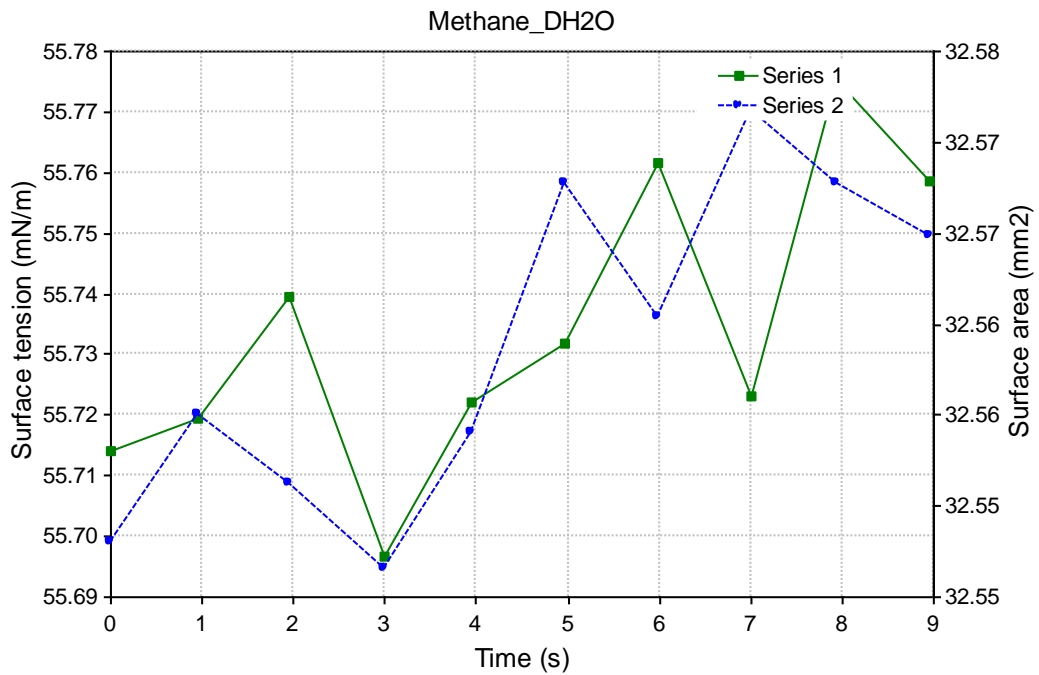
Pressure = 10.515MPa

No.	Time	Gamma	Beta	R0	Area	Volume	Messages	Theta	Height	Width	Opt
1	0.0	54.20	0.351	1.451	36.68	20.80		93.06	4.403	3.068	3
2	0.9	53.27	0.351	1.450	36.69	20.80		93.06	4.402	3.066	3
3	1.9	54.25	0.351	1.450	36.69	20.80		93.00	4.404	3.068	3
4	3.0	54.26	0.351	1.450	36.69	20.80		93.05	4.403	3.067	3
5	4.0	53.33	0.350	1.451	36.69	20.80		93.06	4.403	3.067	3
6	5.0	54.31	0.350	1.451	36.70	20.80		93.06	4.403	3.069	3
7	6.0	52.27	0.351	1.450	36.74	20.84		92.93	4.404	3.067	3
8	7.0	54.27	0.351	1.450	36.69	20.80		93.06	4.402	3.067	3
9	7.9	54.24	0.351	1.450	36.68	20.79		93.01	4.403	3.069	3
10	9.0	54.29	0.351	1.451	36.72	20.82		92.99	4.404	3.066	3

Mean: 54.06 0.351 1.450 36.70 20.81 93.03 4.403 3.067

Stand.dev.: 0.01 0.000 0.000 0.01 0.00 0.01 0.000 0.000
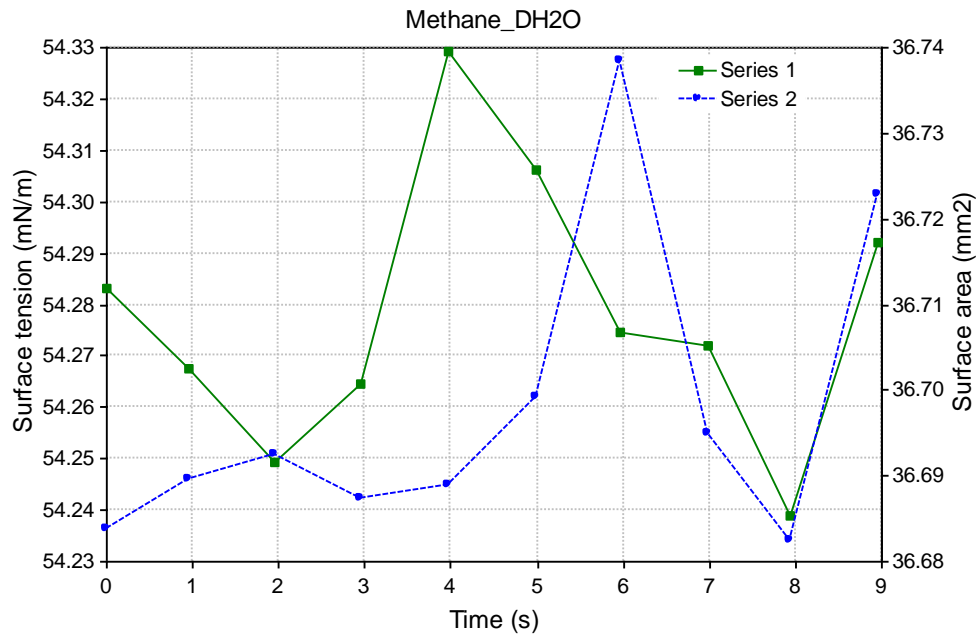
Methane_DH2O

Pressure   = 11.376MPa

No.	Time	Gamma	Beta	R0	Area	Volume	Theta	Height	Width	Opt
						Messages				
1	0.0	52.89	0.345	1.423	35.57	19.56	88.63	4.415	3.007	3
2	1.0	52.87	0.345	1.423	35.58	19.55	88.62	4.415	3.006	3
3	1.9	53.10	0.345	1.423	35.56	19.53	88.66	4.415	3.008	3
4	3.0	53.00	0.345	1.423	35.58	19.54	88.66	4.416	3.008	3
5	3.9	52.92	0.345	1.423	35.55	19.53	88.66	4.416	3.006	3
6	5.0	52.59	0.345	1.423	35.56	19.55	88.56	4.417	3.006	3
7	6.0	52.60	0.345	1.423	35.55	19.54	88.67	4.414	3.006	3
8	7.0	52.63	0.345	1.423	35.57	19.56	88.64	4.415	3.006	3
9	7.9	52.58	0.345	1.423	35.58	19.55	88.57	4.417	3.006	3
10	9.0	52.60	0.345	1.423	35.55	19.55	88.58	4.416	3.004	3

Mean: 52.96 0.345 1.423 35.56 19.55 88.62 4.416 3.006

Stand.dev.:   0.01 0.000 0.000   0.00   0.00   0.01 0.000 0.000
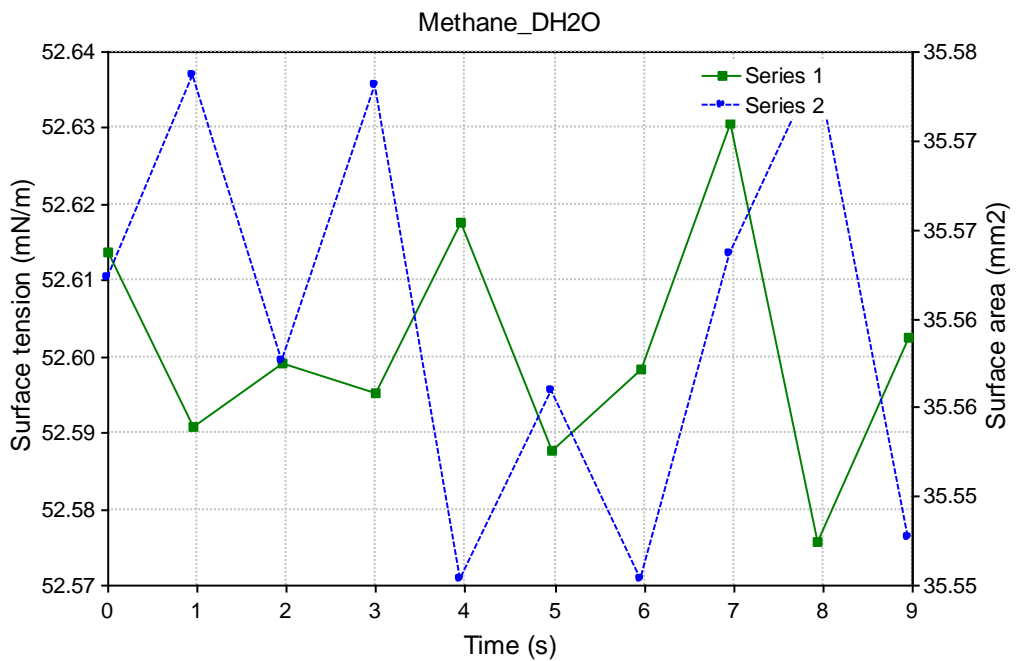
Methane_DH2O

Pressure   = 12.238MPa

No.	Time	Gamma	Beta	R0	Area	Volume	Theta	Height	Width	Opt Messages
1	0.0	50.91	0.351	1.417	34.52	19.23	98.31	4.165	3.013	3
2	1.0	50.92	0.351	1.417	34.49	19.21	98.25	4.165	3.014	3
3	2.0	50.91	0.351	1.417	34.52	19.24	98.28	4.166	3.013	3
4	2.9	50.95	0.351	1.417	34.49	19.22	98.27	4.166	3.013	3
5	4.0	50.90	0.351	1.417	34.52	19.22	98.04	4.171	3.013	3
6	4.9	51.04	0.351	1.418	34.47	19.22	98.44	4.163	3.014	3
7	6.0	50.98	0.351	1.418	34.51	19.23	98.25	4.167	3.014	3
8	7.0	50.97	0.351	1.418	34.51	19.23	98.25	4.167	3.013	3
9	7.9	51.00	0.351	1.417	34.51	19.23	98.21	4.168	3.014	3
10	9.0	50.92	0.351	1.417	34.52	19.22	98.09	4.170	3.012	3

Mean: 50.95 0.351 1.417 34.51 19.23 98.24 4.167 3.013

Stand.dev.: 0.01   0.000 0.000 0.01 0.00 0.04 0.001 0.000

Methane_DH2O
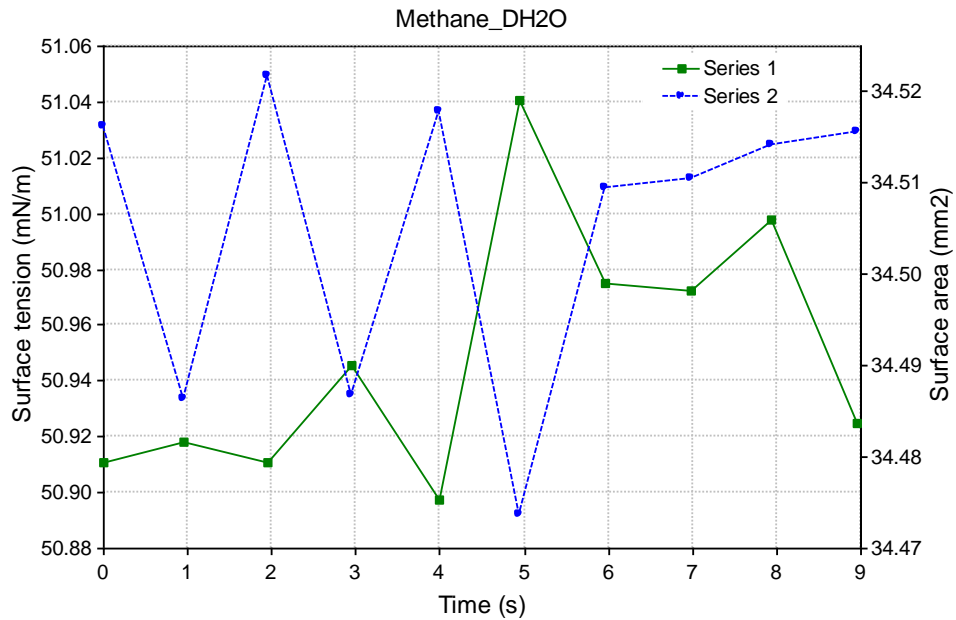
Pressure = 13.100MPa

No.	Time	Gamma	Beta	R0	Area	Volume Messages	Theta	Height	Width	Opt
1	0.0	49.78	0.351	1.392	33.21	18.21	99.40	4.063	2.962	3
2	0.9	46.75	0.351	1.392	33.20	18.21	99.36	4.063	2.963	3
3	1.9	48.79	0.351	1.392	33.21	18.21	99.38	4.063	2.962	3
4	2.9	47.80	0.351	1.392	33.20	18.21	99.39	4.063	2.962	3
5	4.0	48.78	0.351	1.392	33.21	18.22	99.38	4.063	2.963	3
6	4.9	47.76	0.351	1.392	33.21	18.21	99.35	4.064	2.961	3
7	6.0	48.77	0.351	1.392	33.21	18.22	99.36	4.063	2.963	3
8	7.0	49.80	0.351	1.393	33.19	18.21	99.35	4.064	2.962	3
9	8.0	49.78	0.351	1.392	33.21	18.22	99.39	4.063	2.962	3
10	9.0	49.73	0.351	1.392	33.22	18.22	99.32	4.064	2.963	3

Mean: 49.36 0.351 1.392 33.21 18.21 99.37 4.063 2.962

Stand.dev.: 0.01 0.000 0.000 0.00 0.00 0.01 0.000 0.000
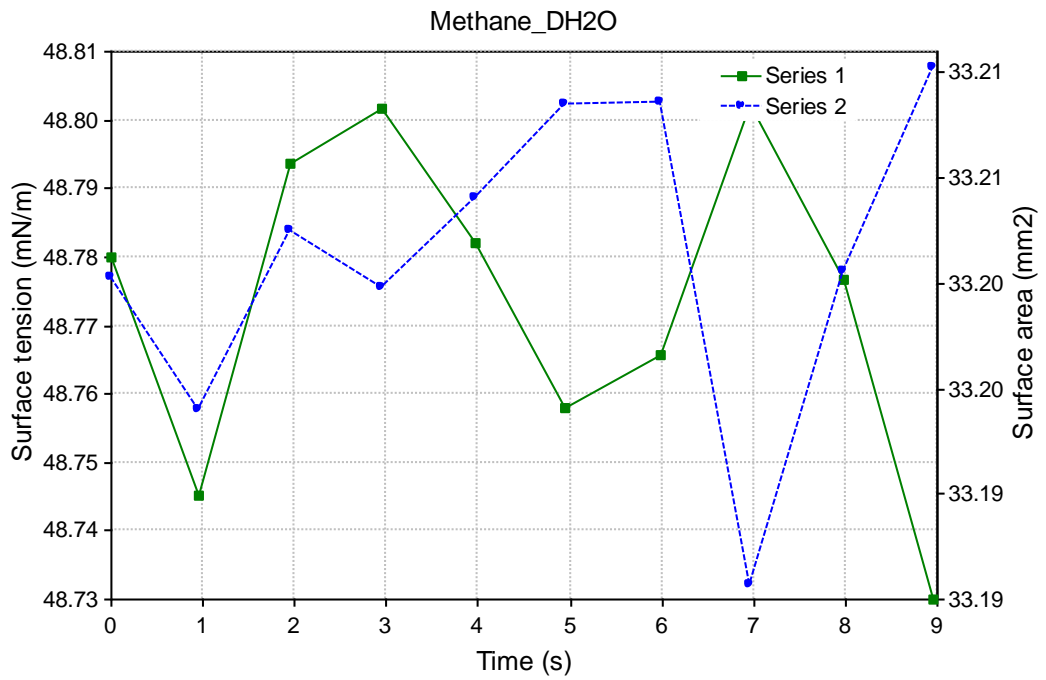
Methane_DH2O

176

Drop Shape Image Analysis

Temperature = 308.15 K
Pressure = 0.172 MPa

Date	: 11/28/2017	Remarks : Comments here
Experiment	: Methane_(DW+PEG)_35	Method : methane_(dw+peg).met
Drop phase	: Methane	Density : 0.007
Extern.phase	: Water	Density : 1.0145
Solid phase	: Steel	Calculation : Optimized cont.

No.	Time	Gamma	Beta	R0	Area	Volume	Theta	Height	Width	Opt
						Messages				
1	0.0	64.89	0.283	1.345	30.33	15.00	77.85	4.126	2.822	3
2	0.9	64.93	0.283	1.345	30.34	15.00	77.63	4.129	2.824	3
3	2.0	64.95	0.283	1.345	30.35	15.01	77.24	4.133	2.823	3
4	3.0	64.96	0.283	1.345	30.34	15.00	77.07	4.136	2.822	3
5	4.0	65.02	0.283	1.345	30.36	15.00	76.78	4.140	2.822	3
6	5.0	65.05	0.283	1.345	30.36	15.00	76.51	4.144	2.821	3
7	6.0	65.11	0.283	1.346	30.37	15.00	76.28	4.147	2.823	3
8	6.9	65.17	0.282	1.346	30.37	15.00	76.02	4.151	2.823	3
9	8.0	65.20	0.282	1.346	30.37	15.00	75.75	4.154	2.822	3
10	9.0	65.23	0.282	1.346	30.39	14.99	75.47	4.159	2.822	3

Mean:		65.05	0.283	1.345	30.36	15.00	76.66	4.142	2.823	
Stand.dev.:		0.04	0.000	0.000	0.01	0.00	0.25	0.004	0.000	
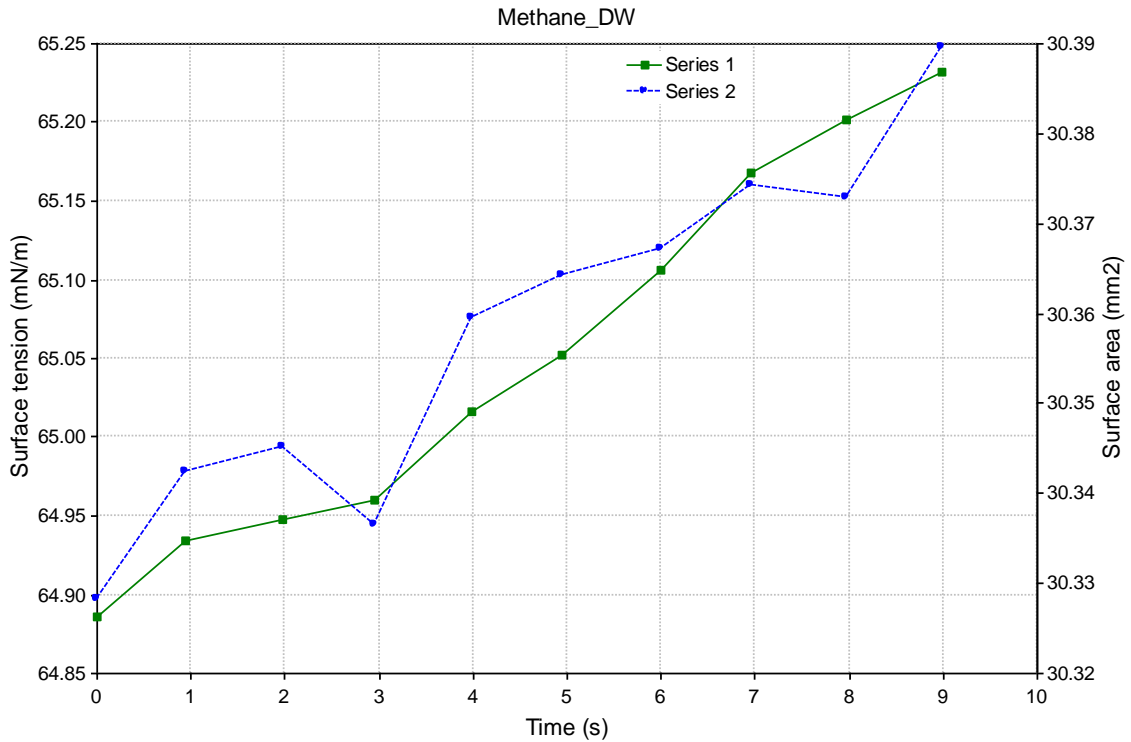
Methane_DW

Pressure   = 1.034 MPa

No.	Time	Gamma	Beta	R0	Area	Volume	Theta	Height	Width	Opt
						Messages				
1	0.0	64.50	0.282	1.338	29.95	14.74	78.35	4.092	2.810	3
2	1.0	64.56	0.282	1.339	29.97	14.75	78.04	4.098	2.811	3
3	2.0	64.66	0.282	1.340	30.00	14.77	77.83	4.102	2.812	3
4	2.9	64.71	0.282	1.340	30.02	14.77	77.62	4.106	2.812	3
5	4.0	64.79	0.282	1.340	30.05	14.78	77.32	4.111	2.814	3
6	4.9	64.88	0.282	1.341	30.06	14.79	77.09	4.115	2.814	3
7	6.0	64.94	0.282	1.341	30.08	14.81	76.91	4.118	2.814	3
8	6.9	65.00	0.282	1.342	30.11	14.83	76.66	4.124	2.814	3
9	8.0	65.10	0.281	1.342	30.13	14.83	76.38	4.129	2.814	3
10	9.0	65.18	0.281	1.343	30.16	14.85	76.03	4.134	2.816	3

Mean: 64.83   0.282   1.341   30.05   14.79   77.22   4.113   2.813
Stand.dev.:   0.07   0.000   0.000   0.02   0.01   0.24   0.004   0.001
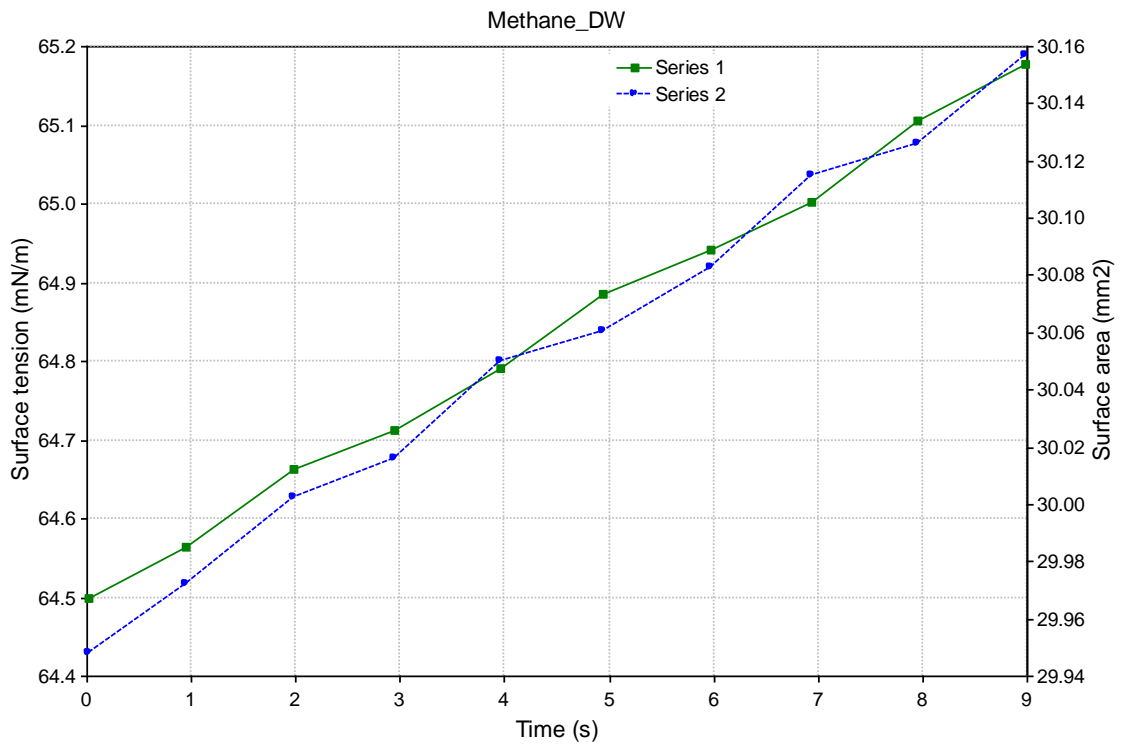
Methane_DW

178

Pressure   = 1.896MPa

No.	Time	Gamma	Beta	R0	Area	Volume	Theta	Height	Width	Opt
						Messages				
1	0.0	63.00	0.279	1.315	28.25	13.85	95.85	3.773	2.771	2
2	0.9	63.00	0.279	1.315	28.30	13.87	95.51	3.779	2.773	2
3	2.0	63.11	0.279	1.316	28.34	13.90	95.36	3.784	2.773	2
4	3.0	63.07	0.279	1.317	28.38	13.92	95.22	3.789	2.775	2
5	4.0	63.15	0.280	1.318	28.42	13.96	95.00	3.794	2.777	2
6	4.9	63.23	0.279	1.319	28.46	13.98	94.85	3.798	2.779	2
7	5.9	63.26	0.280	1.319	28.51	14.01	94.77	3.803	2.780	2
8	7.0	63.27	0.280	1.320	28.53	14.03	94.41	3.809	2.782	2
9	7.9	63.33	0.280	1.321	28.58	14.06	94.30	3.813	2.782	2
10	9.0	63.42	0.280	1.321	28.61	14.08	94.18	3.817	2.784	2

Mean: 63.19   0.279   1.318   28.44   13.96   94.94   3.796   2.777
Stand.dev.:   0.04   0.000   0.001   0.04   0.03   0.17   0.005   0.001

Methane_DW
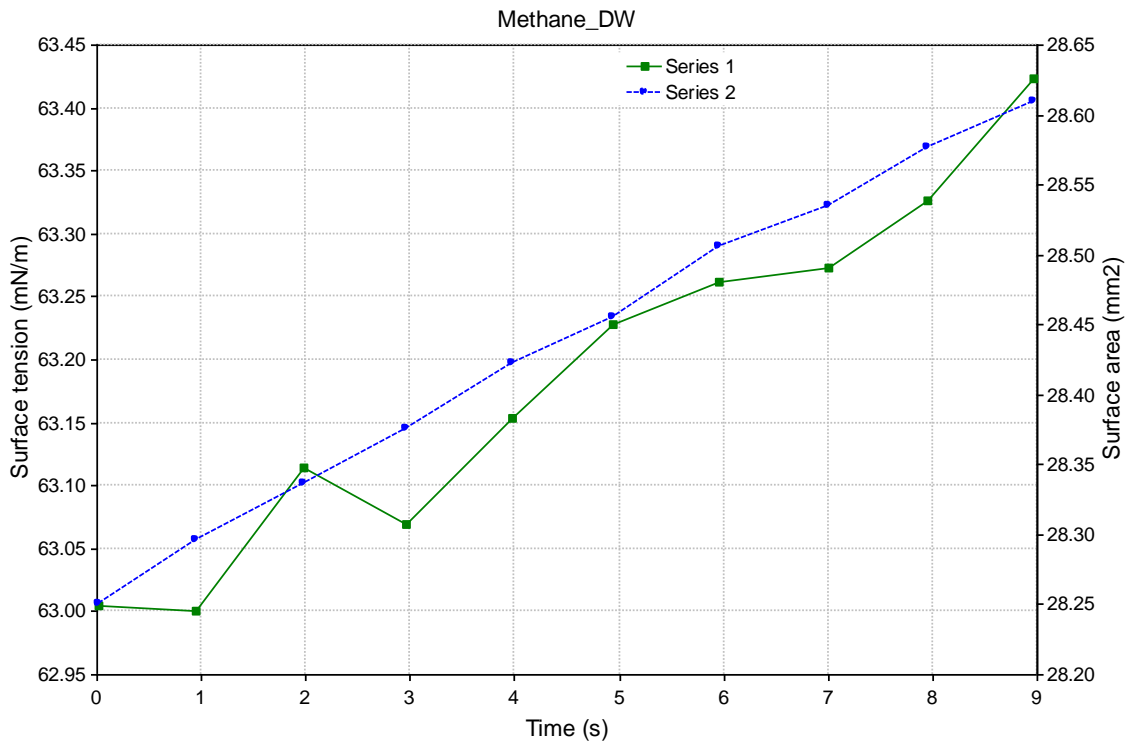
Pressure = 2.758MPa

No.	Time	Gamma	Beta	R0	Area	Volume	Theta	Height	Width	Opt
						Messages				
1	0.0	62.15	0.279	1.306	27.86	13.58	96.75	3.736	2.750	2
2	0.9	62.17	0.279	1.307	27.89	13.60	96.67	3.740	2.752	2
3	1.9	62.19	0.279	1.307	27.91	13.61	96.57	3.743	2.753	2
4	3.0	62.24	0.279	1.308	27.94	13.63	96.45	3.746	2.755	2
5	3.9	62.20	0.280	1.308	27.97	13.65	96.33	3.750	2.754	2
6	5.0	62.25	0.280	1.309	28.00	13.67	96.24	3.753	2.757	2
7	5.9	62.34	0.280	1.309	28.03	13.68	96.12	3.755	2.757	2
8	7.0	62.33	0.280	1.310	28.04	13.70	96.11	3.758	2.758	2
9	7.9	62.36	0.280	1.310	28.07	13.72	95.92	3.762	2.758	2
10	9.0	62.33	0.280	1.311	28.09	13.73	95.76	3.765	2.760	2

Mean: 62.26   0.280   1.309   27.98   13.66   96.29   3.751   2.755

Stand.dev.:   0.02   0.000   0.000   0.03   0.02   0.10   0.003   0.001
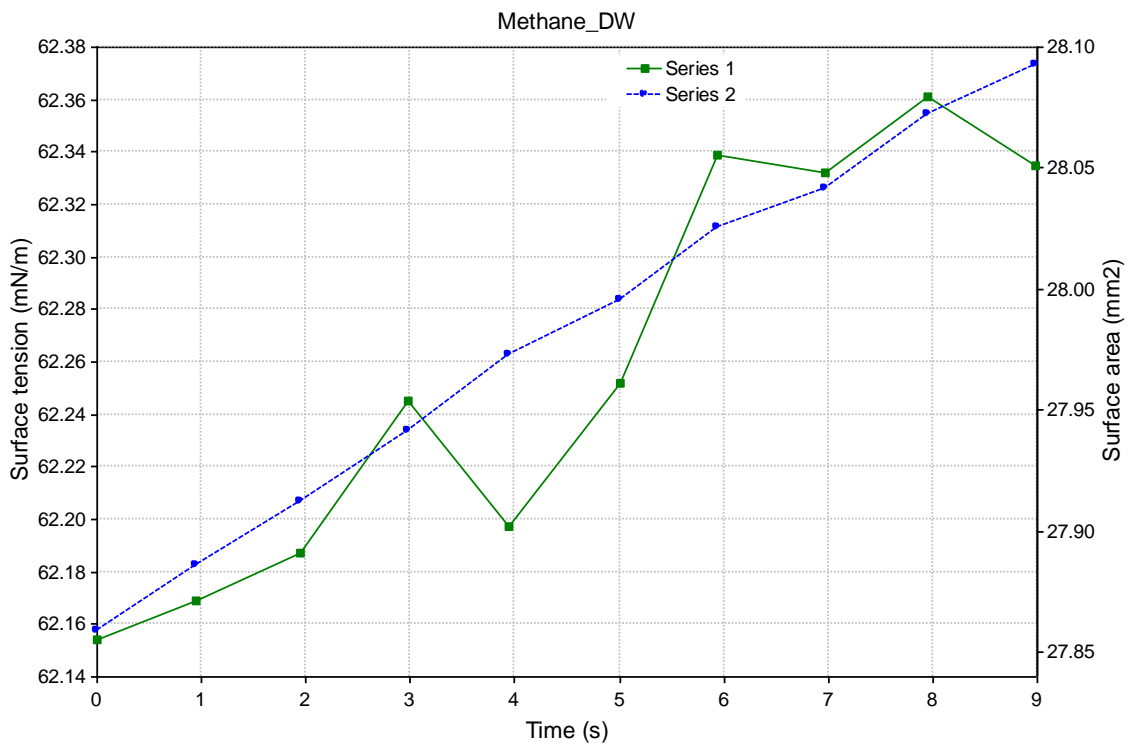
Methane_DW

Pressure = 3.620MPa

No.	Time	Gamma	Beta	R0	Area	Volume	Theta	Height	Width	Opt
						Messages				
1	0.0	61.15	0.280	1.299	27.59	13.39	96.98	3.717	2.736	2
2	1.0	61.30	0.280	1.300	27.64	13.43	96.98	3.721	2.739	2
3	2.0	61.41	0.280	1.301	27.67	13.44	96.82	3.723	2.739	2
4	2.9	61.45	0.280	1.302	27.71	13.46	96.71	3.727	2.741	2
5	4.0	61.48	0.280	1.302	27.76	13.49	96.64	3.732	2.743	2
6	5.0	61.57	0.280	1.303	27.78	13.51	96.48	3.735	2.746	2
7	6.0	61.68	0.280	1.304	27.81	13.53	96.32	3.739	2.745	2
8	7.0	61.72	0.280	1.305	27.86	13.56	96.24	3.744	2.748	2
9	7.9	61.84	0.280	1.306	27.89	13.59	96.07	3.748	2.748	2
10	9.0	61.90	0.280	1.306	27.93	13.62	96.06	3.751	2.749	2

Mean: 61.55 0.280 1.303 27.77 13.50 96.53 3.734 2.743
Stand.dev.: 0.08 0.000 0.001 0.04 0.02 0.11 0.004 0.001
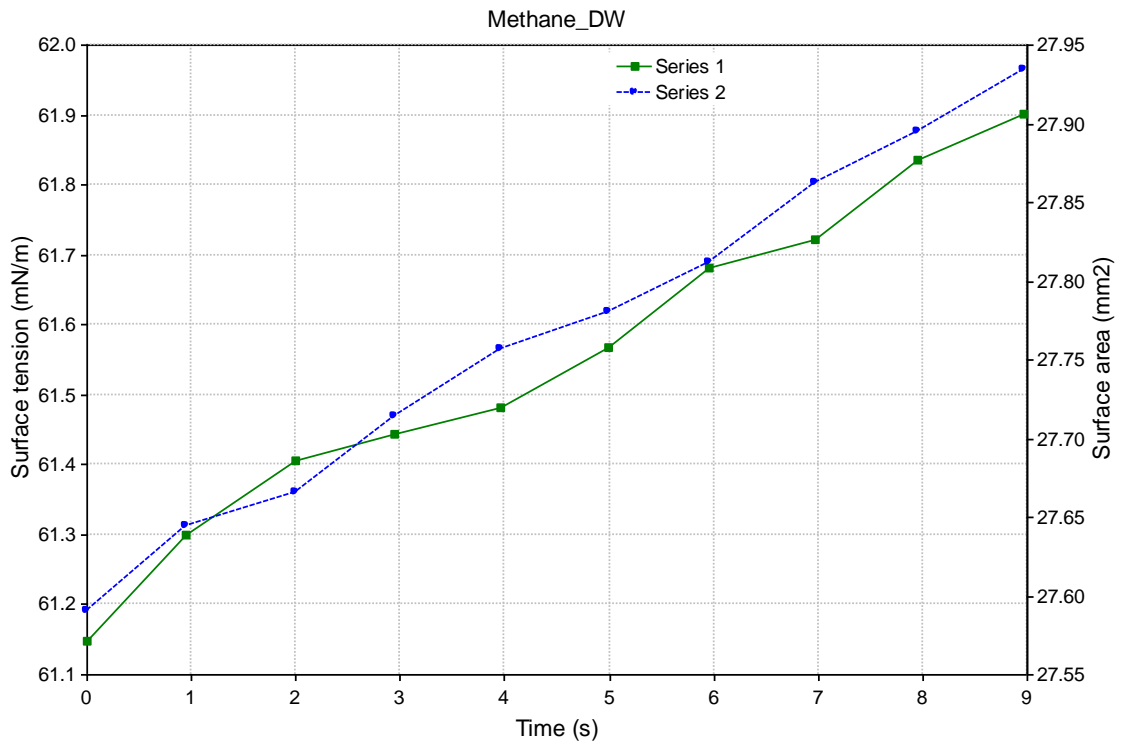
Methane_DW

Pressure   = 4.482MPa

No.	Time	Gamma	Beta	R0	Area	Volume Messages	Theta	Height	Width	Opt
1	0.0	60.89	0.283	1.303	27.98	13.44	85.09	3.897	2.719	3
2	0.9	61.07	0.283	1.304	28.00	13.46	85.08	3.901	2.721	3
3	1.9	61.12	0.283	1.305	28.04	13.48	84.90	3.906	2.721	3
4	3.0	61.13	0.283	1.306	28.08	13.50	84.70	3.911	2.723	3
5	4.0	61.26	0.283	1.307	28.13	13.55	84.47	3.916	2.726	3
6	5.0	61.36	0.283	1.308	28.14	13.55	84.41	3.920	2.726	3
7	5.9	61.45	0.283	1.309	28.24	13.60	84.19	3.925	2.727	3
8	7.0	61.55	0.283	1.309	28.26	13.62	84.05	3.929	2.729	3
9	8.0	61.67	0.283	1.311	28.30	13.65	83.88	3.934	2.731	3
10	9.0	61.70	0.283	1.311	28.31	13.67	83.66	3.941	2.733	3

Mean: 61.32   0.283   1.307   28.15   13.55   84.44   3.918   2.726
Stand.dev.:   0.09   0.000   0.001   0.04   0.03   0.16   0.005   0.001
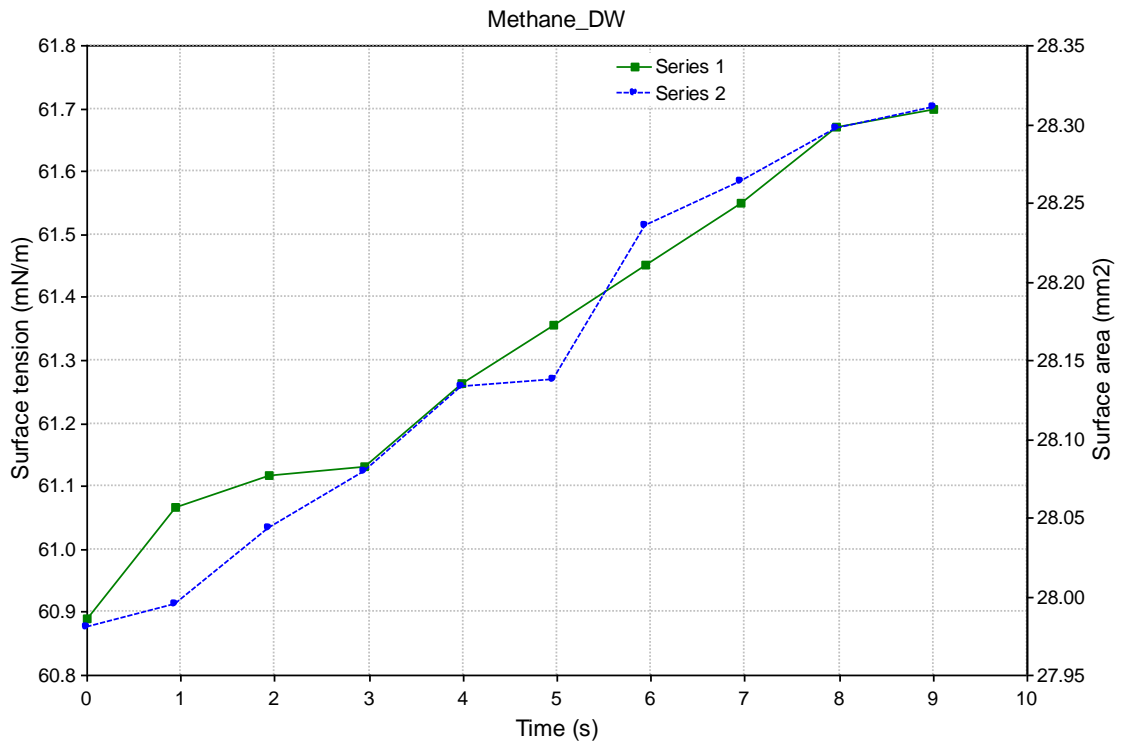
Methane_DW

Pressure   = 5.343MPa

No.	Time	Gamma	Beta	R0	Area	Volume Messages	Theta	Height	Width	Opt
1	0.0	59.01	0.284	1.284	27.12	12.88	87.83	3.807	2.686	3
2	0.9	59.12	0.284	1.285	27.15	12.90	87.76	3.812	2.686	3
3	2.0	59.17	0.284	1.286	27.20	12.92	87.60	3.816	2.688	3
4	3.0	59.27	0.284	1.287	27.24	12.95	87.44	3.820	2.688	3
5	4.0	59.32	0.284	1.288	27.27	12.98	87.38	3.825	2.690	3
6	4.9	59.42	0.284	1.289	27.32	13.00	87.17	3.829	2.692	3
7	6.0	59.46	0.284	1.289	27.36	13.03	87.04	3.834	2.693	3
8	7.0	59.56	0.284	1.290	27.42	13.07	86.82	3.838	2.694	3
9	7.9	59.69	0.284	1.291	27.47	13.10	86.80	3.842	2.696	3
10	8.9	59.82	0.284	1.292	27.47	13.11	86.65	3.846	2.697	3

Mean: 59.38   0.284   1.288   27.30   12.99   87.25   3.827   2.691
Stand.dev.:   0.08   0.000   0.001   0.04   0.03   0.13   0.004   0.001

Methane_DW
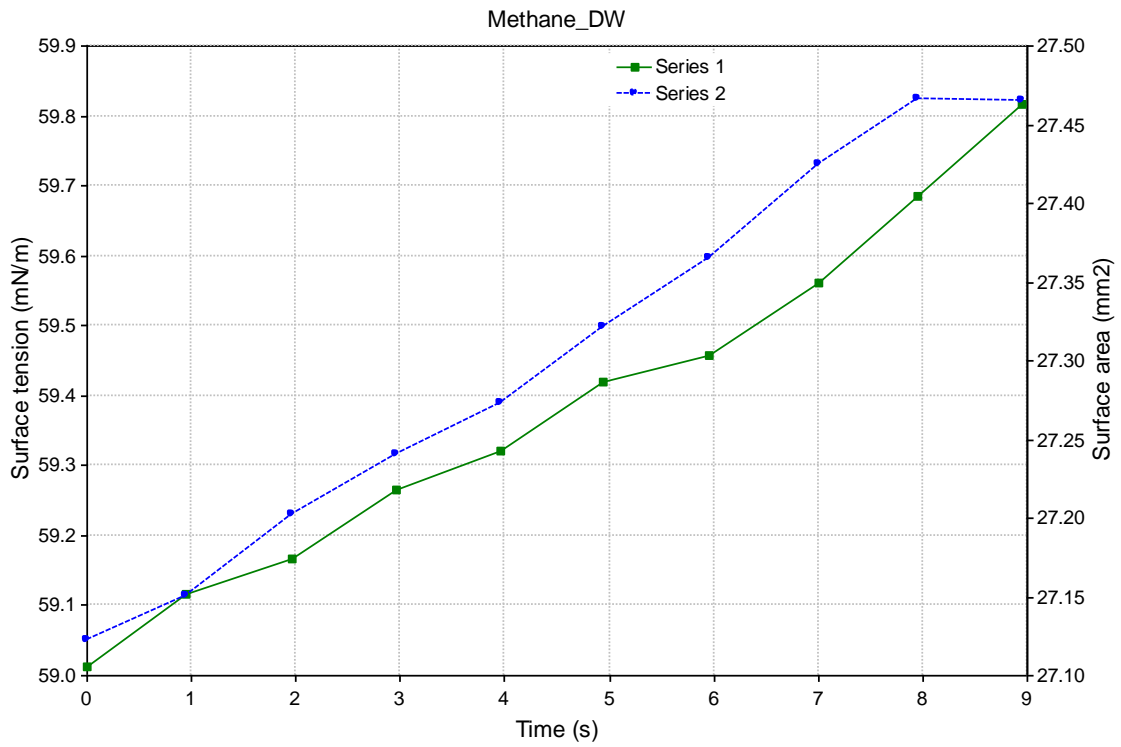
Pressure   = 6.205MPa

No.	Time	Gamma	Beta	R0	Area	Volume	Theta	Height	Width	Opt
						Messages				
1	0.0	58.23	0.286	1.281	27.21	12.85	84.99	3.845	2.679	3
2	0.9	58.23	0.286	1.281	27.24	12.86	84.77	3.848	2.679	3
3	1.9	58.37	0.286	1.282	27.27	12.89	84.76	3.852	2.681	3
4	3.0	58.41	0.286	1.283	27.30	12.91	84.61	3.855	2.683	3
5	4.0	58.51	0.286	1.284	27.32	12.93	84.60	3.857	2.685	3
6	5.0	58.53	0.286	1.284	27.38	12.96	84.24	3.863	2.684	3
7	5.9	58.54	0.286	1.285	27.39	12.96	84.17	3.867	2.687	3
8	7.0	58.62	0.286	1.285	27.40	12.98	83.97	3.871	2.687	3
9	8.0	58.60	0.287	1.286	27.42	12.99	83.97	3.874	2.690	3
10	9.0	58.73	0.286	1.287	27.48	13.03	83.79	3.877	2.690	3

Mean: 58.48   0.286   1.284   27.34   12.94   84.39   3.861   2.685
Stand.dev.:   0.05   0.000   0.001   0.03   0.02   0.13   0.004   0.001
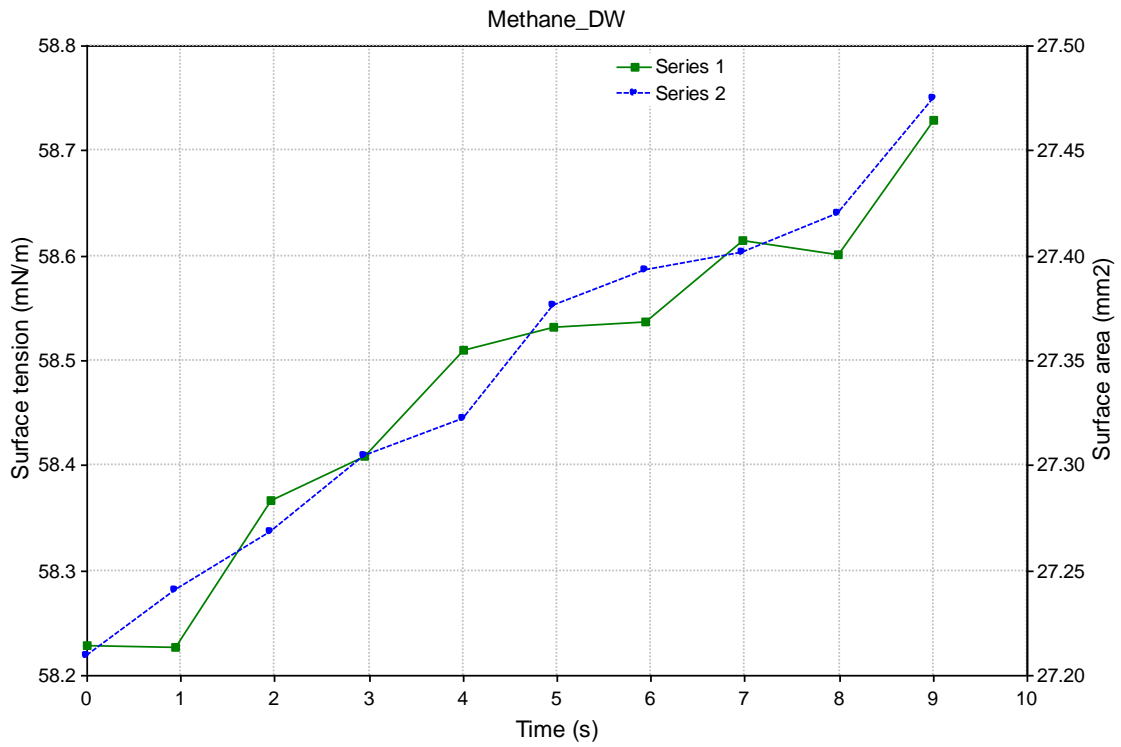
Methane_DW

184

Pressure   = 7.067MPa

No.	Time	Gamma	Beta	R0	Area	Volume Messages	Theta	Height	Width	Opt
1	0.0	57.16	0.286	1.268	26.48	12.41	87.84	3.765	2.655	3
2	0.9	57.18	0.286	1.268	26.50	12.43	87.70	3.768	2.655	3
3	2.0	57.34	0.285	1.269	26.55	12.45	87.69	3.770	2.656	3
4	3.0	57.32	0.286	1.269	26.56	12.46	87.53	3.774	2.657	3
5	4.0	57.38	0.286	1.270	26.60	12.49	87.37	3.777	2.657	3
6	5.0	57.40	0.286	1.270	26.61	12.50	87.30	3.779	2.658	3
7	5.9	57.44	0.286	1.271	26.65	12.53	87.20	3.783	2.661	3
8	7.0	57.54	0.286	1.272	26.68	12.54	87.10	3.785	2.660	3
9	8.0	57.62	0.286	1.272	26.69	12.55	87.08	3.788	2.662	3
10	8.9	57.67	0.285	1.273	26.71	12.57	86.96	3.790	2.662	3

Mean: 57.41   0.286   1.270   26.60   12.49   87.38   3.778   2.658
Stand.dev.:   0.05   0.000   0.001   0.02   0.02   0.10   0.003   0.001

Methane_DW
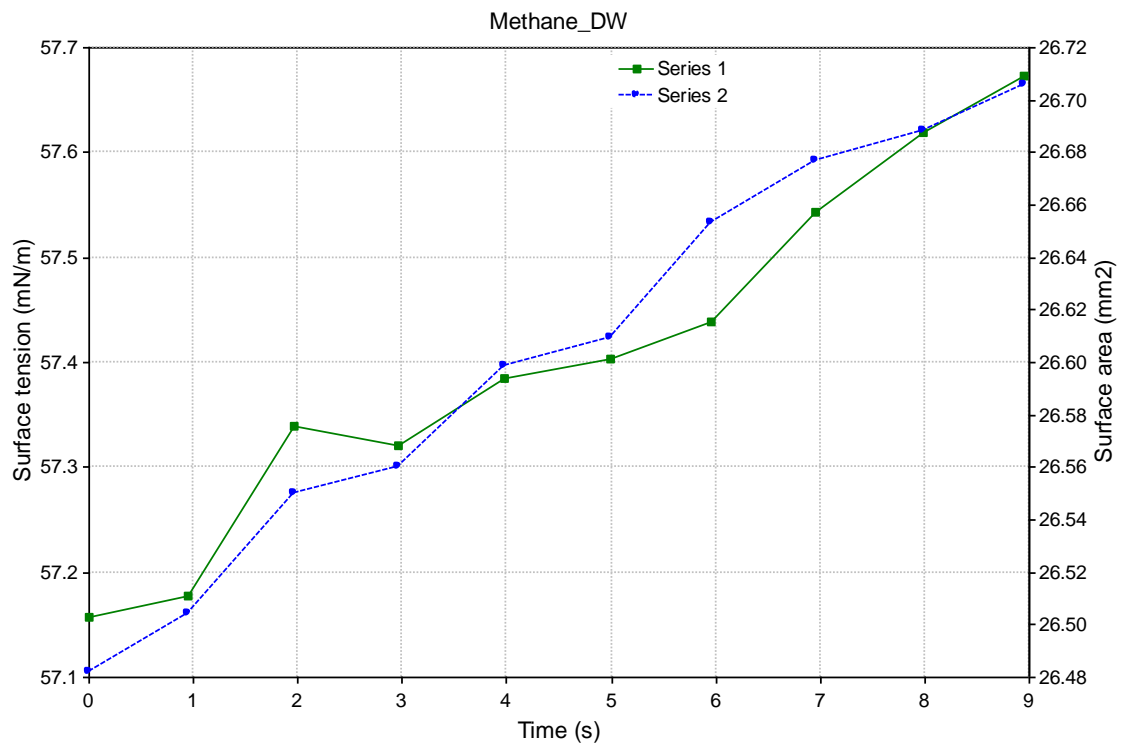
Pressure   = 7.929MPa

No.	Time	Gamma	Beta	R0	Area	Volume	Theta	Height	Width	Opt
						Messages				
1	0.0	55.85	0.286	1.254	25.86	12.01	89.51	3.705	2.630	3
2	0.9	55.92	0.286	1.255	25.89	12.04	89.46	3.708	2.629	3
3	1.9	55.89	0.287	1.255	25.95	12.07	89.01	3.715	2.630	3
4	3.0	55.99	0.286	1.256	26.00	12.10	88.99	3.718	2.632	3
5	4.0	56.06	0.286	1.257	26.01	12.12	88.81	3.720	2.632	3
6	4.9	56.06	0.287	1.257	26.02	12.13	88.82	3.723	2.634	3
7	5.9	56.13	0.286	1.258	26.02	12.13	88.85	3.725	2.634	3
8	7.0	56.26	0.286	1.259	26.06	12.15	88.80	3.728	2.635	3
9	8.0	56.18	0.287	1.259	26.09	12.17	88.57	3.731	2.635	3
10	9.0	56.35	0.286	1.260	26.14	12.20	88.52	3.734	2.637	3

Mean: 56.07   0.286   1.257   26.00   12.11   88.94   3.721   2.633
Stand.dev.:   0.05   0.000   0.001   0.03   0.02   0.10   0.003   0.001

Methane_DW
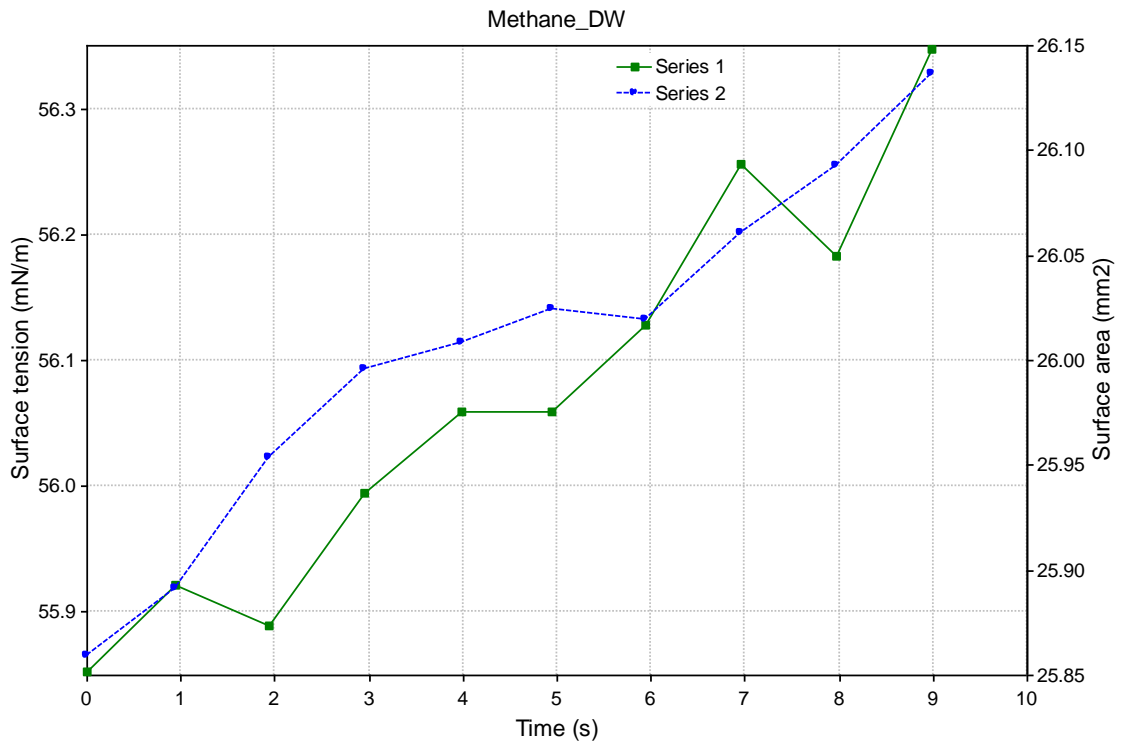
Pressure   = 8.791MPa

No.	Time	Gamma	Beta	R0	Area	Volume	Theta	Height	Width	Opt
						Messages				
1	0.0	55.08	0.287	1.246	25.56	11.82	90.10	3.676	2.614	3
2	0.9	55.06	0.287	1.247	25.59	11.84	89.97	3.680	2.615	3
3	2.0	55.17	0.287	1.248	25.61	11.85	89.93	3.684	2.615	3
4	3.0	55.24	0.287	1.248	25.64	11.87	89.81	3.687	2.617	3
5	3.9	55.24	0.287	1.249	25.66	11.88	89.60	3.691	2.617	3
6	5.0	55.29	0.287	1.250	25.68	11.90	89.53	3.694	2.617	3
7	5.9	55.28	0.287	1.250	25.71	11.91	89.44	3.697	2.618	3
8	7.0	55.38	0.287	1.251	25.73	11.93	89.31	3.700	2.620	3
9	8.0	55.44	0.287	1.251	25.77	11.95	89.09	3.705	2.621	3
10	9.0	55.50	0.287	1.252	25.79	11.96	88.94	3.709	2.621	3

Mean: 55.27   0.287   1.249   25.67   11.89   89.57   3.692   2.618

Stand.dev.:   0.05   0.000   0.001   0.02   0.01   0.12   0.003   0.001
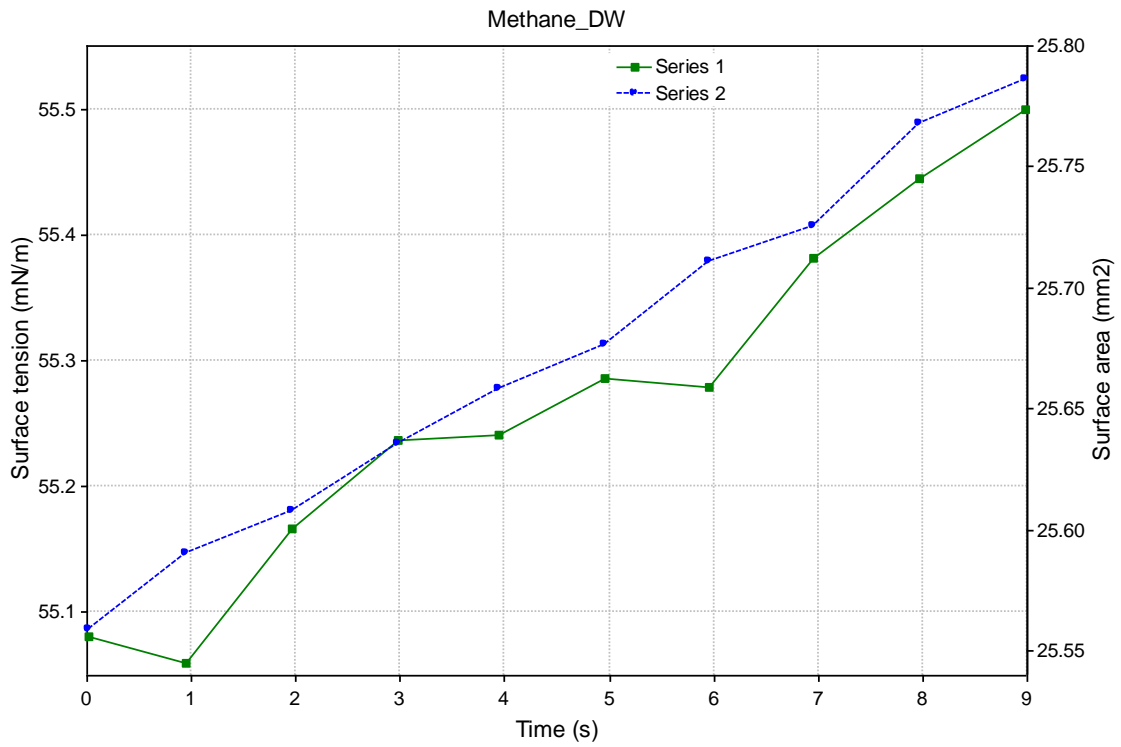
Methane_DW

Pressure   = 9.653MPa

No.	Time	Gamma	Beta	R0	Area	Volume Messages	Theta	Height	Width	Opt
1	0.0	54.04	0.292	1.246	25.94	11.92	80.33	3.828	2.595	3
2	1.0	54.09	0.292	1.247	25.98	11.94	80.03	3.834	2.595	3
3	1.9	54.13	0.292	1.247	25.99	11.95	79.96	3.836	2.595	3
4	2.9	54.20	0.292	1.248	26.02	11.96	79.95	3.838	2.596	3
5	4.0	54.28	0.292	1.248	26.06	11.99	79.63	3.843	2.597	3
6	5.0	54.30	0.292	1.249	26.08	12.00	79.46	3.847	2.598	3
7	6.0	54.44	0.292	1.250	26.11	12.02	79.33	3.851	2.599	3
8	7.0	54.45	0.292	1.250	26.13	12.04	79.12	3.855	2.602	3
9	7.9	54.49	0.292	1.251	26.14	12.04	79.04	3.858	2.602	3
10	9.0	54.54	0.292	1.251	26.19	12.06	78.84	3.863	2.603	3

Mean: 54.30   0.292   1.249   26.06   11.99   79.57   3.845   2.598
Stand.dev.:   0.06   0.000   0.001   0.03   0.02   0.16   0.004   0.001

Methane_DW
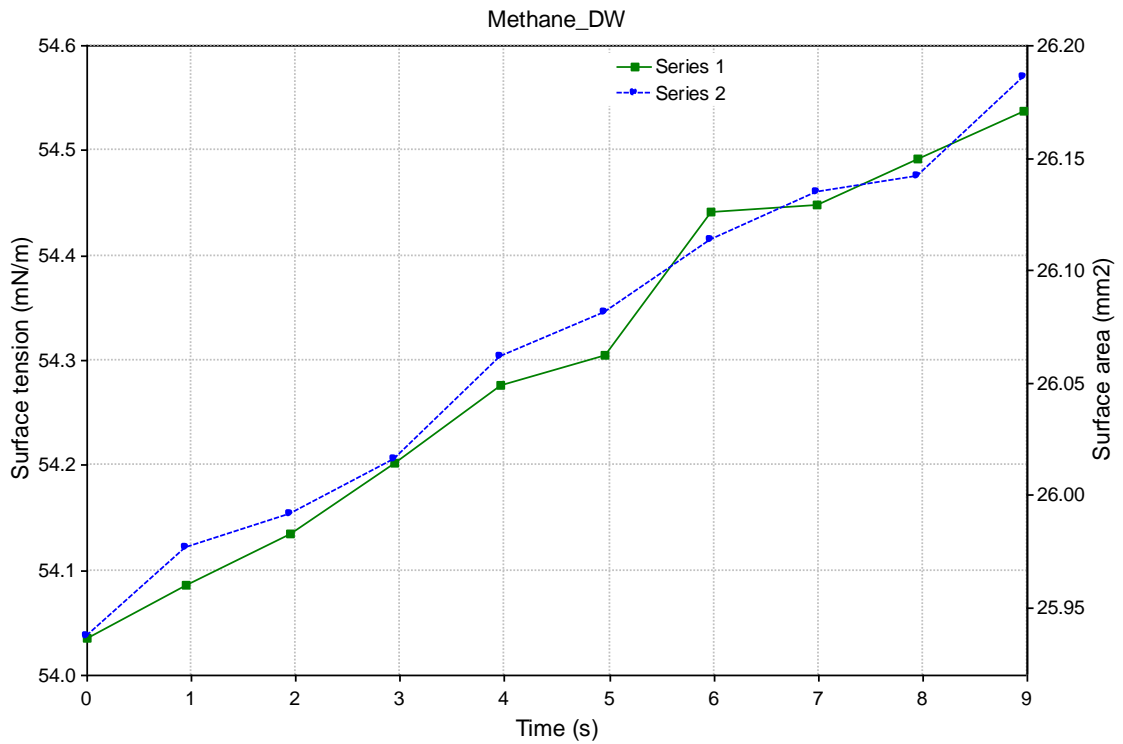
Pressure   = 10.515MPa

No.	Time	Gamma	Beta	R0	Area	Volume	Theta	Height	Width	Opt
						Messages				
1	0.0	53.37	0.287	1.227	24.64	11.27	93.98	3.568	2.578	3
2	0.9	53.43	0.287	1.228	24.67	11.29	93.82	3.572	2.579	3
3	2.0	53.45	0.287	1.228	24.70	11.31	93.71	3.575	2.579	3
4	2.9	53.56	0.287	1.229	24.74	11.33	93.66	3.578	2.582	3
5	4.0	53.64	0.287	1.230	24.76	11.35	93.65	3.580	2.583	3
6	5.0	53.71	0.287	1.230	24.76	11.35	93.64	3.582	2.583	3
7	5.9	53.69	0.287	1.231	24.81	11.38	93.48	3.585	2.584	3
8	6.9	53.74	0.287	1.231	24.85	11.39	93.35	3.588	2.584	3
9	7.9	53.79	0.287	1.232	24.87	11.41	93.36	3.591	2.587	3
10	9.0	53.83	0.287	1.233	24.90	11.43	93.14	3.595	2.588	3

Mean: 53.62   0.287   1.230   24.77   11.35   93.58   3.581   2.583
Stand.dev.:   0.05   0.000   0.001   0.03   0.02   0.08   0.003   0.001

Methane_DW
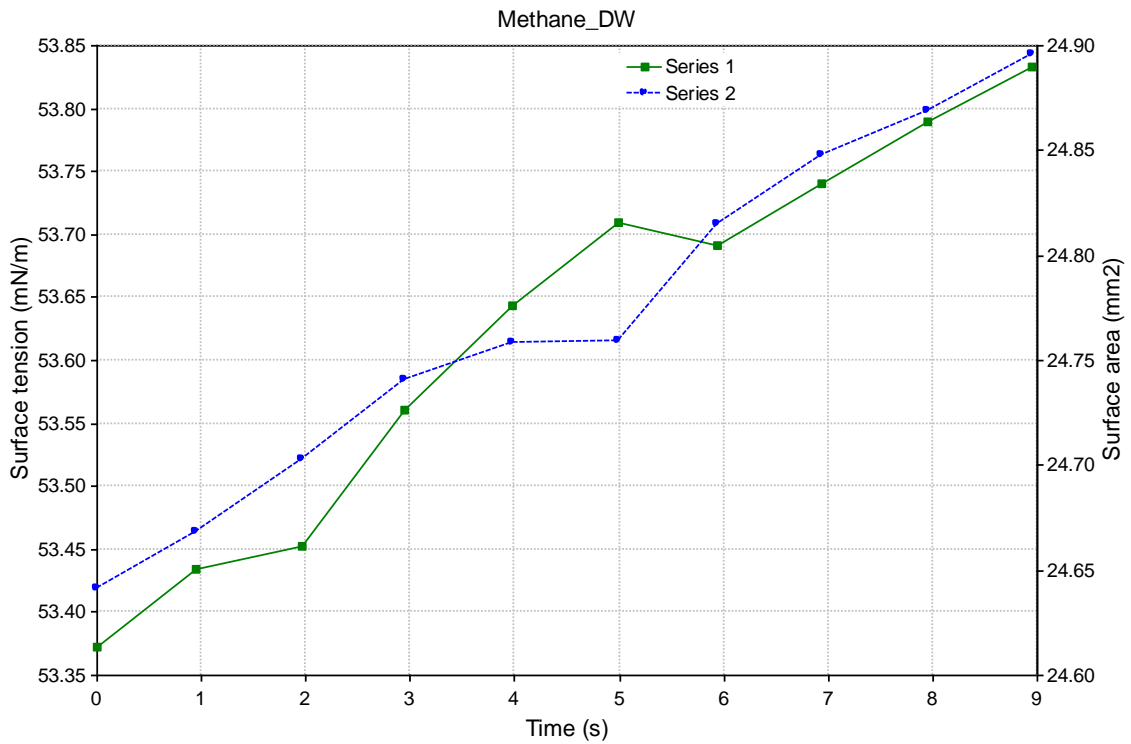
Pressure   = 11.376MPa

No.	Time	Gamma	Beta	R0	Area	Volume Messages	Theta	Height	Width	Opt
1	0.0	51.59	0.289	1.210	23.99	10.84	94.49	3.517	2.544	3
2	0.9	51.61	0.289	1.211	24.03	10.86	94.31	3.522	2.546	3
3	2.0	51.67	0.289	1.212	24.06	10.88	94.16	3.527	2.547	3
4	3.0	51.67	0.289	1.212	24.10	10.91	93.95	3.532	2.547	3
5	4.0	51.82	0.289	1.214	24.15	10.93	93.80	3.537	2.550	3
6	5.0	51.88	0.289	1.214	24.21	10.96	93.60	3.543	2.552	3
7	6.0	51.96	0.289	1.215	24.24	10.99	93.37	3.548	2.555	3
8	7.0	52.00	0.289	1.216	24.29	11.02	93.20	3.552	2.554	3
9	7.9	52.07	0.289	1.217	24.30	11.03	93.15	3.557	2.557	3
10	9.0	52.20	0.289	1.218	24.35	11.06	92.99	3.561	2.559	3

Mean: 51.85   0.289   1.214   24.17   10.95   93.70   3.540   2.551

Stand.dev.:   0.07   0.000   0.001   0.04   0.02   0.17   0.005   0.002

Methane_DW
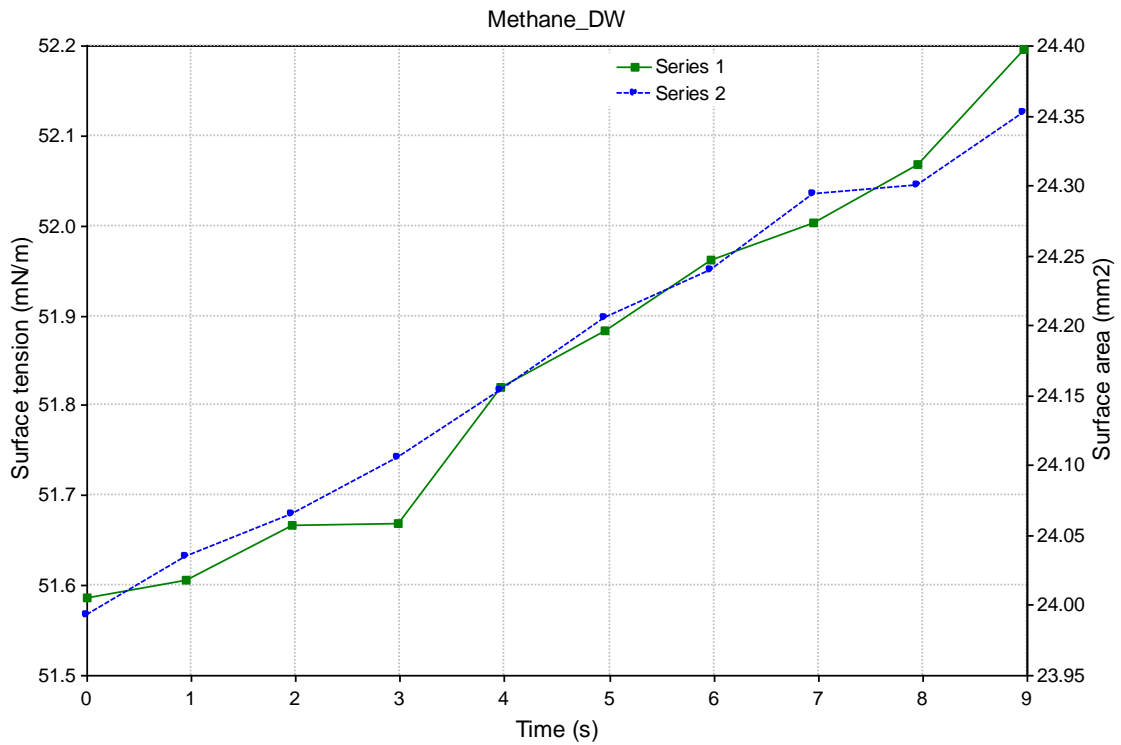
Pressure   = 12.238MPa

No.	Time	Gamma	Beta	R0	Area	Volume	Theta	Height	Width	Opt
						Messages				
1	0.0	50.54	0.290	1.200	23.55	10.58	96.05	3.470	2.523	3
2	1.0	50.65	0.289	1.201	23.59	10.60	95.91	3.474	2.526	3
3	2.0	50.69	0.289	1.201	23.61	10.61	95.78	3.477	2.524	3
4	3.0	50.73	0.290	1.202	23.65	10.64	95.77	3.479	2.529	3
5	4.0	50.76	0.290	1.203	23.67	10.65	95.63	3.483	2.528	3
6	4.9	50.82	0.290	1.203	23.72	10.68	95.46	3.487	2.530	3
7	5.9	50.84	0.290	1.204	23.73	10.68	95.38	3.490	2.531	3
8	7.0	50.87	0.290	1.204	23.75	10.70	95.27	3.493	2.531	3
9	7.9	50.95	0.290	1.205	23.78	10.71	95.10	3.497	2.532	3
10	8.9	51.02	0.290	1.206	23.82	10.73	95.08	3.499	2.534	3

Mean: 50.79   0.290   1.203   23.69   10.66   95.54   3.485   2.529
Stand.dev.:   0.05   0.000   0.001   0.03   0.02   0.11   0.003   0.001

Methane_DW
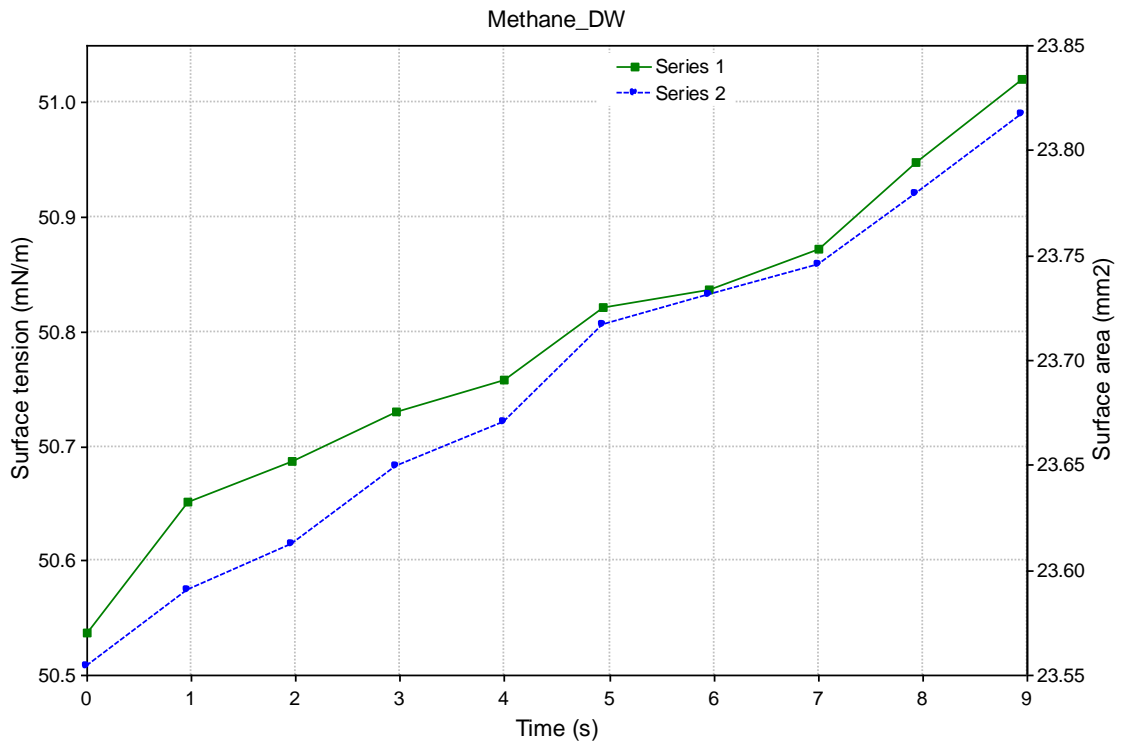
Pressure   = 13.100MPa

No.	Time	Gamma	Beta	R0	Area	Volume	Theta	Height	Width	Opt
					Messages					
1	0.0	49.53	0.289	1.186	23.00	10.20	96.99	3.414	2.500	3
2	0.9	49.61	0.289	1.187	23.07	10.24	96.87	3.417	2.501	3
3	2.0	49.64	0.289	1.187	23.09	10.25	96.74	3.421	2.503	3
4	3.0	49.72	0.289	1.188	23.11	10.27	96.82	3.423	2.505	3
5	4.0	49.79	0.289	1.189	23.13	10.29	96.70	3.427	2.507	3
6	5.0	49.89	0.288	1.190	23.16	10.30	96.64	3.430	2.507	3
7	5.9	49.92	0.289	1.191	23.20	10.32	96.56	3.433	2.510	3
8	6.9	49.96	0.289	1.191	23.24	10.35	96.43	3.437	2.511	3
9	8.0	49.97	0.289	1.192	23.27	10.36	96.34	3.440	2.512	3
10	8.9	50.10	0.289	1.193	23.29	10.38	96.29	3.443	2.513	3

Mean: 49.81   0.289   1.189   23.16   10.30   96.64   3.428   2.507
Stand.dev.:   0.06   0.000   0.001   0.03   0.02   0.07   0.003   0.001
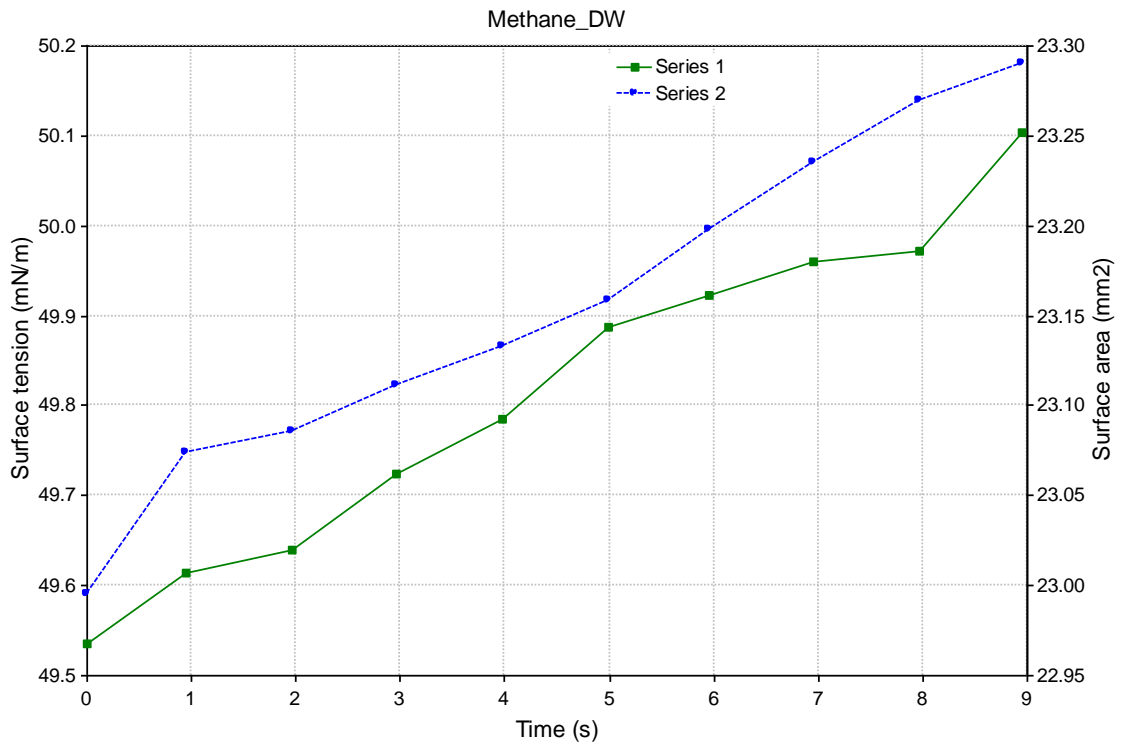
Methane_DW

Drop Shape Image Analysis

Temperature : 308.15 K
Pressure: : 0.172 MPa

Date : 11/28/2017 Remarks : Comments here
Experiment : Methane_(DW+PEG)_35Method : methane_(dw+peg).met
Drop phase : Methane Density : 0.007
Extern.phase : Water Density : 1.0145
Solid phase : Steel Calculation : Optimized cont.

No.	Time	Gamma	Beta	R0	Area	Volume	Theta	Height	Width	Opt
						Messages				
1	0.0	51.26	0.277	1.199	23.50	10.19	72.90	3.709	2.468	4
2	1.0	51.43	0.277	1.201	23.58	10.23	72.78	3.715	2.472	4
3	2.0	51.50	0.277	1.202	23.61	10.25	72.65	3.720	2.473	3
4	3.0	51.58	0.277	1.202	23.63	10.27	72.54	3.723	2.472	4
5	4.0	51.63	0.277	1.203	23.65	10.28	72.41	3.727	2.472	4
6	4.9	51.66	0.277	1.204	23.67	10.30	72.23	3.733	2.475	4
7	5.9	51.74	0.277	1.204	23.69	10.31	72.04	3.735	2.476	3
8	7.0	51.97	0.276	1.205	23.72	10.33	71.79	3.739	2.477	4
9	7.9	52.17	0.276	1.207	23.78	10.36	71.61	3.745	2.479	4
10	9.0	52.32	0.276	1.209	23.86	10.40	71.41	3.754	2.484	4

Mean: 51.73 0.277 1.204 23.67 10.29 72.24 3.730 2.475
Stand.dev.: 0.11 0.000 0.001 0.03 0.02 0.16 0.004 0.001

Methane_(DW+PEG)
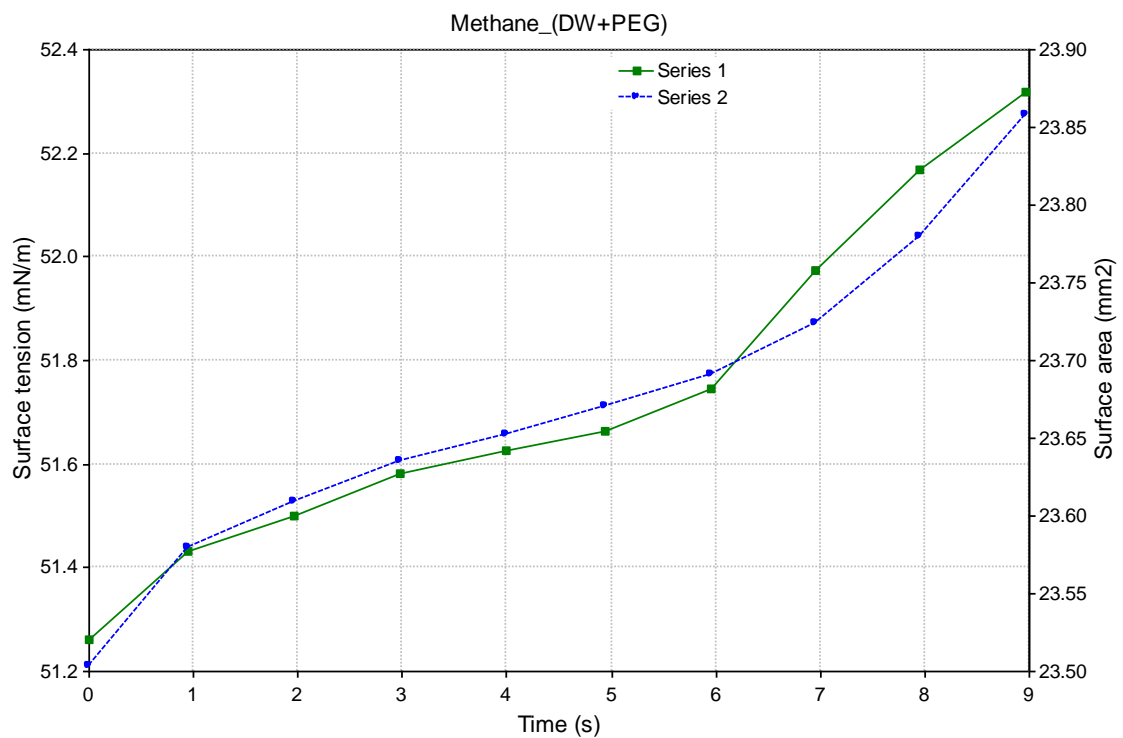
Pressure = 150

No.	Time	Gamma	Beta	R0	Area	Volume	Theta	Height	Width	Opt
						Messages				
1	0.0	55.75	0.278	1.251	25.68	11.48	64.95	3.995	2.558	4
2	0.9	56.14	0.277	1.254	25.84	11.57	64.40	4.010	2.560	4
3	1.9	56.58	0.277	1.259	25.96	11.65	63.84	4.032	2.568	4
4	3.0	57.00	0.276	1.262	26.06	11.71	63.24	4.051	2.575	4
5	4.0	57.44	0.275	1.265	26.15	11.77	62.54	4.069	2.578	4
6	5.0	57.84	0.275	1.268	26.27	11.82	61.94	4.087	2.584	4
7	6.0	58.22	0.274	1.271	26.35	11.87	61.33	4.105	2.588	4
8	6.9	58.68	0.273	1.274	26.40	11.90	60.71	4.121	2.591	4
9	7.9	59.16	0.273	1.278	26.55	11.98	59.98	4.141	2.596	4
10	9.0	59.64	0.272	1.281	26.63	12.03	59.29	4.160	2.600	4

Mean: 57.64   0.275   1.266   26.19   11.78   62.22   4.077   2.580

Stand.dev.:   0.41   0.001   0.003   0.10   0.06   0.60   0.018   0.005
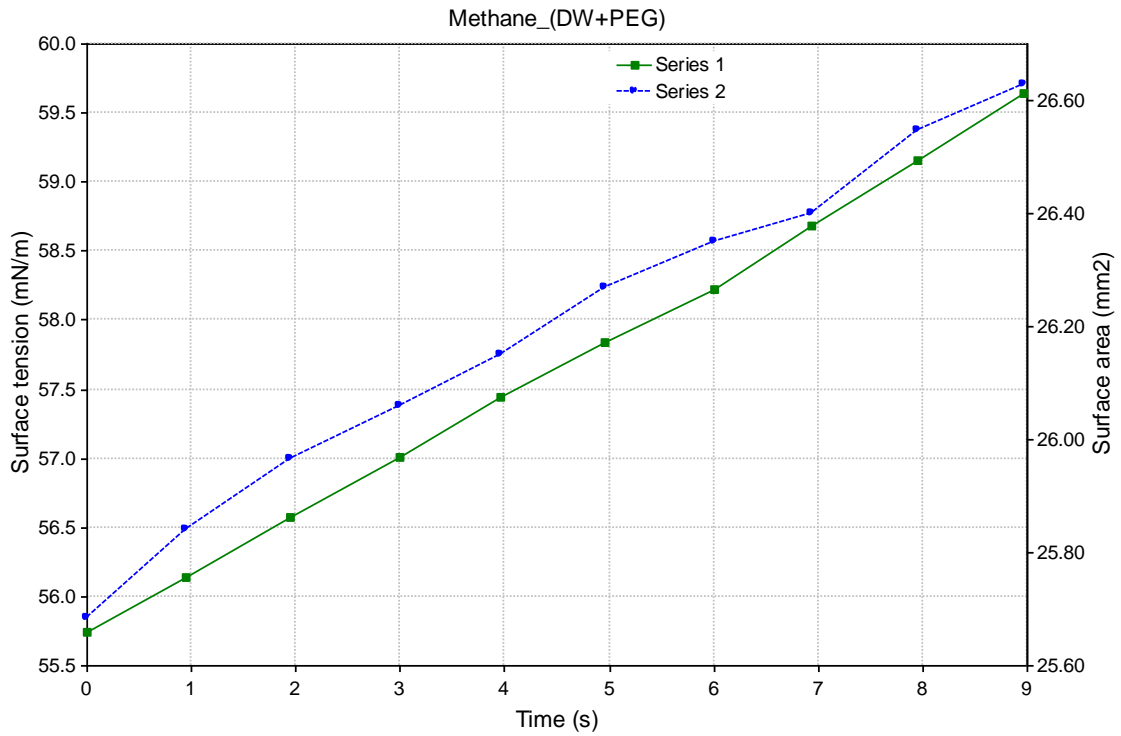
Methane_(DW+PEG)

Pressure   = 1.034 MPa

No.	Time	Gamma	Beta	R0	Area	Volume	Theta	Height	Width	Opt
						Messages				
1	0.0	47.43	0.286	1.171	22.56	9.66	77.60	3.604	2.427	4
2	1.0	48.50	0.285	1.182	22.96	9.90	76.05	3.653	2.446	4
3	2.0	49.40	0.284	1.191	23.29	10.10	74.75	3.694	2.459	4
4	2.9	50.28	0.283	1.200	23.62	10.30	73.36	3.737	2.475	4
5	3.9	50.95	0.282	1.207	23.91	10.46	72.25	3.769	2.483	4
6	4.9	51.46	0.282	1.212	24.07	10.56	71.48	3.795	2.492	4
7	5.9	51.88	0.282	1.216	24.19	10.64	70.82	3.814	2.499	4
8	7.0	52.17	0.281	1.218	24.31	10.70	70.26	3.829	2.502	4
9	7.9	52.66	0.281	1.223	24.47	10.80	69.37	3.854	2.509	4
10	8.9	53.31	0.280	1.229	24.68	10.92	68.39	3.883	2.518	4

Mean: 50.80   0.283   1.205   23.81   10.40   72.43   3.763   2.481
Stand.dev.:   0.60   0.001   0.006   0.22   0.13   0.94   0.029   0.009

Methane_(DW+PEG)
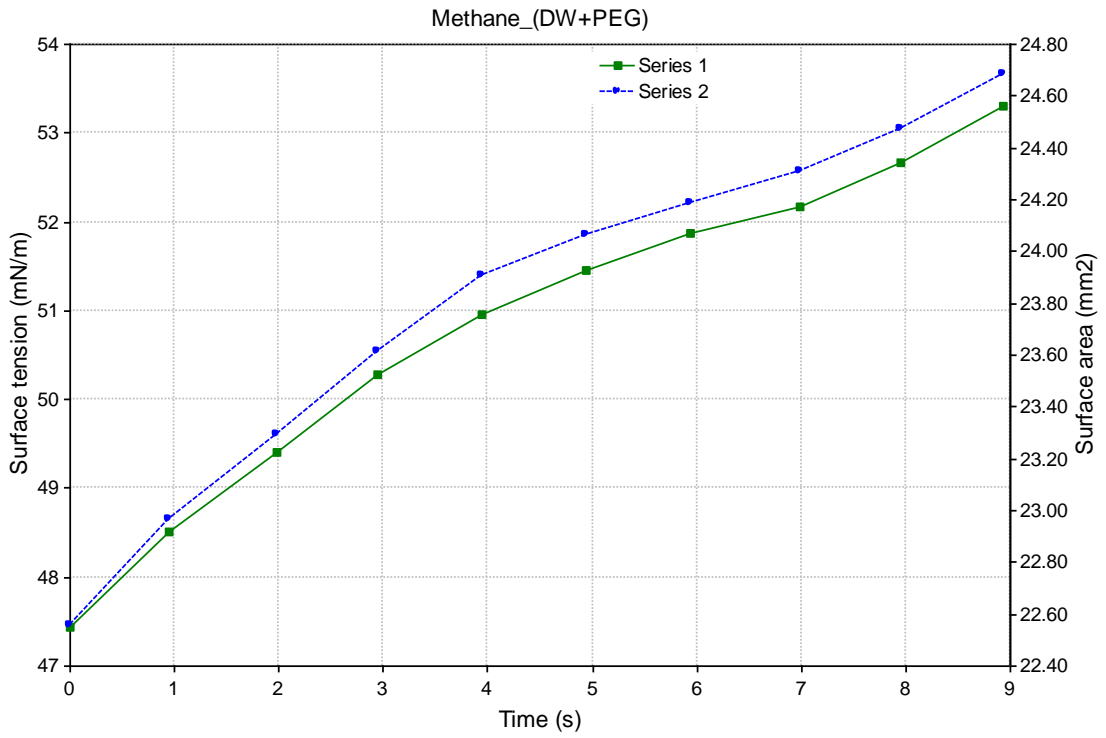
Pressure   = 1.896MPa

No.	Time	Gamma	Beta	R0	Area	Volume	Theta	Height	Width	Opt
						Messages				
1	0.0	53.23	0.280	1.228	24.62	10.90	68.08	3.888	2.509	4
2	1.0	53.43	0.280	1.230	24.69	10.93	67.72	3.898	2.509	4
3	2.0	53.56	0.280	1.231	24.75	10.96	67.40	3.906	2.511	4
4	3.0	53.76	0.280	1.233	24.80	10.99	67.06	3.916	2.513	4
5	4.0	53.92	0.279	1.234	24.84	11.01	66.70	3.923	2.514	4
6	5.0	54.09	0.279	1.236	24.90	11.05	66.39	3.933	2.515	4
7	5.9	54.29	0.279	1.238	24.95	11.08	66.08	3.941	2.517	4
8	6.9	54.43	0.279	1.239	25.00	11.11	65.79	3.950	2.520	4
9	8.0	54.63	0.278	1.241	25.05	11.14	65.46	3.959	2.522	4
10	8.9	54.80	0.278	1.242	25.14	11.19	65.11	3.968	2.524	4

Mean: 54.02   0.279   1.235   24.87   11.04   66.58   3.928   2.515

Stand.dev.:   0.17   0.000   0.001   0.05   0.03   0.31   0.008   0.002
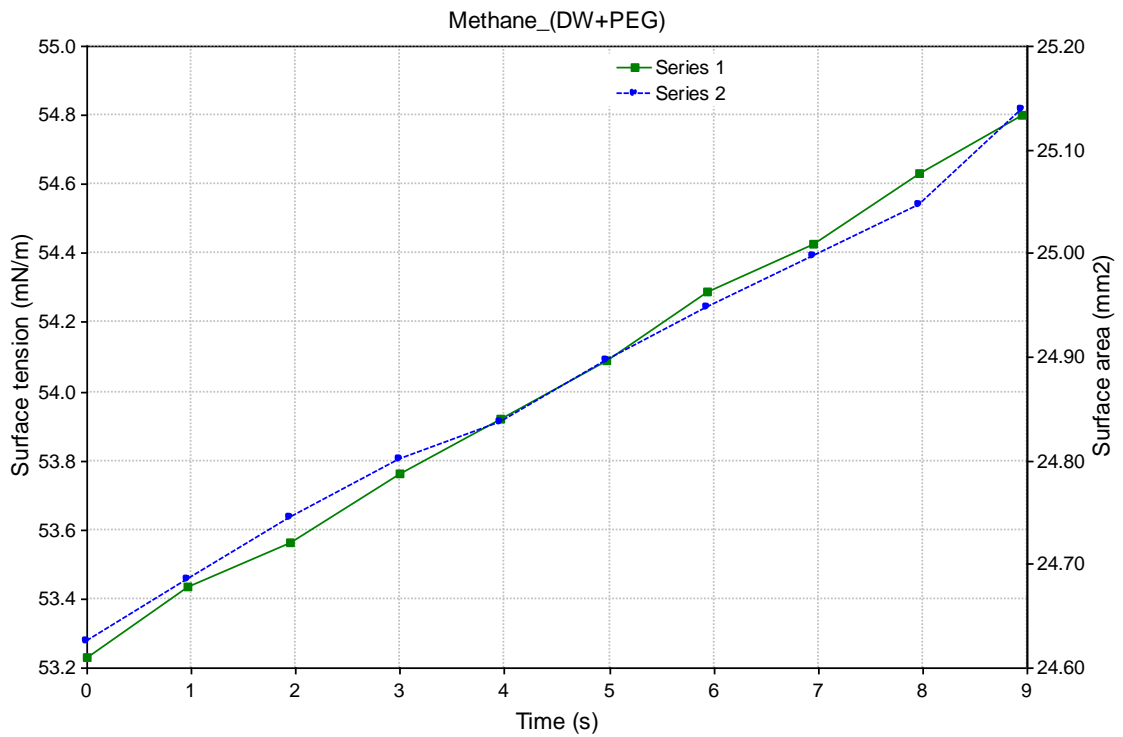
Methane_(DW+PEG)

Pressure = 2.758MPa

No.	Time	Gamma	Beta	R0	Area	Volume Messages	Theta	Height	Width	Opt
1	0.0	53.11	0.280	1.226	24.46	10.73	64.66	3.934	2.489	4
2	0.9	53.35	0.279	1.227	24.55	10.78	64.29	3.941	2.490	4
3	1.9	53.44	0.279	1.228	24.58	10.80	64.02	3.948	2.491	4
4	2.9	53.59	0.279	1.230	24.60	10.81	63.77	3.956	2.492	4
5	3.9	53.74	0.278	1.230	24.63	10.82	63.49	3.961	2.492	4
6	4.9	53.93	0.278	1.232	24.66	10.84	63.21	3.967	2.493	4
7	6.0	54.02	0.278	1.233	24.69	10.85	62.98	3.973	2.494	4
8	6.9	54.18	0.278	1.234	24.76	10.89	62.67	3.981	2.495	4
9	8.0	54.27	0.278	1.234	24.74	10.88	62.37	3.988	2.494	4
10	9.0	54.45	0.277	1.236	24.78	10.90	62.11	3.996	2.496	4

Mean: 53.81   0.278   1.231   24.65   10.83   63.36   3.964   2.492
Stand.dev.:   0.14   0.000   0.001   0.03   0.02   0.27   0.006   0.001

Methane_(DW+PEG)
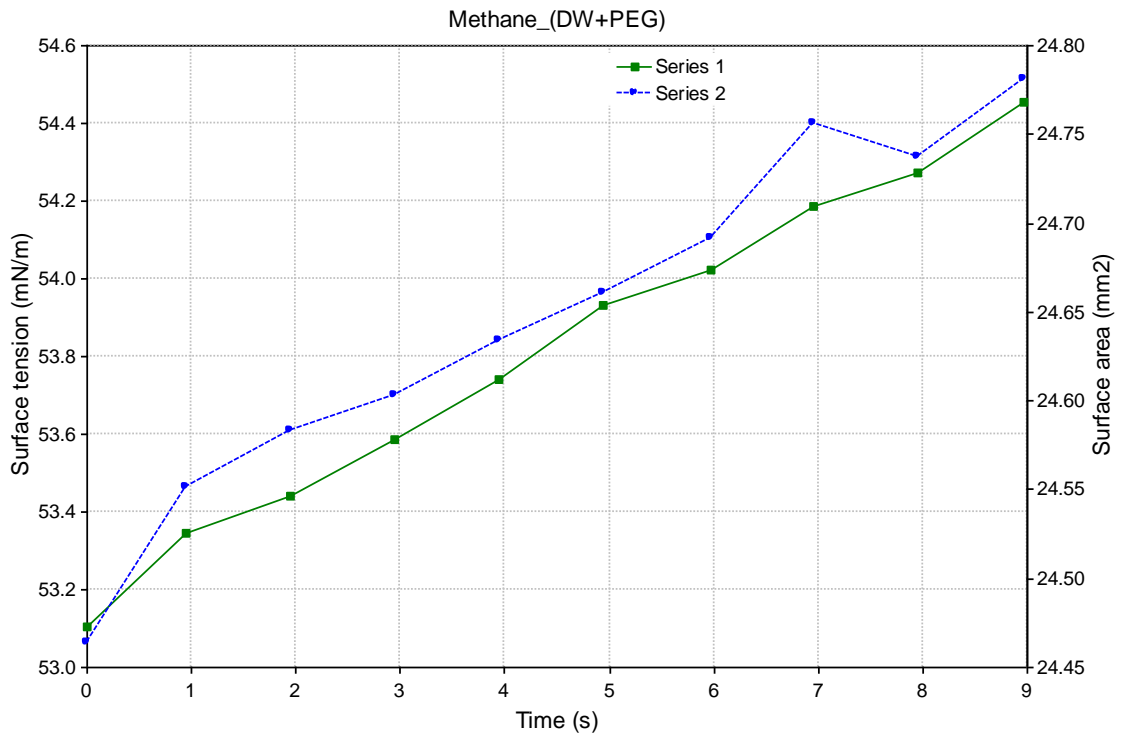
Pressure = 3.620MPa

No.	Time	Gamma	Beta	R0	Area	Volume Messages	Theta	Height	Width	Opt
1	0.0	49.17	0.286	1.192	23.32	10.10	72.86	3.734	2.449	4
2	0.9	49.45	0.285	1.195	23.42	10.16	72.44	3.745	2.453	4
3	1.9	49.70	0.285	1.197	23.51	10.21	71.90	3.760	2.455	4
4	3.0	49.91	0.285	1.199	23.59	10.26	71.46	3.772	2.457	4
5	3.9	50.10	0.285	1.201	23.65	10.29	71.06	3.781	2.460	4
6	5.0	50.25	0.284	1.203	23.67	10.30	70.73	3.791	2.464	4
7	6.0	50.47	0.284	1.205	23.78	10.36	70.24	3.803	2.466	4
8	6.9	50.72	0.284	1.207	23.89	10.43	69.78	3.815	2.470	4
9	8.0	50.94	0.284	1.209	23.92	10.44	69.40	3.825	2.473	4
10	8.9	51.18	0.283	1.211	24.04	10.51	68.91	3.838	2.473	4

Mean: 50.19   0.284   1.202   23.68   10.31   70.88   3.786   2.462

Stand.dev.:   0.21   0.000   0.002   0.07   0.04   0.41   0.011   0.003

Methane_(DW+PEG)
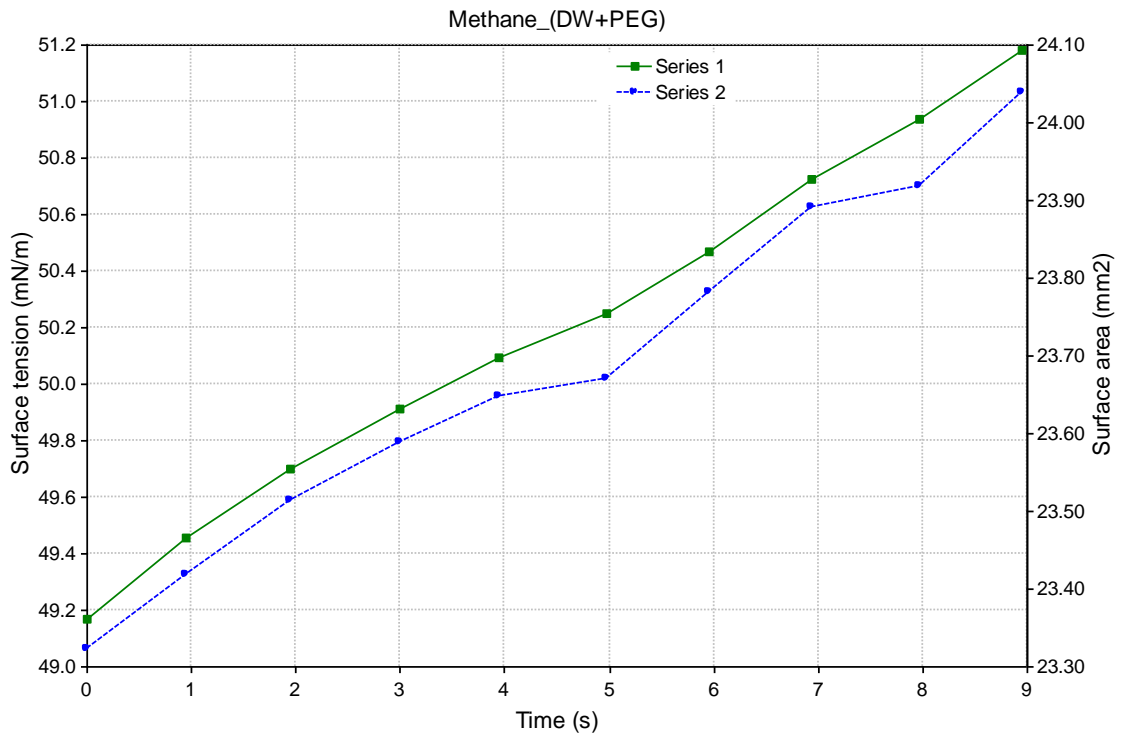
Pressure   = 4.482MPa

No.	Time	Gamma	Beta	R0	Area	Volume Messages	Theta	Height	Width	Opt
1	0.0	46.25	0.288	1.161	22.30	9.42	73.01	3.647	2.393	4
2	0.9	46.45	0.288	1.163	22.34	9.45	72.81	3.655	2.396	4
3	1.9	46.61	0.288	1.165	22.41	9.50	72.43	3.665	2.398	4
4	3.0	46.84	0.287	1.167	22.51	9.55	72.13	3.673	2.402	4
5	3.9	46.99	0.287	1.169	22.56	9.58	71.77	3.683	2.405	4
6	5.0	47.14	0.287	1.171	22.66	9.64	71.42	3.692	2.407	4
7	6.0	47.35	0.287	1.172	22.69	9.64	71.15	3.700	2.411	4
8	7.0	47.48	0.287	1.174	22.75	9.68	70.88	3.710	2.416	4
9	7.9	47.58	0.287	1.175	22.75	9.68	70.59	3.718	2.418	4
10	9.0	47.73	0.287	1.177	22.84	9.73	70.23	3.727	2.419	4

Mean: 47.04   0.287   1.169   22.58   9.59   71.64   3.687   2.407
Stand.dev.:   0.16   0.000   0.002   0.06   0.03   0.30   0.009   0.003

Methane_(DW+PEG)
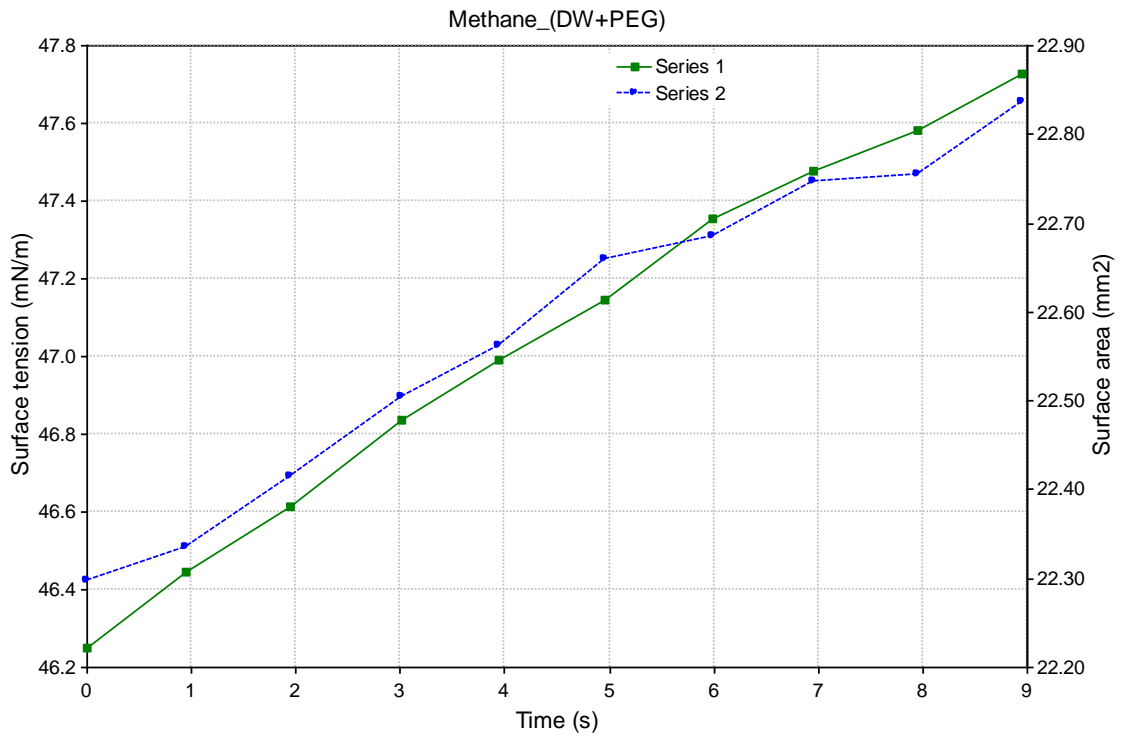
Pressure   = 5.343MPa

No.	Time	Gamma	Beta	R0	Area	Volume	Theta	Height	Width	Opt
						Messages				
1	0.0	46.25	0.290	1.164	22.37	9.50	74.06	3.648	2.398	4
2	0.9	46.30	0.290	1.165	22.39	9.51	73.86	3.653	2.399	4
3	2.0	46.41	0.289	1.166	22.39	9.51	73.73	3.658	2.399	3
4	3.0	46.46	0.289	1.166	22.45	9.55	73.50	3.661	2.401	4
5	3.9	46.54	0.289	1.167	22.49	9.57	73.31	3.667	2.402	4
6	5.0	46.64	0.289	1.168	22.49	9.57	73.19	3.672	2.404	4
7	6.0	46.69	0.289	1.169	22.56	9.60	72.95	3.677	2.404	4
8	6.9	46.79	0.289	1.170	22.58	9.62	72.76	3.681	2.405	4
9	7.9	46.90	0.289	1.171	22.61	9.63	72.56	3.686	2.408	4
10	8.9	47.02	0.289	1.172	22.66	9.66	72.41	3.691	2.408	4

Mean: 46.60   0.289   1.168   22.50   9.57   73.23   3.669   2.403
Stand.dev.:   0.08   0.000   0.001   0.03   0.02   0.18   0.005   0.001

Methane_(DW+PEG)
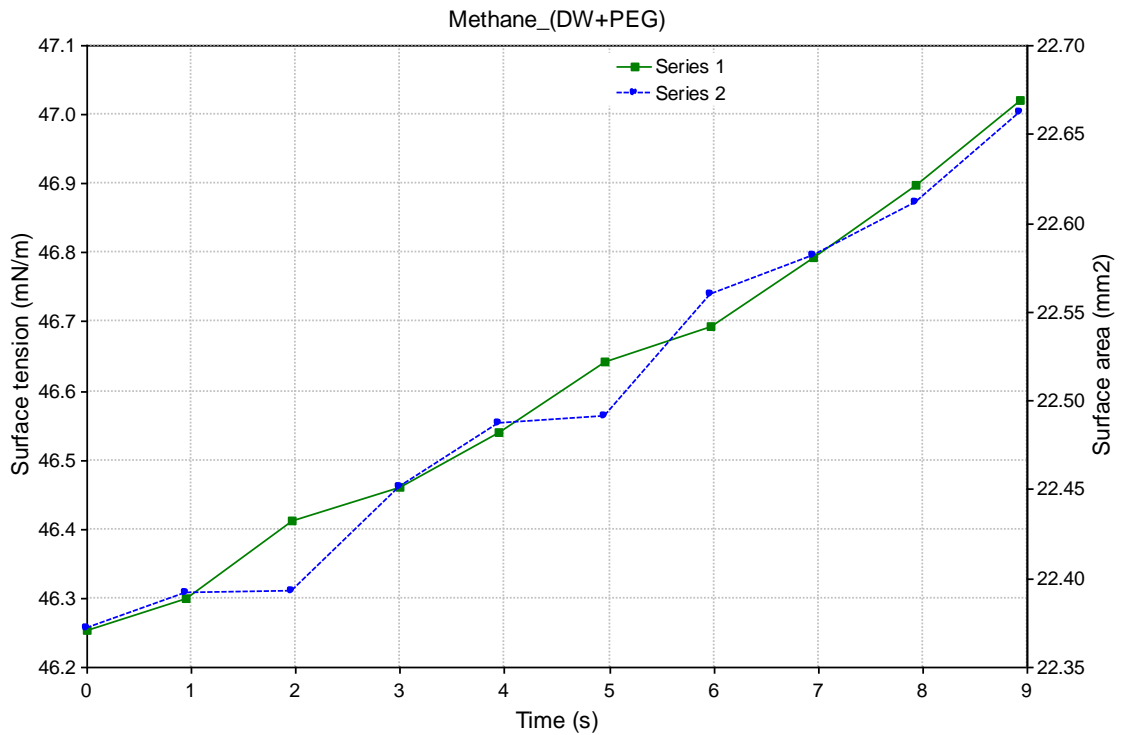
Pressure   = 6.205MPa

No.	Time	Gamma	Beta	R0	Area	Volume	Theta	Height	Width	Opt	Messages
1	0.0	46.48	0.293	1.173	22.72	9.75	75.77	3.666	2.416	4	
2	0.9	46.80	0.292	1.176	22.83	9.81	75.12	3.682	2.418	4	
3	2.0	47.07	0.292	1.179	22.93	9.86	74.45	3.699	2.423	4	
4	3.0	47.40	0.291	1.182	23.04	9.92	73.70	3.717	2.425	4	
5	3.9	47.77	0.291	1.185	23.15	9.98	72.95	3.734	2.430	4	
6	5.0	48.12	0.290	1.188	23.25	10.03	72.16	3.752	2.436	4	
7	6.0	48.52	0.289	1.191	23.38	10.11	71.30	3.770	2.438	4	
8	6.9	48.89	0.289	1.195	23.49	10.17	70.38	3.792	2.441	4	
9	8.0	49.29	0.288	1.198	23.60	10.22	69.47	3.812	2.444	4	
10	9.0	49.75	0.287	1.201	23.70	10.28	68.54	3.833	2.446	4	

Mean: 48.01   0.290   1.187   23.21   10.01   72.39   3.746   2.432
Stand.dev.:   0.35   0.001   0.003   0.10   0.06   0.77   0.018   0.003

Methane_(DW+PEG)
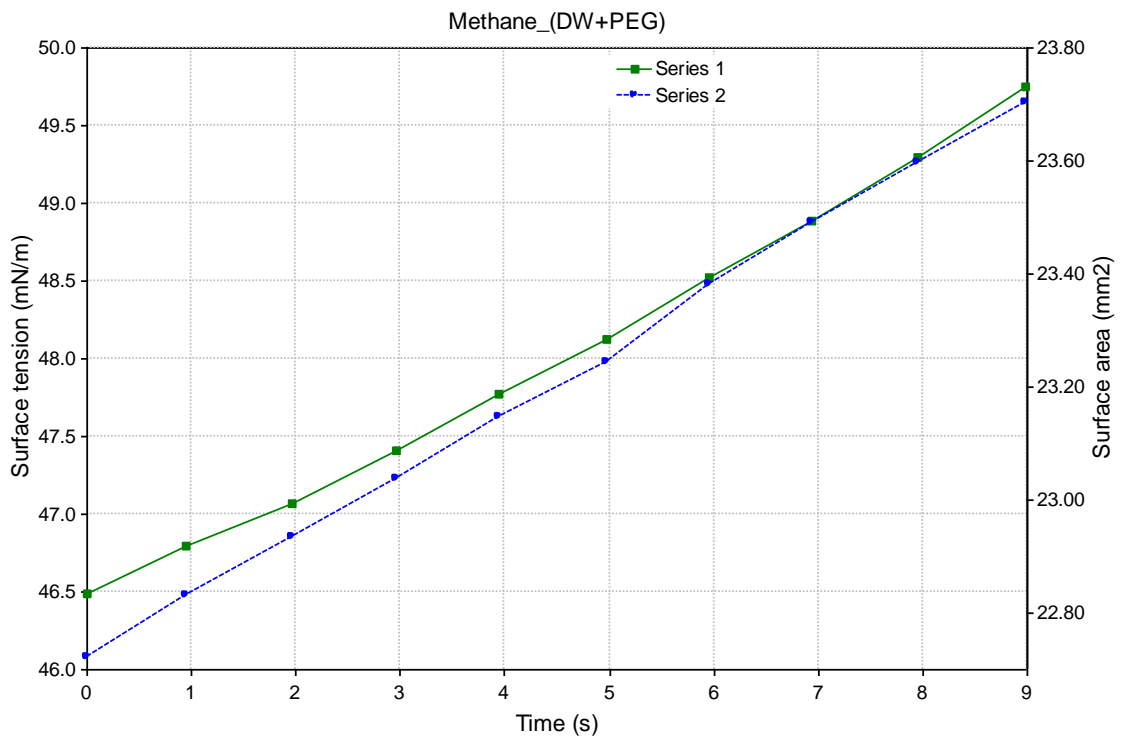
Pressure   = 7.067MPa

No.	Time	Gamma	Beta	R0	Area	Volume	Theta	Height	Width	Opt	Messages
1	0.0	44.25	0.296	1.151	21.97	9.31	78.74	3.571	2.378	4	
2	1.0	44.53	0.296	1.154	22.05	9.35	78.16	3.587	2.384	4	
3	1.9	44.86	0.295	1.157	22.17	9.41	77.48	3.605	2.390	4	
4	3.0	45.24	0.294	1.161	22.29	9.48	76.72	3.623	2.394	4	
5	3.9	45.66	0.294	1.165	22.46	9.57	75.71	3.646	2.400	4	
6	5.0	46.02	0.293	1.168	22.52	9.60	75.11	3.661	2.403	4	
7	6.0	46.40	0.292	1.171	22.67	9.69	74.24	3.680	2.406	4	
8	6.9	46.70	0.292	1.174	22.74	9.73	73.48	3.699	2.408	4	
9	8.0	47.10	0.291	1.178	22.87	9.79	72.60	3.719	2.414	4	
10	8.9	47.47	0.290	1.181	22.97	9.85	71.75	3.738	2.416	4	

Mean: 45.82   0.293   1.166   22.47   9.58   75.40   3.653   2.399
Stand.dev.:   0.35   0.001   0.003   0.11   0.06   0.75   0.018   0.004

Methane_(DW+PEG)
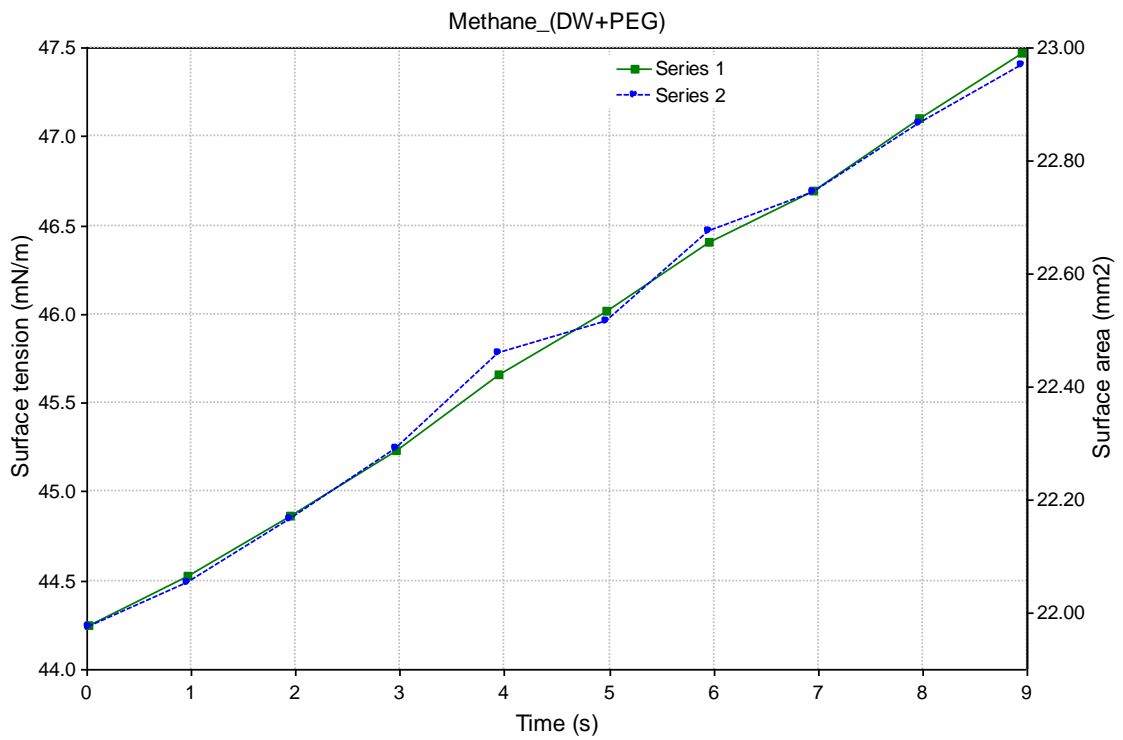
Pressure   = 7.929MPa

No.	Time	Gamma	Beta	R0	Area	Volume	Theta	Height	Width	Opt	Messages
1	0.0	40.69	0.296	1.104	20.26	8.24	79.34	3.420	2.289	3	
2	0.9	40.99	0.296	1.108	20.39	8.32	78.75	3.439	2.295	3	
3	1.9	41.42	0.295	1.113	20.52	8.39	78.12	3.457	2.301	3	
4	3.0	41.66	0.295	1.116	20.67	8.47	77.62	3.475	2.306	3	
5	4.0	42.01	0.295	1.120	20.82	8.56	76.96	3.493	2.312	4	
6	5.0	42.35	0.295	1.123	20.96	8.64	76.42	3.510	2.317	3	
7	5.9	42.65	0.294	1.127	21.09	8.71	75.85	3.528	2.325	4	
8	7.0	43.00	0.294	1.131	21.22	8.79	75.24	3.546	2.332	4	
9	8.0	43.32	0.294	1.134	21.32	8.84	74.69	3.564	2.337	4	
10	9.0	43.68	0.293	1.138	21.53	8.96	73.98	3.582	2.342	4	

Mean: 42.18   0.295   1.121   20.88   8.59   76.70   3.501   2.316

Stand.dev.:   0.32   0.000   0.004   0.13   0.07   0.56   0.017   0.006

Methane_(DW+PEG)

203
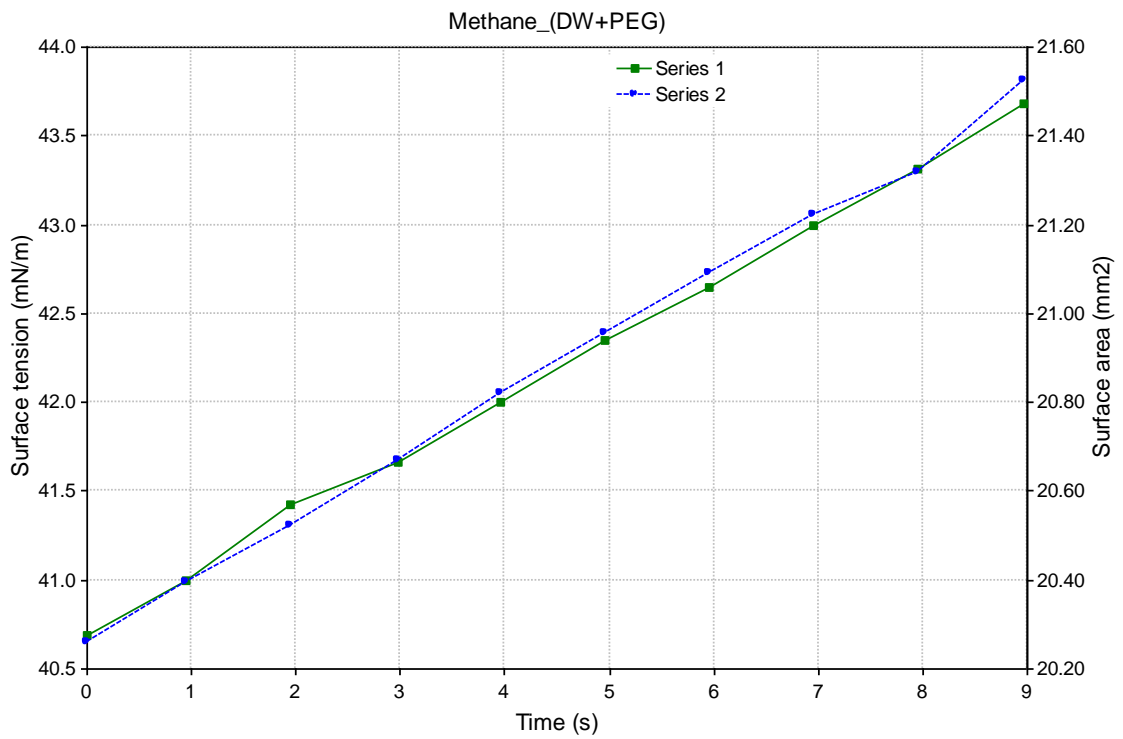
Pressure   = 8.791MPa

No.	Time	Gamma	Beta	R0	Area	Volume	Theta	Height	Width	Opt	Messages
1	0.0	44.62	0.292	1.148	21.84	9.13	71.97	3.637	2.354	4	
2	0.9	45.18	0.291	1.153	21.98	9.20	70.91	3.666	2.364	4	
3	2.0	45.79	0.290	1.159	22.23	9.34	69.81	3.696	2.375	4	
4	3.0	46.35	0.289	1.164	22.40	9.44	68.67	3.726	2.382	4	
5	3.9	46.94	0.288	1.170	22.59	9.54	67.51	3.756	2.388	4	
6	4.9	47.53	0.287	1.175	22.72	9.60	66.42	3.786	2.393	4	
7	6.0	48.20	0.286	1.181	22.93	9.72	65.13	3.818	2.400	4	
8	7.0	48.86	0.284	1.186	23.10	9.80	63.76	3.851	2.405	4	
9	7.9	49.59	0.283	1.191	23.25	9.87	62.37	3.886	2.413	4	
10	9.0	50.52	0.281	1.198	23.42	9.96	60.81	3.927	2.416	4	

Mean: 47.36   0.287   1.173   22.65   9.56   66.73   3.775   2.389
Stand.dev.:   0.61   0.001   0.005   0.17   0.09   1.17   0.030   0.006

Methane_(DW+PEG)
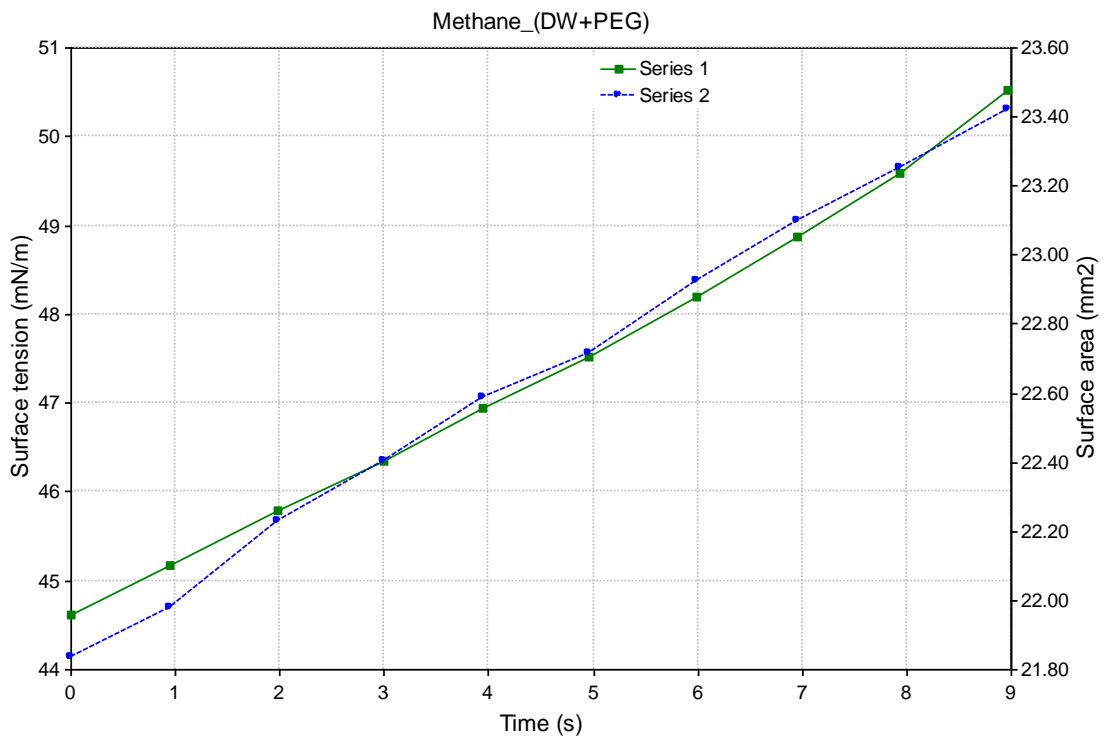
Pressure　　　= 9.653MPa

No.	Time	Gamma	Beta	R0	Area	Volume	Theta	Height	Width	Opt	Messages
1	0.0	43.57	0.294	1.138	21.51	8.94	73.04	3.601	2.341	4	
2	1.0	44.27	0.293	1.145	21.80	9.10	71.67	3.638	2.355	4	
3	2.0	45.02	0.292	1.153	22.02	9.22	70.28	3.677	2.364	4	
4	3.0	45.64	0.291	1.159	22.21	9.32	69.08	3.709	2.372	4	
5	3.9	46.26	0.289	1.164	22.35	9.39	67.96	3.738	2.378	4	
6	4.9	47.09	0.288	1.171	22.63	9.55	66.31	3.780	2.388	4	
7	6.0	47.98	0.286	1.179	22.86	9.67	64.65	3.823	2.395	4	
8	6.9	49.05	0.284	1.187	23.11	9.79	62.64	3.871	2.401	4	
9	7.9	49.30	0.283	1.189	23.13	9.80	62.11	3.884	2.402	4	
10	8.9	49.64	0.282	1.191	23.17	9.82	61.49	3.899	2.404	4	

Mean: 46.78　0.288　1.168　22.48　9.46　66.92　3.762　2.380
Stand.dev.:　　0.69　0.001　0.006　0.19　0.10　1.31　0.034　0.007
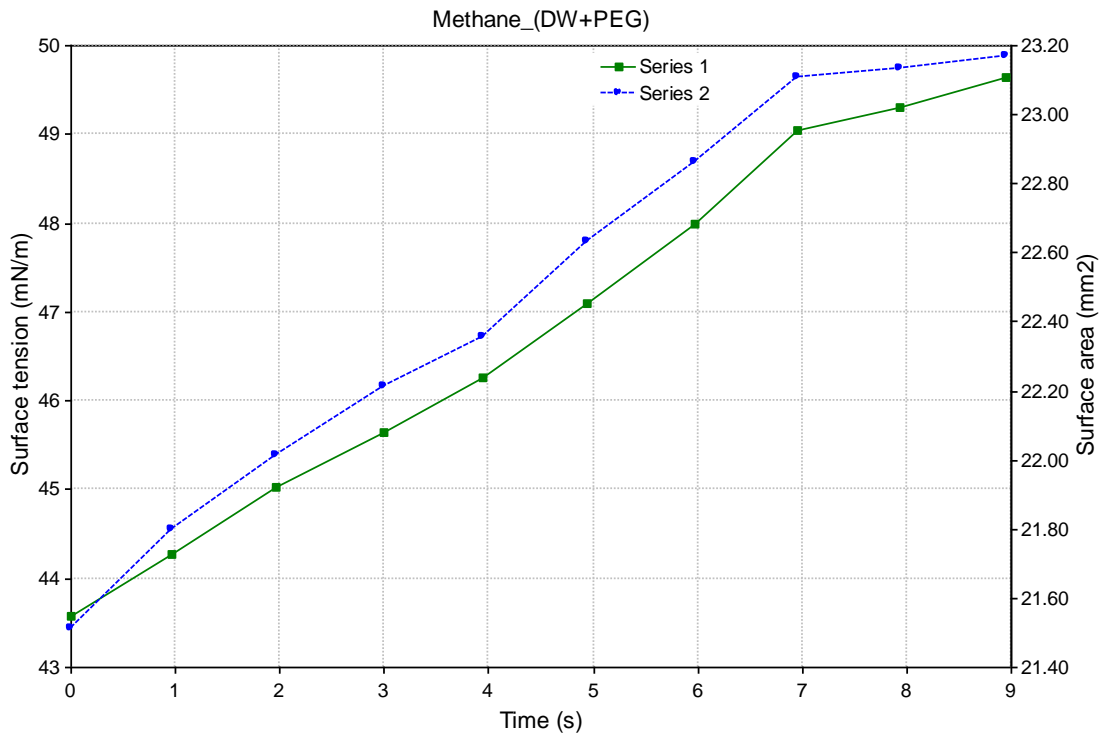
Methane_(DW+PEG)

Pressure   = 10.515MPa

No.	Time	Gamma	Beta	R0	Area	Volume	Theta	Height	Width	Opt	Messages
1	0.0	40.60	0.298	1.106	20.32	8.30	80.68	3.416	2.290	4	
2	0.9	41.95	0.296	1.122	20.90	8.62	78.11	3.491	2.319	4	
3	1.9	43.28	0.295	1.137	21.48	8.95	75.37	3.568	2.340	4	
4	3.0	44.63	0.293	1.151	21.94	9.20	72.73	3.642	2.365	4	
5	4.0	46.05	0.291	1.164	22.42	9.46	69.84	3.718	2.385	4	
6	4.9	47.62	0.288	1.178	22.93	9.74	66.58	3.800	2.402	4	
7	6.0	49.89	0.283	1.195	23.36	9.95	62.27	3.900	2.414	4	
8	7.0	38.48	0.299	1.079	19.32	7.72	83.48	3.300	2.244	4	
9	7.9	39.18	0.299	1.088	19.64	7.91	82.42	3.339	2.256	4	
10	8.9	40.35	0.297	1.102	20.17	8.20	80.28	3.404	2.279	3	

Mean: 43.20   0.294 1.132 21.25   8.81   75.17 3.558 2.329

Stand.dev.:   1.20   0.002 0.012   0.44   0.25   2.26   0.064 0.019

Methane_(DW+PEG)
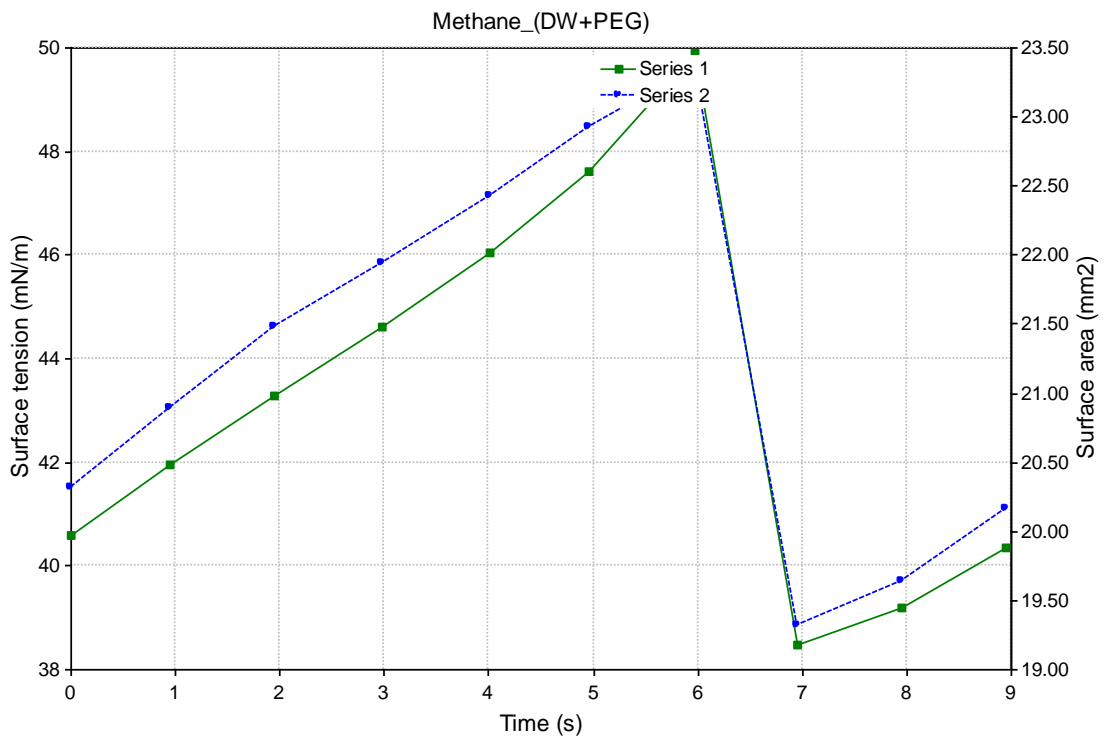
Pressure   = 11.376MPa

No.	Time	Gamma	Beta	R0	Area	Volume	Theta	Height	Width	Opt	Messages
1	0.0	38.55	0.301	1.083	19.55	7.82	79.91	3.362	2.247	3
2	0.9	0.00	0.000	0.000	0.00	0.00	0.00	0.000	0.000	0
3	2.0	39.19	0.300	1.091	19.84	7.98	78.46	3.404	2.259	4
4	3.0	39.63	0.299	1.096	20.00	8.07	77.72	3.426	2.266	4
5	4.0	40.03	0.299	1.101	20.20	8.17	76.82	3.453	2.273	4
6	5.0	40.46	0.298	1.105	20.39	8.28	75.85	3.479	2.278	4
7	6.0	40.87	0.298	1.110	20.58	8.39	75.02	3.502	2.284	4
8	6.9	41.21	0.298	1.114	20.71	8.45	74.16	3.528	2.291	4
9	7.9	41.72	0.297	1.119	20.87	8.54	73.18	3.554	2.297	4
10	8.9	42.13	0.296	1.124	21.05	8.64	72.22	3.578	2.307	3

Mean: 40.42   0.298 1.105 20.35   8.26   75.93 3.476 2.278
Stand.dev.:   0.39 0.000 0.005   0.17   0.09   0.85 0.024 0.006

Methane_(DW+PEG)
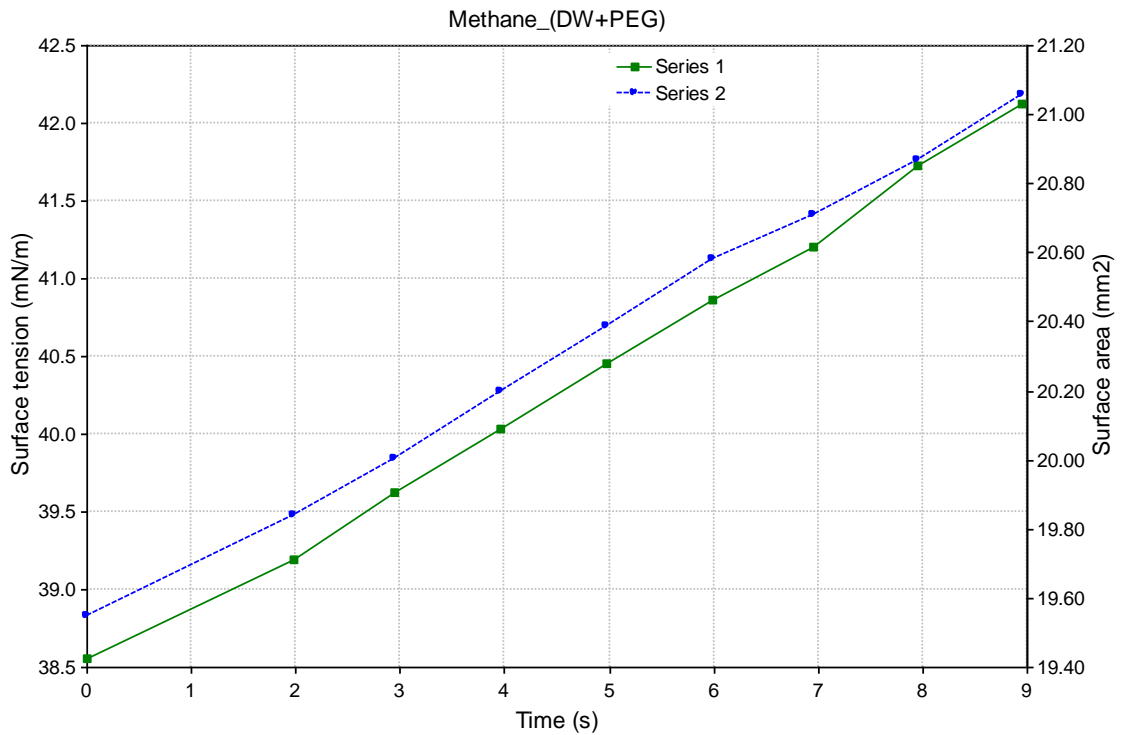
Pressure   = 13.100MPa

No.	Time	Gamma	Beta	R0	Area	Volume	Theta	Height	Width	Opt	Messages
1	0.0	39.53	0.300	1.095	19.98	8.07	79.58	3.402	2.270	4	
2	0.9	39.82	0.300	1.099	20.14	8.16	78.90	3.421	2.278	4	
3	2.0	40.23	0.299	1.103	20.28	8.24	78.17	3.445	2.285	4	
4	2.9	40.67	0.299	1.108	20.44	8.33	77.35	3.469	2.293	4	
5	4.0	41.13	0.298	1.113	20.64	8.44	76.48	3.492	2.297	3	
6	5.0	41.56	0.297	1.118	20.82	8.54	75.58	3.518	2.303	4	
7	6.0	42.12	0.297	1.124	21.04	8.66	74.37	3.552	2.310	4	
8	7.0	42.77	0.296	1.131	21.28	8.79	73.12	3.588	2.322	4	
9	7.9	43.49	0.295	1.139	21.57	8.95	71.58	3.628	2.333	4	
10	8.9	44.39	0.293	1.148	21.87	9.11	69.77	3.677	2.344	4	

Mean: 41.57   0.297   1.118   20.81   8.53   75.49   3.519   2.304
Stand.dev.:   0.51   0.001   0.006   0.20   0.11   1.03   0.029   0.008

Methane_(DW+PEG)